THE UNIVERSITY *of* EDINBURGH

Evaluation of Low-Cost Earth Observations to Scale-Up National Forest Monitoring in Miombo Woodlands of Malawi

Henry Harry Kadzuwa

Submitted for the degree of Doctor of Philosophy

The University of Edinburgh

2023

Declaration

I confirm that this work is my own, except where indicated otherwise. The thesis contains five research chapters and three journal articles (attached separately as electronic copies) that I have published in international peer-reviewed journals, thus, the Journal of Global Ecology and Environment and the International Journal of Forestry Research. The candidate confirms that appropriate credit has been given within the thesis where reference has been made to the work of others. No part of this thesis has been submitted for any other degree or qualification.

The candidate, as principal researcher, performed the following tasks; field data collection, satellite imagery acquisition, data analysis, interpretation of results, thesis writing as well as authoring of the research articles published. Co-authors provided support and guidance on the scope and design of the project, the analyses performed and contributed to the editing of the manuscripts as acknowledged in the published papers.

Signed: …… ……..
Henry Harry Kadzuwa

Date: 28th February, 2023……..

Abstract

This study explored the extent that low-cost Earth Observations (EO) data could effectively be combined with *in-situ* tree-level measurements to support national estimates of Above Ground Biomass (AGB) and Carbon (C) in Malawi's Miombo Woodlands. The specific objectives were to; (i) investigate the effectiveness of low-cost optical UAV orthomosaics in geo-locating individual trees and estimating AGB and C, (ii) scale-up the AGB estimates using the canopy height model derived from the UAV imagery, and crown diameter measurements; and (iii) compare results from (ii), ALOS-PALSAR-2, Sentinel1, ESA CCI Biomass Map datasets, and Sentinel 2 vis/NIR/SWIR band combination datasets in mapping biomass. Data were acquired in 2019 from 13 plots over Ntchisi Forest in 3-fold, *vis-a-vis*; (i) individual tree measurements from 0.1ha ground-based (gb) plots, (ii) 3-7cm pixel resolution optical airborne imagery from 50ha plots, and (iii) SAR backscatter and Vis/NIR/SWIR bands imagery. Results demonstrate a strong correlational relationship (R^2 = 0.7, RMSE = 11tCha^{-1}) between gb AGB and gb fractional cover percent (FC %), more importantly (R^2 = 0.7) between gb AGB and UAV-based FC. Similarly, another set of high correlation (R^2 = 0.9, RMSE = 7tCha^{-1}; R^2 = 0.8, RMSE = 8tCha^{-1}; and R^2 = 0.7) was observed between the gb AGB and EO-based AGB from; (i) ALOS-PALSAR-2, (ii) ESA-CCI-Biomass Map, and (iii) S1-C-band, respectively. Under the measurement conditions, these findings reveal that; (i) FC is more indicative of AGB and C pattern than CHM, (ii) the UAV can collect optical data of very high resolution (3-7cm resolution with ±13m horizontal geolocation error), and (iii) provides the cost-effective means of bridging the ground datasets to the wall-to-wall satellite EO data (£7 ha^{-1} compared to £30 ha^{-1}, per person, provided by the gb system). The overall better performance of the SAR backscatter (R^2 = 0.7 to 0.9) establishes the suitability of the SAR backscatter to infer the Miombo AGB and fractional cover with high accuracy. However, the following factors compromised the accuracy for both the SAR and optical measurements; leaf-off and seasonality (fire, aridness), topography (steep slopes of 18-74%), and sensing angle. Inversely,

the weak to moderate correlation observed between the gb height and UAV FC % measurements (R^2 = 0.4 to 0.7) are attributable to the underestimation systematic error that UAV height datasets are associated with. The visual lacunarity analysis on S2-Vis/NIR/SWIR composite band and SAR backscatter measurements demonstrated robust, consistent and homogenous spatial crown patterns exhibited particularly by the leaf-on tree canopies along riverine tree belts and cohorts. These results reveal the potential of vis/NIR/SWIR band combination in determining the effect of fire, rock outcrops and bare land/soil common in these woodlands. Coarsening the EO imagery to ≥50m pixel resolution compromised the accuracy of the estimations, hence <50m resolution is the ideal scale for these Miombo. Careful consideration of the aforementioned factors and incorporation of FC parameter in during estimation of AGB and C will go a long way in not only enhancing the accuracy of the measurements, but also in bolstering Malawi's NFMS standards to yield carbon off-set payments under the global REDD+ mechanism.

Lay Summary

This study investigated the extent that low-cost and unrestricted remotely sensed imagery data could effectively be combined with tree-level field measurements to support national estimates of Above Ground Biomass (AGB) and Carbon (C) in Malawi's Miombo Woodlands. The purpose of this research was to explore the practicability of scaling-up Malawi's National Forest Monitoring System (NFMS) (which relies on field plot data) using a combination of low-cost optical, but fine resolution imagery acquired from a consumer grade drone and moderate to high quality satellite imagery, while trying to increase accuracy to achieve the global REDD+ mechanism standards and C payments. The research involved three categories of measurements collected over Ntchisi Forest in 2019 as follows; (i) individual tree measurements from 0.1ha field plots, (ii) 50 ha plot low –cost drone imagery and (ii) freely accessed satellite imagery from the following missions; ALOS-PALSAR-2, Sentinel1 and 2, and ESA-CCI-Biomass Map. Results show high correspondence (R^2 = 0.7, RMSE = 11tCha^{-1}) between field AGB and field fractional cover percent (FC %), more importantly between field AGB and drone-based FC % (R^2 = 0.7). Another set of high associations (R^2 = 0.9, RMSE = 7tCha^{-1}; R^2 = 0.8, RMSE = 8tCha^{-1}; and R^2 = 0.7) were detected between the field AGB and satellite-based AGB datasets from; (i) ALOS-PALSAR-2, (ii) ESA CCI-Biomass map, and (iii) S1-C-band, datasets, respectively. These outcomes demonstrate that under the study conditions; (i) FC is more suggestive of AGB and C patterns than the height data (CHM) acquired by the drone, (ii) the drone can collect very high quality RGB data of 3-7cm resolution with a horizontal distance error of ±13m, (iii) the drone can provide the economical means of linking the field measurements to the global satellite EO images at a cost of £7 per ha, in contrast to the £30 per ha, per person provided by the field plot measurement system. The overall better performance of the radar datasets (R^2 = 0.7 to 0.9) over the optical reflectance imagery establishes the suitability of the former to explore the Miombo with high accuracy. Nevertheless, caution should be taken on the following factors

that affected the accuracy for both measurements; leaf-off and seasonality (fire, aridness), topography (steep slopes of 18-74%), and sensing angle. Inversely, the weak to moderate relationship observed between the field-based height and drone-based FC % measurements (R^2 = 0.4 to 0.7) is attributable to the system error that drone height datasets are associated with. The visual analysis on Sentinel 2 measurements demonstrated robust, consistent and identical spatial crown patterns displayed particularly by the leaf-on tree canopies along riverine tree belts and cohorts. They reveal the potential of the Sentinel 2 satellite selected windows in defining the effect of fire, rock outcrops and bare land/soil common in these woodlands. Resampling the satellite imagery to the scale of 50m x 50m or more compromised the assessment accuracy. Therefore, this study deduces that a scale of less than 50m x 50m is ideal for the Miombo. Careful consideration of the aforementioned factors and incorporation of FC parameter during assessment of AGB and C will go a long way in not only enhancing the accuracy of the measurements, but also in supporting the Malawi's NFMS standards to yield carbon off-set payments under the global REDD+ mechanism.

Acknowledgements

My profound gratitude should go to various people who have generously offered support during the past four years, especially; Prof., Iain H. Woodhouse, Dr Steven Hancock, Dr Casey Ryan, and Mr Sam Fleming.

Thanks to my principal supervisor Professor. I.H Woodhouse for his unwavering support, advice and mentorship which have been invaluable for developing my scientific skills and ethics in research, and above all else, in Earth Observations that use optical and active sensors. Many thanks to my second supervisor Dr Steve Hancock whose guidance in UAV data processing using Structure-from-Motion Photogrammetry and data analysis has been key throughout the study.

I am grateful to Dr Casey Ryan for sharing his invaluable knowledge and experience of the tropical ecosystems through the Tropical Land Use platform as well as reading and commenting on pieces of my research presentations made during such meetings. Thanks should go to Dr Courage Kamusoko for his support on Rstudio programming language.

I am indebted to the Commonwealth Scholarship Commission for sponsoring my PhD programme and the Department of Forestry, particularly the Forestry Research Institute of Malawi for providing staff that assisted in field data collection. I am also thankful to the CarboMap and EarthBlox of Edinburgh for the invaluable technical support offered to me throughout my entire PhD programme.

I would like to thank my former flatmate, Dr Andrew Twelves, and the following colleagues; Dr E. Missanjo, Mr M.F. Chirwa and Dr D. Kachamba for the moral support they provided during my study. Last, but not least huge thanks go to the following for the unwavering mental and spiritual support; the Poor Clares Monastery (Lilongwe), Rev. Fr; J. Makoka, C. Kanyambo, H. Makawa, and A. Kadzilawa, Mrs Mchitakupha Banda, Aunt Angella, Rev. Msgr. P. Thawale and His Lordship, Rt. Rev. Bishop P. Chifukwa.

Contents

LIST OF FIGURES

LIST OF TABLES

CHAPTER-1

1.0 INTRODUCTION

1.1 Motivation and Justification

Malawi still relies on field-based measurements for estimating forest biomass and carbon (C), despite the increase in studies that integrate unrestricted Earth Observations (EO) with terrestrial measurements (Government of Malawi, 2019a). This is against the backdrop that ground-based measurement system alone is generally associated with a plethora of setbacks that range from high labour and overhead expenses, definite dimensional and temporal scales to compromised data accuracy, *inter alia* (DeFries et al., 2007; Kachamba et al., 2016; Kadzuwa and Missanjo, 2022a; Petrokofsky et al., 2012).

Forests and woodlands play an indispensable role in the global C cycle through balancing CO_2 concentrations via photosynthesis, and thereby mitigating the impact of global warming and climate change (Dixon et al., 2011; Novotný et al., 2020). Nevertheless, they have been hugely challenged by anthropogenic disturbances, registering a loss of ~2.3 million km^2 between 2000 and 2012, and more recently, 4.7 million hectares per year worldwide between 2010 and 2020 ([FAO] Food and Agriculture Organization, 2020; Hansen, 2013; Ritchie and Roser, 2017). These have contributed to annual global greenhouse gas (GHG) emissions of ~50 gigatonnes of CO_2e[1](*ibid*). This has led to calls for global monitoring of forests and subsequent protection of woodland C stock fluxes *vis-à-vis*; biomass extraction, land use change, forest fires, besides forest growth enhancements (Gonsamo et al., 2017; Prosperi et al., 2020).

One key global intervention is the initiative on reducing emissions from deforestation and forest degradation (REDD+) advocated by the 1992 Kyoto Protocol of the United Nations Framework Convention on Climate Change (UNFCCC) (Patenaude et al., 2005). Under REDD+, C accounting is left to individual national agencies to decide pursuance of the appropriate methodologies with respect to climate change tracking and mitigation (Krug,

[1] CO_2e = Carbon dioxide equivalent. It stands for the number of metric tonnes of CO_2 emissions with the same global warming potential as one metric tonne of another greenhouse gas.

2018). In Malawi, this remains the responsibility of the Department of Forestry (DoF) which commenced piloting such efforts in Nyika and Mkuwazi protected areas, as early as 2008 (Berry et al., 2008). This was prior to officially joining the United Nations REDD partnership in 2014 (Berry et al., 2008; Department of Forestry, 2015; Malawi Redd+ Programme, 2015). However, implementation of the REDD+ efforts in the country has been characterised by a set of intertwined constraints associated with over-reliance on ground-based methods as the major forest monitoring technique (Kadzuwa and Missanjo, 2022a; Neeff et al., 2015). In this work, I focus on the approaches and methods used, or potentially applied in Malawi during estimation of forest biomass and C, with consideration of the cost-effectiveness and their fit-for-purpose.

The dependence on ground-based (gb) methods in Malawi is compounded by insufficient funding that underpins the challenges to developing an effective national forest monitoring system (NFMS) (Malawi Redd+ Programme, 2015; Neeff et al., 2015; Skole et al., 2021). Though gb inventory is primarily, but, not exclusively, renowned for its less sophisticated nature (not requiring much technical computer expertise), its sole employment as a forest inventory method is associated with several drawbacks that include;

(i) high labour and operational costs (DeFries et al., 2007; Kachamba et al., 2016; Mlambo et al., 2017), i.e., £30 per ha per person compared to £7/ha for optical small unmanned aerial vehicle (UAV) airborne surveys (Table 2);
(ii) limited spatial and temporal scale (practically covers small portion of the forest area under research) i.e., 0.126 ha per team per day in comparison to ≥162.5 ha per day for optical small UAV airborne surveys (Table 2) (Mueller, 2012);
(iii) unrepresentative spatial sampling due to inability to access fragile areas such as cliffs, steep slopes, riverbanks, etc. (Petrokofsky et al., 2012), compared to airborne and satellite EO that cover sites regardless of their accessibility; and,
(iv) relative inconsistencies and inaccuracy emanating from various tools and methods used, i.e., use of varied sampling approaches, plot configurations, allometry for biomass calculations and interchange of stem diameter measurement tools (diameter tape versus calliper) (Alegria and Matthews, 2014, 2014; Angelsen, 2008; DeFries et al., 2007; Dube and Mutanga, 2015;

Gaucher et al., 2015; Kachamba et al., 2016; Kadzuwa and Missanjo, 2022a; Malawi Redd+ Programme, 2015; Mlambo et al., 2017; Neeff et al., 2015; Sinha et al., 2015).

Malawi experiences uniquely high annual deforestation and forest degradation that ranged from 22,410 ha yr^{-1} to 38,937 ha yr^{-1} and 42,961 ha yr^{-1} to 71,878 ha yr^{-1} during the period 2000-2009 and 2000-2015, respectively (Skole et al., 2021). Such environmental damage warrants robust forest monitoring methods capable of detecting woody biomass stock loss with minute details i.e., at 20m radius scale, which is the maximum sampling unit plot size for estimating deforestation and degradation in Malawi (Department of Forestry, 2012; Government of Malawi, 2019a). Ideally, these are attainable through spatially explicit means i.e., remote sensing, yet despite the current Malawi's forest status, there is still over-reliance on gb methods alone to monitor and track biomass and C fluxes, a system which comparatively has predefined limitations in space and time dimensions (Table 2) (Petrokofsky et al., 2012).

More striking is that over the past three decades, the dependency on gb data alone has yielded significant inaccuracies and inconsistencies in forest biomass estimations as observed from the following: (i) Standard Operating Procedures (SOPs), (ii) sampling strategies/design, (iii) sampling unit configuration, (iv) stem diameter measurements, and, (v) allometry, (Table 3), *inter alia* (Government of Malawi, 2019a; Kadzuwa and Missanjo, 2022a; McGann, 2015; Skole et al., 2021). Worse-still, under the global REDD+ framework, Malawi still operates within *Tiers* 1 and 2 systems (Ministry of Forestry and Natural Resources, 2021). This is indicative of lower methodological and data accuracy as per standards assessments of the Intergovernmental Panel on Climate Change (IPCC). Consequently, this has stalled the progress of the country's achievements under the REDD+ global scheme.

In this respect, a study on forests noted that AGB estimates of the tropical region where Malawi belongs are associated with; inaccurate measurement of variables, inconsistent allometric models, sampling size and design, and poor representativeness of the sampling network (Petrokofsky et al., 2012).

A different local study that compared remote sensing-derived national land use/land cover (LULC) mapping studies of Malawi revealed significant inconsistencies and variations in procedures, data and results on deforestation, forest degradation rates, hinging on biomass and C in the country (Haack et al., 2015).

Reports have attributed such flaws to bearing incomparable forest biomass and C datasets and results that hamper the accreditation of Malawi's REDD+ efforts, and delay C-based financial payments (Government of Malawi, 2019a; McGann, 2015; Neeff et al., 2015; Skole et al., 2021). Furthermore, these limitations pose an obstacle to the development of Malawi's National Forestry Inventory (NFI) system, which is underway, as noted by the rejection of its initial, though incumbent (2019) Forest Reference Emissions Level (FREL) report by UNFCCC (UNFCCC, 2021). Considering such knowledge gaps, this academic research was designed to support the understanding of how the incumbent Malawi's NFMS technique could integrate low-cost but, moderate to high spatial resolution (HR) remote sensing data to scale-up spatial and temporal coverage while enhancing above-ground biomass (AGB) estimations accuracy with minimal costs.

Remote sensing of forests has been successfully implemented in other low-income countries in the dry tropics, even using freely available datasets. However, attempts to simply transfer methods that have succeeded elsewhere to be used in Malawi have been challenged with substantial difficulties (Haack et al., 2015; Næsset, 2015; Neeff et al., 2015; Ryan et al., 2012, 2012). Hence, to fully exploit the freely available/unrestricted remote sensing data requires either a better understanding of the relationship between forest biomass and remotely sensed parameters (such as radar backscatter) or a more effective bridging between field-based measurements that are the core of Malawi's NFI, and the satellite based-datasets.

In view of these scientific, but uncharted knowledge gaps, thus amidst Malawi's pursuance of the REDD+ mechanism, it was important for this study to explore the following;

i. How efficiently does UAV photogrammetry work in Malawi's Miombo Woodlands considering its fit-for-purpose and cost-effectiveness, given the scale of variation in landscape heterogeneity?
ii. How does it help the researcher understand the spatial variability of Malawi's woodland?
iii. How does it help the researcher understand the efficiency of integrating satellite data into the ground-based measurements? and last though not least,
iv. How might the UAV and satellite datasets be combined to optimise spatial coverage, temporal resolution and enhance data accuracy, all of this within the constraints of cost-effectiveness and other environmental challenges for a Malawi context?

1.1.1 Challenges of Remote Sensing Malawi's Miombo

Miombo Woodlands are the dominant forest biome of Malawi, covering ≥90% of the country's total forestland (23,677km^2), (Figures 4 and 5) (Skole et al., 2021). The woodlands are fragmented and extend across a highly heterogeneous landscape with mosaics of both open and closed canopies (Cassells, 2012; Skole et al., 2021). Besides, they are exposed to unpredictable anthropogenic factors such as fire, wood and charcoal extraction which resulted in some cases, to variant patches of forests C stocks, ranging from 35 to 45Mg ha^{-1} and sometimes to as low as 8Mg ha^{-1}, rendering the woodland's mapping and modelling quite uncertain (Haack et al., 2015; Kamusoko et al., 2014; Kuyah et al., 2014; Skole et al., 2021).

The unpredictable wood/charcoal extraction and fire incidents of Malawi complicate validation, calibration and interpretation of remotely sensed datasets (Figure 42) (Department of Forestry, 2012). This occurs in the way that during the time-lapse between the EO data acquisition and the gb measurements (validation) there is always high chances of biomass reduction due to either wood and charcoal extraction or fire damage, especially during the dry season as the country experiences their high frequencies within a brief time (Department of Forestry, 2012; Nieman et al., 2021; Skole et al., 2021). This partly contributed to the significant variations reported on LULC classification and accuracy revealed by the analysis of the 4 studies conducted during the same period in

Malawi (Haack et al., 2015). Irrespective of the aforementioned factors, the various spatial resolutions of EO used in most of the local studies in Malawi have been too coarse to capture the variability of fragmented landscapes as well as the contribution of the afore-said anthropogenic factors, thereby thwarting mapping efforts of Malawi's Miombo Woodlands (Haack et al., 2015; Skole et al., 2021). For instance, the Landsat Enhanced Thematic Mapper's Thermal InfraRed's 60m spatial resolution (3600m^2 or 0.36ha) of band 6 datasets and the Landsat Multispectral Scanner of 30m spatial resolution (900m^2 or 0.09ha) imagery were used for analysing vegetation i.e., mapping biomass (Haack et al., 2015). However, some fragmented forest mosaics of Malawi are too small i.e., <0.04ha while others are slightly ≤ 1257m^2 (0.12ha, Table 3) to be effectively mapped at the Landsat's imagery minimum mapping units (mmu) (Haack et al., 2015; Skole et al., 2021). This has resulted in serious scale mis-matches (between the mmu and sampling unit plot sizes) and eventually yielded high uncertainty in biomass and C estimates for the previous years in Malawi (Haack et al., 2015; Skole et al., 2021).

Besides, Miombo Woodlands are critically affected by tree leaf-phenology and seasonality, i.e., they experience leaf-off and leaf-on conditions during the dry season (April-October) and wet seasons (November to March), respectively (Fig. 5) (Chidumayo, 1997; Kadzuwa and Missanjo, 2022a; Kamusoko et al., 2014). This renders interpretation of biomass and other woody components difficult as they cause spectral reflectance patterns of the woodland to vary according to tree leaf condition and seasonal change (Kamusoko et al., 2014). This is due to changes of surface moisture or water availability that occurs during the rainy and dry seasons (*ibid*). In Malawi, surprisingly, none of the previous Miombo biomass studies (Domingo et al., 2019; Kachamba et al., 2016; Skole et al., 2021) has meticulously explored how leaf-phenology and seasonality affect AGB estimations, i.e., correlating the effect of leaf-fall and dry season factors with biomass assessments, despite the clear distinction existing between the evergreen riverine and the deciduous sub-forest types (especially during the dry season) constituting the Miombo of Malawi, at least to the author's knowledge.

In addition, most forest cover change assessments that entail C stock monitoring in Malawi focused on government managed (Miombo) lands only, thereby deriving biased

results (Skole et al., 2021). The practice has also resulted in establishing most of the sampling plots for the REDD+ initiative within the government-controlled forests only, yet forests also cover customary and private owned lands as well. This is against the background that under REDD+ mechanism, fine-scale information on forest attributes, primarily acquired through remote sensing is indispensable to the orientation of different management and conservation activities across various forest land tenure (Government of Malawi, 2019a; Kachamba et al., 2016; Skole et al., 2021).

Validating remotely sensed observations using terrestrial data acquired from permanent sample plots (PSPs) is one fundamental element advocated under the REDD+'s measuring reporting and verification (MRV) protocol (Chidumayo, 2019; Zerihun and Tesfaye, 2013). Unfortunately, records indicate that there is no complete wall-to-wall network of permanent sampling plots (PSPs) covering Malawi (Government of Malawi, 2019a; Tetra Tec and Winrock International, 2022, 2021). For instance, from a sample estimate of 663 PSPs computed to sufficiently encompass the country at 95% Confidence Interval (10% error), only 354 (53%) were established by the time the country attempted to conduct a national forest inventory (2019) (Government of Malawi, 2019a; Tetra Tec and Winrock International, 2022, 2021). Unfortunately, to date, the target has not been attained, at least to the knowledge of the author. This predicament renders another significant challenge for the Miombo remote sensing studies especially, under the REDD+ initiative as the scheme requires repeated assessments on designated area, preferably PSPs for consistence and accuracy's sake (Shoch et al., 2013; Vanclay et al., 1995).

Tropical woodland studies on forest monitoring (Southern Africa inclusive) have increasingly recommended the enhancement of terrestrial measurements by integrating remotely sensed EO data as a low-cost option to pursue REDD+ mechanisms (Angelsen, 2008; DeFries et al., 2007; Dube and Mutanga, 2015; Kachamba et al., 2016; Sinha et al., 2015). Research further encourages employment of medium to high resolution Earth Observations from unrestricted sources and low-cost airborne imagery (from commercial UAVs) as an approach to attaining more accurate forest biomass estimations under REDD+ scheme (Ahrends et al., 2021; Bouvet et al., 2018; Kachamba et al., 2016; Mlambo et al., 2017). However, the setback has been that previous LULC studies in

Malawi produced results with considerable inconsistencies and uncertainties, i.e., the minimum mapping unit (MMU) varied from 0.001ha ($25m^2$), 0.8ha ($90m^2$) and 2ha to 100ha, yielding national forest cover percentages with significant errors as they ranged from 18.2 to 28.7% (Haack et al., 2015; Skole and Samek, 2016). In addition, the estimates excluded the trees outside forest (trees on farm) on customary and private land domain (*ibid*). Hence, the deforestation rates estimated by the same studies had significant biases, i.e., ranged from ~6 × 103 ha $year^{-1}$ to 30 × 103 ha $year^{-1}$ while the acceptable ones ranged from 22 × 103 ha $year^{-1}$ to 39 × 103 ha $year^{-1}$ (Skole et al., 2021). These have rendered difficulties in comparison, hence could not be reliably used for the REDD+ purposes (Haack et al., 2015; Kadzuwa and Missanjo, 2022a; Skole et al., 2021).

Despite this, investigations on African woodlands revealed that quantification of the processes of C emissions from tropical land-use change is hindered by limitations of optical remote sensing and ground datasets (McNicol et al., 2018). Malawi is no exception as ~25% of previous gb inventories have had their datasets untraceable and/or irretrievable (Table 3) (Alegria and Matthews, 2014; Kadzuwa and Missanjo, 2022a; Malawi Redd+ Programme, 2015). In some cases, this predicament has left remote sensing/mapping efforts of the country with hitches in planning and consequently, interpretation of the imagery observations due to scanty or unreliable baseline data (Department of Forestry, 2012). This syndrome has subsequently contributed to deterrence of in-depth research efforts that use remote sensing techniques in Malawi's Miombo Woodlands.

Records show that almost one-third of the forest inventory studies in Malawi attempted to employ EO from unrestricted access of Landsat, ASTER sensor aboard the Terra mission (thus DEM) and Google Earth (GE) platform (Table 3). Despite some global and regional efforts undertaken to map the Miombo eco-biome (Baccini and Asner, 2013; McNicol et al., 2018; Saatchi et al., 2011), literature critically exposes there has been minimal efforts by local studies in the country to engage the freely/unrestricted Sentinel or ALOS-2 PALSAR-2 datasets in estimating AGB (Government of Malawi, 2019a; Tetra Tec and Winrock International, 2022, 2021). This is despite the renowned finer spatial and

temporal resolution that the missions' datasets provide, at least to the knowledge of the author.

Remote sensing (RS) technique in forest assessments can be incorporated at either the design (planning stage) and/or estimation (quantification) phases (Saarela et al., 2016). At the design stage, RS can be integrated to stratify forest structure and aid unequal probability sampling while during estimation phase, it facilitates balanced sampling (improves estimates of population parameters either by model-assisted estimation or model-based inference) (Cunliffe et al., 2020; McRoberts et al., 2015; Patenaude et al., 2005; Saarela et al., 2016). Such up-to-date studies have evolved full integration of RS at both stages to the extent of drawing predictive relationship/models and statistically estimate biomass and C, in addition to other woody components, advances renowned to enhance data accuracy, temporal and spatial resolution (*ibid*).

Unfortunately, Malawi's local and national forest biomass assessment statistics over the past 3 decades (Table 3) indicate that only 55% of inventories attempted to integrate RS technique, worse-still, just ~45% of the those studies incorporated the system at a basic palling level i.e., pre-screening and/or stratifying forest areas using arbitrarily visualisations that are prone to high errors (Department of Forestry, 2012; Government of Malawi, 2019a; Malawi Redd+ Programme, 2015).

A renowned forest mapping study employed ALOS-PALSAR-1 radar backscatter measurements to merely identify vegetation and stratify forestland in Malawi's Miombo Woodlands during the 2010 -12 period (Department of Forestry, 2012; Haack et al., 2015). Though the study achieved wider spatial coverage of forestland (compared to the past plot-based inventories) and despite a follow-up synthesis on LULC analysis delivering a forest conversion risk modelling that would have triggered in-depth investigations on spatial forest cover and deforestation risk factors; no deliberate attempt was made to examine the relationship between the ground-based AGB and radar backscatter measurements in these woodlands. Therefore, it was of great interest for this academic study to fill the scientific novelty by examining the correlational relationship of

the parameters using these two datasets, thus against the background of Malawi's Miombo Woodlands challenges.

Forest investigations conducted in the Savannah Woodlands of Cameroon and Uganda, and Miombo Woodlands of Mozambique (Nhambita and Niassa) in 2009, established a positive correlation between gb AGB and L-band backscatter estimations for lower-biomass up to 150 Mg ha^{-1} (±~20%) (Mitchard et al., 2009; Ryan et al., 2011). In sharp contrast, a poor or no correlation pattern between the gb AGB and the L-band radar backscatter measurements was established in Malawi's Miombo Woodlands (Nyika and Mkuwazi protected areas) through a study conducted within the same period (Cassells et al., 2009). This was attributed to; (i) the openness of the forest canopy, (ii) the heterogeneity in tree sizes and locations, and (iii) topography (Cassells, 2012; Cassells et al., 2009). Hence, further studies were encouraged on this, yet up to date, these factors have rarely been explored regarding to their contribution to AGB estimations in Malawi. In contrast, these attributes were not reported to have influenced biomass estimations in the African savannah and Miombo woodlands study, suffice to suggest that their pronounced effect was unique for Malawi in comparison to the other countries. This left a significant knowledge gap for exploring Malawi's circumstances affecting biomass and carbon estimates.

Furthermore, the correlation (between gb AGB and L-band backscatter) drawn in the Savannah of Cameroon and Uganda and Miombo of Mozambique employed regional-scale AGB allometry (Mitchard et al., 2009; Ryan et al., 2011). Nevertheless, application of these allometry were observed to have yielded unreliable results for Malawi's Miombo Woodlands, thus under REDD+ mechanism (Kachamba, 2016). While these findings, in addition to the previous studies, provided the impetus to generate and adopt local allometry for estimating biomass in Malawi's Miombo Woodlands, uniqueness of the country's local circumstances i.e., geographical and topographical attributes were cited as the key reasons for not adopting the allometry despite the woodlands falling under the same Miombo eco-biome stretch with Mozambique (Figure 4) (Kachamba, 2016).

Another key study that examined the applicability of L-band radar backscatter from ALOS-PALSAR cross-polarised-HV measurements in Mozambique's Miombo Woodlands (2007-2009) revealed that datasets could be used, to some extent in detecting vegetation C stocks losses and gains as a low as 12MgCha^{-1}, with 95% confidence interval (Ryan et al., 2012). Despite these findings, another related study emphasised on further work to quantify the uncertainties in the biomass change estimates (Mitchard et al., 2013). While both Mozambique and Malawi share the same Miombo Eco-biome, variations have been observed in the extent of drivers of biomass change in the two countries, suffice to suggest that C stock mapping for Mozambique would have not worked for Malawi's Miombo due to the following;

(i) the minimum level of the detecting C stocks was 12MgCha^{-1} in Mozambique while the stocks of Malawi estimated the same period reached as a low as 8MgCha^{-1} (Skole et al., 2021), hence the difference in the mapping scale would have led to large uncertainty, and

(ii) small-scale farming, the main contributor for biomass change in Mozambique was estimated at an average of 0.2ha, while in Malawi wood and charcoal extraction (quantified at a rate of 15,000ha^{-1}, during the same period) have been the major contributing factors for the change (Kambewa et al., 2007). The difference in the underlying factors for the biomass change, i.e., the anthropogenic activities would have rendered the C stock map model for Mozambique not feasible for Malawi.

Current global efforts on biomass mapping have covered Malawi with the European space Agency's Climate Change Initiative (ESA-CCI) Biomass Map datasets as well as the live biomass stock-change datasets over the 21st century acquired from SAR sensors (Santoro et al., 2021; Xu et al., 2021). Therefore, this incumbent study whose focus was on accuracy of the AGB, and C estimates also employed these C stock change datasets.

Researchers have recommended that low-cost and accurate forest monitoring system remains a top priority for developing tropical countries that practice REDD+ mechanism and experience funding constraints (Kachamba et al., 2016; Mlambo et al., 2017). The studies further explained that employment of high quality third dimension (3D)

photogrammetric observations (from small-UAV) would comparatively be affordable and effective for collecting forest biomass estimates in Miombo Woodlands of Malawi (Kachamba et al., 2016). Nevertheless, critical analysis on previous studies in Malawi reveals that there was no attempt to calibrate and upscale the measurements using SAR backscatter nor has there been any current effort by the local studies to integrate the gb based datasets with the ALOS-PALSAR or Sentinel-1 datasets, regardless of the EO missions unrestricted access current status (Department of Forestry, 2012; Government of Malawi, 2019a; Kachamba, 2016; Skole et al., 2021; USAID PERFORM, 2017).

Ideally, employment of the SAR datasets would have served to leverage the scaling up of the terrestrial measurements by using the structure-*from*-motion (S*f*M) photogrammetric airborne measurements within a short temporal resolution (Table 5) while saving costs, and more prominently, enhancing data accuracy as required by the REDD+ mechanism.

Therefore, to bridge these knowledge gaps while supporting Malawi's REDD+ monitoring, it was of interest for this incumbent academic research to explore further the correlational relationship existing between the gb and the SAR satellite based EO in estimating AGB and canopy spatial distribution while using the airborne based datasets as a link. This entailed employing the gb measurements as reference in analysing the following;

(i) Optical UAV orthomosaics,
(ii) L-and C-band radar backscatter measurements, and
(iii) Visible/NIR/SWIR composite band datasets.

The benefit of the S*f*M propagated imagery over most of the satellite EO (except for the recent i.e., Lidar GEDI (Global Ecosystem and Dynamics Investigation) and ICEsat-2 Missions) is the provision of the 3D or vertical/height advantage, an attribute that improves accuracy of the structure of the terrestrial observations (Hancock et al., 2021, 2019; Phalla et al., 2018; Wang et al., 2018). Unfortunately, datasets from the 2 missions could not have been used by this study due to the following reasons. The missions were launched in 2018 when this research was already underway, hence, it would have been risky and time wasting for this academic study (on the part of the author) to wait for the

missions' datasets, thus in cognisance of the challenges and constraints that newly launched missions incur i.e., failure or deficient performance.

The study also decided not to use these EO/datasets, though the ICEsat-2 Mission render an urge due to their interdisciplinary application to land topography and vegetation canopy heights (Liu et al., 2021; Silva et al., 2021). This is because the high slopes of the mountainous Ntchisi Forest (>30^0) (Table 6) would have presented challenges to both GEDI and ICESat-2 missions, in addition to the tall (>20m) mosaics in some parts of the forest which would have reduced the accuracy of the terrain height estimates (Liu et al., 2021).

Research focusing on the use of height parameter in deriving biomass estimates independently observed that individual tree height remains a better explanatory variable for defining biomass, and its inclusion in allometric models or algorithmic calculations enhances significant accuracies i.e., 6% in biomass estimates (Phalla et al., 2018; Wang et al., 2021). The studies further acknowledged that height estimates can be used to alleviate data signal saturation issues in tropical forests, thereby allowing improved assessment of biomass (*ibid*).

Despite these advantages that UAV SfM photogrammetric data render, it remains costly to operate drones on a large scale due to their non-endurance of long flights (Townsend et al., 2020). It is cost-effective, paradoxically to operate a drone on a small area compared to plot-based inventories (Table 2) (Tang and Shao, 2015; Townsend et al., 2020). As a result, UAV operational costs have been logically used to off-set costs by incorporating freely available datasets from either ALOS-2 PALSAR-2, or S1 and/or S2 satellite missions in most surveys (Odipo et al., 2016; Zhang et al., 2017).

It is therefore, against such a backdrop that this research integrated the gb measurements of individual trees with unrestricted EO datasets from ALOS-2 PALSAR-2, Sentinel-1 and 2, and ESA-CCI Biomass Map by using the UAV orthomosaics as a link in estimating AGB and C in Malawi’s Miombo Woodlands.

The table below provides an overview of the some of the key regional and global scale biomass maps reviewed under this study, in addition to the local scale ones that have been covered under Table 3.

Table 1. Overview of Key Regional and Global Scale Biomass Maps Reviewed

Study	Period/Year of study	Scale	Coverage	Focus	Author/Source
Benchmark map of forest carbon stocks in tropical regions across three continents	2000	Inter-continental	Latin America, sub-Saharan- Africa and Asia	AGB and C stock	(Saatchi et al., 2011)
A first map of tropical Africa's above-ground biomass derived from satellite imagery	2000–2003	Regional	20 million km^2 Tropical Africa,	AGB	(Baccini et al., 2008)
Estimated carbon dioxide emissions from tropical deforestation improved by carbon-density maps	2000–2010	Inter-continental	Tropical America, Africa and Asia (Australia excluded)	AG woody vegetation and C emissions	(Baccini et al., 2012)
Tropical forests are a net carbon source based on aboveground measurements of gain and loss	2003–2014	Inter-continental (pan-tropical)	Tropical America, Africa, and Asia	AG carbon density of live woody vegetation	(Baccini et al., 2019)
Carbon losses from deforestation and widespread degradation offset by extensive growth in African woodlands	2007–2010	Regional	Southern African Savannah Woodlands (Angola, DRC, Malawi, Zambia, Tanzania Zimbabwe, Mozambique)	AG woody carbon stock	(McNicol et al., 2018)
An integrated pan-tropical biomass map using multiple reference datasets	2000–2010	Inter-continental (pan-tropical)	(23.4 N–23.4 S) Tropical America, Africa, and Asia	AGB	(Avitabile et al., 2016)
ESA-CCI BIOMASS Map Project 2021	2010, 2017, 2018	Global	Global	AGB	(Santoro et al., 2021)
Forest biomass retrieval approaches from earth observation in different biomes	2010	Regional	Poland, Sweden, Indonesia, Mexico, and South Africa	AGB	(Rodríguez-Veiga et al., 2019)

1.2 Research Aims, Questions and Objectives

To fully exploit the available RS data requirements which requires a better understanding of the relationship between the woody biomass and remotely sensed parameters or a more effective bridging between field-based measurements that are the gist of Malawi's NFI, and the satellite data; it was of prominent interest for this work to investigate how the UAV based HR photogrammetry may help provide a path to solving one or both problems.

1.2.1 Research aims

This research explored the extent that; (i) optical low-cost small UAV data, and (ii) freely available/unrestricted satellite EO datasets could be effectively combined with (iii) tree-level parameters measured from ground-based plots as a cost-effective, accurate and

coverage enhancement means of estimating AGB and C in the fragmented and rugged terrain Miombo Woodlands while the offering the possibility of upscaling the National Forest Monitoring System (NFMS) of Malawi.

1.2.2 Key research question

The key question that this research tries to answer is: to what extent can low-cost small optical UAV data be effectively integrated with tree-level ground-based measurements to cost-effectively scale up forest monitoring in the challenging Miombo Woodlands of Malawi to support the country's REDD+ initiative?

1.2.3 Specific objectives

The above overarching question was addressed under 4 specific objectives presented chronologically below;

(i) To investigate whether low-cost Structure-*from*-Motion (S*f*M) photogrammetric optical orthomosaics and generated 3D information (canopy height model) allows individual tree crowns to be geo-located and use their structure (height and crown) to estimate AGB and C.

(ii) To use the scaled tree metrics (canopy height and crown diameter acquired from small-UAV photogrammetry, i.e. objective 1) to evaluate the use of SAR backscatter acquired from; (a) ALOS-2 PALSAR-2-L-band, (b) Sentinel-1-C-band and (c) ESA-CCI Biomass Map datasets, and (d) the Visible/Near Infra-Red/Short-Wave Infrared (Vis/NIR/SWIR) composite band measurements from Sentinel-2 in estimating AGB and C in Malawi's Miombo Woodland.

(iii) To compare AGB and crown diameter results from objective ii, thus between ALOS-PALSAR-2 and Sentinel1 backscatter, and the ESA-CCI Biomass Map measurements in terms of (a) accuracy, (b) extent and frequency of coverage, (c) costs, and (d) reliability of operation in the study site's environment, and

(iv) To explore the relationship among the ground-based, airborne-based and satellite-based AGB, C and fractional cover (achieved simultaneously through undertaking the first two objectives).

CHAPTER-2

2.0 CONTEXTUAL BACKGROUND

This chapter provides a general evaluation of forest inventory data acquisition systems in relation to biomass and C assessments. It unfolds the historical backdrop of forest biomass assessment methods applied in Malawi's Miombo Woodlands by highlighting the data collection techniques and their cost estimations. It further encapsulates the ecology and distribution of the Miombo ecobiome by linking it to its primary ecosystem service of carbon balance with a focus on the main carbon pools as identified under the REDD+ mechanism. The section also provides an outline of the parameters of success entailed in forest monitoring system at a national scale as defined within Malawi's context. Finally, the chapter renders an overview of RS concept with a bias towards forest monitoring.

2.1 Forest Data Acquisition Systems and Basis of Cost Estimations

For this study, the forest data acquisition systems have been categorised as follows; (i) ground-based measurements, (ii) optical satellite imagery, (iii) small-UAV Structure-*from*-Motion Photogrammetric Surveys (Optical), (iv) Radar (active sensor), and LiDAR/ALS (active sensor) (Hancock et al., 2021; Mlambo et al., 2017; Woodhouse, 2006).

The forest data acquisition systems and their cost estimations (Table 2) are applicable to various parts of the world forest eco-biomes. This is in exception to the ground-based measurements and to a substantial extent, the small-UAV Structure-*from*-Motion Photogrammetric Surveys (optical) which have been calculated based on the conditions of the Southern Africa Miombo Woodlands. Precisely, the two apply to the REDD+ non-Annex-I partner [2] party context where funding poses a huge constraint, i.e., Malawi, Zambia and Botswana. These three countries were pilot sites under the project entitled 'Development of Integrated Monitoring Systems for REDD+ in the Southern African Development Community (SADC)' (Mueller, 2012).

[2] Non-Annex I partners include developing countries that do not have legally binding greenhouse gas emissions reductions targets under the Kyoto Protocol.

The table below depicts the merits and demerits of data acquisition systems in relation to forest biomass estimations, which have been compared under the context of REDD+ mechanism in Miombo Woodlands of Malawi.

Table 2. Strengths and Weaknesses of Data Acquisition Systems in Relation to Forest Biomass and Carbon Estimations-Malawi's REDD+ Context

No.	System	Spatial Resolution	EMS Region	Carbon Pool	Canopy Penetration	Relative Cost	Relative Cost Considerations	Merits	Demerits
1	**Ground-based measurements**	Coarse	Visible light (λ ≈ 0.4mm – 15mm)	AGB, BGB, Litter, DW & SOC	N/A	£30 per ha per person[3]	Excluding equipment hiring costs[4]	Affordable/ideal for small expanse	High capital & operational costs (time, labour, etc.) Not feasible for rough terrain/inaccessible areas thereby rendering spatial inexplicitness Costly for large expanse
2	**Optical Satellite Imagery**	Coarse-Fine	Visible & IR (λ ≈ 0.4mm – 15mm)	AGB	Coarse-Medium)	£10 per ha (≥ £200/month (20,000GB on internet bundle@£200/month for DoF)[5] during forest resource assessments	Excluding equipment hiring, office space & training costs	Cost-effective for unrestricted access, i.e., Sentinel-2 & Landsat) Effective for areas inaccessible by physical/ground measurements	Costly for commercial satellites, i.e.; IKONOS, SPOT Requires considerable technical training to time optimal data acquisition window, process & analyse data Weather limitations
3	**Small-UAV SfM Photogrammetric Surveys (Optical)**	Coarse-Fine	Visible & IR (λ ≈ 0.4mm – 15mm)	AGB	Ideal for coarse to moderate canopy densities	£7 per ha[6](Excluding; training costs)	Cost-effective/consumer grade-standard (requiring less technical training to operate)	Cost-effective (saves labour & time compared to ground-based measurements & commercial radar or lidar) Covers large expanse & cheap in the long run)[7] compared to ground-based measurements Effective for less dense canopy	Costly for large expanse Saturates in dense canopies Relies on accurate Digital Terrain/Surface Models Affected by weather limitations

[3] (Mueller, 2012)

[4] (Government of Malawi, 2019a; Neeff et al., 2015)

[5] https://www.airtel.mw/Consumer-Newsletter

[6] http://www.precision.mw and author's field survey experience-2019

[7] (Phillips et al., 2016)

4	**RADAR (Active)**	Fine	Microwave (λ ≈ 2.5 –100cm)	AGB, BGB, & SOC	Ideal even for dense canopies (even for lower canopy)	£25 per square km[8] for commercial data (£5 per ha)[9] for unrestricted data	Costly for commercial satellites & cost-effective for unrestricted datasets	Better at detecting 3D forest structures/detects even lower canopy Not affected by weather i.e., clouds etc. Continuous coverage (day & night)	Signal saturation over dense vegetation Requires professional training to acquire and process data (radiometric, geometric corrections, i.e., suffers speckle/precision effects) High payload systems (e.g., 400kg, requires more power and space)
5	**LiDAR/ALS/**	Medium-Fine	Visible and NIR	AGB, BGB, & SOC	Deep penetration (even lower canopy) Direct height measurements	£300 per square km for LiDAR[10], £96, per square km[11] for ALS (~£1 per ha)		Does not suffer signal saturation over dense vegetation Captures ground elevation High precision over hard targets (quality 3D data) Continuous coverage (day & night) Allows direct retrieval of vegetation structure (height)	High initial/capital costs & per unit area cost Requires high level expertise to acquire & process data

[8] https://www.statista.com/statistics/1293877/commercial-satellite-imagery-cost-worldwide/; (Patenaude et al., 2005)

[9] (Government of Malawi, 2019a)

[10] (Hummel et al., 2011; Panjvani et al., 2019; Patenaude et al., 2005)

[11] (Hancock et al., 2021; Hummel et al., 2011, p. 2011; Næsset, 2015)

In this report, the term 'ground-based inventories' has been interchangeably used as 'site-based-measurements/inventory' or 'plot-based inventory/measurements' or 'terrestrial measurements. The different currencies (i.e., $ or €) quoted from the literature reviewed have been converted to British Pound Sterling (£)[12] in Table 2 above for ease of comparison.

The costs for the ground-based and the optical satellite imagery, £120 ha^{-1} (£30, per ha, per person) and £10 ha^{-1} respectively, include total expenses incurred from data acquisition, processing and computation of results pertaining to AGB and C estimations. The charge for the small-UAV Structure-*from*-Motion Photogrammetric Surveys (Optical), was estimated at £7.14ha^{-1} (rounded-off to £7ha^{-1}) includes hiring of equipment, operational (image acquisition and related fieldwork) and data-pre-processing charges. The costs for Radar (£25/km^2), ALS (£96/km^2) and the LiDAR's (£300/km^2) account for image acquisition only (Hancock et al., 2021; Panjvani et al., 2019; Patenaude et al., 2005).

2.1.2 Ground-based measurements

In Malawi's scenario, the plot-based cost estimations displayed in Table 2 factored-in the following key components; (i) labour which is dependent on sampling plot unit size, (ii) data entry and computer-based analysis, (iii) transport, (iv) communication and rentals, (v) food and accommodation, and (vi) field supplies consumed during data collection. These calculations consider the average current exchange rate (26th October 2022-https://www.exchangerates.org.uk/Malawi-Kwacha-MWK-currency-table.html), provided by the central bank of Malawi, the Reserve Bank. They exclude equipment hiring and office space expenses since the two are complimentarily provided by the DOF during forest inventories.

The cost estimations range were fundamentally, but not exclusively synthesised from the following studies;

(i) The author's academic field study conducted in Ntchisi Forest Reserve-2019,

[12] The exchange rates were; $1=£0.71, and £1= €1.16

(ii) A Roadmap for Developing Malawi's National Forest Monitoring System-2015 (Neeff et al., 2015),
(iii) PERFORM Site-Based Forest Inventory Report a Technical Report on Liwonde, Ntchisi and Perekezi Forest Reserves (USAID PERFORM, 2017),
(iv) Development of Integrated Monitoring Systems for REDD + in the Southern African Development Community (SADC) Field Inventory Results: Transboundary Test Area (Malawi-Zambia) (Mueller, 2012),
(v) Forest Resource Mapping Final Report for Implementation Phase (Department of Forestry, 2012),
(vi) An Assessment of Monitoring Requirements and Costs of 'Reduced Emissions from Deforestation and Degradation-2009 (Böttcher et al., 2009), and
(vii) Malawi National Forest Inventory 2018 Analysis Report (Government of Malawi, 2019a).

Despite the funding constraints that Malawi faces, especially when implementing REDD+ efforts, the country still relies on ground-based inventories for collecting data, yet they are deemed expensive, comparatively. A transboundary forest inventory commissioned under the REDD+ MRV-SADC Project covered 52,000 km^2 of Miombo Woodlands (with 604 sampling plots units of 0.3ha each) in Malawi, Zambia and Botswana, cost €210,000 (£181,034, thus ~£30 ha^{-1}) (Mueller, 2012). Though these total expenses were considered fair, they were higher than the average of cost of inventories in the US (United States), UK (United Kingdom), Bolivia, and Costa Rica which ranged from 55 to 172 US$/$km^2$, thus translating to £0.39-£1.22 ha^{-1} (Böttcher et al., 2009).

A roadmap study for Malawi's NFMS estimated that a sum of $100,000 (£76,923) was required to upgrade the country's forest inventory system to attain the global REDD+ standards (Neeff et al., 2015). However, the amount was never realised due to funding constraints, at least to the knowledge of the author. Alternatively, Malawi resorted to site specific forest inventories that are not only conducted on piece-meal basis, but also donor-driven (Figure 2 and Table 3) (Government of Malawi, 2019a; Haack et al., 2015).

Though the site-based inventory approach was adopted as a cost-effective option for monitoring forest in Malawi, its huge setback has been its potentiality to provide project sponsors the leeway to tailor-make data collection procedures to fit their specific goals, which unfortunately, have not been compliant with the global REDD+ standards quite often (Government of Malawi, 2019a; Malawi Redd+ Programme, 2015; Neeff et al., 2015).

Most significantly, donor-driven ground inventories are conducted according to the funder's preference i.e., with modifications to the following; (i) choice of site, (ii) sampling design/approach, (iii) sampling unit plot configuration, (iv) choice of measuring tools, (v) choice of biomass allometry, not to mention of spatial and temporal scales (Government of Malawi, 2019a; Malawi Redd+ Programme, 2015). Strikingly, the inconsistencies applied in the afore-mentioned factors have been the critical parameters rendering the quality of the datasets acquired and their results unsuitable or incomparable to the REDD+ scheme standards, particularly the AGB and C estimates in Malawi (Haack et al., 2015; Kadzuwa and Missanjo, 2022a; Neeff et al., 2015; Skole et al., 2021; UNFCCC, 2021). Unfortunately, this has led to the delay of Malawi's REDD+ progress in attaining the required standards by the laid by UNFCCC (UNFCCC, 2021).

2.1.3 UAV S*f*M photogrammetric system (optical)

The cost of operating UAV surveys varies based on sampling methods and study site conditions (i.e., road network and access, topography) not only within the forest industry, but also in other sectors such as the health and fishing industry (Ene et al., 2016; Phillips et al., 2016; Provost et al., 2020). Due to the scarcity of literature documented precisely on the cost of the same, especially in the African Tropical Woodlands, the estimates on lightweight airborne system indicated in Table 2 above were largely derived, though not exclusively from the following studies;

- The author's academic field study experience during the Ntchisi Forest 2019 biomass and C assessments;
- Costs Associated with the Use of Unmanned Aerial Vehicles for Transportation of Laboratory Samples in Malawi (Phillips et al., 2016);

- A Comparison of Accuracy and Cost of LiDAR versus Stand Exam Data for Landscape Management on the Malheur National Forest-2011 (Hummel et al., 2011);
- An assessment of monitoring requirements and costs of 'Reduced Emissions from Deforestation and Degradation -2009 (Böttcher et al., 2009; Hummel et al., 2011);
- Assessing the Viability of Small Aerial Drones to Quantify Recreational Fishers (Provost et al., 2020).

The calculations factored-in the following expenses; (i) mobilisation from the firm's base (Precision Ltd, in this case) in Lilongwe to Ntchisi and return (200km), (ii) local travel in Ntchisi (from one sampling plot/unit to another), (iii) accommodation, (iv) allowances for fieldwork (data collection) and (v) purchase of materials for Ground Control Points and labour involved for their construction, and (vi) data pre-processing using Precision's (hiring company) equipment. Hence, the per unit area cost (labour inclusive) was calculated as £7ha^{-1}.

2.1.4 Unrestricted/freely available optical satellite imagery

The relative costs associated with the acquisition of the optical unrestricted Earth Observations (EO) were based largely on the pre-paid monthly subscriptions of internet data bundle for the DoF, which is the key cost. Precisely, it was ~500GB per MK5,000 (£500)[13] during forest inventory preparatory period and ≥2000 GB per MK20,000 (£200) during the inventory, translating to £5 per ha. The costs entail the charge for internet data bundle required to download imagery scenes covering the entire country. These were assessed from the DoF's monthly internet bills as well as from internet supplier's link https://www.airtel.mw/Consumer-Newsletter. The calculations assumed that acquisition of the unrestricted imagery DoF does not require separate/additional internet data bundle since the monthly subscriptions had been adequate to support acquisition of imagery i.e., Landsat observations, used during the previous inventories (Table 2) (Berry et al., 2008; USAID PERFORM, 2017).

[13] the current exchange rate is; £1 =1,400 Malawi Kwacha (MK)

Similarly, these costs excluded expenditure on equipment hiring (workstation) and office space because these services are provided by the DoF on complimentary basis (Department of Forestry, 2012). The estimates further discounted expenses for field training of researchers/data collectors on the assumption that the personnel selected were already trained in data acquisition and analysis.

2.1.5 RADAR satellite imagery

Despite several key studies that employed commercial radar-based imagery within the African Savannah, Miombo inclusive, few have reported on the cost estimates involved (Cassells et al., 2009; Mitchard et al., 2013; Ryan et al., 2012; Wingate et al., 2018). The limited use of radar technology in the Miombo region (mostly occupied by non-Annex1 parties) could be attributed to financial constraints that these Least Developed Countries (LDCs) face in that region. The scant use of the datasets could, also be attributed to the challenging technology behind the processing of the datasets with respect to the geometric and radiometric corrections, not to mention their saturation nature during biomass stock estimation, i.e., ~150 to 180 Mg ha^{-1} for cross-polarised L-band data (Mitchard et al., 2013; Næsset, 2015; Wingate et al., 2018).

Hence, the reference on these cost estimations was based on the studies that used both commercial and freely available RADAR datasets in the various forest types i.e., Miombo, Temperate and Mediterranean Woodlands. In that respect, the following studies and links were pivotal in deriving the unit costs of £25/km^2 for commercial datasets and £5/km^2 for unrestricted datasets as displayed in Table 2;

(i) An assessment of monitoring requirements and costs of 'Reduced Emissions from Deforestation and Degradation-2009 (Böttcher et al., 2009; Hummel et al., 2011),
(ii) Forest Resource Mapping Final Report for Implementation Phase (Department of Forestry, 2012),
(iii) Synthesis of remote sensing approaches for forest carbon estimation: reporting to the Kyoto Protocol (Patenaude et al., 2005),
(iv) https://www.statista.com/statistics/1293877/commercial-satellite-imagery-cost-worldwide/, and

(v) https://skywatch.com/earthcache/overview/

2.1.6 LIDAR commercial dataset.

The cost estimates on commercial LiDAR data (Table 2) largely consider the temperate and boreal eco-biomes conditions where they have been extensively applied and fairly the Miombo Woodlands where they have been lowly used. The specific literature on cost estimations of commercial LiDAR studies on Miombo Woodlands of Malawi has not been well documented, at least to the knowledge of the author. Indisputably, this could be attributed to the prohibitive costs that render usage of most of such commercial EO expensive, especially for REDD+ non-Annex-I countries like Malawi.

As a result, the focus of this academic study was on the research that used commercial LiDAR datasets in other countries and the following were key in deriving the costs (Table 2);

(i) Requirements for a Global Lidar System: Space borne Lidar with Wall-to-Wall Coverage (Hancock et al., 2021),
(ii) LiDARPheno – A Low-Cost LiDAR-Based 3D Scanning System for Leaf Morphological Trait Extraction (Panjvani et al., 2019),
(iii) Forest Monitoring with Airborne Laser Scanning in Tanzania-2015 (Næsset, 2015),
(iv) A comparison of accuracy and cost of LiDAR versus stand exam data for landscape management on the Malheur National Forest-2011 (Hummel et al., 2011),
(v) An assessment of monitoring requirements and costs of 'Reduced Emissions from Deforestation and Degradation-2009 (Böttcher et al., 2009; Hummel et al., 2011), and
(vi) Synthesis of remote sensing approaches for forest carbon estimation: reporting to the Kyoto Protocol-2005 (Panjvani et al., 2019; Patenaude et al., 2005).

2.2 Traceable Forest Inventories of Malawi (1991-2019)

This subsection delivers a brief history of the past forest inventories conducted between 1991 and 2019 in the Miombo Woodlands of Malawi. Among other things, it highlights the status of the assessments conducted by underlining the funders, data collection methods, spatial coverage, sampling techniques and key tree parameters focused. The subsection also delivers a critical analysis of the past inventories pertaining to the objectives of this study.

Forest monitoring studies that use novel techniques which provide robust and accurate biomass measurements are not only key to the understanding the global C cycle, but they are also fundamental to assessing emissions from deforestation and forest degradation (Mitchard et al., 2013; Vafaei et al., 2018). Nonetheless, striking a balance between such attributes and accurate results acquired through cost-effective means remains a huge challenge, especially, for the LDCs and/or the non-Annex-I countries, Malawi inclusive (Malawi Redd+ Programme, 2015; Mitchell et al., 2017; Neeff et al., 2015; Romijn et al., 2012).

Unfortunately for Malawi, as aforementioned, the repercussions of the donor preferences come at a cost as significant inaccuracies and inconsistencies pertaining to methods and Standard Operating Procedures have been observed in forest inventories conducted over the past three decades in Malawi (Table 3) (Government of Malawi, 2019a; Kadzuwa and Missanjo, 2022a; McGann, 2015; Skole et al., 2021).

Such datasets that have proven difficult to compare, thereby leading to accreditation of Malawi's REDD+ efforts at a lower tier of methodological and data framework and accuracy (Government of Malawi, 2019a; McGann, 2015; Neeff et al., 2015; Skole et al., 2021).Though not only particular to Malawi, but this problem has also led to a predicament whereby some datasets have technically not contributed to the development of robust NFI system especially in the LDCs practising REDD+ mechanism (Ryan et al., 2012).

More importantly, this has hugely affected the C financial payments as of February 2023; Malawi had not yet received the financial C rewards. Yet, by August 2018, 18 countries including Democratic Republic of Congo (DRC), Ghana, and even Mozambique that

shares a stretch of Miombo woodlands boundary with Malawi) successfully presented their emission reduction programs to the Forest Carbon Partnership Facility (FCPF) of the World Bank in readiness for payment (Köhl et al., 2020; The World Bank, 2018).

In October 2021, Mozambique became the first country to receive the payments to the tune of $6.4 million, while unfortunately, Malawi is still struggling to move on to the level submitting verified and acceptable forest reference emission levels (The World Bank, 2022).

The next illustration (Table 3) entails traceable terrestrial forest inventories conducted in Malawi over the 3 past decades with a focus to underscore the flaws (inaccuracies and inconsistencies pertaining to methods and Standard Operating Procedures) that have proven difficult to compare under REDD+ mechanism. The ground plot dimension of 0.126 ha in this report has hereinafter been rounded off to 0.1ha, for simplicity.

Table 3. Catalogue of Traceable Forest Inventories Conducted in Malawi's Miombo Woodlands: 1991-2019

Study	Source/ Author	Funder	Location & Data Status	Data Collection System	Sampling Design	Sample Size	GNSS used	Parameter Measured	Carbon Pool
National Forest Inventory (1991-93)	*DoF*	IDA, World Bank	Nation-wide, *P*	*Pb & EO* (Satellitenbilder)	*NA*	*NA*	*NA*	*dbh*, *ht*, clear length, species.	*AGB*
Dzalanyama Reserve (1994-95)	*DoF*	Global Environmental Facility	Dzalanyama Reserve, *P*	*Pb*	*NA*	*NA*	*NA*	*dbh*, *ht*, clear length, species.	*NA*
Miombo Inventories (1995-96)	*DoF*	FRP-DFID	Chimaliro & Liwonde, *NA*	*Pb*	*NA*	*NA*	*NA*	*dbh*, *ht*, clear length, species.	*AGB*
Bark Harvesting Project (2005)	*DoF*	FRP-DFID	Phirilongwe Forest Reserve, *NA*	*Pb*	Randomized (branch) sampling - using K- tree methods	*NA*	*NA*	*dbh*, *ht*, species.	*AGB*
Tree Planting and Management for Carbon Sequestration and Other Ecosystem Services (2006-2011)	*DoF* and LTS International, 2013	Malawi Government	Countrywide, *E & P*	*Pb*	Stratified random sampling, 30cm deep soil pits dug in the middle of the field, samples collected from 0-10cm, 10-20cm & 20-30cm soil depths	300	*Not used*	*dbh*, *ht*, root collar, diameter, Soil organic Carbon (SOC), litter, species.	*AGB, BGB, SOC, Litter*
Tree Survey for Right of Way: Malawi Mozambique Interconnector Powerline (2009)	(Chirwa, M. Utila, H. and Kayambazinthu , 2009)	World Bank	Balaka & Mwanza, *E & P*	*Pb* & airborne (aerial photographs for vegetation identification, terrain & slope aspect).	Systematic sampling, (covering a stretch of 75km), concentric nested circular plots of 2m, 5m, 25m, laid at 250m apart	294	*N/A*	*dbh*, *ht*, growth rings of stem disc for age determinatio n, species.	*AGB*
Avoiding Unplanned Mosaic Deforestation and Degradation in Malawi (2008-2009)	(Berry et al., 2009)	USAID-COMPASS II	Mkuwazi & Nyika, *E*	*Pb & EO* (Landsat 7 ETM for forest cover detection & sample plot network derivation)	Random sampling, square plots of 30m x 30m & circular plots of 17.84m radius	203	*N/A*	*dbh, ht*, *cd*, clear length, species.	*AGB, DW, BGB*
Biomass of *Faidherbia albida* under Different Management Regimes (2010)	(Beedy et al., 2016)	ICRAF,	Karonga, Bolero, Makanjila, Salima,	*Pb*	Complete randomised block design, 30m interval	83	*N/A*	*dbh, ht &* crown area	*AGB*

			Bwanje & Mwanza *E*						
Lake Chilwa Climate Change Adaptation Programme (2010-17)	(Chiotha et al., 2017)	Royal Norwegian Embassy	Lake Chilwa Basin (Machinga, Phalombe & Zomba), *E*	*Pb*	Random Sampling	*NA*	*Not used*	*dbh, ht*, species.	*AGB*
Forest Resource Mapping under Forest Preservation Programme (2011-12)	(Department of Forestry, 2012)	Foreign Agency of Japan	17 forest reserves across the country, *E*	*Pb* & *EO* (ALOS-PALSAR-1, AVNIR-2, PRISM & Google Earth for forest cover detection, sample plot derivation & assessment of historical LULUCF)	Systematic sampling. Nested-Circular nested plots of 5.64m & 17.84m radius each, respectively. (0.1ha)	278	*Used*	*dbh, ht*, *cd*, clear length, species.	*AGB, DW, BGB*
Development of Integrated Monitoring Systems for REDD+ in the SADC (2012)	(Mueller, 2012)	SADC-GIZ	Trans-boundary between Malawi & Zambia, *E*	*Pb & EO* (Google Earth & *Rapid Eye for* forest cover detection & sample plot allocation)	Stratified random sampling. Nested T-shaped cluster (0.3ha)	150	*Not used*	*dbh, ht*, *cd*, clear length, species, saplings.	*AGB, DW, BGB*
Distribution and Population Structures of *Adansonia digitata* (2013)	*DoF*	Silva Terra	Countrywide, *P*	*Pb*	Systematic random sampling, 500m grid interval	26 sites		*dbh, ht*, bole height, *cd*, shape of trunk, species.	*AGB*
PERFORM Site-Based Forest Inventory in Liwonde, Ntchisi and Perekezi Forest Reserves (2016)	(USAID PERFORM, 2017)	Protecting Ecosystems and Restoring Forests in Malawi (PERFORM)	Liwonde, Ntchisi and Perekezi Forest Reserves, *E & P*	*Pb & EO*- (LandSat 8 & ASTER DEM). Detection of forest cover, sample plot allocation & additional terrain/slope information	Stratified random sampling. Nested T-Shaped Cluster (0.3ha)	86	*Not used*	*dbh, ht*, *cd*, clear length, species, saplings.	*AGB, DW, BGB*
Dzalanyama Forest Reserve Conservation Project (2017)	(Makungwa, 2017)	JICA	Dzalanyama Forest Reserve, *NA*	*Pb*	Systematic sampling, 2-circular nested plots of 5.64m and 17.84m	*68*	*Not used*	*dbh, ht*, *cd*, clear length, species.	*AGB, DW, BGB*

					radius each respectively (0.1ha)				
Thuma and Dedza-Salima Escarpment Forest Reserves (2017)	(Wildlife Action Group, 2018)	Protecting Ecosystems and Restoring Forests in Malawi (PERFORM)	Thuma and Dedza-Salima Escarpment Forest Reserve, *E & P*	*Pb & EO*- (Google Earth) forest cover estimation & sample plot allocation	Stratified random sampling Nested T-Shaped Cluster (0.3ha)	33	*Not used*	*dbh, ht*, crown diameter, clear length, species.	*AGB, DW, BGB*
National Forest Inventory (2018)	(Government of Malawi, 2019)	Protecting Ecosystems and Restoring Forests in Malawi (PERFORM)	North and South (except Central Region Forests), *E & P*	*Pb & EO*- (Google Earth) Pre-screening and post stratification of areas (plots) under forest cover	Random sampling T-cluster design 6m, 12m, 20m radius plots (0.3ha)	94	*Not used*	*dbh, ht*, *cd*, clear length, species.	*AGB, DW, BGB*

Source: (i) Final Report on Carbon Inventory in Malawi's Forests Capacity to Support Redd+ and National Forest Inventory Activities-March 2015 and, (ii) Malawi National Forest Inventory Analysis-2018.

***Key**: DoF = Department of Forestry; E = Electronic; P = Printed/Hardcopy; EO = Earth Observation(s); Pb = Plot-based field measurement method; DW = Dead Wood; N/A = Not Applicable (information or data not Available or Applicable), ht = height, dbh = diameter at breast height, cd = crown diameter, LULUCF = Land Use, Land-Use Change and Forestry*, *JICA = Japanese International Cooperation Agency*, *USAID= United States Agency for International Development, COMPASS = Community Partnerships for Sustainable Resource Management, SADC-GIZ = Southern African Development Community - German Agency for International Cooperation, FRP-DFID = Forestry Research Programme - Department for International Development, GNSS = Global Navigation Satellite System*

The global REDD+ scheme advocates country wide assessments of forests that are representative of its realms' population either by; (i) sampling, or better-still, (ii) complete tally (wall-to-wall mapping), and/or (iii) a combination of the two as part of routine forest monitoring (Gaucher et al., 2015). While the complete tally option sounds comprehensive, regrettably, Malawi, since officially embracing the REDD+ mechanisms in 2014 has never afforded such a wall-to-wall forest survey at one go due to in adequate funds (Government of Malawi, 2019). The closest efforts were pursued during the 2018 ground inventories when all the 3 regions representing Malawi had some of their forest reserves inventoried (*ibid.*). Unfortunately, some key REDD+ forest sites in central and southern regions of the country i.e., Dzalanyama and Namizimu were not sampled, resulting in non-comprehensive sample representation of the country. This could be attributed partly to the lack of funds compounded by non-existence of the national grid of permanent sample plots.

Malawi reports to UNFCCC on climate change status through literature that focuses on GHGs emissions and sinks plus the associated mitigation and adaptation interventions (Government of Malawi, 2011; UNFCCC, 2021). Key documentation consists of the following reports;

(i) National Communications (NCs),
(ii) Biennial update Report (BuRs),
(iii) Intended Nationally Determined Contributions (INDC),
(iv) National REDD+ Strategy, and
(v) Forest Reference Emission Levels (FREL) (Government of Malawi, 2011; Ministry of Forestry and Natural Resources, 2021).

Malawi's Second National Communication acknowledged uncertainties in the GHG fluxes reported in 2011 and attributed them to the use of default (*Tier 3*) values/methods (Government of Malawi, 2011). The report indicated that the Forestry and Other Land Use (FOLU) subsector contributed significantly both as a net source of CO_2 (19,243 Gg) and a sink of CO_2 (889.4 Gg). While these source values are almost 20 times larger than

the sink values, the report revealed that much of the sink function is explained by the individual trees grown outside forests and on abandoned croplands i.e., those managed under agroforestry systems which unfortunately are often are not sampled during the ground-based forest inventories (Skole et al., 2021).

A different report indicated that deforestation alone in Malawi accounted for 1,236,631 tonnes of carbon dioxide equivalent per year ($tCO_2e.yr^{-1}$) during the period 2006-2016 (Ministry of Natural Resouces Energy and Mining, 2019). However, this was deemed a misrepresentation by a key study which estimated the contribution of deforestation and degradation from 2010 to 2015 to be $4.2^8 \times 106$ $tCO_2e\ yr^{-1}$ and 3.49×10^6 $tCO_2e\ yr^{-1}$, respectively (Skole et al., 2021). The later findings, however, are statistically closer to those reported by Malawi's Third National Communication which estimated 315.61 Gg $CO_2e\ yr^{-1}$ as of 2017 (Ministry of Forestry and Natural Resources, 2021). The inconsistencies in generating the GHG emissions estimations can be attributed partly to lack of using a wall-wall PSPs structure that would have generated values from institutionalised locations with consistent comparisons, though at a cost.

To circumvent this challenge, most studies have advocated the use of satellite imagery that provide wall-to-wall coverage. More importantly, the introduction of the free/ unrestricted EO datasets with moderate to high spatial resolution has tried to solve this challenge.

Hence, it was in the interest of this research to follow this course and fill the knowledge gap by integrating the ground-based forest inventory datasets with the global coverage of the unrestricted imagery from the ALOS-PALSAR- Sentinel 1 and 2, and ESA-CCI Biomass Map satellite missions in Malawi's Miombo Woodlands operating under the REDD+ project.

The next two figures portray site-based plot measurements field experience and the distribution of the donor-funded site-based inventories conducted over under the REDD+ mechanism during the past recent years in Malawi.

Figure 1. Site-based plot measurements-Ntchisi Forest-2019; (Top)-Crown diameter measurements taken from the long and short axes of the crown intersected at 90^0, and (Bottom) – Verification of horizontal distance from plot-centre to tree using a linear tape.

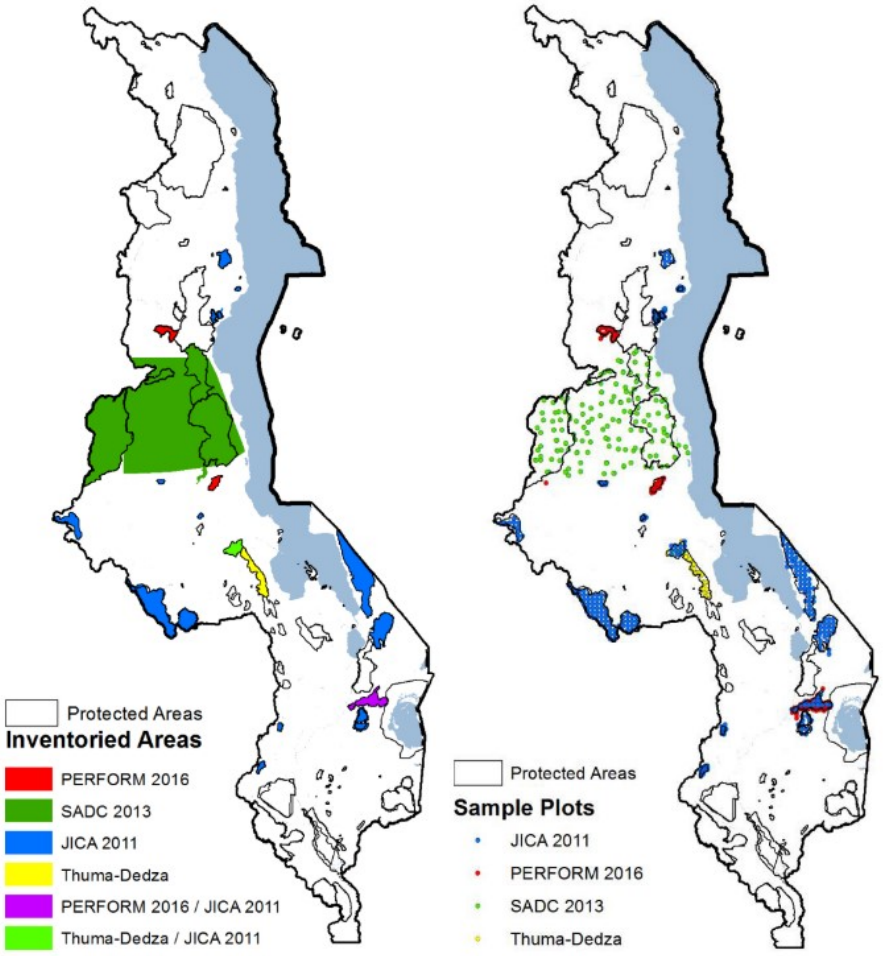

Figure 2. Map of fragmented site-based inventories under REDD+ mechanism in Malawi (2011- 2016); funded by different donors, bearing varied sampling designs, different sampling unit-plot configurations, besides using varied allometry for AGB calculations. *Source:* Malawi National Forest Inventory 2018 Analysis Report.

The piece-meal ground inventories highlighted in the maps above do not only reflect the financial constraints encountered by Malawi, they, on the other hand, call for an encompassing solution that would curtail these inventory challenges associated with data and methods while making advances under the REDD+ umbrella. Recently, there has been an increase in the use of low-cost optical SfM photogrammetric datasets acquired through UAVs to improve forest monitoring in the tropical woodlands of non-Annex I parties practising REDD+ mechanism (Angelsen, 2008; DeFries et al., 2007; Dube and

Mutanga, 2015; Kachamba et al., 2016; Kamusoko et al., 2014; McNicol et al., 2018; Michelakis et al., 2015; Mlambo et al., 2017; Ryan et al., 2012).

2.3 Miombo Woodland Distribution and Ecology

The Miombo Woodlands (hereinafter 'Miombo' for short), or interchangeably referred to as 'woodlands', are seasonally dry ecosystems which can be characterised by an open tree canopy and a contiguous grass layer (McNicol et al., 2018). They are a type of Savannah located in the Southern Africa and dominated by trees of the sub-family *Caesalpinioideae* of the *Leguminosae*, belonging to the genera *Brachystegia*, *Julbernardia* and *Isoberlinia* (Chidumayo, 1987).

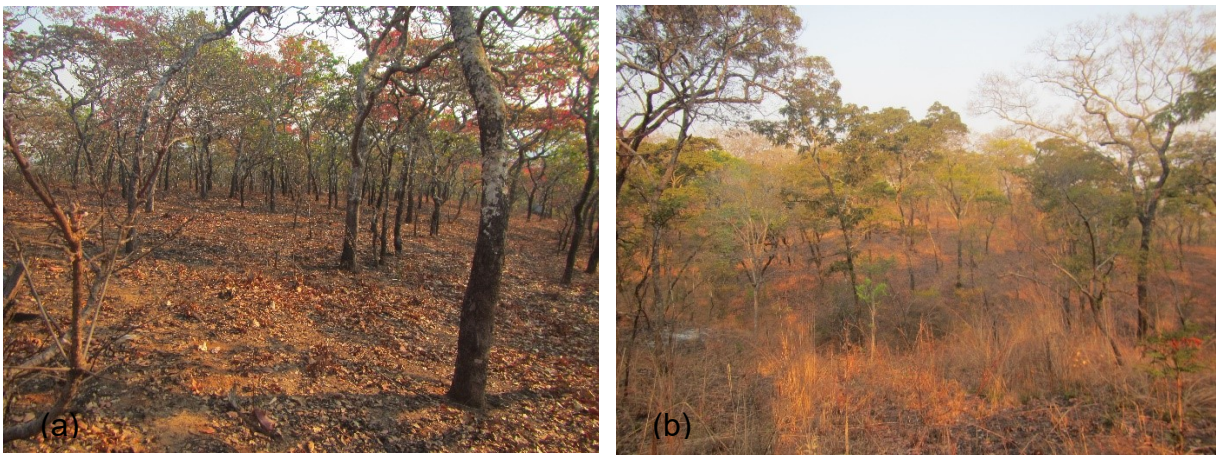

Figure 3. Miombo Woodland Outlook-Ntchisi Forest Reserve; (a) sparse distribution showing open canopy closure dominated by *Brachystegia species* inside forest, and (b) intermix of grass and sparsely distributed Miombo trees at the forest edge.

The Miombo are recognised by their floristic richness and widespread swathe (~2.7 million km^2) of the African sub-humid tropic zone, stretching from DRC, Angola and Tanzania in the north, through Zambia, Malawi and Mozambique, up to parts of Botswana in the south (Figure 4) (Campbell et al., 2007; Kayambazinthu et al., 2005). The Miombo eco-biome experiences a mean annual precipitation range of 650-1,500mm. More than 95% of annual rainfall occurs during a single 5-7months' wet season, thus from October/November to March/April (Cauldwell and Zieger, 2000; Chidumayo, 1997;

Desanker et al., 1997; Frost, 1996). Notably, a few sites within the region receive more than 5% of their total mean annual rainfall during the dry months.

The Miombo Woodlands are divided into dry and wet categories, following their rainfall pattern in zone of occurrence (Chidumayo, 1994). Dry Miombo occur in the south portion of Southern Africa region, precisely Malawi, Mozambique, and Zimbabwe, in areas receiving less than 1,000mm of rainfall annually (Ribeiro et al., 2015). In contrast, the wet Miombo Woodlands exist widely in the eastern Angola, DRC, northern Zambia, south-western Tanzania, and central Malawi, specifically within areas receiving >1,000mm rainfall per annum (Ribeiro et al., 2015).

The Miombo ecosystem occurs in geologically old and nutrient-poor soils with the dominant soils belonging to the order Oxisol (Chidumayo, 1997; Frost, 1996). These are highly weathered old soils dominated by aluminium, iron oxides and low-activity clays. They are typically acidic (pH between 4.2 and 6.9) and contain low Cation Exchange Capacity (CEC:1.80-25.10 me100/g) (Chidumayo, 1997). They are further characterised by low ranges of essential elements i.e., 0.02-0.62% for nitrogen, 0-54 ppm for phosphorous while the Total Exchangeable Bases (TEB) is 0.35-20.78 me100/g (ibid). The soils portray a low range of carbon content (0.3-3.8%) and low concentration of organic matter, with an average of 1% and 2% in the topsoil for dry and wet Miombo, respectively (Chidumayo, 1997; Ribeiro et al., 2015; Walker and Desanker, 2004). These can be attributed to the abundant termite activities and frequent fire incidences that the woodlands experience (Cauldwell and Zieger, 2000; Chidumayo, 1997).

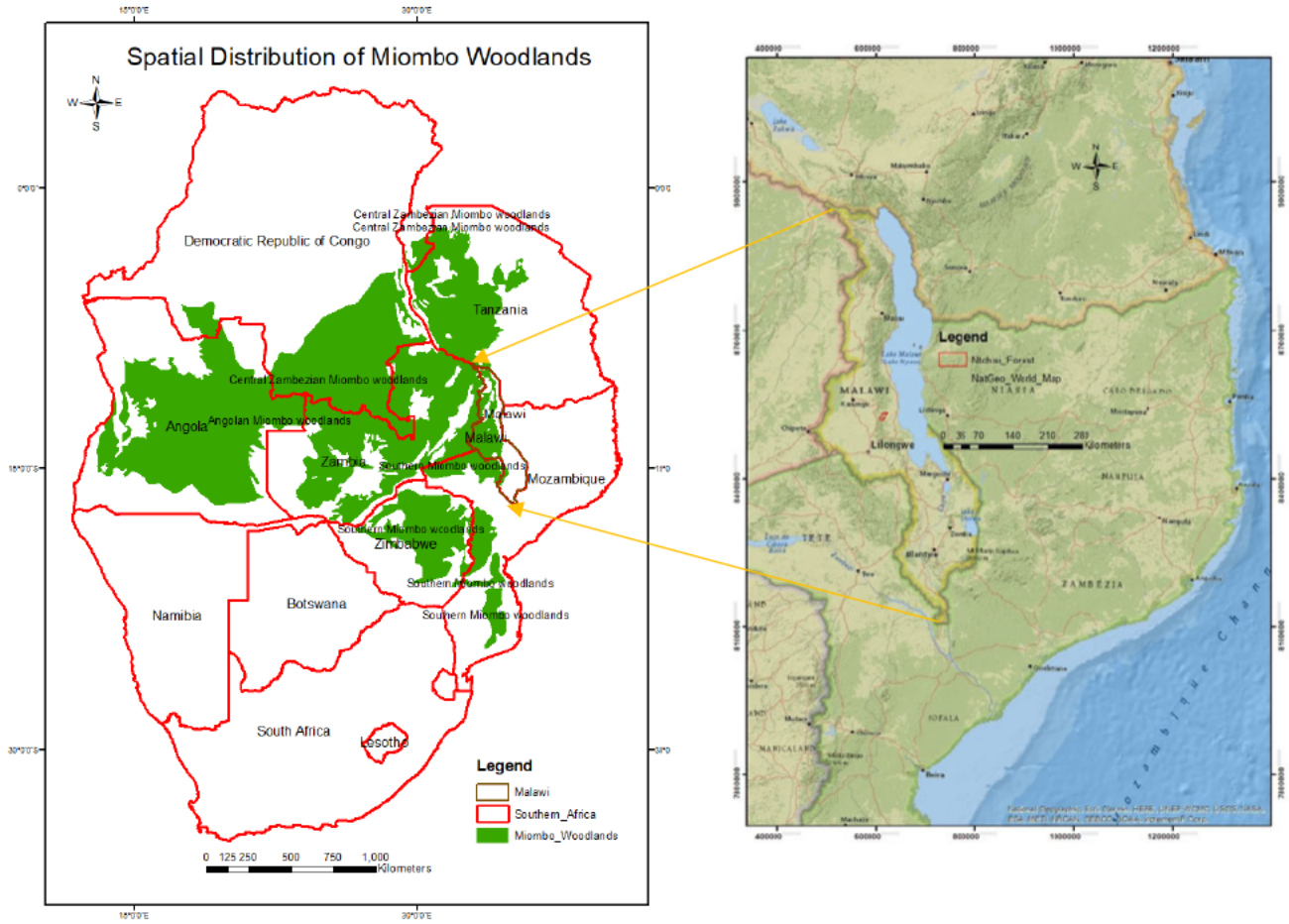

Figure 4. Spatial distribution of part of Central and Southern Miombo Eco-biome (green) covering Malawi in relation to other countries practicing REDD+ mechanism within the sub-humid tropic zone of the Southern African Development Community Region

Source: *https://www.worldwildlife.org/publications/terrestrial-ecoregions-of-the-world*

2.3.1 Role of Miombo woodlands in Malawi

While Malawi's forests cover 32,370km^2 representing 25% of the country's total surface land area, about 90% of the forestland spans over Miombo landscape (Skole et al., 2021). The majority of Malawi's Miombo woodland is confined to protected areas as follows;

(i) forest reserves (8,076 km^2),

(ii) national parks and wildlife reserves (9,680 km^2), and

(iii) customary land forests (8,843 km^2) (Government of Malawi, 2019a; Ribeiro et al., 2015).

The woodlands provide a wide range of biophysical ecosystem goods and services that ensure sustainability of the environment and livelihoods of people, especially to those living within their vicinity. These range from food, fuelwood, fibre medicine, construction material in form of timber, poles, sticks, and stakes, to large scale biodiversity conservation, maintenance of the global C cycle, soil, and water management services (Kayambazinthu et al., 2005; Ribeiro et al., 2015).

About 15 million urban dwellers within the Miombo Woodlands of Southern Africa depended on wood or charcoal as source of energy around 1990 (Campbell, 1996). Nevertheless, >96% of Malawi's population relies on the woodland largely for fuelwood in form of charcoal and firewood (Drigo, 2019; Ministry of Natural Resources, Energy and Mining, 2017). Most recent statistics show that wood biomass as of 2019, accounted to ~89% of Malawi's national energy consumption budget, most of which was extracted from the woodlands (Mulvaney et al., 2011; Neeff et al., 2015).

The forest products and services in Malawi contribute 6.9% of the country's GDP through; domestic and export product sales, employment, and tourism (Drigo, 2019; Ministry of Natural Resources, Energy and Mining, 2017). Besides, the woodlands are a source of wide range non-timber products which include; fruits, bush meat, edible insects and caterpillars, bees wax, honey, traditional medicines, mushroom and materials for tool handles and household utensils (Gumbo et al., 2018; Ngulube, et al., 1999; Ryan et al., 2012). Extraction of these products and services from the woodlands simultaneously offers employment and income through their sales and remittances (Kerr, 2005).

As mentioned earlier, forests (which are dominated by the Miombo) in Malawi also act as both the main net source and sink of CO_2 thus, (19,242.86 Gg) and (889.4 Gg), respectively (Government of Malawi, 2017, 2011).The woodlands are further depended for agriculture as they are encroached through opening new farmland that involves clearing of trees. This has hugely affected forest biomass and C stocks to the extent that

some of Malawi's woodlands currently comprise open forest mosaics of low C levels ranging from 35 to 45Mg ha^{-1} and in some cases, as low as 8Mg ha^{-1} (Skole et al., 2021).

2.3.2 Miombo phenology and seasonality

In contrast to Boreal eco-biomes, Miombo can be characterised as tropical forests that exhibit a deciduous nature (seasonally put on and shed off leaves), bear low height of mature trees (7-15m) and low canopy closure on large areas with bare soils, shrubs and thickets in varying intensity and transition forms (Figures 3 and 5) (Chidumayo, 1997). Studies on Miombo tree phenology have demonstrated that they experience leaf-fall (shed foliage) during dry season and leaf-on morphological changes during rainy season (Chidumayo, 1997; Kamusoko et al., 2014). The figures below depict Miombo trees during the transition from leaf-on to leaf-fall and during the leaf-fall period of 2019 in Ntchisi Forest Reserve.

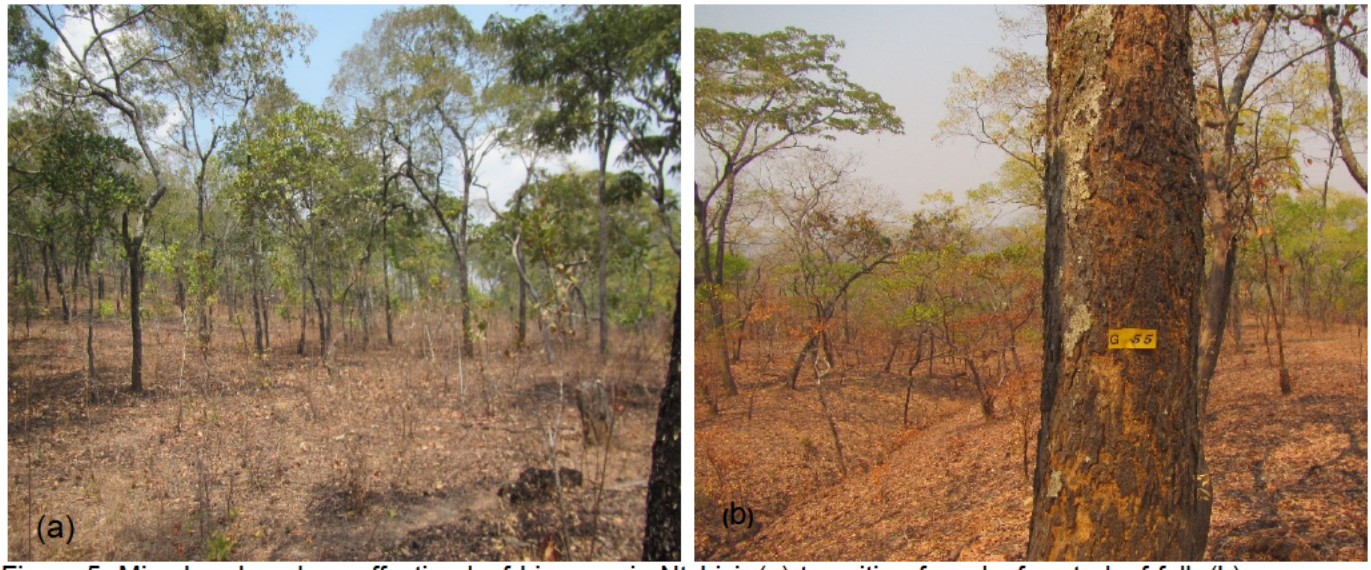

Figure 5. Miombo phenology affecting leaf biomass in Ntchisi: (a) transition from leaf-on to leaf-fall, (b) leaf-fall in hot sunny weather (hazy) during the peak of dry season, and *Brachystegia* species (tree ID: G 55) partially scorched by fire.

Mapping of the Miombo is challenged by technical constraints associated with phenology and seasonality which collectively act as disincentives to study their biomass (Chidumayo, 2019; Kamusoko et al., 2014). The Miombo display complicated growth and phenological variations by exhibiting high degree of spatial heterogeneity in form of tree

density patterns, tree size and leaf dynamics (*ibid*). These studies observed further that such attributes are influenced by anthropogenic factors such as land use, i.e., harvesting and farming that consist of cropping, pasture, fire and walking habits of herbivores, *inter alia*. While the soil type exemplifies a natural factor, cumulatively these aspects contribute to the development of vegetative mosaics that alternate between closed and open canopies (Frost, 1996; Kamusoko et al., 2014). The intermix of wooded grassland and bushland mosaics (Figure 3b) render difficulties to distinctly quantify the trees' biophysical properties such as canopy cover and structure in remotely sensed imagery (*ibid.*).

Miombo cover is influenced by significant seasonal changes that vary according to water/moisture availability and correspondingly to a particular period of season (Kamusoko et al., 2014; Zimba et al., 2022). While the flush of new leaves occurs prior to start of the rainy season (Frost, 1996), their full development in Miombo trees takes place during the peak/mid rainy season, thus between January and March. Leaf development serves to provide biomass detectability in EO (Figure 6). However, cloud cover peaks during the same period (Lupala et al., 2015) and potentially leads to insignificant variation in tree leaf detectability in terms of spectral signature (Kamusoko et al., 2014). This artefact compromises the quality of EO and further renders difficulties in imagery interpretation. Hence, cloud cover highly contributes to compromised accuracy in biomass and C estimations of the Miombo and in the end, this predicament jeopardises remote sensing studies using optical sensors. As a result, there is usually scant data and studies on Miombo, particularly those that relate tree biomass to spectral detectability or remote sensing in general (Bouvet et al., 2018; McNicol et al., 2018).

During leaf-fall, in the dry season (May-October), Miombo provide a limited window for RS that uses optical data (Figures 6) though there is less cloud cover (Nyasulu et al., 2020; Phiri and Nyirenda, 2022). This is due to the shedding of leaves and loss of moisture which facilitate biomass detection since the detectability of vegetation largely depends on moisture content and leaf biomass (Chidumayo, 2001; González-Jaramillo et al., 2019; Morsdorf et al., 2009). However, the loss of moisture also affects biomass detection when using SAR measurements since the backscatter intensity is a function of

the surface moisture, *inter alia*, (Woodhouse, 2006). The figure next displays proposed mapping windows for Miombo Woodlands using remote sensing in Malawi.

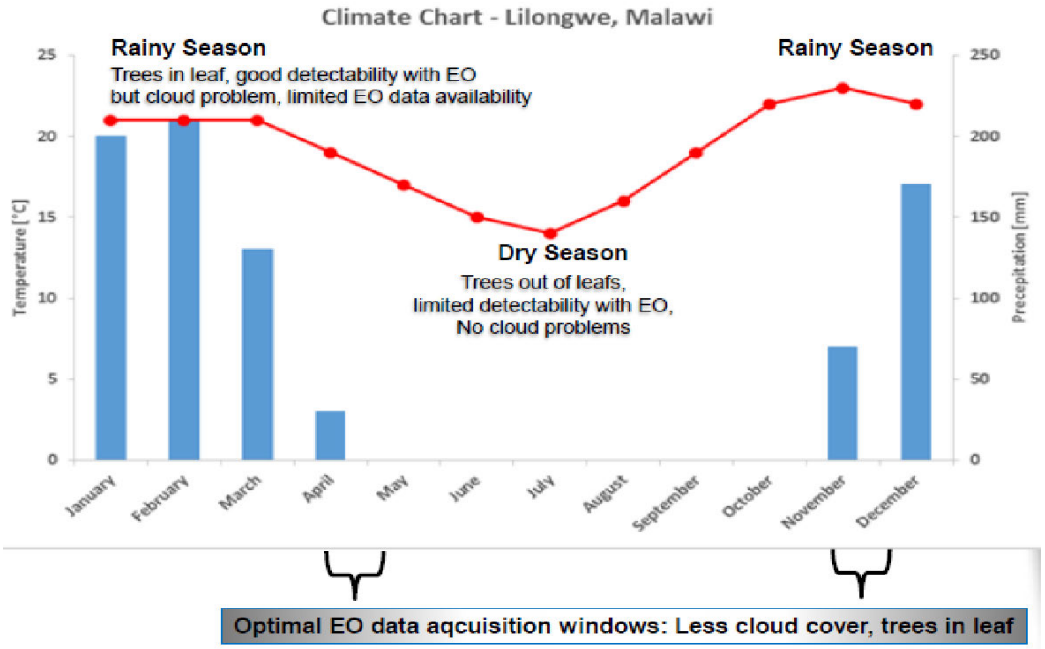

Figure 6. Proposed EO data acquisition windows for Malawi's Miombo Woodlands; rainy season providing better window in contrast to dry season (though with cloud cover between January and April), rendering challenges for optical remote sensing.

Source: **ESA- GAF-AG Dry Forest Mapping Workshop, April 2015, - Malawi**

The chart above suggests the rainy season as an ideal period for optical EO acquisition in contrast to the dry season though it is also cautious about the presence of cloud cover particularly between January and April. The information was presented to the forestry sector of Malawi (Department of Forestry inclusive) at a workshop entitled 'ESA Dry Forest Mapping' held in Lilongwe in 2015. It was organised by GAF-AG of Germany under the sponsorship of the European Space Agency (ESA).

Despite the proposed/ideal windows for RS, no documented attempt was made to validate the suggested periods in relation to biomass assessments in Malawi's Miombo

Woodlands, at least to the author's knowledge. Hence, it was in the interest of this study to bridge this knowledge gap by conducting a survey that detects AGB and crown pattern using EO covering both windows and validating the results using ground-based measurements.

Due to significant vegetation biomass changes shown during leaf-on and leaf-fall periods, studies encourage acquisition of multi-seasonal data i.e., post-rainy and dry seasons (in contrast to mono-season) to account for seasonality or vegetation phenology variations not only in Miombo (Kamusoko et al., 2014). Unfortunately, the minimal key studies that covered mapping of Miombo also used single-date satellite imagery most of which failed to capture dynamic vegetation changes in the Miombo ecosystem (Chidumayo and Gumbo, 2010).

2.4 Forest Carbon Pools and National Forest Monitoring System

The key role of forests with regards to Climate Change has been recognised as a C sink whose domain contains above and below-ground terrestrial regenerative C stored as biomass (Dixon et al., 2011; Novotný et al., 2020). Such recognition prompted categorisation of forest biomass into five main pools as follows; (i) AGB, (ii) Below Ground Biomass (BGB), (iii) Deadwood, (iv) Litter, and (v) Soil Organic Carbon (SOC), (Table 4) (Bhattarai et al., 2016; Goetz and Dubayah, 2011).

The AGB pool constitutes the majority of woody biomass in tropical forests, besides it is relatively easy and cost-effective to measure when used as a study parameter, compared to the BGB which involves destruction sampling (Government of Malawi, 2019a; Iman, et al., 2017; Kachamba et al., 2016; Novotný et al., 2020; USAID PERFORM, 2017). Hence, the AGB is the mostly frequently used pool in biomass studies (Iman, et al., 2017).

The table below covers a description of the main C pools as adopted by the Malawi REDD+ programme.

Table 4. Five Global Key Forest Pools for Estimating Biomass and Carbon Adopted by Malawi

Carbon Pool	Description
Above Ground Biomass (AGB)	Woody and herbaceous biomass of living vegetation above the soil surface that includes; trees, shrubs, palms, bamboo, vines and other living plants.
Below Ground Biomass (BGB)	Biomass of live roots >2 mm diameter that includes; the coarse roots, trees, shrubs, and other living plants.
Dead Wood	Non-living woody biomass that is larger than the litter pool. It includes both standing deadwood and down deadwood lying on the surface >15cm diameter.
Litter	Non-living biomass on the soil surface that is larger than the soil organic matter (>2mm) and smaller than the dead wood (<15cm).
Soil Organic Carbon (SOC)	Organic carbon in mineral or organic soils to a specified depth (30cm is the default depth, but sometimes measured up to 1m deep).

Source: (Bhattarai et al., 2016; Ministry of Natural Resources Energy and Mining, 2016).

Tree parameters measured from the C pools during forest inventories may slightly vary, but the six main elements include; (i) species, (ii) height (ht), (iii), diameter at breast height (*dbh*), (iv) crown diameter or canopy cover (v) stocking density, and (vi) stand density (Appendix I).

As the REDD+ global standards have been laid for comparability and repeatability's sake, they govern the recognition of measuring parameters and C pools that include definitions of forest, deforestation, and forest degradation (Romijn et al., 2012). A country's definition of 'forest' may vary contextually, but fundamentally originates from the one developed by the Food and Agriculture Organization of the United Nations (FAO-UN) which describes 'forest' as 'land spanning >0.5 hectares with trees >5 meters and a canopy cover of >10%, or trees able to reach these thresholds *in-situ*' (https://www.fao.org/). The definition is exclusive to land that is predominantly under agricultural or urban land use.

Malawi's definition of forest reflects the country's national LULC system as used for mapping purposes, and it refers to 'land with woody vegetation that has a dominant class in a minimum mapping area of 0.5 ha, with a minimum 10% crown closure and a potential height of 5 meters at maturity' (Ministry of Natural Resouces Energy and Mining, 2019).

Invariably, deforestation is defined as the conversion of forest to another land-use or the long-term reduction of the tree canopy cover below the minimum 10% threshold ([FAO] Food and Agriculture Organization, 2020). Both deforestation and forest degradation remain key challenges that contribute highly to C emissions as explained earlier, yet their estimation and documentation is characterised by inconsistencies and large uncertainties in Malawi (Haack et al., 2015; Skole et al., 2021).

The aspect of estimating biomass and C stocks is a pre-eminent step in accounting for forest goods and ecosystem services under REDD+ mechanism (The World Bank, 2018). The diagram next depicts the schematic set up of the REDD+ mandatory pre-requisites in relation to the pillars that construe the NFMS element.

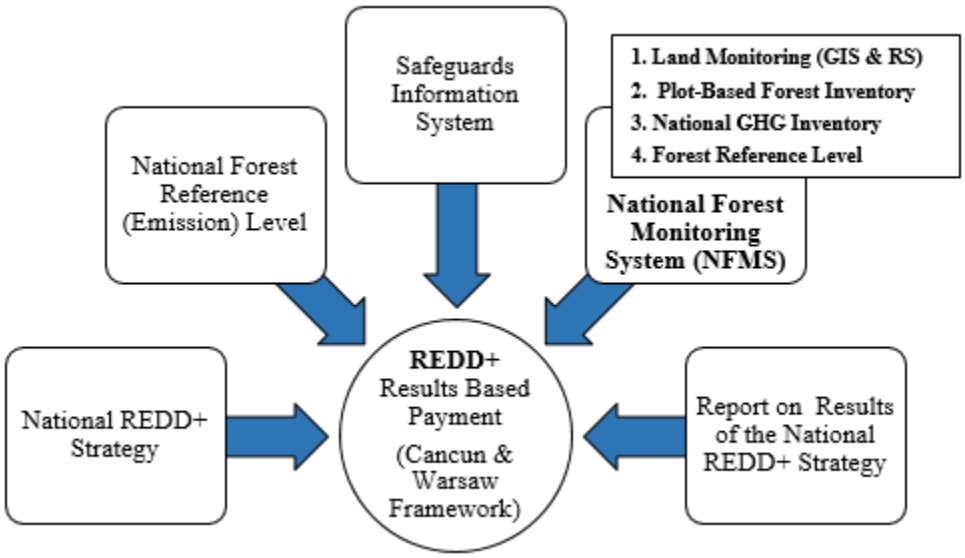

***Key**: GIS= Geographical Information Science; RS=Remote Sensing; GHG= Greenhouse Gas.*

Figure 7. Mandatory requirements and NFMS pillars adopted by REDD+ Project and the National Green House Gas Inventory in Malawi. Their strict adherence leads to carbon payment accreditation.

However, prior to realisation of C payments, the REDD+ mechanism requires institutionalisation of the following five core elements, *visa-a-vis*; (i) National REDD+ Strategy/Action Plan, (ii) Safeguard Information System, (iii) National Forest Reference (Emission) Level, (iv) National Forest Monitoring System (NFMS), and (v) Report on the Results of the National REDD+ (Figure 7) (Goetz and Dubayah, 2011; Government of Malawi, 2011; Malawi Redd+ Programme, 2015; Neeff et al., 2015).

The National Forest Monitoring System (NFMS) refers to a system for recording and monitoring land use while developing data on fluxes of GHG emissions and removals related to forests with the aim to assess performance of REDD+ activities (Hugel et al., 2018).

Implementation of the national GHG emission inventories and REDD+ schemes hinge on the development of MRV guidelines which are based on knowledge of the extent, C density and change of forested areas (Duncanson et al., 2014). Since REDD+ is established on the fundamental premise of payment-for-performance, requiring an account of forest biomass losses and associated C emissions and/or enhancing C sinks, it is imperative that such measurements are not only accurate, but also repeatable (Goetz and Dubayah, 2011; Goetz et al., 2015; Köhl et al., 2020).

While each of the REDD+ requirements (Figure 7) are reliant on technologies for forest measurement and monitoring that requires financial backstopping, the pivotal constraint with most developing countries, Malawi inclusive, has been inadequate financial resources to support operations that would be done to satisfy these conditions effectively (Goetz et al., 2015; Neeff et al., 2015; Romijn et al., 2012).

One of the central stages prior to accruing REDD+ carbon payments involve rigorous data collection that is followed by calculation of emission reductions (Nomura et al., 2019). The process includes acquisition of the extent of Forest-related emissions/Reference Levels (RLs), MRV, and safeguards through a procedure known as forest inventory (Nomura et al., 2019; The World Bank, 2018). Generation of the RLs is based on the historical rate of emissions and adjusted if necessary to account for national circumstances (*ibid*). The level of emissions emanating from the implementation of REDD+ activities is calculated by comparing MRV emission reductions to RL which is regarded as a benchmark rate (Goetz et al., 2015; Ministry of Natural Resouces Energy and Mining, 2019). Unfortunately, under the current plot-based inventory system, Malawi's key report Forest Reference Emissions Level was rejected due to inconsistencies observed in the methods and data employed (UNFCCC, 2021).

The transition from reliance on plot-based measurements only to their integration with EO is recognised as a remarkable stride in REDD+ monitoring systems, precisely among non-Annex 1 parties (Fankhauser et al., 2018; Kachamba et al., 2016; Moreno et al., 2016; Wang et al., 2009). Regrettably, comprehensive forest inventories are conducted at a prohibitive cost for Malawi and other LDCs, as a result these countries resort to the traditional ground-based system that often sample across small areas. This is against the REDD+ criteria which advocates integration of the remote sensing technology for more expanded, consistent, accurate and monitoring (Goetz et al., 2015; Romijn et al., 2012). In addition, (Goetz et al., 2015) noted that to meet the REDD+ requirements, consistent and repeatable measurements must be attained through integration of RS i.e., validation and calibration of remotely sensed estimates using ground-based measurements.

However, due to the afore-mentioned constraints that largely hinge on methodology, costs and data quality, Malawi is yet to attain the expected REDD+ standards in consistently tracking down the forest related C emissions (acquired through biomass estimation) and receive C payments (Ministry of Natural Resouces Energy and Mining, 2019; UNFCCC, 2021).

2.5 Forest Inventory Parameters of Success in Malawi

Though integration of EO with terrestrial forest measurements is key to accuracy enhancement of biomass estimates under the global REDD+ mechanism, it has unluckily, not yet been accorded as a mandatory requirement in Malawi's Standard Operating Procedures (SOPs) for estimating AGB (Government of Malawi, 2011; Skole and Samek, 2016). This is in comparison with other African REDD+ member states that employ satellite EO and have further registered incredible strides such as Uganda, DRC, Tanzania and Mozambique (Köhl et al., 2020; The World Bank, 2018).

Critical to the NFMS remains the tracking of forest C sinks and emissions which is also fundamental to an MRV system that relies upon forest inventories to consistently generate data (UNFCCC, 2014). While NFI acts as the primary source to estimate country level biomass, particularly AGB estimates, such exercises are ensured to be temporally

accurate, bear exceptionally fine spatially scaled and accurate data at an appropriate cost (Goodbody et al., 2017; Hilker et al., 2008). However, standards of such requirements and recommendations respective to most tropical forests have been scant. While those available for Miombo have ranged from being country-specific to site-based, it leaves an open question as to how accurate and robust their national spatial and temporal scales should be to attain the REDD+ standards (Government of Malawi, 2019a; Mueller, 2012; Neeff et al., 2015).

Integration of RS methods into datasets acquired via classical means in forest ecology studies indispensably demands in-depth understanding of their relative strengths and weaknesses on biomass retrieval (Bond et al., 2010; Köhl et al., 2020; Romijn et al., 2012). In this regard, various temporal and spatial resolutions plus the costs incurred during biomass estimates are central to the success of the assessments, especially among the non-Annex-I parties which experience funding limitations (*ibid*). Hence, in the context of Malawi, this forms the gist of this academic study that focused on enhancing accuracy, spatial and temporal coverage while minimising costs incurred during monitoring of Miombo biomass and carbon fluctuations.

Thorough examination on the 'Roadmap for Developing Malawi's NFMS' as well as the meta-analysis of Malawi's LULC Mapping Standards reveals that they emphasised to conduct forest inventories every 5 years in Miombo Woodlands to bolster the forest monitoring system (McGann, 2015; Neeff et al., 2015). In the same regard, local studies in Malawi indirectly highlighted the overall key standards acceptable on mapping accuracy (uncertainty) as ~85% Confidence Interval with 10% precision error (McGann, 2015; Miewald and Oduor, 2014; Neeff et al., 2015).

Though this was received with substantial interest by the Malawi REDD+ fraternity, critical analysis on LULC/inventory studies conducted in 2010 and sponsored by different organisations, i.e., (i) JICA, (ii) FAO and (iii) RMCRD/US-EPA revealed a series of overall mapping accuracies; 87.6%, ~80%, and 89.2%, respectively, that were accepted in the country (Department of Forestry, 2012; Haack et al., 2015; Neeff et al., 2015). Therefore,

this academic research inferred on such standards which were later adopted as the benchmark for the succeeding forest inventory exercises (Miewald and Oduor, 2014), unless officially documented otherwise, thus, not to the knowledge of the author.

The NFMS Roadmap study further recommended that a sum of $100,000 (£76, 923[14]) was required to support the Malawi's NFI system to attain the standards of the global REDD+ mechanism (Neeff et al., 2015). Naively, the study never estimated the key costs required for a single NFI exercise, not even on sampling unit plot or hectare basis, despite the existing plot configurations of 0.1ha (20m circular plots) or 0.3ha for the 3-T cluster circles (of 20m radius each) (Table 3 and Figure 5) (Department of Forestry, 2012; Neeff et al., 2015).

Despite this, an international plot-based forest inventory study conducted in 2012 calculated a range of €3.37-€4.04 per km^2, *ceteris paribus,* as an average cost for a terrestrial inventory (Mueller, 2012). The study sponsored by the SADC-GIZ[15], covered the Miombo Woodlands of Malawi, Zambia and Botswana. This incumbent study, however, estimated the inventory costs by factoring-in inflation and/or depreciation of the Malawi Kwacha currency between 2012 and 2019. These years account for the period when the previous forest inventories occurred as well as the data collection year for this current research. The calculations factored-in 20% as the maximum inflation value per km^2 i.e., (€348 per plot of 0.3ha + 20% = €417 per plot of 0.3ha or simply £360[16] per plot of 0.1ha). Therefore, for simplicity's sake, in this study, £360 per plot of 0.3ha or (£30 per ha per person, Table 2) is calculated as the standard cost for terrestrial forest inventory under the studied conditions of the Malawi's Miombo Woodlands.

In summary, this incumbent study presents the NFI parameters of success in Malawi (as synthesized from the literature reviewed and from the experience of the ground-based inventories) as follows;

[14]The exchange rate was £1= $1.30 in 2015

[15] SADC-GIZ = Southern African Development Community- Deutsche Gesellschaft für Internationale Zusammenarbeit GmbH,

[16] The exchange rate was £1= €1.16 in 2012

(i) 80-95% overall mapping accuracy obtained at 95% Confidence Interval (CI) and ≤10% precision error (Miewald and Oduor, 2014; Neeff et al., 2015; Saunders, 2014), and

(ii) £30 per ha per person as an average cost of ground-based inventory (Malawi Redd+ Programme, 2015; Miewald and Oduor, 2014; Mueller, 2012).

2.6 Generic Remote Sensing Techniques

This subsection delivers the concept of remote sensing by highlighting its concise history as used under forest monitoring. It provides a critical analysis of the application of the remote sensing in Malawi's Miombo Woodlands with reference to the previous forest inventories conducted.

The reliance on remote sensing (RS) for acquisition of information about environmental processes can be traced to have been triggered by the launch of the first earth observatory satellite for forestland monitoring called Earth Resources Technology Satellite (ERTS) in July 1972 (Kondratyev et al., 1973). The satellite mission was launched by the United States of America, and it was later renamed LandSat.

Remotely sensed forest ecology data such as Earth Observations (EO) provide enhanced and feasible alternative besides complimenting manual observations with a short revisit time, referred to as temporal resolution (Lechner et al., 2020; Ribeiro et al., 2012). An increase in the availability of freely available and unrestricted EO has equally rendered enhanced access of global datasets with frequent revisit time and improved coverage (Alleaume et al., 2018). Notwithstanding the repeatable observations over large areas that would prohibitively be costly and time-consuming, RS also provides access to a consistent and large historical archive that characterises change detection such as land use and land cover formations, i.e., LandSat that spans over 40 years with space-based land surface observations (Roy et al., 2016).

The technology has been used for mapping the distribution of forest ecosystems, global fluctuations in plant productivity with season, and the 3D structure of forests, involving

identification, locating and characterisation of object features (Lechner et al., 2020). Among others, EO are preferred due to their improved spatial resolution and wall-to-wall coverage, thus even in areas that would have been rendered inaccessible and consequently left un-surveyed in contrast to ground-based measurements (Westoby et al., 2012). Most of vegetation assessments retrieved from RS studies have proven indispensable to improving bottom-up C flux estimates due to their incorporation of both changes in forest extent and biomass density (Duncanson et al., 2014).

However, the extent and quality of the estimates depends on the type of sensor used. It is, therefore, fundamental to understand the nature of an object feature under RS as it determines the instruments and type of sensor to be used. Correspondingly, it determines the platform on which to mount the sensor. These attributes warrant a RS system to be characterised as either active or passive, thus depending on their sensor's sensitivities and artefacts.

2.6.1 Passive remote sensing

Passive sensors measure illumination or energy radiated as emission or reflected from the sun or other radiating objects by Earth's surface or atmosphere (Woodhouse, 2006). While there are passive microwave sensors used to generate global biomass maps using "vegetation optical depth" (VOD) methods (B. Li et al., 2021; Moesinger et al., 2022; Zhang et al., 2021), the term 'passive' as applied under RS in this study is interchangeably used with 'optical' and denotes a condition where solar energy is reflected from the Earth's surface as the sensor does not actively emit its own radiation (Lechner et al., 2020; Woodhouse, 2006).

Passive sensors highlighted in this study operate within the four regions of the electromagnetic spectrum (EMS) ~ 0.4 - 2.5μm, namely; (i) Visible (Vis), (ii) Near-InfraRed (NIR), (iii) Short-Wave Infrared (SWIR), and (iv) Thermal Infrared (TIR) (Figure 8). Notable satellites with passive sensors aboard include; LandSat, Sentinel-2, Rapid Eye and, ASTER and MODIS aboard Terra and Aqua missions. The next figure shows the range of wavelength regions within the EMS.

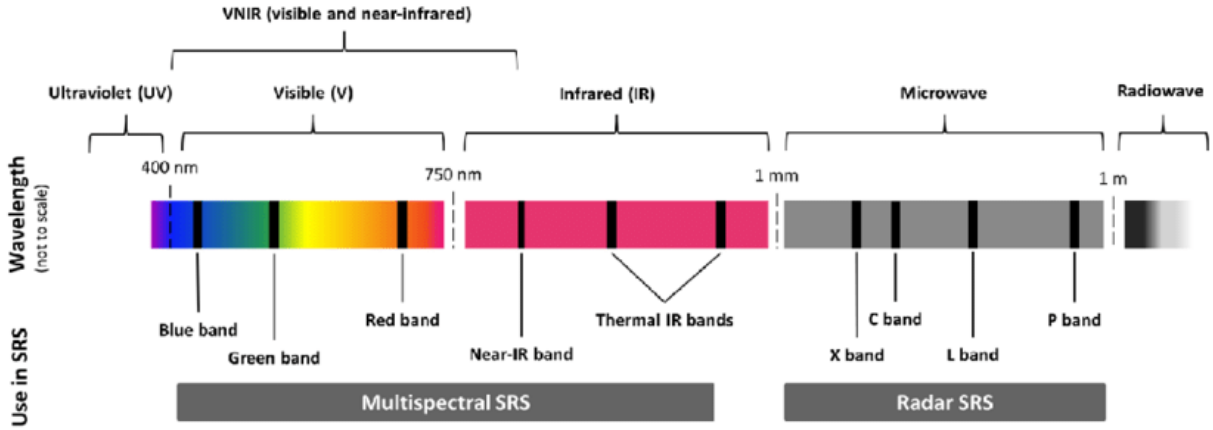

Figure 8. Electro-magnetic Spectrum (EMS) Remote Sensing Windows arranged from Low to High Wavelength Regions. Key: SRS=Satellite Remote Sensing.

Source: https://www.researchgate.net/figure/The-spectrum-of-electromagnetic-radiation-not-to-scale-and-its-use-in-satellite_fig1_324537528

Both passive and active sensors may employ a range of bandwidth depending on the purpose for which they were designed, and characteristics that affect the spatial and spectral quality i.e., accuracy of the Earth Observations retrieved (Matsuoka et al., 2013).

While the most common regions of the EMS employed for monitoring vegetation under passive sensors include; (i) Visible, (ii) NIR and (iii) SWIR; the ones preferably used in vegetation studies (forestry inclusive) are NIR and SWIR wavelengths due to their high reflectance on vegetation (Fitzgerald, 2010). Studies on multisource data comparisons noted that optical datasets have a complementary role as their integration to RS methods increases biomass estimation accuracy (Avitabile et al., 2011).

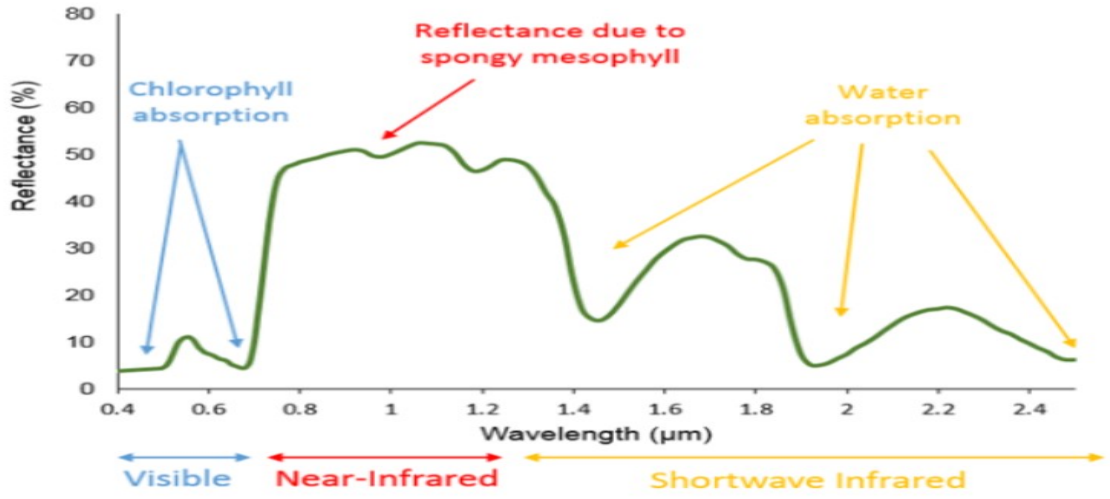

Figure 9. Vegetation Spectrum showing the percentage of reflectance and spectral signature in micrometers (µm); absorption in the Red and Blue wavelengths, and reflection in the Green and Near Infrared (NIR) wavelengths. Source: GAFAG, 2019. Cloud Based Forest Monitoring Workshop, Munich-Germany.

Vegetation spectrum reflectance entails a synthesis of reflection from structure and texture of plant parts and canopies (Roy, 1989). Since leaf cover and canopy development is related to many plant and canopy variables, majority of the studies have for years used the normalized difference vegetation index (NDVI) to relate to many important plant characteristics such as leaf area index to aboveground biomass (Fitzgerald, 2010; Roy, 1989). Therefore, NDVI simply refers to a graphical indicator most widely characterised in plant studies which is correlated with green leaf cover and consequently biomass set by the plant physiology i.e., canopy (*ibid)*.

However, the use of NDVI in characterising green leaf cover and biomass in Miombo Woodlands and other vegetation is limited by the leaf phenology and seasonality that render it useful only during the wet season when trees and other vegetation put on leaves, in contrast to the dry season when they are shed-off and/or damaged by fire (Pettorelli et al., 2005; Ribeiro et al., 2012).

A study on Miombo canopy land surface temperature and phenological phase and showed that Normalized Difference Water Index (NDWI) and NDVI, (as indicators of water

content and plant physiology, respectively) begin to decline immediately following the end of the rainy season in early April (Zimba et al., 2022).

Documented evidence on forest inventories conducted since 2009 to date in Malawi indicates that only 38% (6 out of 16) surveys attempted to integrate EO data acquired from passive and active satellite mission sensors, though at a very basic level (Table 3), at least to the knowledge of the author (Department of Forestry, 2012; Government of Malawi, 2019a). While 31% of the studies managed to employ RS for stratification and sampling purposes, only 6% (one) attempted to use RS at the estimation stage of biomass and C (Table 3). Among the 31%, one was conducted in Mkuwazi and Nyika protected area whereby it engaged data sets acquired by passive sensors of the LandSat 7 ETM+ imagery areas for stratification sampling during forest inventory (Berry et al., 2009) Disregarding these low statistics, one unresolved area is that the Mkuwazi and Nyika study did not use the EO to model and quantify forest biomass and C changes, and neither did it attempt to scale up the gb measurements by using low-cost airborne imagery as a means of enhancing coverage and accuracy of the estimates.

Another key transboundary Miombo Woodland study conducted from 2012 used RapidEye and Google Earth imagery to stratify and sample plots spanning eastern Zambia and central-western Malawi (Mueller, 2012). While the merit of this study lies in the introduction of the T-cluster sample plot-design which complies with the global REDD+ mechanism standards; it nonetheless did not explore whether low-cost i.e., unrestricted access EO could alternatively be used for estimating biomass given the conditions of the Malawi's Miombo Woodlands, though notwithstanding the imagery's commercial status.

Despite being widely used, the LandSat 8 satellite imagery bands are known to generate a low correlation with vegetation biophysical properties such as biomass due to their coarse spatial resolution of 30m (Puliti et al., 2018). In a different study, the LandSat 8 EO (datasets acquired from passive sensors) were used to stratify forest cover areas and derive sample plot-network, thus at a design stage in Liwonde, Ntchisi and Perekezi

Miombo Woodlands of Malawi (2016) (Table 3). It remained an open question whether the ground-based measurements (with sampling plots units of 1257m^2) could have been further employed for validation and/or calibration of these free access Earth Observations (30m spatial resolution or 900m^2) to enhance accuracy of the biomass estimates. This is due to the scale mismatch between the sampling plot size and the Landsat imagery pixel resolution.

In addition, despite the coarse resolution, it is also clear that there was never an attempt to step up the efforts to explore a correlation characterise the relationship between the individual tree metrics (height, crown diameter and *dbh*) and AGB generated from the ground-based measurements and their corresponding measurements from the wall-to-wall imagery datasets.

Another study employed Google Earth platform imagery for pre-screening forest ground sample plots, when Malawi attempted to conduct a National Forest Inventory in 2018 (Government of Malawi, 2019a). Nevertheless, the design of the study, as previously mentioned was somehow subjective as it skipped most of the protected (forest and wildlife reserves, national parks and other forestlands) that significantly represent the Miombo Woodlands of central Malawi (Figure 10). Besides, the Google Earth imagery provided relative coarse resolution for ground sampling accuracy of the *in-situ* plots (0.1ha) to the extent that stratification accuracy was highly compromised, i.e., most of the crop fields were misclassified as forestlands in the northern region. Such a predicament triggered the need for this incumbent academic study to employ EO of medium to fine resolution i.e., radar backscatter imagery from ALOS-PALSAR, S1, S2 and ESA CCI Biomass Map datasets (with unrestricted access) and the low-cost but VHR optical UAV airborne orthomosaics (Figure 11) to enhance accuracy and coverage of the AGB estimates.

Studies on multisource data comparisons noted that optical datasets have a complementary role as their integration to RS methods increases biomass estimation accuracy (Avitabile et al., 2011).

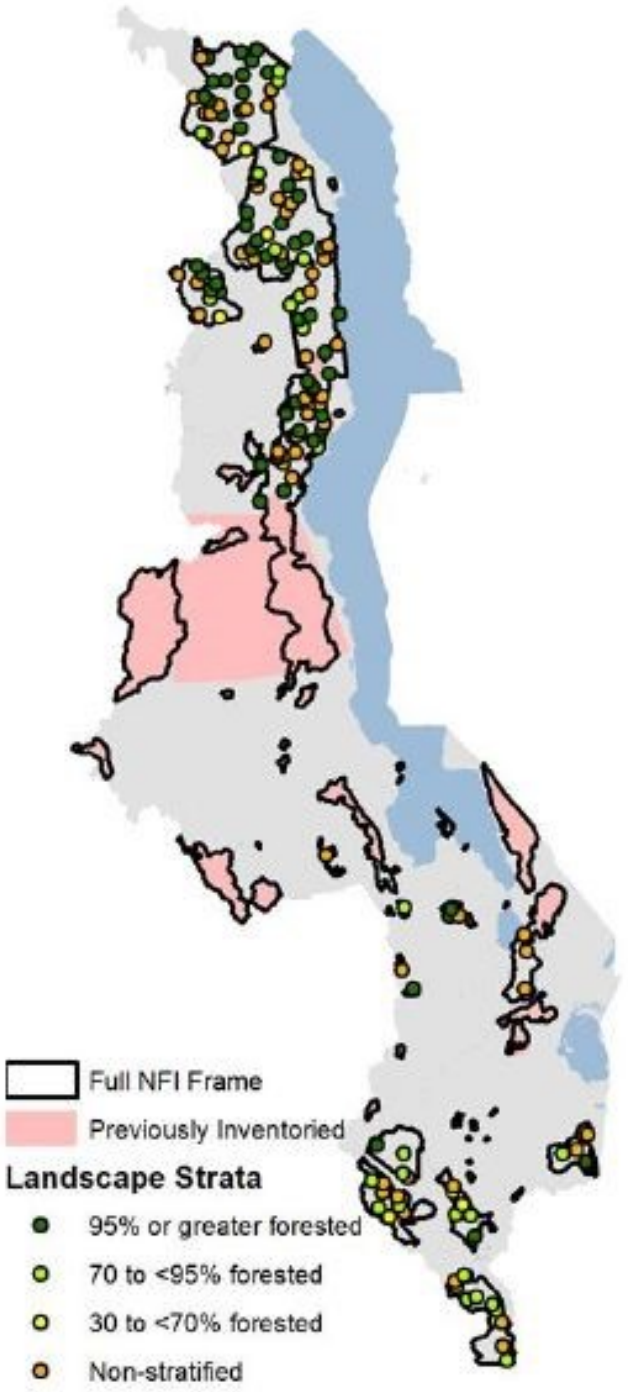

Figure 10. 2018 NFI Sample Plot Distribution without key Central and Southern Region Protected Forests of Malawi (denoted as previously inventoried). The exclusion of these key forests rendered the 2018 inventory non-representative. *Source*: *Malawi National Forest Inventory 2018 Analysis Report* (Government of Malawi, 2019a).

Figure 11. Miombo tree canopy density aerial view of Ntchisi Forest acquired by fine spatial resolution optical sensor aboard DJI-Phantom 4 Pro+ during 2019 post-rainy season. Sparse canopy cover characterises most Miombo Woodlands especially during dry season due to leaf-off condition.

2.6.2 Active remote sensing

In contrast to passive remote sensors, active sensors generate their own illumination by transmitting pulses of microwave radiation (i.e., Radio Detection and Ranging, abbreviated as RADAR) and then use specialized receiver system to measure reflected (or more precisely, scattered) signal from the area of interest (AOI) (Woodhouse, 2006), while the Light Detection And Ranging (LiDAR) sensor transmit visible/NIR radiation (K. Liu et al., 2017; Silva et al., 2021). Some of the active sensors aboard satellite missions that use RADAR system include; ERS, RADARSAT, ALOS-PALSAR, and Sentinel-1. These primarily, but not exclusively, use the wavelengths greater than 3cm (<10GHz) where the atmosphere becomes transparent (Woodhouse, 2006).

A study on generation of a benchmark of forest carbon stocks in tropical regions across America, sub-Saharan Africa (covering Malawi and other countries), and Southeast Asia

combined ground-based and Lidar datasets from ICESat and accounted for 49%, 25%, and 26% of the total stock, respectively (Saatchi et al., 2011). However, for the estimations in sub-Saharan Africa, including the Savannah Woodland the study used a general allometry ($AGB = 0.35h^{2.05}$) which is different from the local allometry for the Malawi's Miombo Woodlands ($AGB = 0.104 \times dbh^{1.92} \times ht^{0.845}$ and/or $AGB = 0.218 \times dbh^{2.32}$) (Kachamba, 2016; Saatchi et al., 2011). Hence, the allometry used in the pan-tropical estimations were unreliable for Malawi's Miombo and they yielded uncertainties in the AGB stock estimations (Kachamba, 2016).

A different study that focused on comparisons between;(i) the above-mentioned pantropical biomass maps, and (ii) maps on estimations of CO_2 emissions from tropical deforestation datasets (Baccini et al., 2012), both of which used active sensors (spaceborne LiDAR) dataset exposed substantial estimate differences in Miombo Woodlands of Africa (Malawi inclusive) and other forests (Table 1) (Baccini et al., 2012; Mitchard et al., 2013; Saatchi et al., 2011). This was attributed to differences in the spatial distribution of biomass and spatial pattern of forest cover change.

Unfortunately, these map datasets were also used to make decisions at sub-national and national-level activities in relation to REDD+. The same trend of has been true for several inter-continental and pan-tropical studies that generated biomass and carbon maps covering Africa, Malawi inclusive (Table 1).

A key local study that employed radar backscatter imagery datasets in Malawi's Miombo Woodlands established a poor correlation (R^2 ranged between 0.01-0.16) between the plot-based biomass measurements and the ALOS-PALSAR based biomass in 2008 (Cassells et al., 2009). These results were inconclusive, and the study recommended further studies on the same.

A different study conducted between 2010 and 2012 employed ALOS-PALSAR-1 pan-sharpened imagery to augment assessment of forest biomass and carbon over 17 forest reserves distributed across the Miombo woodlands of Malawi (Department of Forestry, 2012). The radar backscatter measurements were engaged to assess historical land

use/land use change (LULUCF) and derive sample plot units (Table 3) as a means of stratification and sampling the forest. Still, the question of central interest would be to interpret the plot-based biomass estimations using the imagery's observations through a modelled correlation, an important aspect that the 2012 study did not address.

Besides, the investigations did not attempt to explore the cost-effective means of estimating forest AGB since the ALOS-PALSAR-1 datasets were not free of charge that time, thus against the backdrop of the financial challenges of Malawi's forest monitoring system (Neeff et al., 2015). Hence, to address these gaps, this academic study employed the unrestricted active remotely sensed datasets of different spatial resolution from Sentinel-1 (S1), ALOS-2 PALSAR-2 and ESA-CCI Biomass Map missions over Ntchisi Forest Reserve of Malawi.

2.6.2.1 Sentinel1 Mission

Operated by ESA, the Sentinel1(S1)-mission was launched in April 2014, and it comprises two polar-orbiting satellites that operate day and night, regardless of the weather (Torres et al., 2012). The mission captures data with minimal atmospheric noise that may require less processing, in contrast to other mission datasets e.g., LandSat 8 datasets which though free access as well are highly characterized by considerable cloud cover (Li et al., 2020; Phiri and Nyirenda, 2022; Torres et al., 2012).

The main operational mode of S1 features a wide swath of 250km with a high geometric (typical 20m-Level-1 product resolution) and radiometric resolutions suitable for many applications (Torres et al., 2012). The S1 Synthetic Aperture Radar (SAR) instrument acquires data in four exclusive acquisition modes namely; (i) Strip Map (SM), (ii) Interferometric Wide swath (IW), (iii) Extra Wide Swath (EW), and (iv) Wave (WV) (Torres et al., 2012). For this Miombo study, the interest was on IW, a mode that caters for forest biomass estimation which is a task that directly falls within the mission's Land Monitoring category.

Data in the IW is acquired in three swaths, thus using the Terrain Observation with Progressive Scanning (TOPSAR) imaging technique (Torres et al., 2012). The data

products of S1 distributed by ESA include; (i) raw Level-0 data (for specific usage), (ii) processed Level-1 Single Look Complex (SLC) data, and (iii) Ground Range Detected (GRD) levels 1 and 2 (*ibid*). The Level-1 data contain multi-looked intensity and are projected to ground range using an Earth ellipsoid model only while the Level-2 Ocean (OCN) data are retrieved for geophysical parameters of the ocean (systematically distributed).

The twin polar satellites (Sentinel-1A and 1B) are phased at 180^0 to each other in sun-synchronous manner (Torres et al., 2012). The mission has a 12-day repeat cycle and 175 orbits per cycle (Table 5). Therefore, a single S1 satellite is capable of mapping global land masses in the IW swath mode once in every 12 days thus, in a single pass (ascending or descending) while the constellation offers 6 days' exact repeat cycle at the equator. With such an advantageous temporal resolution, S1 mission provides latest data within the given period. This renders an urge to support monitoring of vegetation changes within the growing season that may not be necessarily possible with other satellites. Hence, this forms the rationale behind its preference for the incumbent academic study that estimates AGB change and crown spatial pattern within over a given period.

Unlike the passive sensors, the SAR sensors have the advantage of operating at wavelengths with less impediments by cloud cover or lack of illumination (Urbazaev et al., 2018; Woodhouse, 2006). As the SAR sensors transmit their own microwave signal to irradiate the energy backscatter from the ground, the backscatter measurements get influenced by the terrain surface/roughness, i.e., the more the roughness or structure on the ground, the greater the backscatter (Woodhouse, 2006). A study on radar backscatter observations derived from the QuikSCAT sensor (focusing on the effect of sloping terrain over the North American Monsoon region) showed that backscatter is dependent on the local incidence angle caused by changes in slope (Mladenova and Lakshmi, 2009).

On the hand, backscattering from bare rocks (occurring at the rock-air boundary) is renowned for its influence on surface roughness signal reflectance (Kamusoko et al., 2014; Woodhouse, 2006). More structurally complex targets such as forests tend to

appear brighter due to signal interaction with leaves, branches and trunks that result in higher proportion of the signal being transmitted back to the sensor (*ibid.*). This attribute is important for the forest biomass detection and estimation.

2.6.2.2 ALOS-2 PALSAR-2 Mission

Another mission that renders unrestricted active remote sensing datasets (since January 2016) is the Japanese Phased Array L-band Synthetic Aperture Radars of (PALSAR-2) (https://www.eorc.jaxa.jp/ALOS/en/dataset/fnf_e.htm). The Japanese Aerospace Exploration Agency (JAXA) generate global 25m resolutions mosaics and forest/non-forest maps that are acquired by the PALSAR sensors. These are aboard a mission referred to as Advanced Land Observing Satellite (ALOS) and ALOS-2. While the spatial resolution (size of one pixel) is ~25m x 25m, the temporal resolution is one year. The L-band refers to the operating frequency range of 1–2 GHz and wavelength range of 30–15cm in the EMS (Figures, 8 and 9). Owing to its low bandwidth, because of low frequency, L-band is the easiest to implement for many applications comparatively to other higher frequency ranges like C and S band. Consequently, it is one of the main operating ranges used by various applications such as radars, global positioning systems (GPS), radio, and telecommunications and aircraft surveillance.

The PALSAR/PALSAR-2 are effectively employed for studying global environmental changes such as global warming, loss of biodiversity and forest change detection. Significantly, the latter domain has been used for this study to estimate forest AGB stock of Ntchisi. The L-band Synthetic Aperture Radars (SAR) on ALOS and ALOS-2 provide the capability to observe land surface regardless of clouds, an attribute that gives it an edge for rendering essential information about forest changes in tropical regions. This attribute provides the suitability for engaging such datasets in the tropical Miombo Woodlands of Malawi, where cloud clover is an issue (Nyasulu et al., 2020; Phiri and Nyirenda, 2022).

The mission’s orbit is sun-synchronous and has a height of 628 km, inclining at 97.9º. The local sun time of the mission is 1200 ± 15 min during daytime, and this contributes to

the generation of quality imagery. The mission's datasets comprise several guide categories which include; (i) Disaster monitoring, (ii) Land monitoring, (iii) Agricultural monitoring, (iv) Natural resource exploration, and (v) Global Forest monitoring. Under the latter, the mission seeks to resolve global level environmental issues such as global warming. It accomplished this by deriving from global monitoring of tropical rain forests that is used to identify C sinks to relevant organisations. This domain is of particular interest to this Ntchisi Forest study as it has rendered data/estimates for forest AGB and C. It is this facet of capturing seasonal variations that fits seamlessly into the Miombo research which entails tree species that exhibit great seasonal variations i.e., leaf-on and leaf-fall, rendering difficulties in detecting and estimating AGB and C changes when other satellite mission's datasets are employed (Chidumayo and Gumbo, 2010; Kamusoko et al., 2014).

The next table displays historical attributes of ALOS-PALSAR and Sentinel missions in relation to their heritage ones.

Table 5. Comparison of Sentinel and ALOS-PALSAR against Other Heritage Missions

	LANDSAT 1-8	SPOT	ALOS PALSAR	SENTINEL-1	SENTINEL-2
Mission lifetime	1972-present	1986-present	2006-present	2014-present	2015-present
Instrument principle	Scanner	Push broom	L-band SAR	Single C-band SAR	MSI-Push broom
Repeat cycle (days)	16	26	46	12 (at equator)	5 (at equator)
Swath width (km)	185	2 x 60	60,70	400	290
Spectral bands	7	4	L-band	C-band	13
Spatial resolution (metres)	30, 60	2.5, 10, 20	25	5, 20, 40	10, 20, 60
Data Access	Unrestricted	Not free (press order)	Unrestricted for some period	Unrestricted	Unrestricted

Source: *Sentinel-2 User Handbook 2015*

2.6.2.3 GEDI Mission

Data from the Global Ecosystem and Dynamics Investigation (GEDI) instrument of the NASA Earth Venture Instrument (EVI) Mission launched in December 2018 is another

potential source but was not preferred by this incumbent study. The instrument can be characterised as a geodetic-class light-detection and ranging (Lidar) that comprises 3 lasers (full-waveform recording) which produce 8 parallel tracks of observations. Each laser fires 242Hz, illuminating 25m spot (footprint) on the surface over which 3D structure is measured.

GEDI's ability to estimate C stocks enables the estimation of land use change's impact on CO_2 concentrations (Hancock et al., 2019; Silva et al., 2021). This potentially enables quantification of biomass and C stocks sequestered as well generating future projections. The system also provides high resolution geo-located elevation data that can improve the global Digital Elevation Models (DEMs) for the 3D aspect. Quite relevant to this academic study would have been the fact that GEDI data provides biomass and C stock estimates. The following parameters that have also been investigated under this study; (i) forest canopy height and relative height metrics, (ii) canopy vertical structure (profile metrics), and (iii) surface elevation (https://www.earthdata.nasa.gov/learn/articles/first-gedi-data-available).

Nevertheless, the choice of not using the mission's datasets was because it would have been risky and time wasting for this academic study (scheduled for 2018-2022) to wait for the GEDI datasets as the mission was launched in the same year this study commenced. This is in cognisance of the challenges and constraints that newly launched missions face such as failure or substandard performance.

However, Lidar in contrast to other sensors, can address multi-layer nature of forests by using full wavelength to provide accurate biomass estimation (Zianis et al., 2016). The technology is also used as a direct method for height and canopy measurements rather than being used in allometry as it is the case with radar backscatter measurements (*ibid*). Lidar relies on processing of HR digital airborne waveform from which vertical information can be produced (Zianis et al., 2016).

Nevertheless, Lidar technology has basic limiting factors associated with costs. Despite the Airborne Laser Scanner (ALS)/LiDAR renowned as the primary data sources for the

3D information on forest vertical structure, they are an expensive means and applied on commercial basis (Table 2). Therefore, this renders the low-cost optical sensors best alternatives for obtaining accurate height while complimenting conventional plot-based measurements methods over Lidar/ALS (White et al., 2013).

Briefly, in as far as RS is concerned, the REDD+ participating countries engage primarily, but not exclusively, the NFI systems to estimate forest biomass and C fluxes, thus respective of their capacities that include; EO from optical remote sensors (satellite or UAVs photogrammetric surveys and/or active remote sensors (LiDAR/ALS and Radar) (Fankhauser et al., 2018; McRoberts et al., 2015; Mlambo et al., 2017; Wang et al., 2009; Zhang et al., 2017).

CHAPTER-3

3.0 – METHODOLOGY

3.1 Description of Study Site and Rationale

The study was conducted in Ntchisi Forest, a state controlled Miombo Woodland located in the central district of Malawi called Ntchisi (Lat., -13.3205 E and Long., 34.0419 S) (Figure 12). The district lies ~96km to the north of Lilongwe, Malawi's capital city and it borders with 3 districts namely; Nkhotakota to its north and east, Kasungu in the north-west and Dowa to its south and west, respectively (Figure 12) (Ntchisi District Assembly, 2014).

Ntchisi Forest was declared a protected area in 1924 and spans over 9,720ha that entail undulating mountainous terrain with an altitudinal range of 600-1675m above sea level (ASL) recorded within its plots (Figure 13). With a peak elevation of 1702m (ASL), the reserve has a mix of rough rolling slopes, especially on the eastern side and gentle slopes ranging from 5-74% (Figure 13, Table 6). These extreme slopes render accessibility difficult, though they are tourists' attraction spots (Ntchisi District Assembly, 2014, 2007).

The forest comprises three core vegetation types namely; (i) *Brachystegia*, (ii) Montane Evergreen Forest, and (iii) Riverine Forest. The latter juxtaposes to perennial streams while the Montane evergreen forest patch is located on the southern ridge of Ntchisi Forest Mountain, characterised by large emergent of *Newtonia species* (Ntchisi District Assembly, 2014). The dominant Miombo trees in the forest are of the genera*;* *Brachystegia*, *Julbernadia* and *Diplorhynchus* (Ntchisi District Assembly, 2014). The three most abundant species within the *Brachystegia* genera include; *B. buseii*, *B. boehmii* and *B. manga* (USAID PERFORM, 2017). The soils in the reserve are classified as a mixture of poor sand, localised within the *Brachystegia* vegetation chunk and blackish-loam soils ubiquitous within the montane mosaic.

The figures below display, (i) the map of Ntchisi Forest in relation to some REDD+ Pilot sites in Malawi, and (ii) the topographical outlook of the reserve.

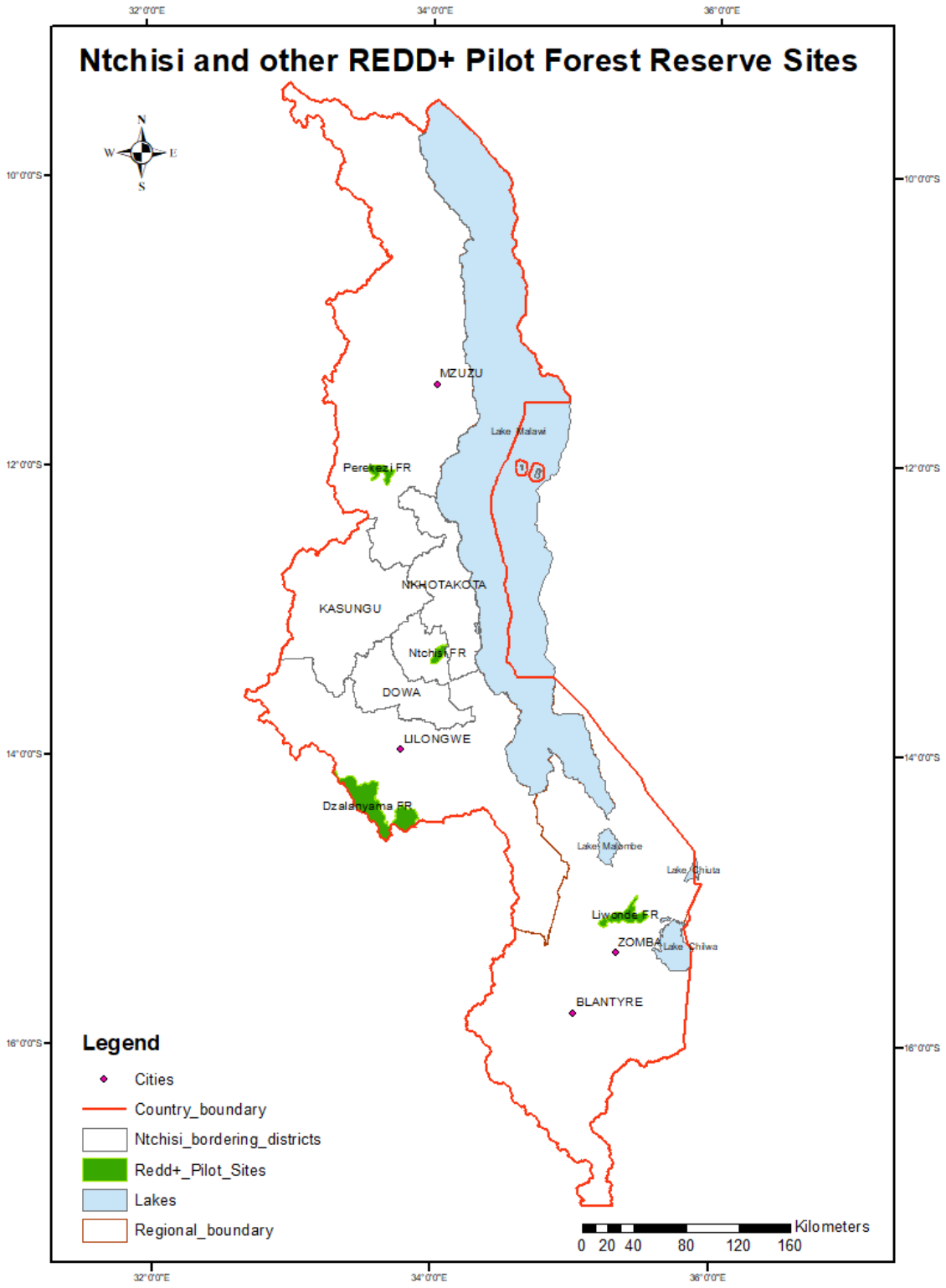

Figure 12. Location of Ntchisi Forest Reserve, a REDD+ pilot site of Malawi in relation to bordering districts and some key REDD+ sites where ground-based measurements are conducted in Malawi.

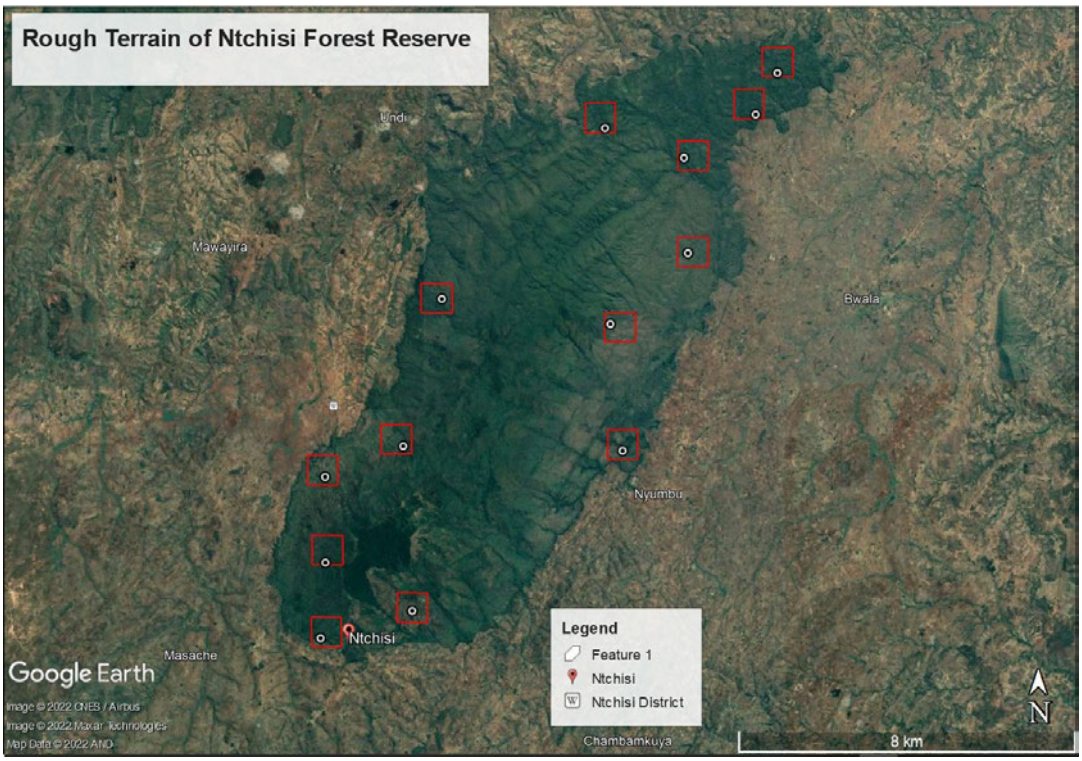

Figure 13. Ntchisi Forest mountainous terrain; (top)-Ground plot-centroids (white-dots) and 50ha UAV square plot-box distribution (red) overlaid on Google Earth imagery, 2022, (bottom)-eastern topographical view of its terrain.

The table below displays some elevation attributes of Ntchisi Forest recorded at each sampling unit plot centroid during both the 2019 and 2016 ground inventories.

Table 6. Ntchisi Forest Topographic Attributes Acquired during 2016 and 2019 Ground Study

Plot	Plot number	UTM Easting	UTM Northing	Elevation (m)	Slope %	Slope Condition	Distance from boundary (km)
Mpamila	12	0610161	8520969	1344	48	Extremely steep	1.3
Nyanga	13	0607984	8520324	1332	12	Steep	0.7
Mandwe	6	0610894	8528310	1079	18	Steep	0.8
Kasakula	9	0616733	8524713	764	5	Flat	1.5
Chenche	5	0615166	8529363	716	10	Fairly steep	1.7
Msankhire	3	0614781	8532317	832	19	Very steep	1.3
Mndinda	1	0618875	8533606	681	12	Fairly steep	2.3
Kajaliza	2	0618355	8532624	669	10	Fairly steep	1.2
Mkomba	4	0616651	8531612	713	11	Fairly steep	1.7
Chanika	7	0614888	8527699	847	36	Extremely steep	2.8
Chifwelekete	8	0609963	8524839	1206	74	Dangerously steep	1.8
Mnguluwe	10	0608108	8524124	1212	37	Extremely steep	0.9
Sambakunsi	11	0608106	8522106	1498	32	Extremely steep	1.5

Ntchisi experiences a humid subtropical climate characterised by alternating dry winter and scorching summer seasons. Rainy season commences in October/November, peaks in January and ends in April. Annual rainfall ranges from 1200-1400mm, providing a season which alternates with the dry period that comes between May and November. An annual temperature range of 19-25^{0}C is experienced with an alternate of cool and warm weather (Ntchisi District Assembly, 2007).

The reserve's catchment falls within Kalira and Chikwatula Extension Planning Areas which are under the authority of Traditional Authorities; Vuso Jere, Kasakula and Nthondo (Ntchisi District Assembly, 2014). The forest is under co-management regime, an administrative arrangement between the Central Government of Malawi (Department of Forestry) and the surrounding villages. These two parties share roles and responsibilities in governing the forest.

Ntchisi Forest Reserve was selected as a study site for this academic research due to the following reasons. First, it is more significantly a pilot-study area for the REDD+ mechanism in Malawi (Figure 12). Despite this national importance, illegal wood harvesting in form of firewood, poles, charcoal, and timber remain key threats of its

woody component since 2007 (Chinangwa et al., 2016; Ntchisi District Assembly, 2014, 2007; USAID PERFORM, 2017).

Second, the forest has an established network design of permanent sampling plot units laid in 2016 which provides a better leverage for scientific comparisons and analysis of biomass estimates (Government of Malawi, 2019a; USAID PERFORM, 2017). Third, the reserve's canopy density status of ≥50% multi-storey (in some parts) provides the better testing threshold for the high resolution RGB airborne observations employed in this study (Table 8) (USAID PERFORM, 2017). Technically, this attribute was envisaged to be advantageous to this study because the operation of the UAV's Structure-*from*-Motion photogrammetry requires a sparse canopy for the ground surface detection which is critical to the development of a 3D structure used for AGB estimations (Kachamba et al., 2016; Mlambo et al., 2017).

Fourth, Ntchisi Forest has uniquely undergone several management arrangements in comparison to other REDD+ pilot sites in Malawi, i.e., Liwonde and Perekezi Forests, (Figure 12), where their management regimes have changed only. Such management regime has contributed to its Ntchisi's current forest biomass status as follows;

(i) Co-management system involving the state and surrounding communities (2003-2014, and from 2018 to present). This is arrangement that entails demarcation of the forest into management blocks following the chunks allocated to the villages that hold stake in its management (Chinangwa et al., 2016; Government of Malawi, 2019a; Ntchisi District Assembly, 2014),

(ii) Single–entity management arrangement whereby traditional leaders fundamentally manage the reserve as one communal entity, in contrast to block management (2014-2018) that subdivides the forest into blocks/coupes (Government of Malawi, 2019a), and

(iii) State-controlled arrangement (1924 to 20020 whereby the reserve was entirely managed by the Government of Malawi.

Since forest management techniques influence the status forests i.e., growing stock, volume, density, biomass *inter alia* (Ali et al., 2007; Bouriaud et al., 2019; Chinangwa et al., 2016; Routa et al., 2011), it was of significant interest for this academic research

to incorporate Ntchisi Forest as a study area basing on the governing systems as they inform the available AGB stock.

Furthermore, the choice of the study site was also based on its unique topographic aspect (mountainous, rock outcrops, and steep slopes) and its biophysical factors such as manageable size (9,270 ha), seasonal fires, riverine and upland tree species patterns (Figures 5 and 13). These provided an enabling and encompassing analysis of spectral reflectance of RS methods strengths and limitations whose effect on AGB accuracy has never been statistically explored in Malawi, at least to the knowledge of the author.

3.2 Research Study Design

Data acquisition for the entire study was three-fold, *vis-a-vis*;

(i) *in-situ*/plot-based measurements (individual tree level parameters),
(ii) optical airborne imagery acquired by a sensor aboard small-UAV DJI Phantom 4 Pro+ RTK, and
(iii) Satellite imagery acquired by; (a) Sentinel 2, and (b) radar backscatter measurements from ALOS-PALSAR-2, Sentinel-1 and ESA-CCI Biomass Map missions.

Following (Puliti et al., 2018), this study analysed regression relationships to assess accuracy (through validation and calibration) of the EO using the ground-based measurements as reference datasets. Hence, the parametric relationships tested were as follows;

(i) tree-level ground-based (gb) height and airborne canopy height model (CHM),
(ii) tree-level (gb) AGB and airborne based AGB,
(iii) gb fractional cover percentage (FC%) and airborne based FC%,
(iv) gb AGB and airborne based FC%,
(v) gb AGB and ALOS-PALSAR-2 AGB,
(vi) gb AGB and Sentinel-1AGB, and
(vii) gb AGB and ESA CCI Biomass Map data (AGB)

The diagram below (not drawn to scale) represents a schematic illustration of datasets acquired and integrated in this study. It further presents the design (in descending order) on how the remotely sensed datasets (imagery) were analysed and compared, thus using the ground datasets and the UAV imagery as the reference and the link, respectively, in this study.

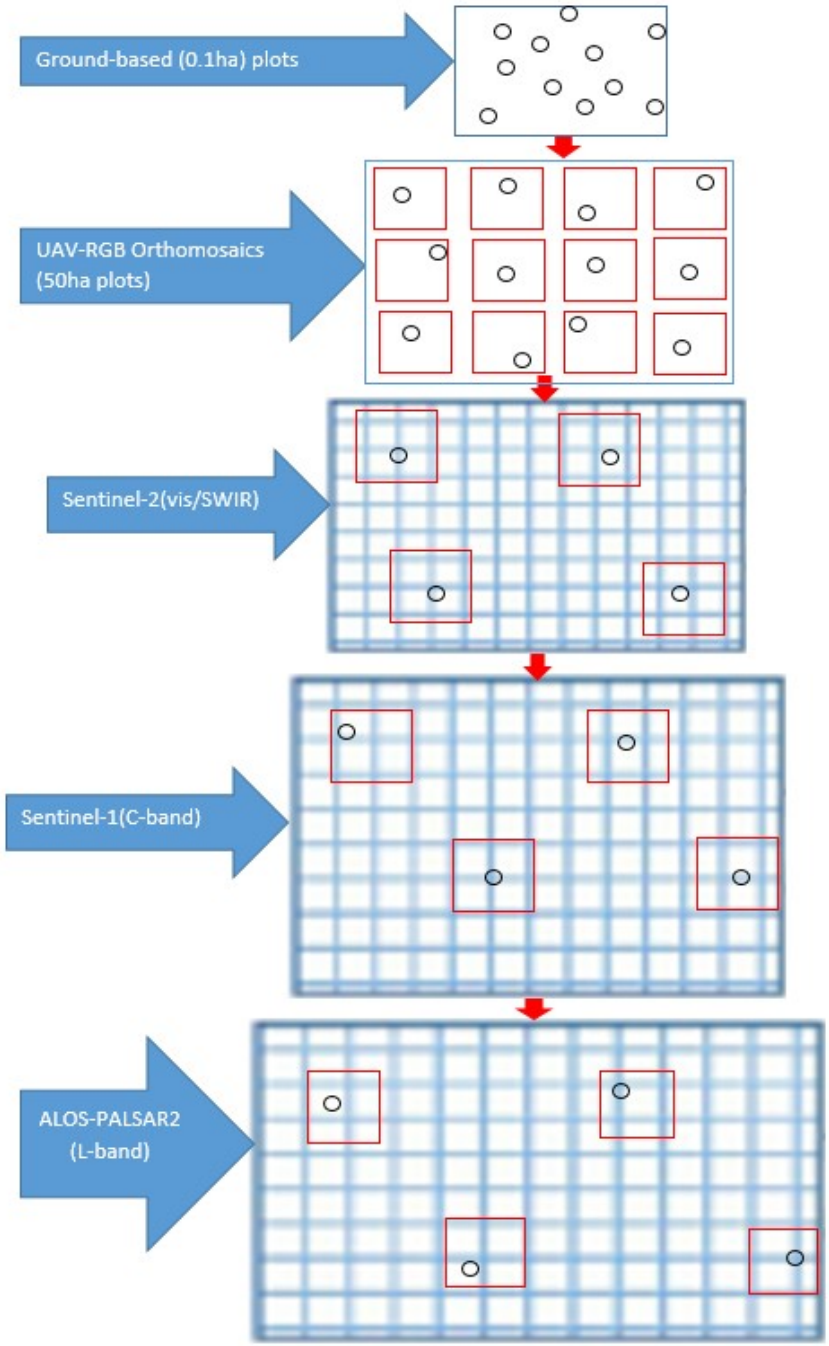

Figure 14. Schematic workflow for study datasets integration-(top-bottom); (i) Ground-based measurements from 0.1ha plots, (ii) Optical airborne imagery of 50ha square plots-(3-7cm pixel

resolution), (iii) Sentinel-2 20m pixel resolution imagery, (iv) Sentinel-1 20m pixel resolution imagery, and (v) ALOS-PALSAR-2 25m pixel resolution.

NB: ESA-CCI Biomass Map datasets have not been displayed in the schematic diagram above because part of them comprise the L- and C- band EO represented by the ALOS-PALSAR and Sentinel-1 missions.

3.2.1 Ground-based sampling design

Individual tree plot-based measurements were collected for a period of five consecutive days, thus from 17-21 September 2019. The study inherited a multi-stage sampling design which integrated random stratified sampling techniques during the 2016 Malawi REDD+ site-based inventory (Government of Malawi, 2019a; USAID PERFORM, 2017). The stratified sampling phase incorporated forest management coupes demarcated to cover all forest management blocks of Ntchisi Forest (Ntchisi District Assembly, 2007; USAID PERFORM, 2017). This was deliberately arranged to allow each of the 13 surrounding villages that holds management stake in Ntchisi Forest management to bear representation in the sampling frame.

This was followed by systematic random sampling whereby sampling unit plots were computed at a minimum spacing of 90meter square grids (network) canvassing the reserve. The network generated a minimum of 13 randomly sampled points that became plot centroids of 20metre radius circles (0.1ha) (Figure 15), sufficient to attain a 95% Confidence Interval (CI) of 95% and a 10% precision error (Pearson et al., 2005; USAID PERFORM, 2017). The 13 points were incorporated as the permanent sample plots centroids for the subsequent inventories, thus considering the REDD+ monitoring that emphasises repeatability of measurements (Chidumayo, 2019; Zerihun and Tesfaye, 2013).

The next figure shows a design of a ground plot-sampling unit used by this study in Ntchisi Forest in 2009.

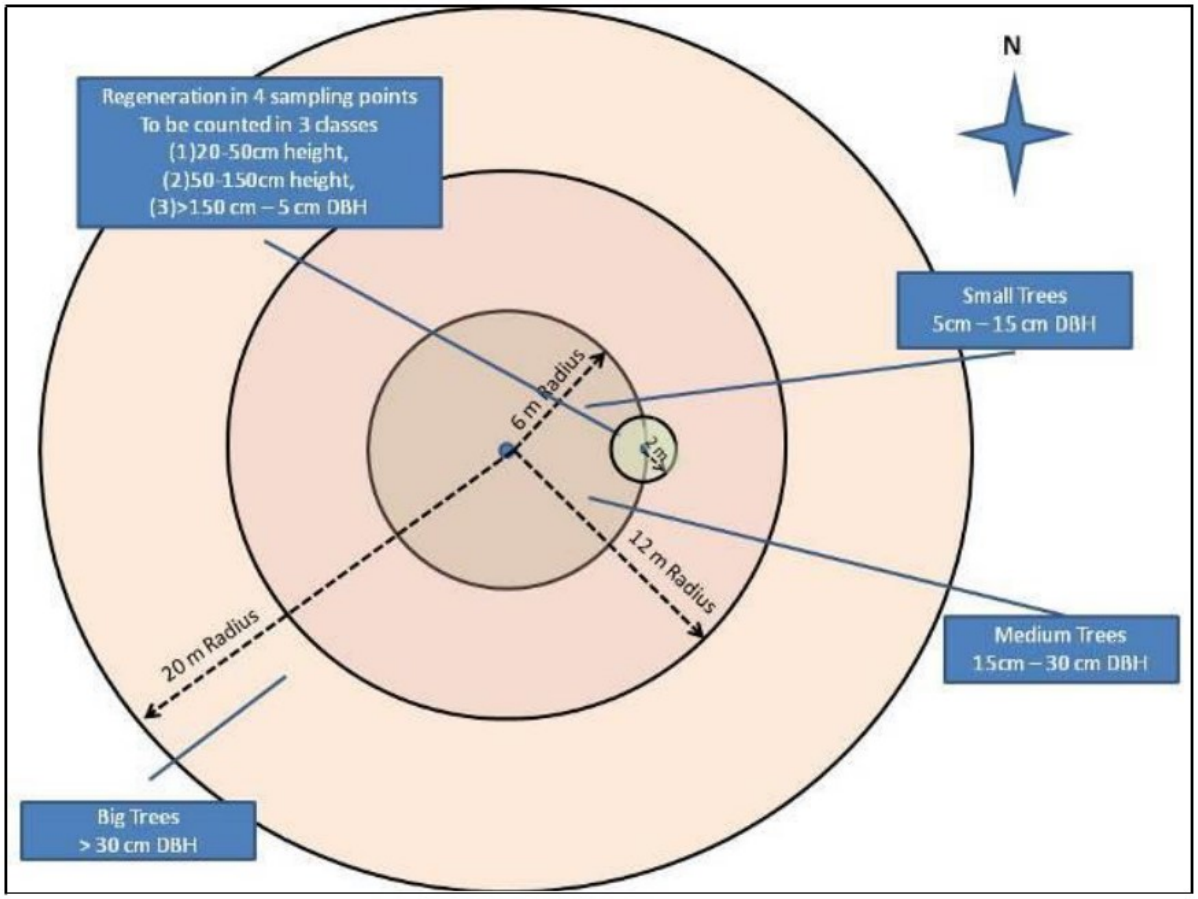

Figure 15. Four fixed concentric circular plot design in permanent sampling units used for ground-based measurements during 2016 and 2019 inventories in Ntchisi: plot cluster radii include, 2m, 6m, 12m and 20m for the regeneration, small, medium and large plots, respectively.

The 2016 REDD+ sponsored inventory of Ntchisi increased sample size from 13 to 18 units to ensure that each village forest management block was represented. However, this academic study maintained the original 13 due to funding limitations and this did not compromise the pre-set CI (95%) and precision error (10%), respectively.

3.2.2 Ground-based measurements

Hand-held Garmin GPSMap 64x receivers set to the projection WGS84 UTM zone 36S were used for plot navigation. A minimum positional accuracy of ±3m or was maintained prior to marking waypoints (recording *xy* position of target features). Using each plot centroid as reference, four fixed concentric circular plots bearing 2m, 6m, 12m and 20m radius each respectively, were laid and inventoried (Figure 15). Plot alignment was achieved using pocket prismatic compasses and adjustable ranging rods. Plot perimeter boundaries were marked using measuring tape and coloured flagging tape and/or chalk.

Individual tree parameters were measured beginning from the plot-centre stretching outward, following the Azimuth direction. Each measured tree was tagged with an identification number (Fig. 5b) that was also captured by inbuilt GPS camera and/or steel camera embedded with GPS function. This was done to ascertain the georeferenced location of each feature attribute. Digital-still images were also taken to depict status of the plots i.e., regenerants, standing trees, lying/leaning trees, deadwood any other attribute deemed important (Figures 5, 17, 41 and 42).

Using a threshold of *dbh* ≥5cm, 216 trees of varied sizes were measured and recorded per each plot (Table 7). Key variables and parameters recorded included; (i) individual diameter at breast height (*dbh*), taken at 1.3m above-ground-using diameter tape, (ii) total tree height (*ht*)–using hypsometer, (iii) crown diameter (*cd*) (*max.* and *min,*)-using measuring tape, (iv) tree and regenerants botanical names, (v) trees *xy* geocoordinates using handheld GPS set, (vi) plot centre geocoordinates (centroids) using handheld GPS set, (vii) Azimuth angle (bearing in degrees) of each tree from the plot centre–using a prismatic compass, and (viii) distance of each tree from the plot centre-using measuring tape (Appendix II).

The next table shows dimensions and threshold of cluster sampling subplot units inventoried in Ntchisi Forest.

Table 7. Dimensions and Threshold for Plot Measurements used in Ntchisi

Subplot	DIMENSION			
	Radius (m)	Area (ha)	Area (m^2)	*dbh* (cm)
Regeneration	2	0.001	12.57	≤5
Small	6	0.011	113.14	5-14.9
Medium	12	0.045	452.57	15-29.9
Large	20	0.126	1257.14	≥30

For each tree measured, its code was documented using a species list catalogue provided by the Forestry Research Institute of Malawi (FRIM). The species were later deciphered to their full botanic names prior to transferring the records into Microsoft Excel data sheets for statistical computing and graphics. These were later uploaded in GenStat (18.1 for Windows) for further modelling and analysis.

The flowchart below depicts key tasks undertaken and parameters measured during the plot-based survey in Ntchisi Forest.

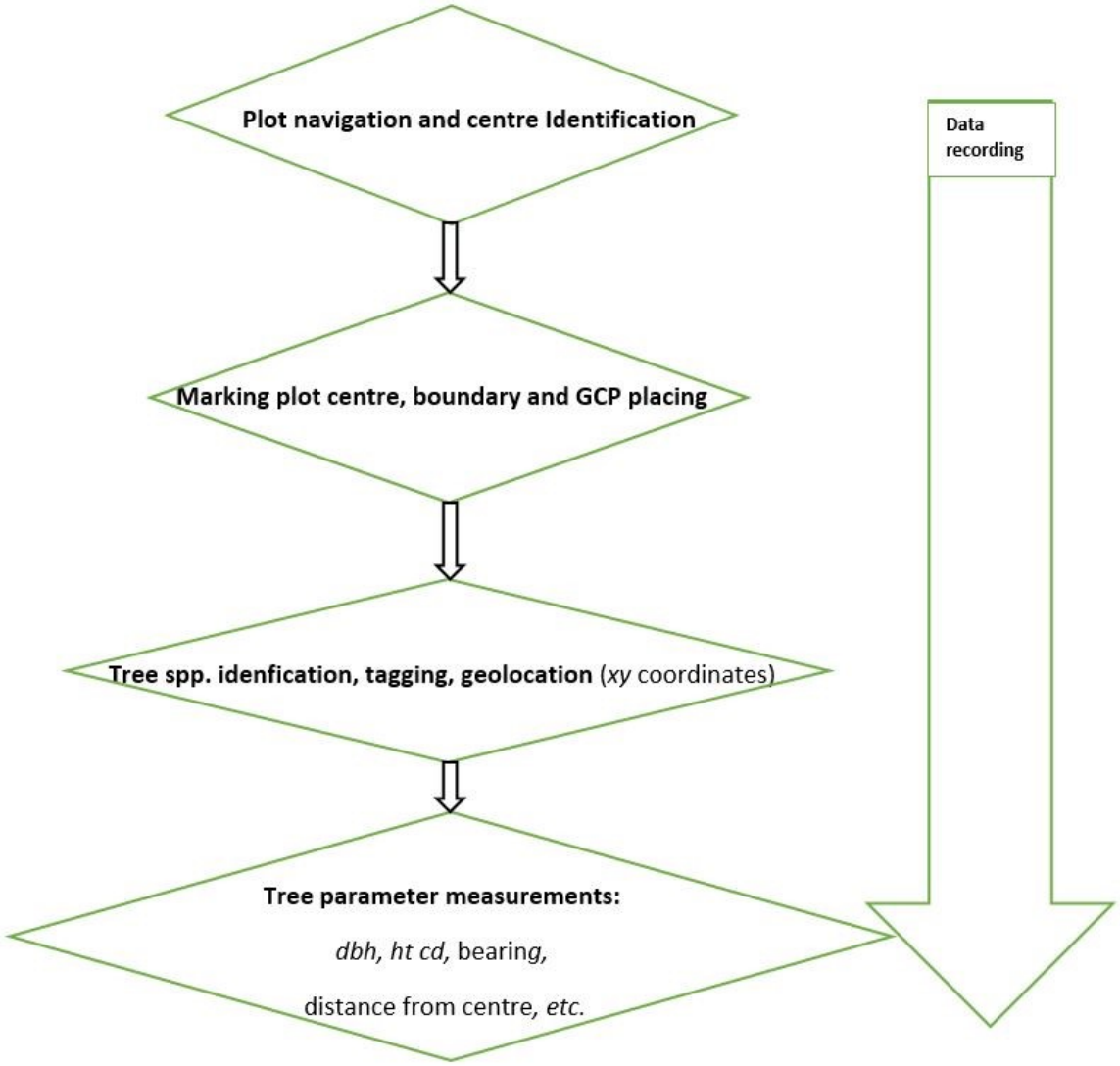

Figure 16. Top-Bottom: Schematic representation of key tasks undertaken, and parameters measured during ground-based inventory in Ntchisi Forest-2019.

3.2.3 AGB computation

Calculation of AGB encompassed all live trees measured in the 20m, 12m and 6m radius plots (Fig.15 and Table 7). The computations covered several stages termed as follows in this report; (i) sampled plot area, (ii) horizontal projection of radii, (iii) area of horizontal eclipse, (iv) scaling factor, and (v) employment of allometry (Government of Malawi, 2019a; Kachamba et al., 2016; USAID PERFORM, 2017).

3.2.3.1 Sampled plot area

This is an initial stage that calculates the dimensional area which is a tree's biomass covers basing on sample plot size and shape. Hence, this involved area calculation of 216 (*n*=216) individual live trees observations whose *dbh* measurements fell within the threshold of ≥5cm and were measured in the sub-plots of 20m,12m and 6m radius. The area of each of the nested sub circular plot was calculated using the following formula:

$A = \pi r^2$, (Equation a)

Where:

A = the area of the nest (circle),

π = pi (3.14), and

r = radius of the nest.

3.2.3.2 Radii horizontal projection and associated assumptions

Measuring of C was premised on the assumption that C pools data i.e., AGB are expressed on the horizontal projection of a land unit area, hence, where plots fall on slope ground adjustments were done to reflect the true horizontal projection (ellipse) (Government of Malawi, 2019a; Skole and Samek, 2016; USAID PERFORM, 2017).

Another assumption was that since ellipses have two radii, the first is parallel to the horizon while the second is parallel to the slope (*ibid*). Therefore, the horizontal projection of the radii lying along the slope was computed using the following formula;

$R_{slope–horizontal} = R_{field} * \cos \theta$ (Equation b)

Where:

$R_{slope–horizontal}$ = projected horizontal length of the radii lying parallel to the slope in the nest, thus measured in meters (m),

R_{field} = radius of the nest, measured in the field (m), and

cos θ = cosine of the slope measured in degrees.

3.2.3.3 Area of horizontal ellipse

As a step further, estimation of area of horizontal ellipse entailed the following calculations:

$NA = \pi * R_{field} * R_{slope-horizontal}$ (Equation C)

Where:

NA = horizontally projected area of a circular nested plot in square meters (m^2),

R_{field} = the radius of the nest measured in the field (m), and

$R_{slope-horizontal}$ = the projected horizontal length of the radii lying parallel to the slope in the nest (m).

3.2.3.4 Scaling factor (SF)

Prior to the calculations, a scaling factor (*SF*) was applied to scale up dimension (area) values for each subplot and convey the estimates of C to a hectare basis (1ha). The step involved conversion of the subplot area's unit measurements in square meters (m^2) to per hectare basis (1ha) as follows.

SF = 10,000/NA, (Equation d)

Where;

SF = *Scaling Factor* to convert per hectare basis (dimensionless),

10,000 = number of square meters (m^2) in one hectare, and

NA= horizontal projected area of nested plot (in m^2).

3.2.3.5 Employment of allometry

This stage involved factoring-in of the AGB allometry. A comprehensive forest biomass study observed that the previous models (pan-tropical) used in Malawi i.e., (Cairns et al., 1997; Chave et al., 2005), were unreliable (underestimated and overestimated) because they were tested using different sites whose conditions do not match Malawi's Miombo Woodlands (Kachamba, 2016). For this reason, this study employed the allometry specifically developed and tested in Malawi's Miombo trees as published by

(Kachamba et al., 2016). For comparison of sake, this research explored the two allometric equations, thus; the one that factors-in *dbh* only (Equation 1) as well as the one that factors both *dbh* and *ht* (Equation 2) (Kachamba, 2016) rounded-off to 3 significant numbers as indicated below;

Equation 1: $AGB = 0.218 \times dbh^{2.32}$

Equation 2: $AGB = 0.104 \times dbh^{1.92} \times ht^{0.845}$

The results obtained after employing the allometry are in the kilogram units of dry matter (kg.d.m.), otherwise referred to as AGB in this case. As a last step, a carbon fraction of 0.47 for all the Miombo tree species measured is multiplied by the AGB to convert the biomass into carbon terms ($tCha^{-1}$) (Government of Malawi, 2019a; Kachamba, 2016; USAID PERFORM, 2017).

3.2.4 Tree crown measurements

While Crown measured in meters (m) as (i) depth (C_{dep}, m), crown radius (C_r, m), and/or (iii) crown diameter (C_d m) remain the main crown dimensions that can be measured in the field, forest studies of AGB in Malawi's Miombo Woodlands mostly focus on C_r and C_d parameters (Government of Malawi, 2019a; USAID PERFORM, 2017). Crown radii are measured in the four cardinal directions (north, south, east and west) or eight (north, north-east, north-west, south, south-east, south-west, east and west) (Loubota Panzou et al., 2020). Such measurements are taken from ground projections of crown edge to stem centre, with the researcher taking the reading/viewing the edge of the canopy standing perpendicular to the line of the bole (*ibid*).

Individual tree crown analyses for this study focused on C_d computed using an ellipsoid formula for each tree whereby two crown measurements were taken perpendicular to each other, thus following the 2016 Ntchisi Forest inventory (Figure 1) (USAID PERFORM, 2017). The C_d parameter is used to estimate crown area (C_a, m^2) which eventually yields canopy percentage cover/density. The crown area is defined as the outermost perimeter (envelope) of the crowns forming part of the upper canopy level (dominant and/or co-dominant stratum) (Gonsamo et al., 2013).

On the hand, crown cover is defined as a physical measurement of the sum of tree crown vertical projection areas divided by the horizontal area of observation unit on which the trees are growing (*ibid*). While the equation for calculating area of a circular plot has been aforementioned, the crown area is estimated by using the formula for the area of an ellipse (π * half of the maximum diameter * half of the diameter at 90°). For clarity's sake, the crown area has been calculated as follows;

$(C_a, m^2) = (\pi x\ C_{r\_NS}\ x\ C_{r\_EW})$

Where; C_a, m^2 = crown area calculated in square metres,

π (pi) = 3.142,

C_{r_NS} = mean of C_r north and C_r South, and

C_{r_ew} = mean of C_r east and C_r west.

Computation of crown cover should be explicit with regards to the within crown gaps and/or the crown overlapping phenomena. In this study, fractional cover percentage was derived from the crown area measured from Ntchisi Forest Reserve. Fractional Cover (FC) simply refers to the proportion of an area in the field/ground that is covered by the crown of trees expressed as percentage of the total area (Zhang et al., 2019). Furthermore, the stand/plot percent canopy cover can be calculated as well and fundamentally, it refers to the percentage of the ground area directly covered by trees (Gonsamo et al., 2013). The fractional cover percentage of each plot, which is calculated as follows;

Fractional cover %= (CA/PA) *100%;

Where CA=crown area per plot,

PA = plot area = 1257m^2 (0.1ha)

3.2.5 Caveats in terrestrial measurements and their mitigation

3.2.7.1 Geolocation errors

The use of handheld GPS receivers (Garmin GPSMap 64x) in marking target feature waypoints i.e., individual trees and plot centroids is affected by positional accuracy.

While this may potentially happen due to poor signal (weak signal strength) during clouds, windy weather or under slightly dense canopy; this source of error was mitigated as follows. First, waypoints of each plot centroid and individual trees were uploaded using the 2016 inventory datasets as *a priori* set up. These were then validated during this academic ground survey navigation and plot identification to ensure that they coincide. As part of the etiquette, the GPS sets were let to attain a minimum of ≤3m accuracy, upon being switched on, thus prior to marking waypoints.

Second, only the Garmin GPSMap 64x brand were used through-out inventory. This ensured that the waypoints and plot boundaries were systematically recorded with minimal error calibrated by the same GPS brand.

In addition, the ground survey ensured that the measurements were conducted in PSPs whose origin and extent were traced by presence of metal bars pegged into the ground during the 2016 inventory. This assisted in locating the origin of the pot centroids as reference points.

3.2.7.2 Overlapping and overhanging trees

Some of the individual trees measured, especially those growing in cohorts showed their overlapping and overhanging attributes (Figure 17), i.e., in Kasakula and Chifwelekete.

Figure 17. Crown overlapping and overhanging of individual trees; rendering difficulties in sighting their tips and crown delineation, consequently affecting height and crown diameter measurements and AGB estimation accuracy.

While the crown overlapping and overhanging of individual trees were localised in highly rugged and sloppy terrains, ground -plot slope adjustment was conducted to mitigate this potential source of error.

3.3 UAV Imagery Acquisition

Digital airborne RGB imagery were acquired using UAV in 4 days, thus from 23-25 September and on 6 October 2019. The survey flight missions were operated on DJI Phantom 4 Pro+ RTK (Real-time Kinematic) quadcopter platform carrying a 1” CMOS SENSOR (2.52µm-1) with a 20 Megapixel resolution (Figure 18).

Figure 18. DJI-Phantom-4 Pro+ quadcopter, turned on in readiness for vertical take-off in Ntchisi Forest. Preference of the drone was due to its vertical take-off/landing (VTOL) capability, suitable for the rough mountainous terrain of the forest reserve.

The UAV, a 2016 release, was manufactured by the Shenzhen DJI Sciences and Technologies Ltd, in Shenzhen City of Guangdong Province in China. The flights were programmed on Map Inner (v3) software. The UAV was hired from Precision Malawi, a local firm based in Lilongwe, the capital city of Malawi.

Its imaging sensor has 5472x3078 pixels fitted to a 3-axis stabilized gimbal to maintain effective imagery acquisition angles. It has an autofocus feature that enabled it to capture still *JPEG* scenes at 3-7cm pixel sensor resolution (Ground Sampling Distance) for this study. The sensor is embedded with a mechanical shutter for controlling light while mounted on the multirotor. The shutter enables the camera

sensor to remove the detrimental 'jello' effect, an attribute that ensures generation of professional images with low noise. In contrast to the fixed wing, the multirotor craft was preferred for easy vertical take-off/landing (VTOL) in the rough mountainous terrain of Ntchisi Forest. The wavelength range of the sensor was 2.4 to 5.8GHz frequency bands, with a maximum controllable range of 4.3miles (~7km).

Image acquisition involved 13 flight missions of ~50ha square boxes (0.71km x 0.71km) sampled following the 13 randomly distributed terrestrial plots design that employed the multi-stage sampling approach (stratified and random techniques) explained earlier. This ensured that the UAV flight boxes, otherwise referred to as UAV plots overlaid the terrestrial plot centroids to enhance geo-spatial referencing (Fig. 22, 23 and 24), thus following (Puliti et al., 2018). Hence, at each of the 13 terrestrial plot centroids, corresponding ground control points (GCPs) were placed, and their respective waypoints marked using handheld GPS sets (Garmin GPSMap 64x), (Fig. 19). The imagery was acquired in WGS84 (EPSG: 4326) projection, at a flying altitudinal range of 120-150m above-ground-level (AGL). Detailed key flight settings have been depicted in (Table 8, below).

Table 8. Key Settings for Unmanned Aerial Vehicle Flight Surveys in Ntchisi Forest- 2019

UAV Make	Sensor Type	GSD	Flights Day [1]	Images plot [1] (mean)	Flight Endurance (min)	Flight Altitude AGL (m)	Wind Speed Resistance (m.s [1])	On-board GPS Accuracy (m)	Front and End Overlaps
DJI-Phantom-4 Pro+ Quadcopter	1" 20-Megapixel CMOS	3-7cm	2-3	338	20	120-150	20 Knots	5-6	83% (front) 84% (end)
	With mechanical shutter	Terrain dependent	Access & weather dependent		Weather dependent	Terrain dependent	Max.	RTK	Terrain dependent

The GCPs constituted square plywood panels painted by 4 equal alternating black and white sections (like chessboard) deliberately painted to enhance visibility. Hence, as the GCPs geolocations (xy-coordinates) were also recorded on-board GPS using the RTK system, their positions got validated during the visual inspection of the rectified orthomosaics.

The figure below demonstrates the mounting of the GCPs that were used as original points of reference especially for the airborne flight survey.

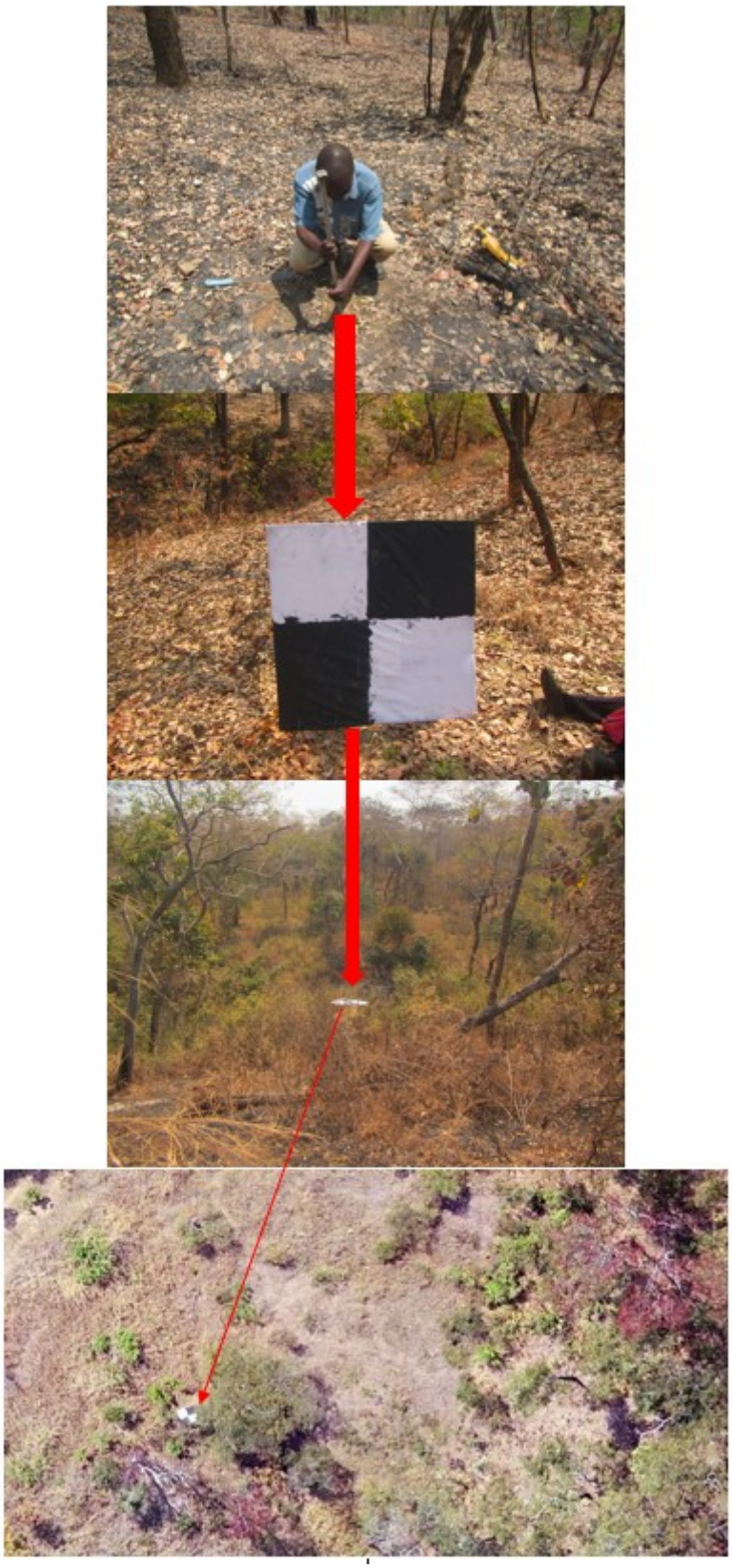

Figure 19. GCP used as the original point of reference in ground-based and airborne surveys; Top-Bottom; (i) marking of ground-plot centroid for the GCP, (ii) outlook of GCP board, ready to be placed on the ground plot-centre, (iii) GCP placed on ground-plot centre, and (iii) GCP located in an aerial orthomosaic.

In a survey, the use of GCPs and Differential Global Positioning System (DGPS) or Global Navigation Satellite System (GNSS) portable base stations enhance global/absolute positional accuracy of the target ground features. Position accuracy in navigation refers to a degree of conformance between the estimated or measured position and its true position (Specht, 2021). Nevertheless, due to cost limitations it was not affordable for this academic study to hire a portable DGPS or GNSS base station. Section 3.3.5 details how this challenge was mitigated.

3.3.1 Generic S*f*M photogrammetry

Acquisition and processing of the airborne data covering Ntchisi Forest Reserve involved Structure-*from*-Motion (S*f*M) photogrammetry. The technique borrows its basic principle from conventional stereoscopic photogrammetry in that it also involves resolving of 3D structure from a series of overlapping offset-images captured from a camera sensor to form a scene (Fig. 20-left) (Westoby et al., 2012). Nevertheless, S*f*M differs from the traditional system in that scene geometry, camera positions and orientation of the camera are automatically resolved; thus, without the need to specify, but uses an algorithm (*a priori*) which constitutes a network of targets having known 3D positions (*ibid*).

While a stereoscope uses a single stereo pair of photographs to construct a 3D position (height), the S*f*M technique employs multiple overlapping photographs as input into feature extraction besides the reconstruction algorithms. S*f*M engages an algorithm that estimates height structural model of a scene from overlapping two-dimensional (2D) image sequences taken from various locations and orientations above the focused scene (Westoby et al., 2012).

During SfM photogrammetric process, scene geometry, camera positions and orientation are resolved simultaneously using highly redundant, iterative bundle adjustments procedure (Chu et al., 2018; Westoby et al., 2012). The resolution is based on features' database automatically extracted from a set of multiple overlapping images. Hence, by employing S*f*M, the UAV-extracted canopy height is usually determined by means of canopy height models (CHM) obtained from the point-cloud data (Chu et al., 2018). The next illustration shows a DJI-Phantom-4 Pro UAV and the S*f*M Photogrammetry technique.

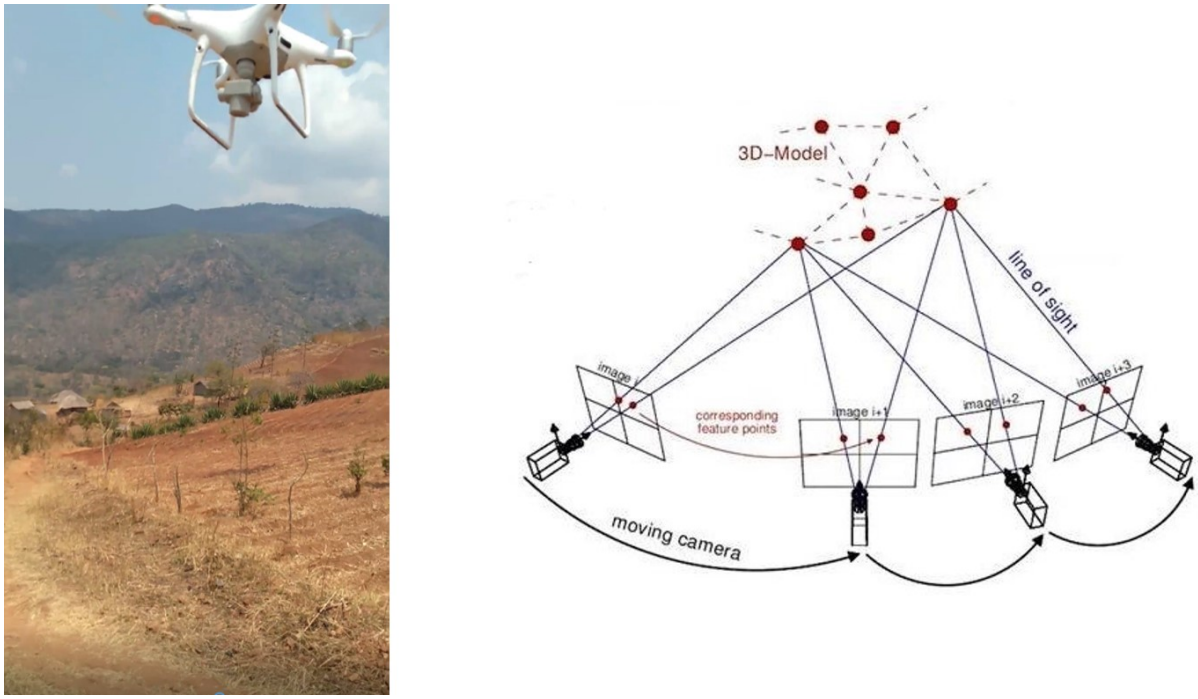

Figure 20. (Left)- DJI-Phantom-4 Pro UAV with camera sensor mounted on a gimbal, imaging at nadir angle; vertical take-off to Msankhire plot (P3) flight mission in Ntchisi Mountain Forest; (Right)-Structure-*from*-Motion (S*f*M) Photogrammetry technique showing a moving camera acquiring overlapping images from different perspectives that are used to construct a third dimensional (3D) model.

Source: (i) DJI-Phantom-4 Pro UAV-Author's own captured during in Ntchisi (2019), (ii) S*f*M principle-*theia-sfm.org* (2016).

3.3.2 Ntchisi Forest UAV image processing

The airborne observations acquired were processed in Agisoft Metashape Professional 1.4 (Table 9) using SfM photogrammetry technique under four main stages, *vis-à-vis*; photo alignment, point-cloud building, generation of mesh and building of orthomosaics (Table 9), as follows. The initial step involved photo-configuration whereby the software algorithmically searched common points on the photographs prior to matching them. This entailed finding positions of the camera for each picture (i.e., Fig. 20-left) and refining camera calibration parameters.

The second step involved building point-clouds and this required generation of data points that had matched. For this study, the point-clouds were classified into ground and vegetation feature classes because the prime interest was to separate the height of tree vegetation (canopy height) from the ground level layer.

The subsequent phase ensured exportation of the point-clouds to yield bare earth ground level input referred to as Digital Terrain Model (DTM), which is also a product of Digital Elevation Model (DEM). Using the exported material, a surface mesh called Digital Surface Model (DSM), was generated in a process otherwise termed as mesh building.

The fourth stage involved generation of orthomosaics, which basically cascades the merging of geometrically rectified (aligned) photos into a large composition structure representing a 3D scene.

The table below presents a brief chronological flow of the main tasks and parameter settings involved during S*f*M photogrammetric image processing undertaken for this research.

Table 9. Main Steps and Parameter Settings Employed during S*f*M Photogrammetry.

Task	Parameter
Align Photos	Accuracy: High Projection Type: Geographic WGS84 (EPSG:4326) Pair selection: Generic Preselection Reference preselection: Source Key Points Limit: 40,000 Tie points:4,000
Build Dense	Quality: High Depth Filtering: Moderate
Build Mesh	Source Detail: Dense cloud Surface Type: Arbitrary (3D) Quality face count: High Interpolation: Enabled Select Point Classes:
Build DEM	Source data: Dense cloud Interpolation: Enabled Surface Type: Arbitrary (3D) Quality face count: High Select Point classes: Ground
Build Orthomosaic	Surface: DEM Blending Mode: Mosaic Hole filling: Enabled

The relative absolute height values of the resulting dense point-clouds were normalised using the DTM obtained from the orthophotos. Optical RGB spectral band information was used to generate 3D outputs in *JPEG* format and as an ultimate step,

while the outputs (orthomosaics, DSM, DTM and CHM) were converted into *Tiff* for further analysis and interpretation.

3.3.3 Canopy Height Model generation and extraction

Application of an algorithm for each plot's 3D point-cloud data was set to conduct a geographic analysis that filtered DTM mesh from corresponding DSM structure in ArcMap (10.8.1) software. The process engaged the Map-Algebra function of the Spatial Analysis Tool, whereby each DTM mesh was mathematically subtracted from DSM using an Algebraic Boolean expression in the Raster Calculator. This yielded a preliminary CHM layer with values of different vegetation strata growing on the ground i.e., grass, shrubs, herbs and trees, etc. Since the minimum height of all the trees measured during ground-measurement was 2m, this was set as a threshold condition (i.e., >=2) for filtering the preliminary CHM of trees from lower vegetation.

The variables for determining canopy height included maximum and median values. These were interpolated to a regular grid corresponding to DSM. Extraction of such values was conducted by overlaying point shapefile layers containing *xy* geocoordinates of individual trees measured during plot-based survey, but identified and geo-located on the UAV orthomosaics of each plot in ArcMap software. The GCPs, as previously mentioned, were the reference points for any target feature for geo-rectification purposes.

For each DTM generated, extract-variables were derived describing plot-level canopy height in GeoTiff. These included, but were not limited to, maximum and mean values, standard deviation coefficient of variation, kurtosis, skewness, and percentiles. The values extracted from the CHM were later used for determining parameter relationships i.e., height, crown cover as well as predicting AGB, and C stocks for the reserve.

3.3.4 Canopy cover generation and extraction

UAV crown cover based on pixels from the CHM were separately computed for canopy cover percentage on a 20m radius scale, thus using crown diameter data from the 13 ground-based plots as reference data. The process involved overlaying 20m radius ground-sample plot layers onto the CHM point clouds layer in ArcGIS 10.8.1 software.

This ensured that the airborne CHM datasets were extracted and calibrated from the exact positions of the ground-plots. The purpose was to determine whether the optical airborne datasets (at the 3-7cm resolution) could be employed to identify the geo-locations of the individual trees as an initial step prior to estimating AGB, respective of objective 1 of this study.

The initial task involved visual inspection of correct *xy* geo-locations (coinciding) of the point clouds and ground-based tree locations using the RGB orthomosaics while using GCPs as reference points. During the process, buffer layers of 20m radii were created using the GCPs waypoints as centroids. Using the 'Extract by Mask' function under the Spatial Analyst Tools of in ArcMap, forest cover/canopy pixels values depicting the proportional coverage of crown covered and non-covered areas were extracted from the CHM.

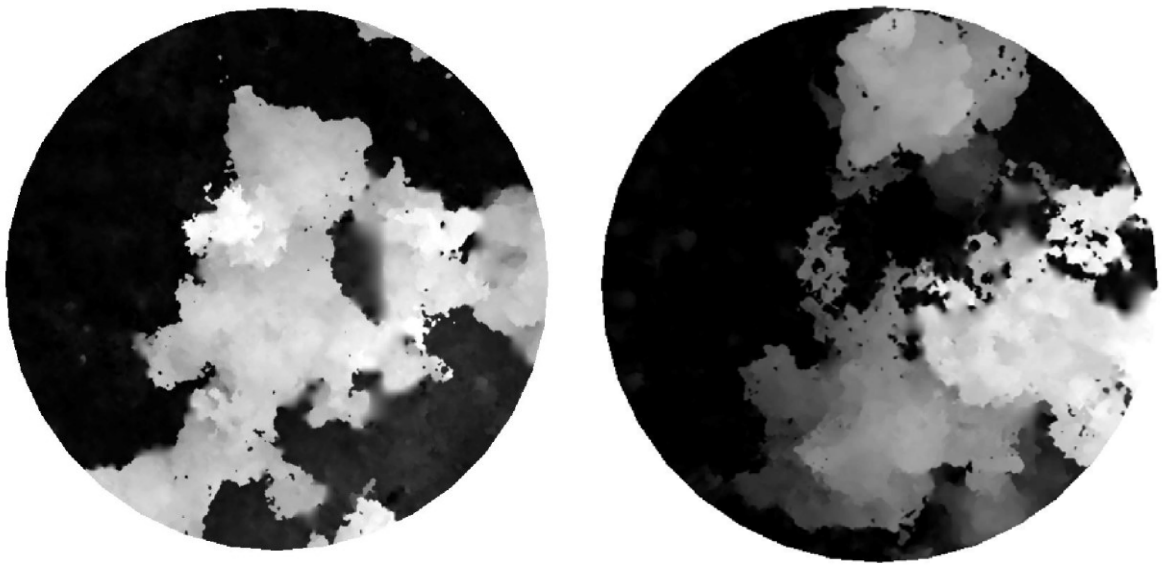

Figure 21. CHM point-clouds in greyscale; for P9 (left) and P11 (right) of Ntchisi Forest Reserve 20m radius ground-plot scale at ≥2m threshold. White colour denotes canopy cover while black denotes low or no canopy cover.

Source:(Kadzuwa and Missanjo, 2022b)

The pixel values extracted from the point-clouds were exported to Microsoft Excel 2016, and finally to GenStat 18.1 where they were tested against the ground-based measurements for their relationship using co-efficient of determination (R^2) and Root Mean Square Error (RMSE).

3.3.5 Caveats in airborne observations and their mitigation

The following were the key caveats and/or sources of error associated with the airborne observations; (i) phenology and seasonality changes, (ii) position error, and (iii) wind-speed upsurge.

3.3.5.1 Phenology and seasonality challenges

The airborne imagery acquisition was initially scheduled for the period between April and July 2019 in Malawi. This was the timing when the rains had just stopped and more importantly, the Miombo trees had leaves-on, thus for ideal signal detection using optical sensors (Figure 5) (Chidumayo, 2015, 1997; Kadzuwa and Missanjo, 2022b; Kamusoko et al., 2014). Unfortunately, this was affected by the countrywide protests of the Malawi 2019 Tripartite Elections results. This resulted to shifting the exercise to September and October 2019, unluckily, when some tree species lost their leaves (leaf-off season) due to trees morphological response to dry season (Figure 5) (Chidumayo, 1997). This partly affected the spectral as well as structural detection of tree biomass as the branches and crowns were not properly resolved in the UAV imagery. Consequently, it yielded uncertainties as noted during extraction of CHM whereby some low and null values were generated from trees that lost leaves, i.e., Plots P1, P2 and P6, *inter alia,* and to a significant extent, affected parametric data correlational observations.

While the most obvious remedy would have been re-surveying the forest in the next immediate leaf-on window, thus April-May 2020, this option was not feasible, unfortunately, due to funding constraints. It could not have materialised either due to the global lockdown conditions imposed to curtail the spread of Covid-19 pandemic, which resulted to a ban on both local and international travels in 2020.

Nevertheless, the errors were partly offset technically, thus by running a median (low pass) filter over the CHM, from which maximum height values were extracted within a 5x5 kernel (window size) which is regarded optimal for minimising local variation (Lindsay et al., 2019; Reitz et al., 2022).

Again, as explained in section 3.3.3 (Algebraic Boolean expression applied in the Raster Calculator thus under CHM generation and extraction), the setting of ≥2 metres

threshold (as the minimum height) for the CHM also contributed to addressing this error. The threshold was determined based on the current (2019) gb data as well as the previous (2016) inventory conducted in the same forest whereby 2m was the average minimum height of all the individual trees sampled. The threshold filtered out the understory vegetation (i.e., the herbs, shrubs, and grasses) inter-spaced with the Miombo trees (Figure 5) and enhanced accuracy of the estimates.

3.3.5.2 Morphological and anthropogenic challenges

Akin to the gb measurements, some trees displayed overlapping and overhanging patterns which rendered difficulties in delineating their individual crowns and consequently their *xy* locations. This affected the accuracy of their AGB calculation. Research on Subtropical tree-species classification using airborne and Lidar data observed that overlapping of adjacent canopy affected accuracy of estimated individual crown diameter and tree height (Shen and Cao, 2017).

In addition, the (i) thorny and leafless nature of some *Acacia* species dominant in P1 and P2, (Fig. 51), and (ii) forest fire that scorched the same plots rendered difficulties in interpreting and comparing of canopy and biomass of these two datasets (Fig. 42). This was due to the contribution of both attributes to the reduction of leaf surface area and greenness of the targets features (trees) which consequently affected the spectral and structural detection of tree leaves and crowns that constitute biomass.

Similarly, these morphological errors were compensated by running the low-pass filter which is renowned for reducing local variation (Lindsay et al., 2019).

3.3.5.3 Position accuracy

Since no base station DGPS/GNSS was employed, as aforementioned, the positional accuracy was affected. This was mitigated using the original coordinates recorded the 2016 terrestrial inventory *(a priori* values) as reference *xy* points in relation to those recorded in the airborne imagery acquired by the RTK–GPS aboard the UAV. This involved the identification 2016 permanent sample plot centroids that were monumented with a metal bar and validating their coordinates. The centre of each GCP was deliberately coincided with the ground plots centroid for easy identification as well as for geo-referencing purposes.

Mitigation of the positional error process involved calculating the average of the 2016 and the incumbent 2019 inventory (with predictable accuracy) of the plot centroids and tree positions acquired by the Garmin GPSMap64x handheld receivers in the permanent sample plots. To this effect, a generic spatial horizontal geolocation uncertainty of ±13m (positional accuracy) was observed throughout the imagery. This was mitigated by adjusting the imagery using the ground-plot centroid GCPs in ArcMap 10.8.1 software

3.3.5.4 Terrain and viewing angle

Airborne studies noted that aircraft position and orientation may result to error in measurements, thus in addition to the flying height above ground level (AGL) (Booysen et al., 2021; McKee et al., 2019). The mountainous landscape of Ntchisi which has a varied altitudinal plot range, estimated between 600-1720m (*asl*) rendered this artefact inevitable for the DJI-Phantom-4 UAV sensor used.

A key study exploring optimisation of GCPs and Independent Control Points (ICPs) on rectification of high-resolution satellite imagery observed that the former are required for geometric correction of x and y positions to improve the overall image during ortho-rectification (Hariyanto et al., 2019). In this respect, the terrain and viewing angle errors encountered in UAV imagery were mitigated by adjusting the images using the GPCs (with validated xy coordinates) placed at the centroids of permanent sample plots as reference points.

3.3.5.5 Wind speed upsurge

The eastern part and coincidentally the (windward) side of Ntchisi Forest is just ~25km away from Lake Malawi (Figure.12). This attribute exposes the forest to the effects of the South-easterly winds, locally known as ‘Mwera’ that blow over the lake to the mainland (Magrath and Sukali, 2009; Streefkerk et al., 2022). The winds are high with prevailing velocity known to cause property damage, especially to fishing boats and vegetation in Malawi (*ibid*).

During the flight missions covering Plots 8 and 3 (P8 and P3), the survey was challenged by the sharp rise of the Southeasterly wind. The UAV wind speed sharply peaked beyond the expected maximum of 10.4 $m.s^{-1}$ thus to 13.1 $m.s^{-1}$. Such an

upsurge affected image capture by rendering temporary *xy* positional shifts of tree crown-point features that form the canopy height. This resulted to poor structure detection (of the maximum and lower limits of the crown) as detected by RGB camera sensor aboard the UAV. The shifts affected the combination sets of pixel values of features in the overlapping images, which would have become tie-points captured during S*f*M photogrammetric process as observed by several key studies (J. Chen et al., 2022; Uyttendaele et al., 2001; Westoby et al., 2012). As a result, the would-be tie-points became slightly different in each image, thereby rendering each scene entirely different while forming a pattern of trees that is either redundant or wrongly located on the orthomosaics.

A tropical forest study where optical and Lidar UAV airborne surveys were contrasted, observed that increasing the front and side-overlap in the imagery to 80%–85% (e.g., by increasing altitude, and/or flying slower), potentially improves results of estimations (McNicol et al., 2021). In this regard, this problem was also resolved in 2-fold for this study; first, the flight height was increased from 120m to 150m AGL and this automatically adjusted camera front and side overlaps, thus from within the range of 70-72% and 83-84%, respectively. This improved the tie-point resolution.

Second, the persisting tie-point challenges were resolved by stitching of the scenes which was done by the Precise Company in Lilongwe, Malawi.

3.4 Satellite Imagery Acquisition and Key Properties Considered

This study acquired 2019 radar backscatter measurements from ALOS-2-PALSAR-2 and Sentinel-1-C-band and optical imagery from Sentinel-2 covering Ntchisi Forest Reserve, thus in addition to the ground-based measurements and the UAV orthomosaics. While the specific details have been elaborated separately in the subsequent sections, thus under each mission, the table below provides an overview of the key specifications of the satellite imagery employed.

Table 10. Primary Specifications of Acquired Satellite Imagery Used

Satellite	Acquisition Date/ Scene ID	Res.	Level	EMS Band	Spectral/ Polarisation
ALOS-2PALSAR-2	S13E033_19, S13E034_19	25m		L	HH+HV
Sentinel-1	12-04-2019, 28-10-2019	20m	L1-GRD	C	VV+VH
Sentinel-2A	28-07-2019, 31-10-2019	20m	L2	VIS, NIR SWIR,	-

Source: Japanese Aerospace Exploration Agency and Sentinel Hub EO Browser (powered by European Space Agency-ESA). Key: Res. =Resolution, EMS= Electromagnetic Spectrum.

For the radar backscatter EO, this study considered their SAR sensor properties that may lead to geometric distortions due to the nature of their oblique angle of observation (side-looking), inherent attributes in all radar systems (Meyer, 2019; Woodhouse, 2006). These distortions have been categorised as; (i) foreshortening, (ii) layover, and (iii) shadowing (*ibid*).

Under foreshortening condition, the SAR sensor facing slopes of the features under observation appear closer to the sensor as they diverge significantly from the surface onto which their slant range are projected (Woodhouse, 2006). In the case of a symmetric mountain, for instance, it would seem to be leaning towards the sensor in the radar image. While the extent of foreshortening depends on both the system's look angle and on the object's slope angle, its effects decrease with increasing look angle the target (Meyer, 2019).

On the other hand, layover can be exemplified as being related to foreshortening in the way that its condition occurs in areas where the slope angle is greater than the look angle (Meyer, 2019; Woodhouse, 2006). Foreshortening may turn into layover e.g., in areas of steep slopes combined with steep incidence angles. This can result to the tops of mountains being imaged ahead of their base while backscatter from mountains may overlay with image information at closer and farther image ranges. Similarly, layer over can also be compensated if the look angle is increased (*ibid*).

The shadow distortion condition occurs when the look angle is comparatively greater (than 90^0 in the direction away from the instrument) to the extent that areas behind the target such as a mountain cannot be seen by the sensor. Shadowing is more of a factor of local slope in relation to the imaging geometry as opposed to the absolute

height. Alternatively, radar image shadows can be described in principle as completely black and sharply defined since they correspond to areas where there is a complete lack of received information (Woodhouse, 2006). The shadow effects increase with increasing look angle, and they correspond to the region that lies behind objects in the imaged scene from which there is no return echo (backscatter/radar silence area) (*ibid*).

Even though the major advantage of the ALOS-2-PALSAR-2 and the Sentinel-2 2019 EO used in this study is that they were already orthorectified at the time of their acquisition, research has revealed that topography–related image distortions cannot be entirely removed (Meyer, 2019). Their geometric distortions effect over Ntchisi Forest which is a mountainous cannot be completely overruled, hence; these have been highlighted under the results and discussions of this report.

As the SARs transmit microwave signals at an oblique angle, they measure the backscattered portion (in the direction of the sensor) of the signals to analyse features on the surface (Woodhouse, 2006). In this regard, the choice of the SAR sensors for this study also considered the scene parameters that affect radar backscatter (cross-section) measurements indispensable to analysing features on the surface. Radar backscatter intensity is primarily, but not exclusively affected by the following parameters;

i. surface roughness - determines how much energy is directed back to the sensor,
ii. dielectric constant (surface moisture) - of the imaged object guides whether how deep signals may penetrate scattering surface,
iii. wavelength (influence of frequency) - determines how deep the energy can penetrate an object target,
iv. signal polarisation - describes the orientation of the plane of oscillation of a propagation signal that effects the brightness of the image, and
v. incidence radiation angle- the angle between a ray incident on a surface and the line perpendicular to the surface at the point of incidence called the normal (Brolly and Woodhouse, 2012; Cutler et al., 2012; Ryan et al., 2012; Woodhouse, 2006). The individual effect and interplay of these parameters has also been covered under the results and discussions of this research report.

The table below displays some of the important technical details of space-borne SAR sensor considered prior to imagery data acquisition. These were reviewed for consideration under this study due to their unrestricted accessibility (for non-commercial use).

Table 11. Key Details of Some Significant Space-borne SAR Missions Providing Unrestricted Imagery

Sensor	Lifetime	Band/Wavelength & Frequency	Polarization	Resolution	Repeat cycle (days)
ALOS-1	2006-2011	L-band λ =24.6cm	FBS: HH, VV FBD: HH/HV, HH/VH PLR: HH/HV/VH/VV ScanSAR: HH, VV	FBS:10x10m FBD:20x10m PLR:30x10m ScanSAR:100m	46
SENTINEL-1	2014	C-band λ = 05.6cm	Single: HH, VV Dual: HH/HV, VV/VH	Stripmap: 5x5m IW: 5x20m EW: 20-40m	Satellite:12 Constellation: 6
ALOS-2 PALSAR-2	2014	L-band λ =24.6cm	Single: HH, VV, HV, VH Dual: HH/HV, VV/VH Quad: HH/HV/VH/VV	Spotlight: 1x3m Stripmap:3-10m ScanSAR:25-100m	14
ESA CCI BIOMASS MAP (3rd version)	2018	L-band λ =24.6cm (for Alos-Palsar)	WB	100mx100m (Resampled)	46 (for Alos-Palsar)
SEASAT	1978	L-band λ =24.6cm	HH	Az:25m; Rg:25m	

Source:(Meyer, 2019). **Key**: IW=Interferometric Wide Swath, EW=Extra Wide Swath, H= Horizontal, V=Vertical, Az=Azimuth, Rg=Range, WB=Wide Beam

3.4.1 ALOS-2 PALSAR-2 radar backscatter measurements

Two scenes of ALOS-2-PALSAR-2 2019 Forest/non-forest radar backscatter Ground Range Detected (GRD) dual-polarised horizontal-horizontal (HH) and horizontal-vertical (HV) mosaic datasets were acquired from the Japan Aerospace Exploration Agency link (*https://www.eorc.jaxa.jp/ALOS/en/palsar_fnf/data/2019/html2/download.htm*) covering Ntchisi Forest Reserve. They were accessed on 7th April 2021, and they comprise; (i) S13E033_19, and (ii) S13E034_19 which are both Fine Beam, mode #2 Dual polarisation Ascending pass Right-Looking-2019 (F02DAR) tiles. Their cell size (spatial/pixel resolution) is 25m x 25m. These datasets were created by mosaicking SAR images in backscattering coefficients with the same pixel resolution.

Apart from unrestricted access, employment of the ALOS-2 PALSAR-2 EO for this study was based on the ability of its SAR sensor to operate in the long wavelength's region (L-band, λ=23 cm). This attribute enables its signal to penetrate through forest canopies. The other advantage is that the PALSAR sensor operates regardless of cloud condition. These SAR aspects fit quite well in this Tropical Miombo Woodlands study of the Sothern Africa, whose trees are broadleaved, thus requiring long wavelength of radar energy to be detected. Besides, Malawi lies within a region where cloud cover is common (Phiri and Nyirenda, 2022), thereby requiring EO that are not highly affected the cloud condition.

These HH+HV cross-polarisations were preferred to VV because the correlation of biomass and backscatter is usually better for longer wavelengths i.e., (L-band) and for cross-polarised measurements since the latter's response is dominated by the canopy contribution rather than the surface component (Woodhouse, 2006). Primarily, these ALOS-2 PALSAR-2 images rendered the advantage of having their geometric distortions and topographic effects already corrected, to some extent, thus during their acquisition.

In addition, the deeper canopy penetration attribute renders L-band (~23 cm wavelength) SAR imagery sensitive enough to forest biomass and eventually detect deforestation, besides being less affected by soil conditions when compared to shorter wavelengths (Woodhouse, 2006). The appropriateness of the ALOS-2 PALSAR-2 (L-band) imagery for Ntchisi Forest Reserve lies in the fact that the Miombo trees (of Ntchisi Forest, the study site inclusive) are broad-leaved and therefore become the suitable target feature for the ALOS-PALSAR signals.

The acquisition period of the ALOS-PALSAR datasets used for this study was deliberately timed together with the collection of ground reference data and the airborne orthomosaics over the same study site, thus September to October 2019. The matching of the temporal resolution of the datasets was intended to optimise comparability and render significant interpretation.

Vegetation studies have discouraged the use of single-date satellite imagery (one period datasets) on the basis that they fail to capture dynamic vegetation changes in the ecosystem (Kamusoko et al., 2014; Kellndorfer et al., 2014; Woodhouse, 2006).

Inversely, two-time periods datasets (dry and wet season) are recommended for meaningful comparisons and interpretation due to their seasonal and phenological changes (*ibid*). On the contrary, this did not hold for ALOS-PALSAR-2 datasets in this study because their temporal resolution is one year. Apart from being relatively less affected by the weather conditions, the use of these single date SAR backscatter measurements has been compensated by incorporating two-time periods of wet and dry season EO from Sentinel 1 and 2.

3.4.2 ALOS-PALSAR imagery pre-processing

The Ntchisi Forest Reserve perimeter boundary vector dataset was acquired from the Surveys Department of Malawi as a shapefile layer that defines the study area. This was followed by re-projection of all the data-layers to GCS_WGS_1984 (Datum: D_WGS_1984) which was the original coordinate system for the ALOS-PALSAR and Sentinel datasets.

The subsequent step involved inspecting the overlay and data interoperability of the data layers conducted in QGIS (3.10) software. This was followed by clipping of the 13 plot boxes using 50ha UAV airborne plots as the dimension scale.

Below is a map depicting the ALOS-PALSAR radar backscatter measurements sampling plot-unit distribution over Ntchisi Forest.

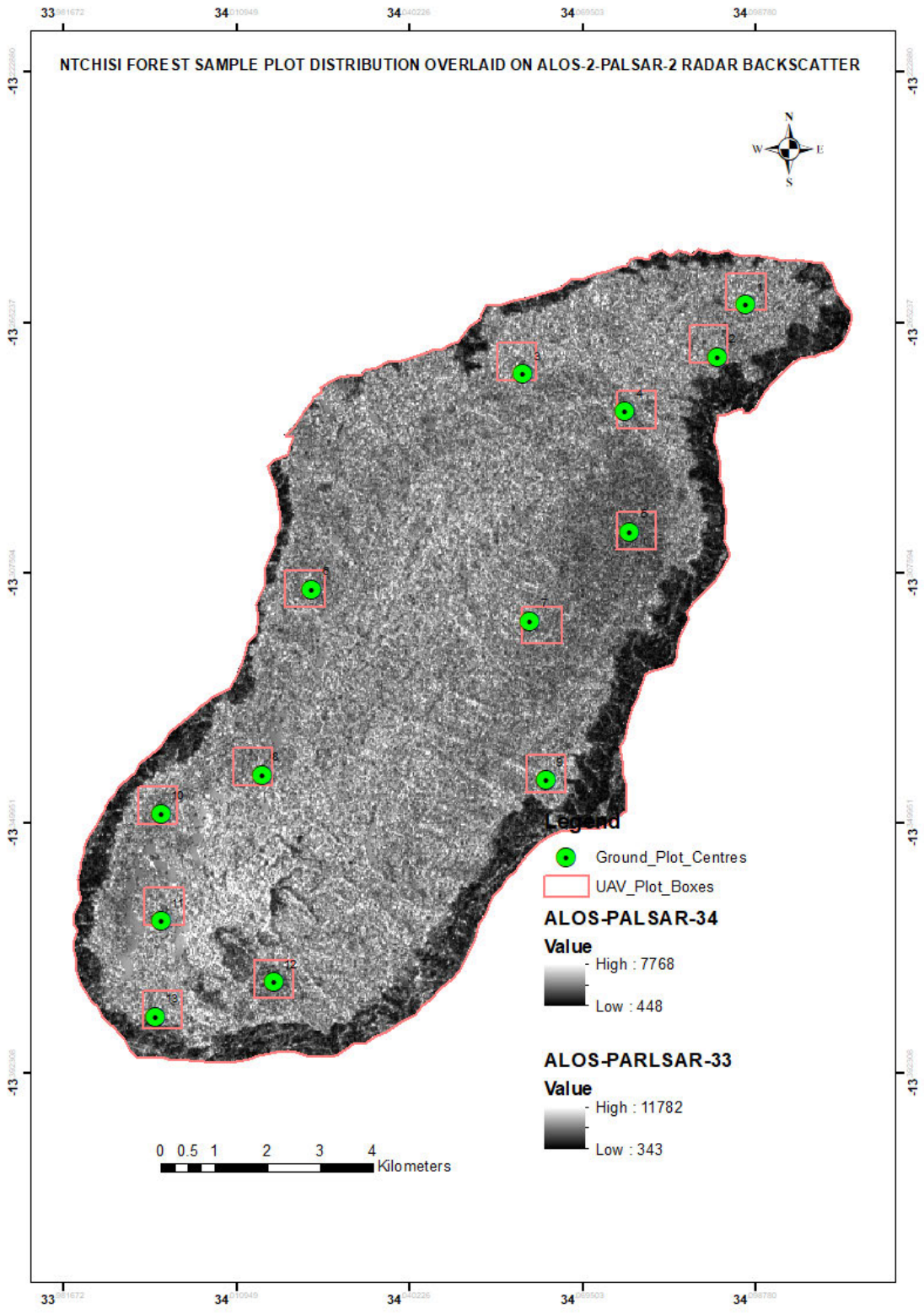

Figure 22. Ntchisi Forest Reserve sampling plot unit distribution for ALOS-PALSAR. Two separate imagery scenes (ALOS-PALSAR-33 and 43 with digital number values ranges of 343-11782 and 446-7768 respectively) were required to cover Ntchisi Forest. Low reflectance (deep gray) on the forest edge in contrast to high reflectance in the interior characterising deforestation and forest cover, respectively. Big squares represent UAV 50ha (0.71km X0.71km) plot boxes overlaid on ALOS-2 PALSAR-2 (L-band) imagery while the green circles (inset), represent ground plots (20cm radius) and the black dots represent plot centroids, where GCPs were placed.

The disparity between the value ranges of the two scenes (343 to 11783 for the ALOS-PALSAR-33 and 448 to 7768 for ALOS-PALSAR-34) is attributed to the effect of structural and dielectric constant properties and surface scattering of the target, i.e the Miombo forest canopies (Cutler et al., 2012; Woodhouse, 2006). This was induced by the differences in the times that the two scenes passed the reserve in the two separate portions they cover it. The value disparities signify the direct influence of the varying environmental conditions observed in the forest during the various months of the year with regard to the relative dryness and the leaf-on or off condition of the target areas (Chidumayo, 2001; Urban et al., 2018; Vrieling et al., 2018).

3.4.3 Sentinel-1 data acquisition and processing

The study also acquired two-time periods (wet and dry seasons) 2019 Sentinnel-1-C-band SAR (radar backscatter) cross-polarised (VV+VH) decibel-gamma0 orthorectified datasets covering Ntchisi Forest Reserve. These were acquired from the EO browser website, thus; https://apps.sentinel-hub.com/eo-browser. The datasets were accessed on 25th March 2021 as Interferometric Wide swath (IW) products of 10m x 10m (spatial resolution). Their spatial pixel resolution was 20m and they were acquired in the WGS 84 (EPSG: 4326) coordinate system (Figure 23).

These wet and season datasets comprise of scenes captured on 12th April 2019 and 28 October 2019, respectively. The timing of the acquisition period was based on the following considerations;

(i) Seasonal phenology in the wet season (immediate post-rain data), but prior to leaf senescence (months of April–June),
(ii) Dry season (September-November), and
(iii) Scenes with minimal cloud cover (especially those with or close to same imagery date).

The choice of both the wet and dry season datasets was to mask out the seasonal and phenological effects while utilising the proposed ideal remote sensing window for Miombo (Figure 6). Since radar backscatter intensity gets affected by surface moisture (Woodhouse, 2006); it is correspondingly affected by the spectral reflectance of Miombo woodland cover that is highly influenced by water/surface moisture availability as a factor of the short rainy and long dry seasons that alternate in the tropics (Chen

and Wang, 2008). One of the key benefits with S1 (acquired from the EO browser website) is the provision of the already orthorectified datasets.

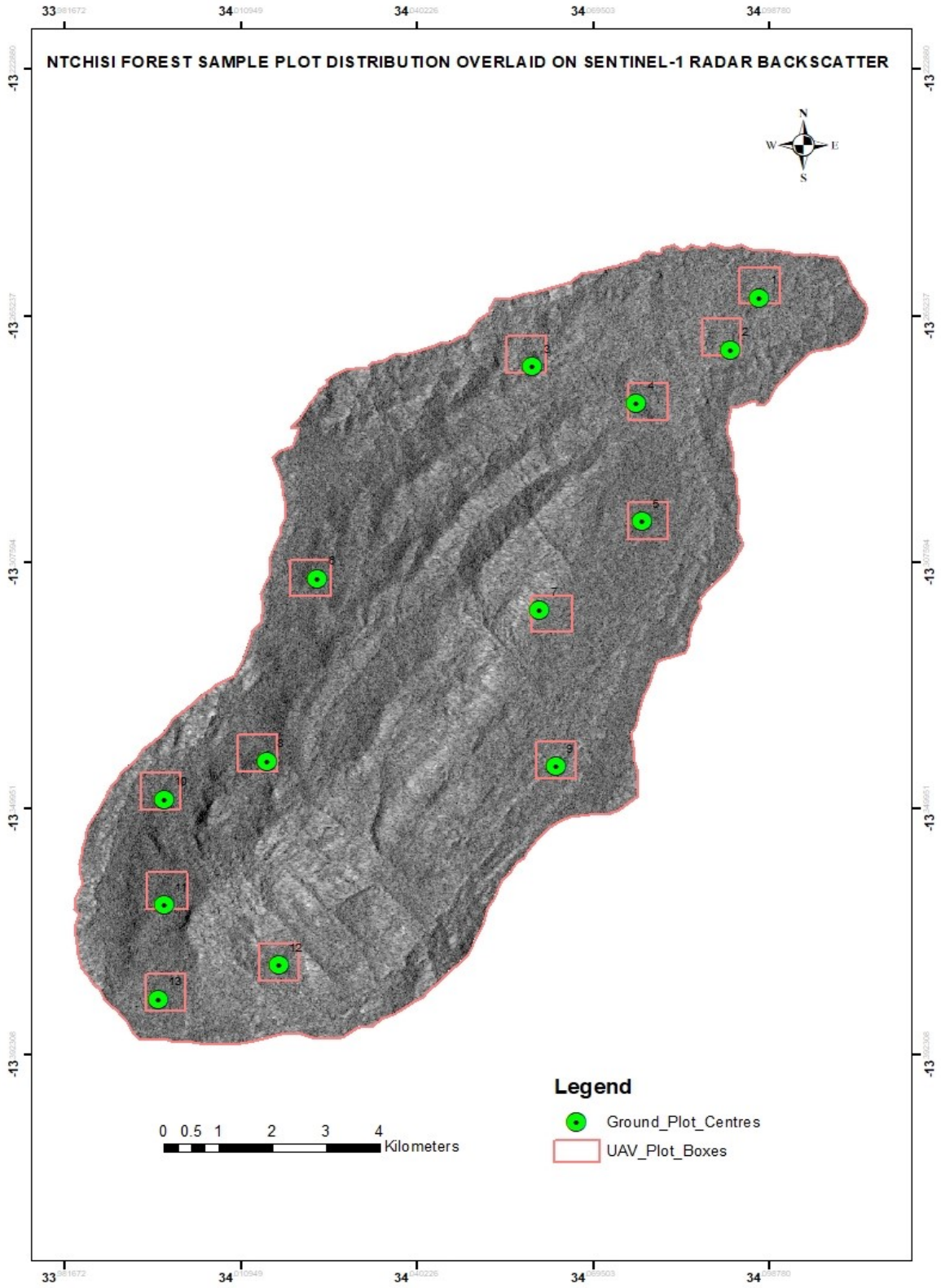

Figure 23. Ntchisi Forest Reserve sampling plot unit distribution for Sentinel-1: Big squares represent UAV 50ha (0.71km x 0.71km) plot boxes overlaid on sentinel-1 (C-band) Imagery while the green circles

(Inset), represent ground plots (20cm radius) and the black dots represent plot centroids, where GCPs were placed.

3.4.4 ESA-CCI AGB data acquisition and processing

This study has also employed open-source datasets provided by the European Space Agency's (ESA) Climate Change Initiative (CCI) Biomass Project. The ESA-CCI biomass map version 3 datasets were derived from a combination of EO from the Copernicus Sentinel-1 mission, Envisat's ASAR instrument and JAXA's ALOS-1 and 2, depending on the year (Santoro et al., 2021). Besides being unrestricted, the datasets were also preferred because they render quantified AGB stocks. Precisely, the datasets comprise global maps of AGB for four epochs (mid 1990's, 2010, 2017 and 2018) and use a map at a grid of 1km spacing, with a target relative error of less 20% where AGB exceeds 50Mgha^{-1} (Santoro et al., 2021).

For this study, the ESA CCI Biomass Map 2018 datasets covering Ntchisi Forest were acquired on 06/07/2022 from the following link; https://climate.esa.int/en/projects/biomass/. The specific tile covering Ntchisi Forest was coded by default as follows; S10E030_ESACCI-BIOMASS-L4-AGB-MERGED-100m-2018-fv3.0.tif.

The 2019 datasets (covering the base year for this research) would have been quite suitable for this study, nevertheless, these were not available under the ESA CCI mission, thus during the planned data acquisition period for this study. Instead, the 2018 AGB stocks were acquired as the closest temporally.

The 2018 datasets used include estimates of AGB stock in units of tonnes/ha i.e., Mg/ha as provided by the raster imagery. The imagery datasets comprise of the AGB stock calculated in mass, thus expressed as oven-dry weight of the woody parts (stem, bark, branches, and twigs) of all living trees excluding stump and roots for the year 2018.

3.4.5 SENTINEL-2-L2A VISIBLE/NIR/SWIR visualisation scenes

Wet and dry season 2019 optical Sentinel-2 L2A scenes covering 28 July 2019 and 31 October 2019 period for Ntchisi Forest Reserve were acquired in April 2021. These L2A-were acquired from the EO Browser (https://apps.sentinel-hub.com/eo-browser/) in the descending orbits. The datasets were in Visible/Near InfraRed and Short-Wave Infra-Red (Vis/NIR/SWIR) composite band visualisations.

The table below shows the bands, wavelength, and resolution characteristics for Sentinel-2A Multispectral Instrument.

Table 12. Sentinel-2A Multispectral Instrument (MSI) Bands, Wavelength and Resolution

Sentinel-2A MSI			
Band	**Spectral Region**	**Wavelength Range (nm)**	**Resolution (m)**
B1	Coastal aerosols	443	60
B2	Blue	458-523	10
B3	Green peak	543-578	10
B4	Red	650-680	10
B5	Vegetation Red Edge	698-713	20
B6	Vegetation Red Edge	733-748	20
B7	Vegetation Red Edge	773-793	20
B8	NIR	785-899	10
B8A	NIR (Vegetation Red Edge)/narrow	855-875	20
B11	SWIR	1565-1655	20
B12	SWIR	2100-2280	20

As depicted from Table 12 above, the SWIR composite band combination (B12), the Visible/NIR's Vegetation Edge (B8A) and the Visible Red (B4) operate within 2100-2280nm, 855-875nm and 650-665nm ranges of the EMS respectively. However, the SWIR region is divided into SWIR1 (1500–1800nm) and SWIR2 (2000–2400nm) (Benseghir and Bachari, 2021; Neuwirthová et al., 2017; Wang et al., 2018).

Generically, the Vis/NIR/SWIR band combination of the Sentinel-2 imagery was preferred due to its improved spectral resolution (10-20m) within the EMS windows. Particularly, the red-edge (RE) band has low reflectance over vegetation canopy due to its strong absorption of chlorophyll (Chen et al., 2018; Puliti et al., 2021; Wang et al., 2018). The RE band renders a high correlation with various physiological vegetation parameters, such as nitrogen and eventually, biomass (Wang et al., 2018).

The RE spectral region lies in the sharp change of canopy reflectance range between 680nm and 750nm, where a slope occurs (Table 12) (Wang et al., 2018). This attribute of the B5 and B6 provides a huge advantage for describing the status of plant pigments and health over other EMS bands. Hence, Sentinel-2 Vis/NIR/SWIR band combination, especially the red-edge is commonly used for detecting and assessing

vegetation cover as well as improving biomass estimation accuracy (C. Li et al., 2021; Wang et al., 2018).

The SWIR composite band of Sentinel-2–L2A imagery displays vegetation in various shades of green i.e., the darker shades of green indicate denser vegetation while the brownish are indicative of bare soil and/or built-up areas (*ibid*). In contrast, under the Vis/NIR regions of the EMS, the healthy vegetation absorbs strongly in the Red band and reflects strongly in NIR. In general, darker shades of green indicate denser vegetation (Wang et al., 2021). In this respect, vegetation (Miombo trees inclusive) appears in shades of green and is reflected in the B8A, otherwise known as the Vegetation Red Edge (865nm) of the Vis/NIR region.

While the NDVI would have also been an appropriate technique to estimate AGB in the study, preference of SWIR band combination was primarily due to the following local conditions of the study area that are better monitored in this composite band combination;

(i) Fire occurrences observed during the ground and UAV surveys (newly burnt areas) in the following plots; P7, P8, P9, P10, P11, P12, and P13,
(ii) Mountainous nature of the forest with distinctive rock outcrops, in addition to the bare lands within the reserve (in all the plots except P1 and P2),
(iii) Cultivated soils surrounding the entire boundary of the forest reserve (P9, P10, P13), and
(iv) Extremely hot temperature (29.2^{o}C to 42.1^{o}C) and dry condition observed during the survey period (September to October 2019) (Government of Malawi, 2019b), all of which are better attributes for distinction of the spectral reflectance within the SWIR region.

The SWIR's attribute of being negatively correlated to water content (Benseghir and Bachari, 2021), renders another advantage for its preference since it is known to detect newly burnt land, features that reflected highly in these channels. This artefact remains ideal for detecting the fire that scotched Miombo Woodlands of Ntchisi Forest.

The SWIR band combination has in other studies been successfully used to explore leaf-water content, water stress, forest fires, phenology, water bodies, soil moisture

and drought (Benseghir and Bachari, 2021). For the Ntchisi 2019 study, all the ecological circumstances hold i.e., forest fires and seasonal loss of tree leaves were conspicuous even during the ground and airborne surveys (Fig 42, 59 and 50) rendering the selection of the S2 SWIR datasets prominent.

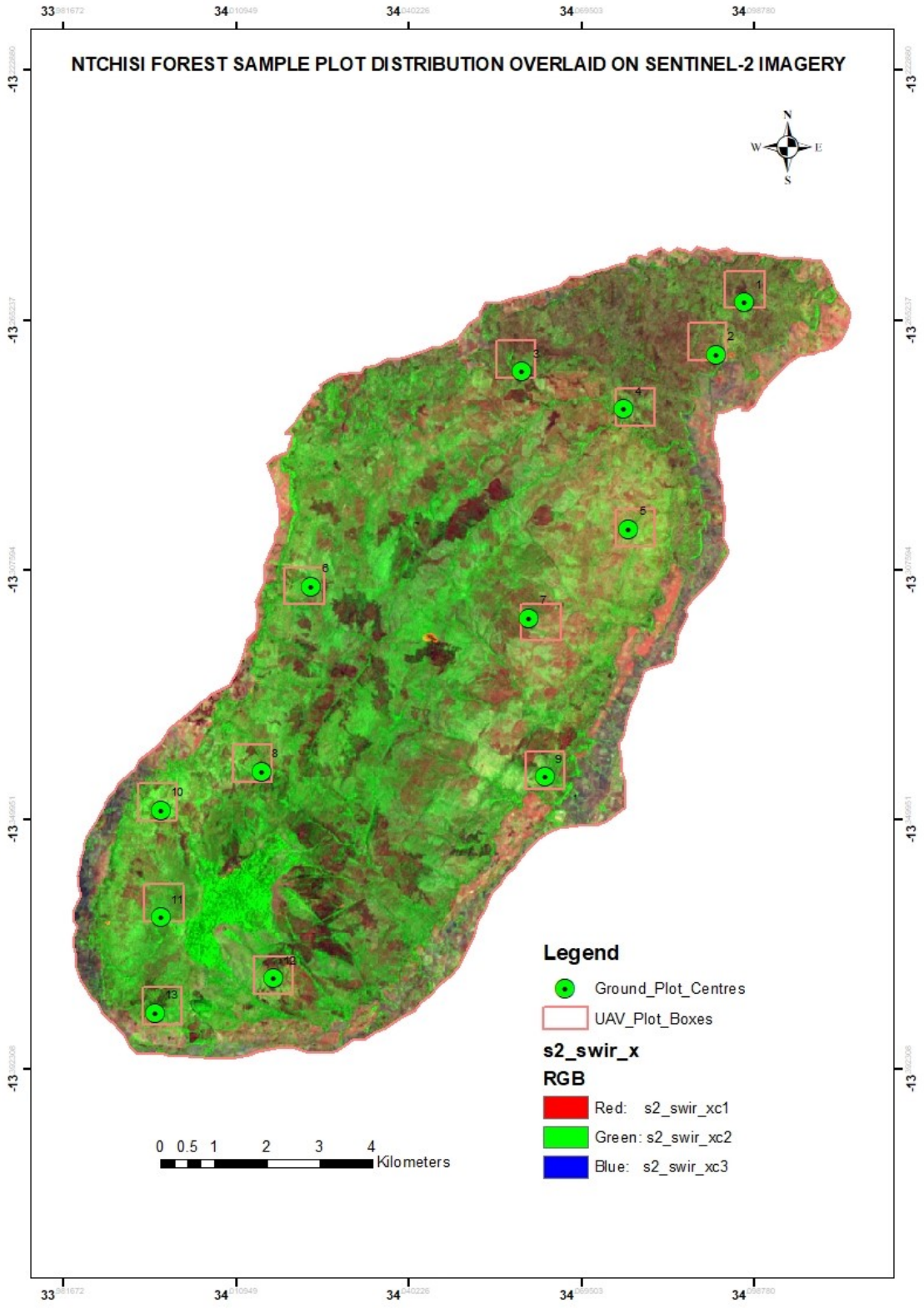

Figure 24. Ntchisi Forest Reserve sampling plot unit distribution for Sentinel-2: Big squares represent UAV 50ha (0.71km X0.71km) plot boxes overlaid on Sentinel-2-SWIR-band imagery while the green circles (inset), represent ground plots (20cm radius) and the black dots represent plot centroids where GCPs were placed. Key: s2= Sentinel-2, swir=Short wave infrared, x= extracted imagery data layer.

3.5 Imagery Data Resampling

Resampling of the EO imagery was carried out in both Erdas Imagine (2020) and ArcGIS (ArcMap10.8.1) software for better comparisons and imagery optimisation. The UAV orthomosaics, ALOS-PALSAR, Sentinel-1 and 2 imagery datasets (7cm, 25m, 20m and 20m pixel spatial resolution, respectively) were coarsened to provide an equal chance for better comparison at different scales. Precisely, this involved determination of AGB stock correlation at plot and pixel-by-pixel level for the quantitative analysis, and determination of the tree crown spatial pattern distribution (homogenous or heterogeneous arrangement) for the qualitative analysis.

The resampling process entailed downsizing of the scene's spatial resolutions (*xy* cell sizes) as follows;

(i) UAV orthomosaic plot scenes of DSM and CHM originally from 710m x 710m (0.71km x 0.71km) each to 25m, 50m and 100m pixel spatial resolution, respectively,

(ii) ALOS-2 PALSAR-2 radar backscatter originally from 25m x 25m to 50m and 100m pixel spatial resolution, respectively,

(iii) Sentinel-1-C radar backscatter (IW) (decibels) originally from ~10m (grid) or 20m x 20m to 50m and 100m pixel spatial resolution, respectively, and

(iv) Sentinel-2 Vis/NIR/SWIR imagery originally from ~20m to 50m and 100m pixel spatial resolution, respectively.

The choice of the 100m x 100m pixel spatial resolution as a sampling scale was on the basis that the area dimension (10,000m^2) is equal to 1ha (hectare) which is a standard unit measure for AGB in Malawi (Government of Malawi, 2019a). The dimension is also the original pixel spatial resolution scale of the ESA-CCI Biomass Map datasets used in this study (Santoro et al., 2021).

On the other hand, the 50m x 50m pixel spatial resolution scale was chosen because the dimension is equivalent to a quarter of a hectare (0.25ha or ~0.3ha) which is a dimension more or less equal to the size most ground sampling plot units of the T-

cluster design in Malawi (Government of Malawi, 2019a; Mueller, 2012; USAID PERFORM, 2017).

The use of different pixel resolutions was to determine the efficient scale at which each EO imagery would estimate AGB biomass, C, and fractional cover with regard to accuracy.

Below is a schematic diagram outlining the generic pre-processing workflow of the EO layers during the resampling process.

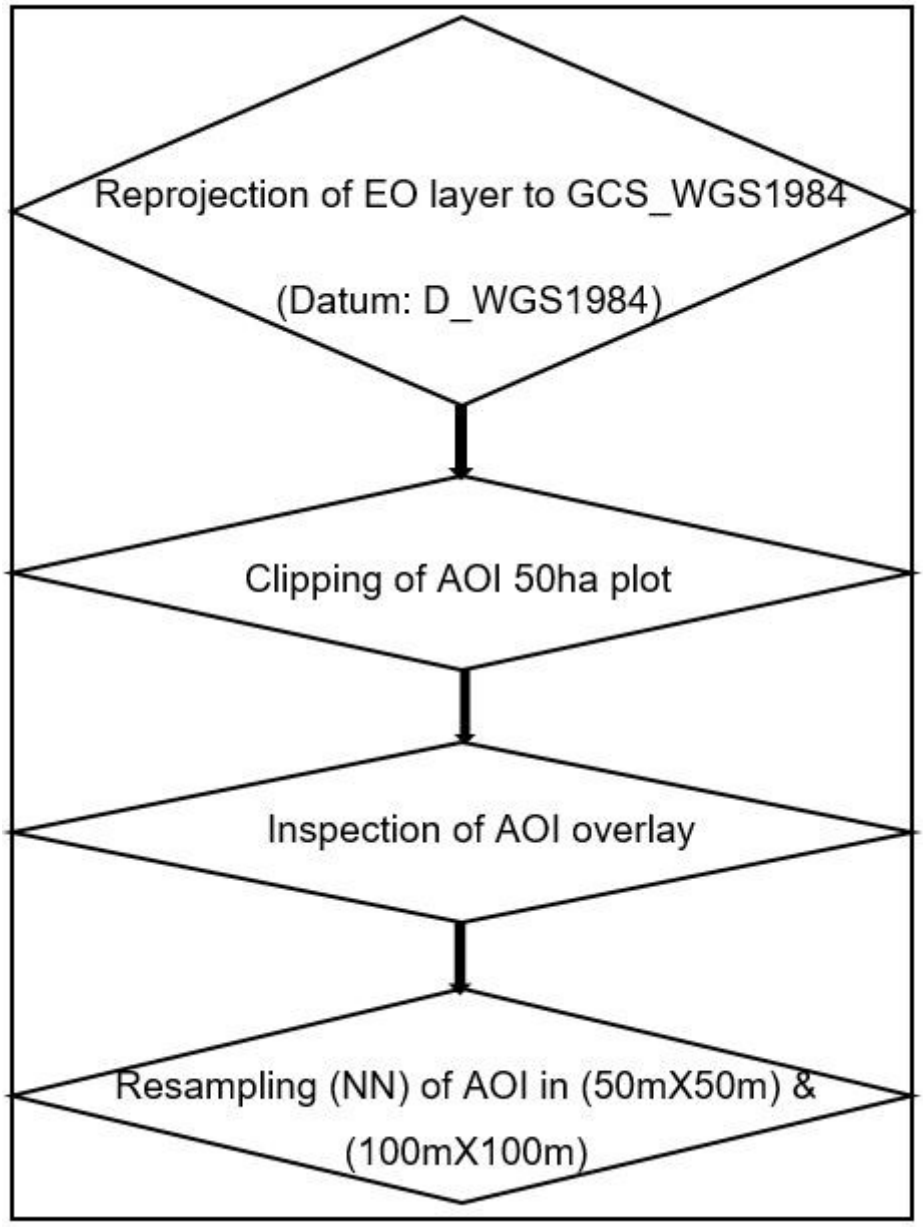

Figure 25. Schematic workflow of fundamental imagery pre-processing stages outlining the generic pre-processing tasks performed on the EO layers up to the resampling stage.

During resampling, the Nearest Neighbour and Bilinear Interpolation techniques were applied. The former was employed during crown distribution pattern visual (qualitative) analysis due to its efficiency in minimising changes to pixel values since it has got a record of avoiding generation of unwanted values during such a process (Baboo and Devi, 2010; Qin et al., 2003). In addition, it was preferred for its suitability to process discrete datasets (*ibid*), i.e., land cover since the interest of the visual analysis was to determine whether an area is covered by forest (tree crown cover) or not followed (Baboo and Devi, 2010; Qin et al., 2003).

Despite its challenges of changing the pixel values to some extent, Bilinear Interpolation technique was preferred for the quantitative data analysis only (visual imagery interpretation) due to its ability to infer pixel-by-pixel value as used in the correlations of the imagery continuous (AGB) datasets, thus, as recommended by previous studies (Baboo and Devi, 2010; Qin et al., 2003). Engagement of the technique took advantage of the Miombo Woodlands forest cover structure which is continuous dataset with no distinct boundaries; thereby rendering it easy to distinguish canopy cover and bare area surface patterns using closest pixel related points (Accadia et al., 2003; Kim et al., 2019; Solberg et al., 2015)

CHAPTER-4

4.0-RESULTS AND DISCUSSIONS

This chapter delivers the analysis and outcomes pertaining to the datasets employed by this research. It displays the trends assumed by the AGB and C stocks, and the crown spatial distribution patterns over Ntchisi Forest, *vis-à-vis*; (i) ground-based (gb) measurements, (ii) airborne observations, and (iii) satellite EO. It further provides their explanation with regard to local circumstances of the forest reserve.

While data patterns have been explained with the aid of bar charts, scatter plots and tables, the parametric correlational relationships explored were derived through the Analysis of Variance (ANOVA) technique following the Linear Regression (LR) method. This was done to test the statistical differences between their treatments' mean values determined using the Fishers' Least Significant Difference (LSD) set up.

A probability value (p-value) was set at 0.05 level of significance and the Pearson's co-efficient of determination (R-squared), Root Mean Square Error (RMSE) and Bias they were employed to explain the relationships observed between the treatments. The simple and straightforward relationships were analyses in Microsoft Excel (16) while the relatively complicated ones were computed using GenStat (18.1) and RStudio (R-3.6.1) programming software.

4.1 Ground-based Data Analysis and Trends

This subsection renders trends observed after analysing the gb measurements acquired over Ntchisi Forest, and more importantly, conveys explanations to the patterns. The key variables tested include; (i) *dbh* and height, (ii) *dbh* and crown diameter, (iii) AGB and *dbh* of dominant (10 largest diameter) trees per plot, and (iv) AGB and fractional cover (Crown Area).

Table 13 below shows a summary of the total number of plots, individual trees and AGB in tonnes of carbon (tC) sampled in Ntchisi Forest.

Table 13. Summary of 2019 AGB stock estimated from the 13 Permanent Sampling Units of Ntchisi Forest at 95% Confidence Interval, and 10% Precision Error, using Local Allometry (Equation 1 and 2) derived from (Kachamba, 2016).

No. of Plots	Tree Observations	Mean AGB ($tCPlot^{-1}$) (0.1ha)		Mean AGB ($tCha^{-1}$)	
		Equation 1	Equation 2	Equation 1	Equation 2
13	216	2.7	2.6	44.5	43.3

From the total 13 circular ground-plots of 20m radius (0.1ha), a sample of 216 individual tree observations was measured and its AGB computed using both Equation 1[17]and Equation 2[18] in Table 13, above. The employment of both allometry was for comparison's sake.

Overall, the plots registered on average, AGB values of 44.5$tCha^{-1}$ and 43.3$tCha^{-1}$ using Equation 1 and Equation 2, respectively. The total mean AGB per each plot (0.1ha) were 2.7$tCha^{-1}$ and 2.6$tCha^{-1}$ for Equation 1 and Equation 2, correspondingly. These findings were compared to the 2016 Ntchisi inventory and the 2018 and 2020/21 countrywide terrestrial assessments and they portray a consistent and expected pattern of estimates and predictions of not only the AGB and stocking density, but also the *dbh* and height parameters, *inter alia* (Government of Malawi, 2019a; Tetra Tec and Winrock International, 2021, 2022; USAID PERFORM, 2017).

For instance, the 2016 study's mean AGB estimate (using Equation 1) was 45$tCha^{-1}$, while the incumbent study's is 44.5$tCha^{-1}$ and the current statistics also fall within the expected range (Government of Malawi, 2019a; Skole et al., 2021). The marginal biomass reduction of 0.5$tCha^{-1}$ registered by this study's analysis (2019) compared to the 2016 inventory is attributed to the effect of escalated anthropogenic threats projected since 2007, which include wood extraction (firewood, charcoal, poles, and timber), dry season fire and grazing (Chinangwa et al., 2016; Ntchisi District Assembly, 2014, 2007). Many of these factors were also physically encountered during this study's data collection period in October 2019 (Figure 42).

Table 14 and Figure 26 below display the range and mean values of *dbh* and *ht,* indispensable parameters that determine AGB and canopy cover, estimated per plot in Ntchisi Forest.

Table 14. Tree Dbh and Height Parameter Value Ranges for Ntchisi AGB Estimations

Plot Name	Plot Number	*dbh* (cm)		*Height* (m)	
		Minimum.	*Maximum.*	*Minimum.*	*Maximum.*
Mndinda	1	6.7	53.5	2.7	16.2
Kajaliza	2	31.9	49.0	13.3	20.0
Msankhire	3	6.0	31.5	2.9	15.1
Mkomba	4	8.0	53.3	4.9	17.8
Chenche	5	5.0	59.5	4.0	14.4
Mandwe	6	11.8	41.9	5.3	12.1
Chanika	7	11.3	31.8	7.4	16.0
Chifwelekete	8	6.5	42.7	4.0	27.6
Kasakula	9	5.5	45.1	2.3	20.1
Mnguluwe	10	5.4	35.6	2.4	11.9
Sambakunsi	11	7.4	33.2	3.2	8.9
Mpamila	12	6.0	32.7	2.9	11.6
Nyanga	13	11.2	52.9	6	16.4
Plot Overall Mean		**10**	**42**	**4.7**	**16.0**

Key: *dbh (*cm*)* = diameter at breast height in centimetres, *ht* (m) = tree height in metres.

Forest studies have recommended that accurate *dbh* and *ht* variables remain significant indicators for quantifying morphological characteristics that determine growth and yield models which can render AGB and C stock estimates (Heo et al., 2019; M. Liu et al., 2017). In this study, both the *dbh* and height parameters were used to inform the AGB and fractional canopy cover, parameters that have an indispensable role in linking the ground-based measurements to the airborne and satellite imagery in the subsequent sections.

The next figure derives a graphical comparison of the *dbh* and *ht* parameters observed per plot basis. These have been plotted using their mean values.

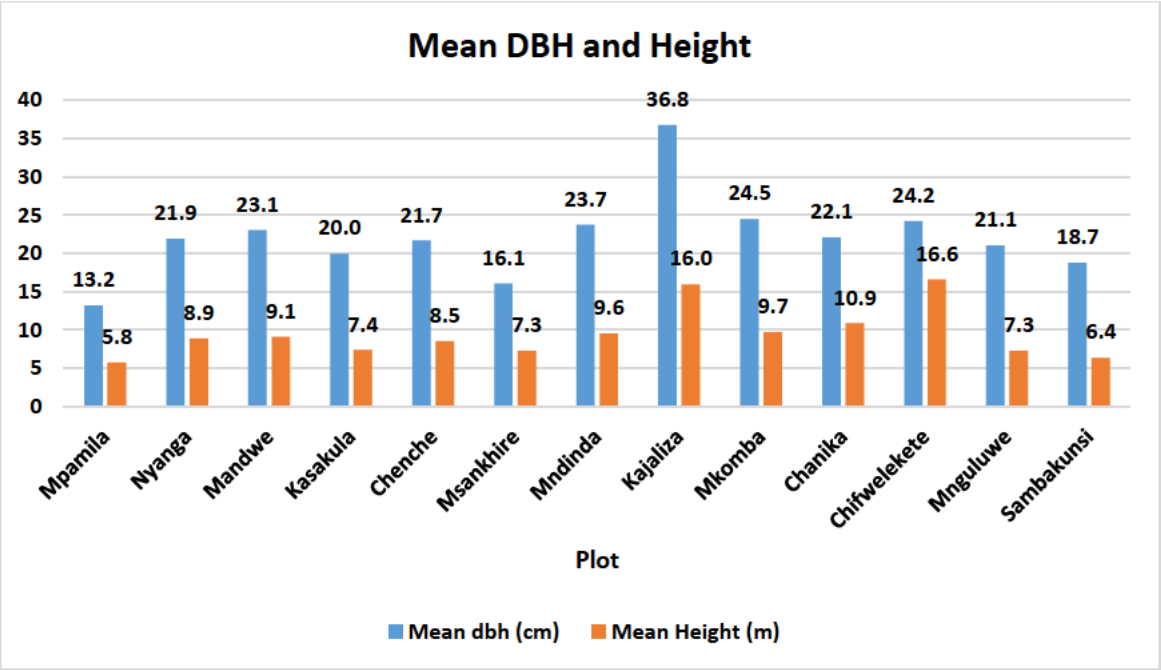

Figure 26. Comparison of plot mean *dbh* and height (*ht*) values measured from the 13 ground sample plots of Ntchisi Forest Reserve. The plot mean parameter[19] range for *dbh* and *ht* are correspondingly; 13.2-36.8cm and 5.8-16.0m while the overall individual tree *dbh* and *ht* intervals are; 5.0 to 59.5cm and 2.3 to 27.6m, respectively.

These *dbh* ranges (13.2-36.8cm and 5.0 to 59.5cm for plot mean and individual trees, respectively) and height range statistics (5.8-16.0m for plot mean and 2.3 to 27.6m, correspondingly) display a wide interval of observations, suggesting a complex effect of both the anthropogenic and natural factors subjected to the Miombo Woodlands of Ntchisi. A study on regeneration dynamics of Miombo noted that the Woodlands are subjected to various human induced and natural disturbances, better understood at plot level basis than wider scales (Syampungani et al., 2016).

Precisely, forest utilisation through wood extraction, fire and livestock grazing that trample down young regenerants are the major contributing factors to these variations in Ntchisi Forest (Chinangwa et al., 2016; Ntchisi District Assembly, 2007). In addition, site conditions such as soils, light (affecting forest density) and micro-climate potentially contribute to the observed wide range values of *dbh* and *ht* measurements in forests (K. Liu et al., 2017). The wide range pattern exposed by these parametric values in Ntchisi could be used to leverage potential sustainability and succession of

[19]Plot mean parameter = Total sum of parameter measurements (i.e., *dbh* or *ht*) per plot divided by number of individual parameter measured

the trees, should the disturbances be curtailed. However, an account of these anthropogenic factors and their effect on AGB, canopy cover and other woody components has been presented from Figure 27 onward.

Table 15 below shows AGB per plot (0.1ha plots), stem density[20] and area coverage of forest management blocks and plots covering Ntchisi Forest.

Table 15. Summary of AGB Stock and Stem Density Measured during Ntchisi Forest Inventory

Block	Area (ha)	Plot No	Mean AGB ($tCha^{-1}$)		Stem Density	
			Eq1 (*dbh*)	Eq2 (*dbh* & *ht*)	Stem $plot^{-1}$	Stem ha^{-1}
Mpamila	252.92	12	29.4	23.4	15	119
Nyanga	125.77	13	66.5	61.2	24	191
Mandwe	373.81	6	25.1	22.7	10	80
Kasakula	848.62	9	50.4	42.7	20	159
Chenche	804.4	5	59.5	55.2	22	175
Msankhire	689.67	3	50.5	43.4	22	175
Mndinda	439.34	1	47.7	44.2	16	127
Kajaliza	207.26	2	25.1	29.9	7	56
Mkomba	472.75	4	58.3	55.9	19	151
Chanika	819.12	7	35.8	39.3	11	87
Chifwelekete	420.54	8	68.8	99.2	24	191
Mnguluwe	262.01	10	25.2	20.0	10	80
Sambakunsi	361.04	11	36.2	25.8	16	127

In Table 15 above, Ntchisi Forest portrays a diverse range of AGB stocks and stem density. The AGB ranged from as low as $25.1tCha^{-1}$, singly, for both Mandwe and Kajaliza, to as high as $68.8tCha^{-1}$ for Chifwelekete.

The figure below displays the stem density statistics measured on ground plot scale of Ntchisi Forest.

[20]Stem or tree density = Sum of all stems per given plot, or block level

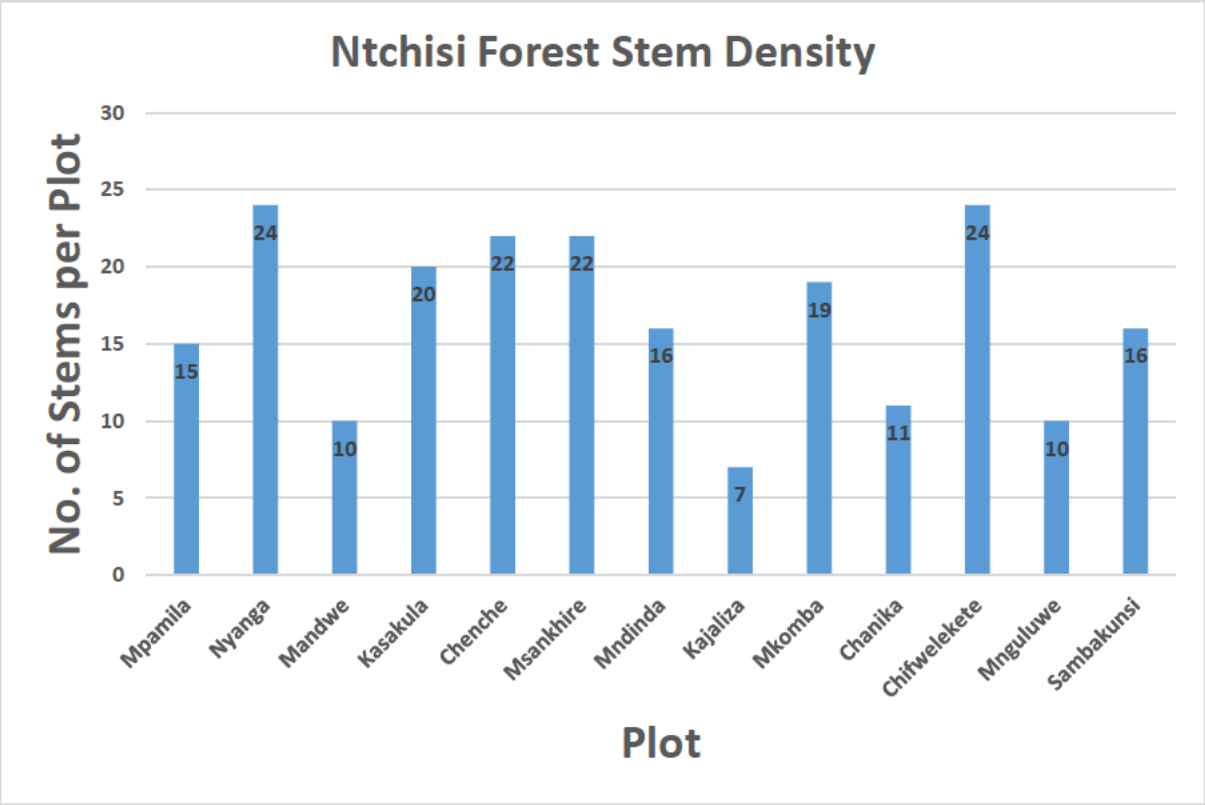

Figure 27. Stem density measured in Ntchisi Forest Reserve: The average stand density[21] is 17 stems plot^{-1} while the overall mean stocking density[22] is 132 stems ha^{-1}. The stem density variations per plot define the anthropogenic activities with which each plot is subjected to i.e., fire, wood harvesting.

Though the diverse range of values could be attributed to the edaphic factors such as differences in soil fertility and structure, (Gonçalves et al., 2017); the AGB and stems density variations in Miombo Woodlands are mostly ascribable to the differentiated anthropogenic pressure that the various localised plots (representing villages) are accounting, i.e., wood extraction and forest fire (Syampungani et al., 2016; Tetra Tec and Winrock International, 2022, 2021). This is a generic trend for not only Malawi's Miombo Woodlands, but, for the entire Miombo eco-biome (Syampungani et al., 2016).

In the figure above, such patterns are conspicuous in the plot statistics of Chifwelekete, which presents a stable tree population in contrast to Kajaliza which portrays the potential for more tree loss due to fire. Such observations manifest the

[21]Stand density = Sum of all plot stems measured per hectare

[22]Overall mean stocking density = Average of the sum of all stems measured in all plots and extrapolated per hectare

social and environmental economic factors that define forest degradation and deforestation of the Miombo Woodlands in the Southern Africa (Kalaba et al., 2013; Munthali, 2013; Munthali and Murayama, 2015).

Besides registering most dangerous steep slope (74%), Chifwelekete plot sits deep inside the Ntchisi Forest, ~1.7km from the peripheral in contrast to Kajaliza which is fairly flat (10% slope), but it is only ~1km away from the forest boundary (Fig. 22 and 23). A deforestation modelling study on Malawi's Miombo Woodland (Dzalanyama Forest) revealed that factors such as short distance to the forest, existence of roads/paths (accessibility) and forest settlement/edge encourage communities to exploit wood resources more and contribute to forest loss (Munthali and Murayama, 2015). Inversely, the long distance and rugged terrain of Chifwelekete contributed to its better conservation by default, thereby attaining higher biomass compared to the Kajaliza (Table 15).

Additionally, Chifwelekete and Nyanga plots registered the richest stand density of 24 stems plot^{-1} each, followed by Msankhire and Chenche with 22 stems plot^{-1} each. The least stocked plot was Kajaliza (7 stems plot^{-1}). Nevertheless, despite this stand density, Kajaliza recorded the largest plot mean *dbh* (36.8cm) and second highest mean height (16m) (Fig. 26). In reverse, Mpamila recorded the lowest mean *dbh* (13.2cm) and second least mean height (5.8m), yet, it has a high stand density, thus slightly more than double (15 stems plot^{-1}) that of Kajaliza.

The above-mentioned trends typify the tree stand ecological economics on growing space and nutrients whereby an increase in growing space of trees correspondingly results to increase in *dbh* (Peters, 2005; Theron and Bredenkamp, 2004). These studies further observed that where trees grow with high stand density that might have induced low *dbh*, thinning/selective, harvesting is introduced to yield an increment in *dbh* (*ibid*). Therefore, for Kajaliza, despite being prone to fire that is escalated by the dry and hot-micro-climate of the area (Government of Malawi, 2019b); the same fire occurrences play the role of thinning through killing and inhibiting other trees and vegetation that would have competed with the remaining measured trees for growing space and nutrients. As a result, despite contributing to the reduction of stand density comparatively, fire positively renders considerable indirect effect of inducing *dbh* and *ht* growth (Fig. 26, 27 and Table 15) (Theron and Bredenkamp, 2004).

The opposite scenario holds for Mpamila which recorded slightly more than double as much (15 stems plot^{-1}) as Kajaliza. In this case, the higher density induced competition for growing space and tree nutrients, resulting to low mean *dbh* and height. These trends uniquely characterise Miombo Woodland stands whereby distribution of stems frequencies decrease with increasing *dbh* parametric value*s*, otherwise, referred to as inverse *J*-shape curve (Gonçalves et al., 2017; Isango, 2007; Peters, 2005; Syampungani et al., 2016).

Figure 28 below depicts tree species abundancy[23] and richness[24] enumerated on ground-based plots of Ntchisi. An index code for the tree species presented is provided separately (Appendix III).

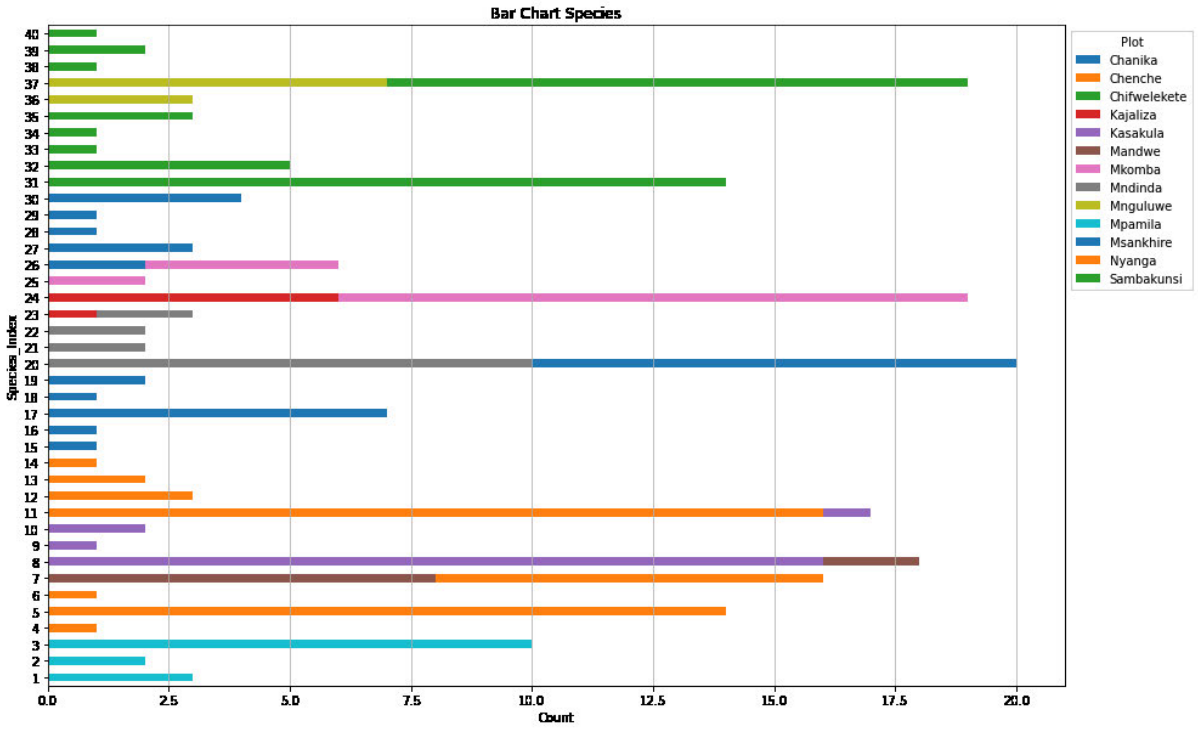

Figure 28. Plot-based species richness and abundance of Ntchisi Forest; Kasakula and Chenche are most abundant plots with a total frequency count of 16 species comprising *Brachystegia bussei* and *B. manga* each, respectively, followed by Msankhire (6) species and Mnguluwe, Kajaliza and Mandwe with 2 each.

[23] Species abundance is the frequency of the same species in an area or community

[24] Species richness is the count of different species in a given an area e.g. per plot

On average, Kasakula and Chenche emerged the most abundant plots, registering a total frequency of 16 species each, comprising of two species, namely; *Brachystegia bussei* and *Brachystegia manga*. Msankhire recorded the highest species richness totalling to 6 while a record of 2 was enumerated from Mnguluwe, Kajaliza and Mandwe, each. Generally, the plots showed high variation in terms of species composition. The figure below illustrates the species biodiversity and abundance of Ntchisi Forest enumerated during the ground-based measurements in 2019.

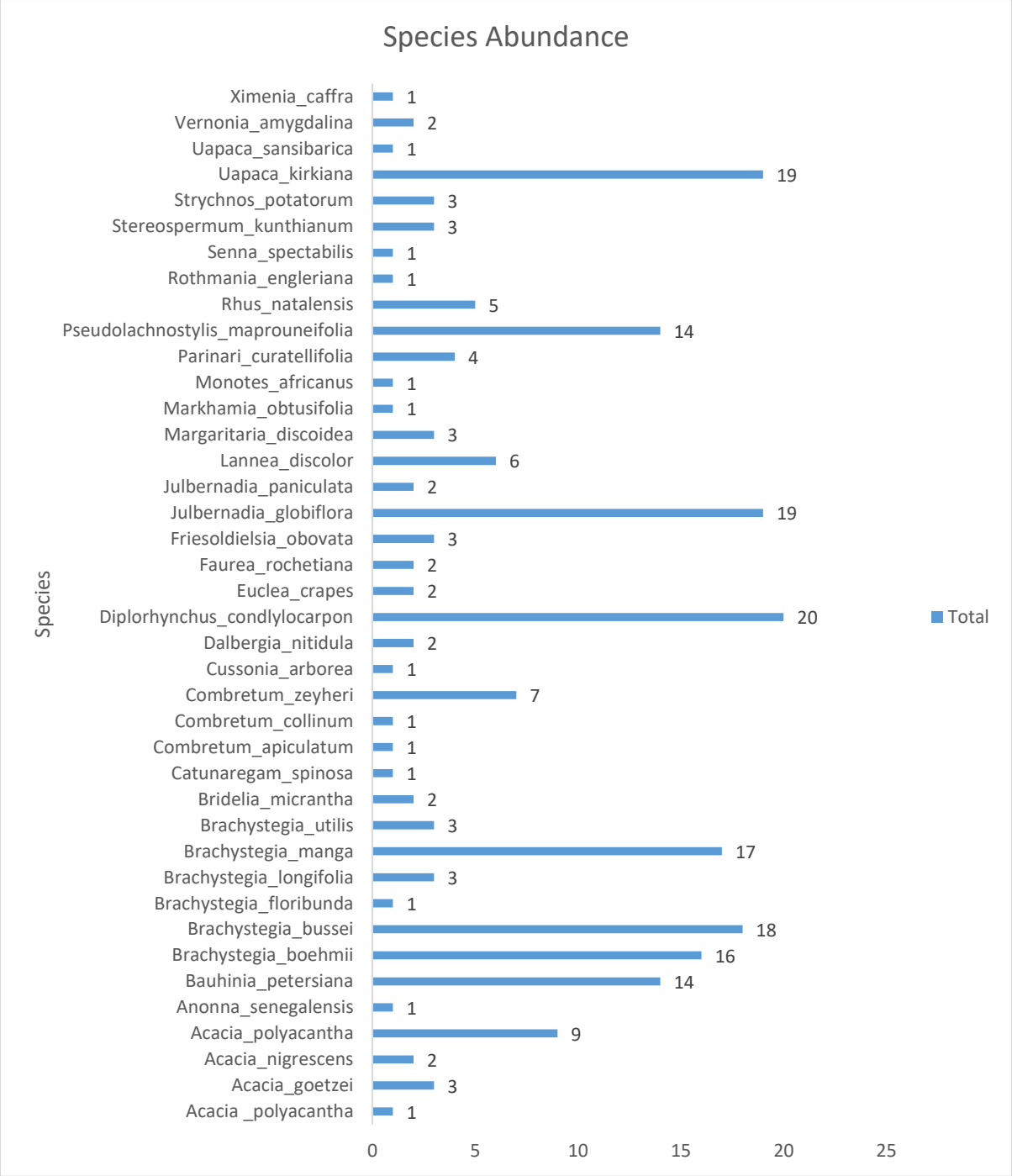

Figure 29. Species diversity and abundance of Ntchisi Forest enumerated during the 2019 ground-based inventory. 40 distinct species identified, 6 dominant ones include; *Diplorhynchus condylocarpon*, *Julbernadia globiflora*, *Uapaca kirkiana*, *B. bussei, B. manga* and *B. boehmii*. The dominance of *D. condylocarpon* signifies the effect of fire disturbance, resulting to plant habitat secondary succession that gives chance to fire-resilient species at the expense of the previous dominant ones.

Figure 29 above, depicts tree species diversity[25] and abundancy enumerated during the ground-based inventory. A total count of 40 distinct species of live trees were

[25] Species diversity is the number of different species that are represented in a given community.

identified in the field, out of which the 6 are dominant ones and these include; *Diplorhynchus condylocarpon*, *Julbernadia globiflora*, *Uapaca kirkiana*, *B. bussei*, *B. manga* and *B. boehmii*, listed in order of abundance. The least 3 abundant species include; *Monotes africanus*, *Uapaca sansibarica* and *Ximenia caffra*.

While *U. kirkiana* is a light demanding and semi-fire tolerant species, *D. condylocarpon* is on the other hand, an understory and fire tolerant species (Chidumayo, 1997; Gonçalves et al., 2017). Hence, their emergence in the dominant category is characterised with plant habitat succession, thus after the plots were exposed to fire and selective harvesting (*ibid*). This entails that forest fire and wood extraction impacted hugely on the previously dominant species through inhibiting their regeneration, thereby giving chance to the current species to dominate.

Notwithstanding edaphic factors, the species variations characterise the unique niche that each species ecologically plays in each habitat/plot or site, though strong environmental changes caused by anthropogenic factors such as fire and wood extraction also contributed (Chidumayo, 1997, 1991; Gonçalves et al., 2017; Isango, 2007; Kalaba et al., 2013; Wale et al., 2012).

The current species richness of 40 is slightly lower than 55, thus, the total count recorded during the 2016 Ntchisi Forest inventory (USAID PERFORM, 2017). The decrease can be attributed to site edaphic differences induced by the lower number of plots (13 compared to the 18 inventoried in 2016) that translated to correspondingly less site diverse covered by this incumbent study, due to funding limitations. Previous studies observed that differences in Miombo tree species diversity may arise due to site variations and strong environmental changes caused by human induced activities, among others (Gonçalves et al., 2017; Isango, 2007).

Nevertheless, employment of 13 sampling units for this academic study did not compromise the pre-set sampling probability of CI (95%) and precision error (10%), but rather followed the initial sampling plan set during the 2016 REDD+ inventory. Despite realising the sufficient sample size of 13 plots under the pre-set CI, the 2016 study resampled five extra plots (adding up to 18) to attain a representation of all the villages participating under the forest management block system. Though more of a managerial decision (aimed at avoiding conflicts among the communities governing the forest) than

a statistical one, this yielded a higher species density than the one observed under this study, thus with 13 sampling plot units.

Besides, research has noted that a species richness range of 40-55 is considered higher diversity and potentially an indicator of greater stability for a Miombo community structure (Isango, 2007). Again, the reduction in species richness is partly attributed to the interplay of fire and wood extraction, events that were spotted even during the field inventory and have been well documented by previous studies (Chinangwa et al., 2016; Ntchisi District Assembly, 2014, 2007). Furthermore, research in Miombo Woodlands has revealed wood harvesting and fire as the major factors affecting tree species diversity and succession in the long term (Chidumayo, 1997; Gonçalves et al., 2017).

In Miombo Woodlands, wood extraction in form of charcoal, timber and poles is quite associated with species loss due to its nature of targeting specific tree species of preferential diameter classes (Chidumayo, 1997, 1991; Kalaba et al., 2013). For instance, high calorific value species (i.e., diameter ≥10cm of *B. boehmii*, *B*. *bussei* or *B. utilis* are targeted for charcoal) whereas high bending and splitting strength species of *J. paniculata and J. utilis* are preferred for timber and poles (Chidumayo, 1991; Kalaba et al., 2013). In this regard, it is not surprising for this incumbent study to record a noticeable decline of the tree species in question, at least when compared to the 2016 inventory.

Except for *D. condylocarpon*, the rest of the dominant species also prevailed as the most abundant during the 2016 inventory. Despite *J. globiflora and Brachystegia spp.* regarded as the typical dominant trees of Miombo ecosystem (Chidumayo, 1997), the emergence of *D*. *condylocarpon, (*a sub-dominant species) in the dominant category is attributed to the effect of high fire frequency and light intensity alterations on woodland structure and composition (Lawton, 1964; Maquia et al., 2013). Under Miombo ecological composition, *D. condylocarpon* is fire-resistant, better still known to withstand repeated burning or fierce dry fire seasons (*ibid*). This has rendered its gradual dominance.

During the ground data collection for this study, fire and post-fire occurrences were encountered, i.e., burned biomass, in all the plots (Fig. 42). The emergence of *D. condylocarpon* in the dominant category confirms the ecological disturbance rendered

by forest fire (Chidumayo, 1997). This is in addition to other anthropogenic factors such as wood extraction that open the canopy and enhance light conditions which in turn induce growth of the initially sub-species to dominate (Chidumayo, 1997; Chinangwa et al., 2016; Ntchisi District Assembly, 2007).

4.1.1 Plot-based tree crown analyses

The crown cover computations for this study adopted the following assumptions;

(i) Individual tree crowns fell inside the 20m radius circular plots, and
(ii) Tree crown overlaps and clumping encountered in some plots and some of these trees shared the same *xy* coordinates (Fig. 17 and 41).

During the ground data analysis, the following parameters were considered in relation to AGB;

(i) The contribution of biggest/dominant trees (10 large diameter trees of each plot) to AGB,
(ii) Canopy cover, and,
(iii) Fractional cover (expressed as a percentage).

The next figure displays the mean crown diameter (*cd*) values per plot calculated from the individual trees measured during the ground inventory.

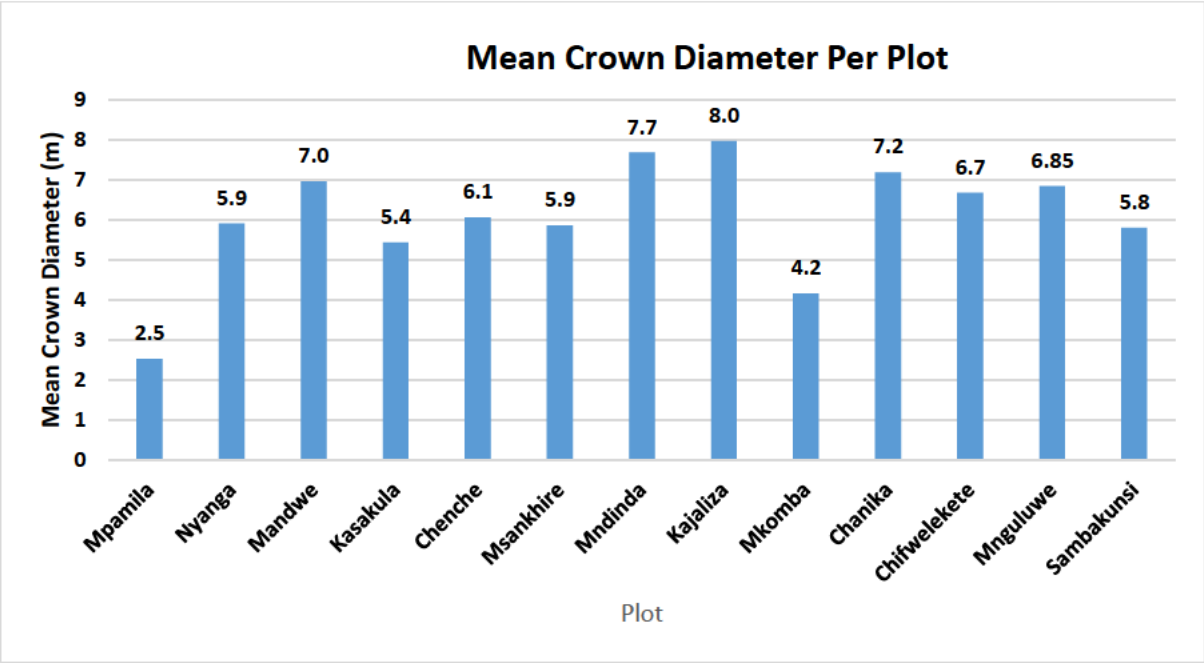

Figure 30. Mean crown diameter per each of the 13 ground-sampling plot units of Ntchisi Forest calculated from individual trees measured during the 2019 terrestrial inventory. The parameter statistics depict a wide range of 2.5 to 8.0m characterising tree stand ecological economics on growing space and nutrients influenced by harvesting, fire and other environmental factors.

The mean crown diameters (*cd*) ranged between 2.5 and 8.0m, registered by Mpamila and Kajaliza, respectively. Though with the greatest mean *cd*, Kajaliza has paradoxically, the least stock (7 stems plot^{-1}) while Mpamila despite the low mean *cd* has more than double the stem density of Kajaliza (15 stems plot^{-1}). Similarly, this trend epitomises the tree stand ecological economics on growing space and nutrients as explained earlier. Therefore, it was expected for the trees in Mpamila plot, which are more (higher stem density) to experience higher competition for nutrients and light, thereby succumbing to reduced *cd* structure of its trees.

The next figure displays the percentage contribution of dominant trees to AGB calculated in each plot of Ntchisi Forest.

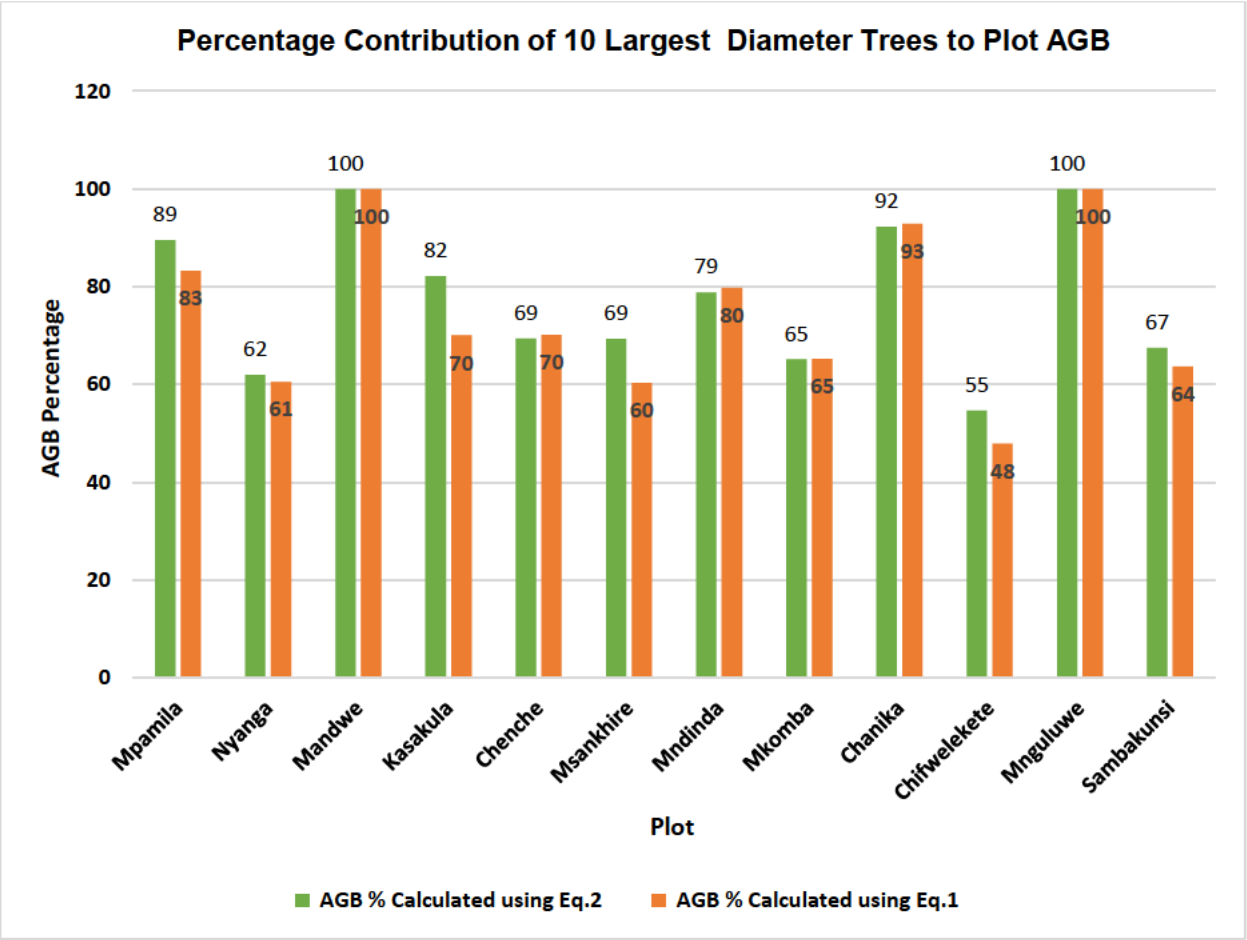

Figure 31. Percentage contribution of ten largest diameter (dbh) trees to plot AGB. The dominant trees contribute 55-92% of the AGB stock suggesting biomass is factor of tree size in Ntchisi Forest.

Computation of percentage contribution the 10 largest diameter trees per plot (0.1ha) to AGB showed a significant range of 55-92% trees sampled using Equation 2. Kajaliza was excluded as its total sample of 7 trees did not meet the threshold of ≥10 trees. However, Mandwe and Mnguluwe registered 100% of AGB contribution because each one had a sample of exactly 10 trees.

The trends of the contribution of dominant trees to AGB and their percentage range suggest that the AGB of Ntchisi is more dependent on structural biomass (size) of trees than just their relative numbers (stem density). This conforms to the premise that in tropical forests, large trees store significant amounts of C in woody components thereby regulating forest C stocks and dynamics (Ali et al., 2019; Piponiot et al., 2022; Slik et al., 2013). In some cases, large trees may be responsible for the 75% of the total forest volume variations (Meyer et al., 2018). Therefore, the AGB of Ntchisi Forest is characterised as being proportional to the size of the trees, implying the more the

huge trees available, the more the AGB they provide, thus following the given assumption (Meyer et al., 2018).

Mpamila is located slightly more than double as much farther from the boundary (~1.8km) and has portrayed exceptionally high AGB contribution (89%) compared to Nyanga (62%), which is also closer to the peripheral of the reserve (0.8km).These observations provide a good fit to the established investigations that accessibility perpetuated by short distance in Miombo Woodlands contributes to enhanced wood extraction and ultimately decrease in the forest loss, while the opposite is true (Manyanda et al., 2021; Munthali and Murayama, 2015). These findings typify the influence of the proximate drivers of deforestation degradation in Miombo Woodlands of Malawi (Munthali and Murayama, 2015).

4.1.2 Crown area and AGB

The table below displays statistics computed from the crown projected area of individual trees sampled in each of the 13 sampling units of the Ntchisi Forest during the 2019 ground-based survey.

Table 16. Ground Plot (0.1ha) Summary Trends for Canopy Cover from Tree Crown Measurements of Ntchisi

Plot no.	Plot name	*Min*. CA plot^{-1} (m^2)	*Max*. CA plot^{-1} (m^2)	Σ CA plot^{-1} (m^2)	Σ Plot FC %
Mpamila	12	1.4	26.4	87	7
Nyanga	13	3.8	130.3	758	60
Mandwe	6	3.4	97.9	447	36
Kasakula	9	2.0	69.5	535	43
Chenche	5	0.1	166.9	832	66
Msankhire	3	7.2	90.2	661	53
Mndinda	1	19.6	143.1	817	65
Kajaliza	2	17.0	132.3	432	34
Mkomba	4	5.1	160.7	1004	80
Chanika	7	5.5	123.4	516	41
Chifwelekete	8	1.7	77.0	939	75
Mnguluwe	10	2.8	70.4	345	27
Sambakunsi	11	4.8	94.8	505	40

Table 16 above shows crown projected area or simply crown area[26] (CA) statistics comprising minimum (min.), maximum (max.), mean and fractional cover[27] percentage (FC %) of each plot of 0.1ha (1257m^2) estimated during ground-based measurements. The range of CA per plot is 0.1-166.9m^2 while that for the total CA is 87-1004m^2. Mkomba registered the highest fractional canopy cover (FC) (80%) followed by Chifwelekete (75%) and Chenche (66%) while the least (7%) was recorded in Mpamila. Correspondingly, these three densely covered plots have displayed an above-average trend mean *dbh* and mean height of >21cm and 8.5m, respectively. This is in contrast to Mpamila's mean *dbh* and mean *ht* of 13.2cm and 5.8m, respectively (Fig 26). These observations signify a positive relationship between *dbh* and height. They further support the premise that there is strong correlation between tree *dbh* and crown size measured during field-based assessments (Gonzalez-Benecke et al., 2014; Shimano, 1997).

The low fractional cover of Mpamila is attributed to its biophysical nature of being easily accessible due to the vaialability of footpaths, roads and bicycle tracks. These structures are extensively used by tourists and officials from Ntchisi Forest Plantation (Government of Malawi) and Ntchisi Forest Lodge for management and commercial purposes. Despite being far from the forest peripheral, the road/paths network facilitates access to wood exploitation and fire incidents in Miombo (Chidumayo, 1997; Munthali and Murayama, 2015). The remarkable footpath network further caters for shortcut to south-west part of villages surrounding the mountain forest. Invariably, these structures orchestrate reasonable access to the plot's wood resources and accelerate harvesting of targeted species, as exposed by the dominance of trees of the lower *dbh* class (6-14.9cm, Table 15) i.e., 11 out of 15 representing 73% in the plot (Fig. 26).

Additionally, wood harvesting in Mpamila potentially prompted by the dominance of *B. boehmii* i.e., 8 out of 15, representing 53% (Fig. 28 and 29), which is slightly more than half of the plot's species richness. The high wood extraction is prompted by the

[26]Crown area is the outermost perimeter (envelope) of the crowns that form part of the upper canopy level (dominant and (or) co-dominant stratum)

[27]Fractional cover refers to the proportion of an area that is covered by each member of a pre-defined set vegetation or land cover types i.e., individual trees in plot, block or forest

species' high calorific value, an attribute that provides an edge for their firewood and charcoal preference over other species (Chidumayo, 2019; Chiteculo et al., 2018). Retrogressively, this has left Mpamila with many juvenile trees whose crowns are not yet fully developed to contribute considerable fractional cover (Fig. 26).

Mkomba, Chifwelekete and Chenche plots are also located moderately deep inside the forest, hence, their distance attribute relatively deters communities from accessing wood products, resulting to higher FC% and *dbh* (Fig. 24) as observed by the previous study (Munthali and Murayama, 2015). Besides, Chifwelekete sits on an extremely dangerous terrain (~74% slope, Table 6), canvassed by several drifts and streams, biophysical factors that further dissuade communities from travelling to extract wood resources. This supports the assumption that in the tropics, wood exploitation and deforestation are facilitated by flat topography (Mendes et al., 2019). A review on study spatial pattern in Miombo Woodlands established a negative correlation between deforestation/forest degradation and distance from some biophysical factors, i.e., the farther communities are located from rivers, roads, and forest boundary, the less the deforestation and/or degradation occurs (Munthali and Murayama, 2015).

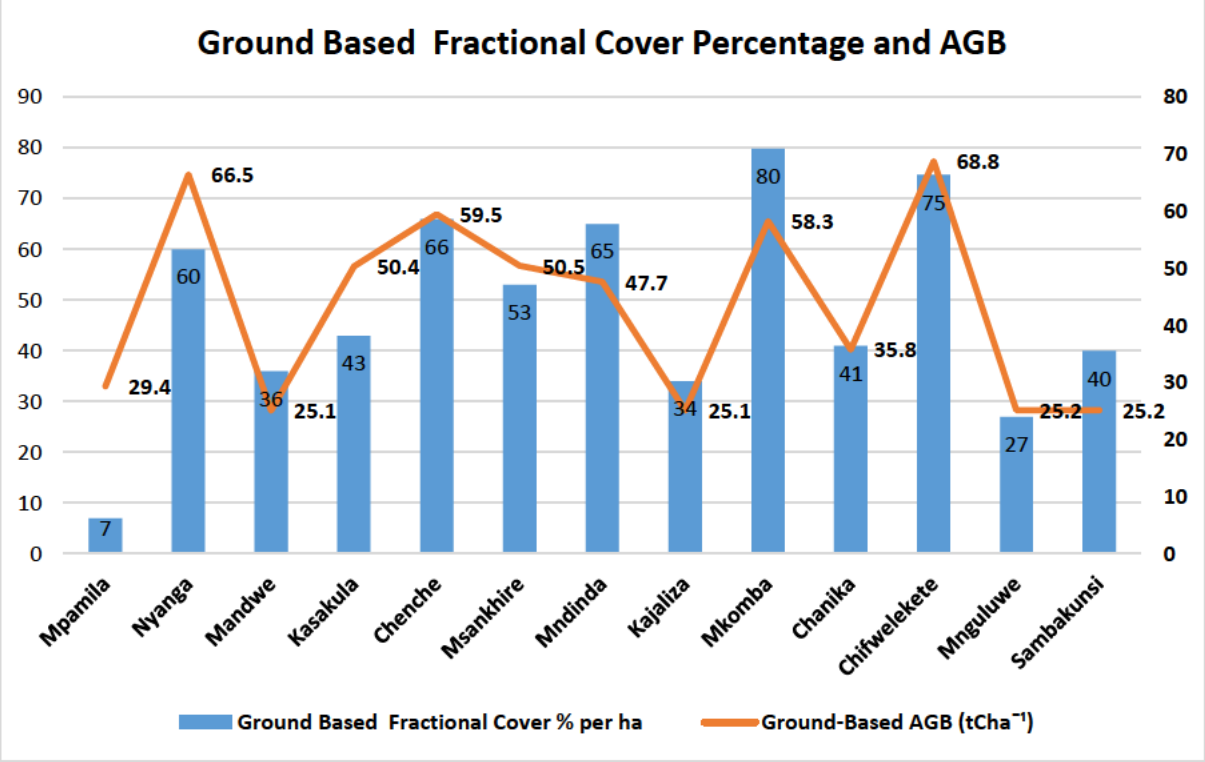

Figure 32. Trend of ground-based AGB ($tCha^{-1}$) and ground-based canopy cover percentage (FC %); derived from individual tree measurements of the 13 ground-plots covering Ntchisi Forest; showing high correspondence between FC % and AGB ranging from 7- 80% for FC % and 25.1- 68.8$tCha^{-1}$ for AGB.

The summary statistics drawn from the canopy cover[28] and AGB derived from the individual tree measurements and AGB stock per each plot indicate a fractional cover percentage range of 7-80% and an AGB range of 25.1-68.8$tCha^{-1}$, respectively. The two parameters have displayed a similar pattern i.e., the low fractional cover percentage of Mpamila (7%) and Mnguluwe (27%) have correspondingly demonstrated low values of AGB 29.4$tCha^{-1}$ and 25.2$tCha^{-1}$ while the higher fractional cover percentage of Chifwelekete (75%), Mkomba (80%) and Chenche (66%) have registered equally higher values of AGB (68.8$tCha^{-1}$, 58.3$tCha^{-1}$ and 59.5%), respectively. This suggests how well correlated the FC and AGB are, however, their detailed explanation is well articulated using R^2 covered under section 3.1.3.

The figure below shows the frequency distribution and percentage of canopy cover estimated using the tree crown diameter measurements of the ground-based plots.

[28]Forest canopy cover, also known as canopy coverage or crown cover, is defined as the proportion of the forest covered by the vertical projection of the tree crowns.

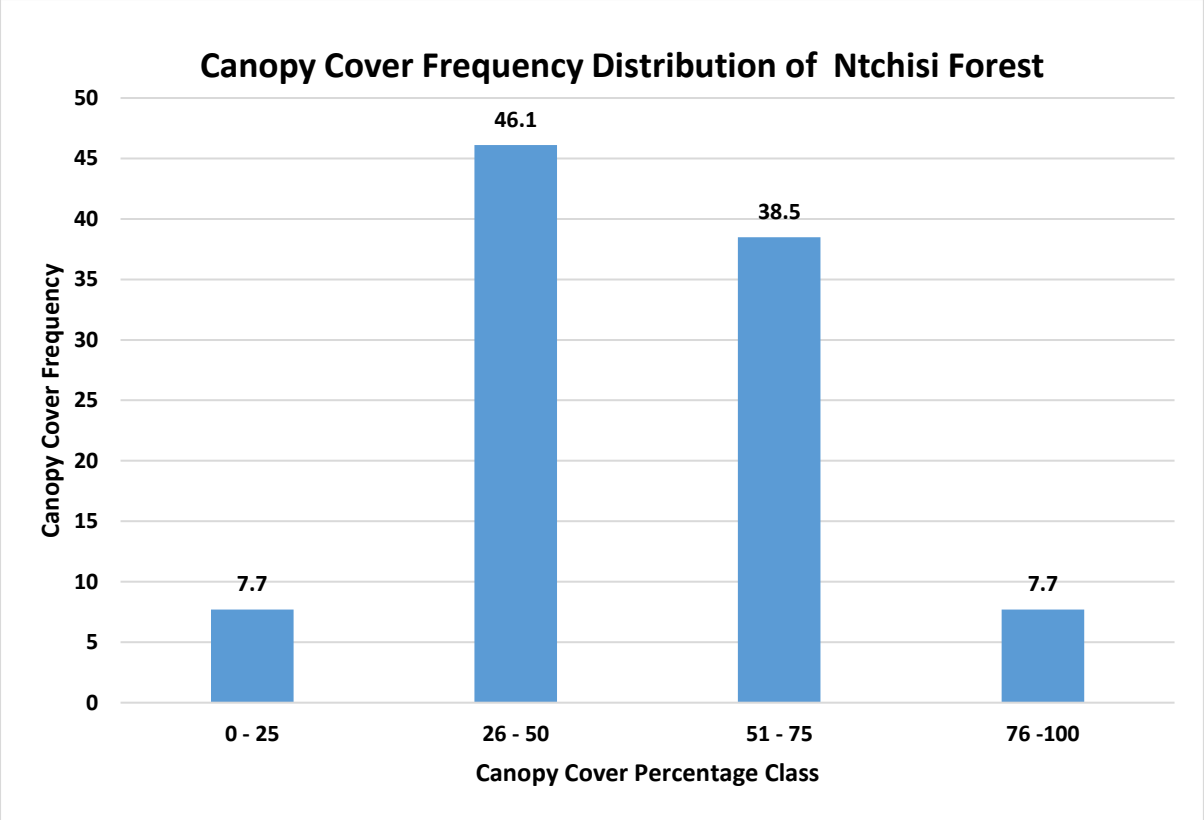

Figure 33. Frequency distribution and percentage density of canopy cover estimated from tree crown diameter measurements sampled in Ntchisi Forest Ground Plots. 46.1% of the forest is covered with moderate canopy density (25-50%) followed by 38.5% with relatively high canopy density from the percentage class of (51-76%). The two density classes yielded 84.6% of canopy cover density.

The figure 33 portrays the frequency distribution of canopy cover estimated using the tree crown diameter measurements of all the 13 ground-based plots sampled in Ntchisi Forest. It further derives the canopy cover density in percentage. The trend shows that the reserve has more areas (46.1%) with moderate canopy densities (25-50%) followed by those (38.5%) with higher canopy densities (51-75%). While this implies the reserve is well covered by forest (84.6%), the 7.7% cover within the range 76-100% suggests there are few areas densely covered by trees. Some of these have individual tree crown overlaps and/or multi-story canopies which were also observed during the 2016 inventory (USAID PERFORM, 2017).

Inversely, the low canopy density (7.7%) from the 0-25% range can be attributed to the intensity of the anthropogenic activities such as wood extraction (firewood, timber, poles, charcoal etc. for both domestic and commercial use), effect of fire and grazing

that the reserve encounters (Fig. 42) (Chinangwa et al., 2016; Ntchisi District Assembly, 2007).

4.1.3 Parametric correlational relationships of ground measured variables

This section delivers the correlational relationships of tree parameters analysed using the coefficient of determination (R^2). Initially, the ground-based parameters (*dbh*, height and crown diameter) were subjected to an exploratory regression analysis to uncover how they relate with each other. This was followed by analyses that involved upscaling of the datasets through calibration and validation (through regression technique) of the airborne and satellite EO while using the ground-based (gb) measurements as reference data.

Initially, the following set of regression analyses were run in order to establish the relationship of the gb and the low-cost optical airborne based datasets; (i) gb individual tree height versus airborne (UAV) based height, (ii) gb fractional cover versus UAV-based fractional cover, and (iii) gb AGB and UAV based fractional cover. Upon establishing the correlational relationship of the gb and the UAV based measurements, the next stage involved upscaling the datasets using the unrestricted satellite EO. This was done by conducting regression analyses of the following; (i) gb AGB versus ALOS-PALSAR-2 based AGB, (ii) gb AGB versus ESA-CCI biomass Map based AGB, and (iii) gb AGB versus Sentinel-1C-band measurements.

During the preliminary analysis, some relationships were inexplicit due to the environmental factors encountered at the time of data acquisition *visa-vis*; (i) tree phenological and seasonal changes (fire inclusive), (ii) terrain, (iii) abrupt wind speed changes encountered during UAV flight missions (afore-mentioned in section 2.8). In such circumstances, regression analyses served to better clarify the relationships. Studies reveal that regression models have been used to select independent variables and improve the coefficient of determination (Adame-Campos et al., 2019; Kadzuwa and Missanjo, 2023; Kronseder et al., 2012).

The diagram next demonstrates the correlation of the gb measurements involving individual tree *dbh* and crown diameter parameter values of 10 largest trees (dominant) from each of the 13 plots of Ntchisi.

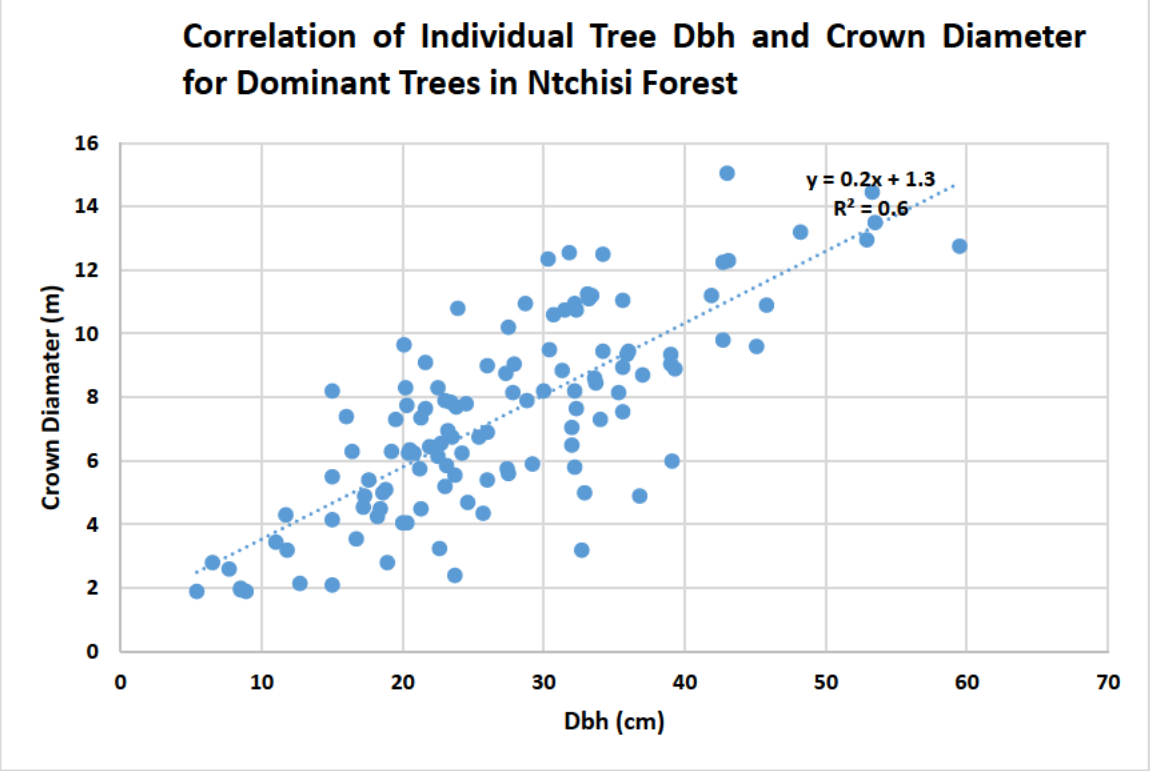

Figure 34. Correlation of dominant individual tree *dbh* and crown diameter sampled from 10 largest diameter trees of each of the 13 ground sampling plot units of Ntchisi Forest. Yielded a positive correlation of $R^2 = 0.6$, suggesting crown cover is dependent on the stem form (*dbh*) of the trees in the forest.

The *dbh* and crown diameter parameter values of plot dominant trees (10 largest diameter trees) in Figure 34 above show a positive correlation ($R^2 = 0.6$) signifying that the crown cover of the forest is dependent on the stem form of the trees. Tree *dbh* and height are key parameters that define AGB, at least inferring from the local models developed for Malawi's Miombo Woodlands (Government of Malawi, 2019a; Kachamba, 2016; USAID PERFORM, 2017; Wildlife Action Group, 2018). However, the positive correlation showcased above suggest that even both *dbh* and crown diameter can be used reliably and independently to inform/estimate AGB and C patterns in Miombo Woodlands of Malawi.

Nevertheless, some trees in the plots, i.e., one sampled from Chenche (P5) (Fig. 35) and the other from Kajaliza (P2) exhibited declining (small) crown expanses (0.3m and 0.1m, respectively) and these were a few examples among many that exhibited such attributes. The two trees sampled were leaning, yet, sprouting while recovering from fire that degraded their original crowns. Such trees have however affected the

correlational relationships and more importantly, the AGB estimates at large. Research indicates that while dominant plants bear linear diameter-height trajectories, the suppressed display curved patterns, with diameter growth declining more than height growth (Fig. 35) (Sumida et al., 2013).

The next figure shows the status of the canopy cover density of one of the Miombo plots captured during the 2019 ground based AGB inventory.

Figure 35. Low canopy cover density of plot 5 (P5) due to fire and wood extraction sampled in Ntchisi Forest; (i) open/sparse canopy cover, (ii) learning and sprouting trees bearing small sized crown, and (iii) uneven height and wide range of diameter classes due to fire and wood extraction. These affect biomass estimations modelling.

Dry season forest fire contributes to the structural changes of the Miombo woody biomass thereby affecting biomass mapping efforts (Chidumayo, 1997; Kamusoko et al., 2014; Ryan and Williams, 2011). A study focusing on modelling of Miombo showed that the woodland's tree populations and biomass are overly sensitive to fire intensity i.e., large stems (>5 cm dbh) are vulnerable to fire, with top-kill rates of up to 12% in

intense fire (Kadzuwa and Missanjo, 2023; Ryan and Williams, 2011). A recent study on the effects of drivers and their variations on stem density and aboveground carbon removals in Miombo woodlands of mainland Tanzania revealed that fuelwood and charcoal caused higher degree of tree removals (Manyanda et al., 2021).

Further analysis involving all trees sampled per plot in this study exposed a diverse range of strengths of correlation, thus from R^2 0.5 to 0.8 (Fig. 37). This, therefore, implies that there are different environmental and anthropogenic factors leading to the variations in plot-level AGB and C stocks and they ought to be well understood to accurately estimate the stocks in these Miombo Woodlands.

The next figure is a scatter plot displaying the relationship of gb AGB in $tCha^{-1}$ and gb fractional cover percent analysed from the 0.1ha 13 sampling ground plots of Ntchisi Forest.

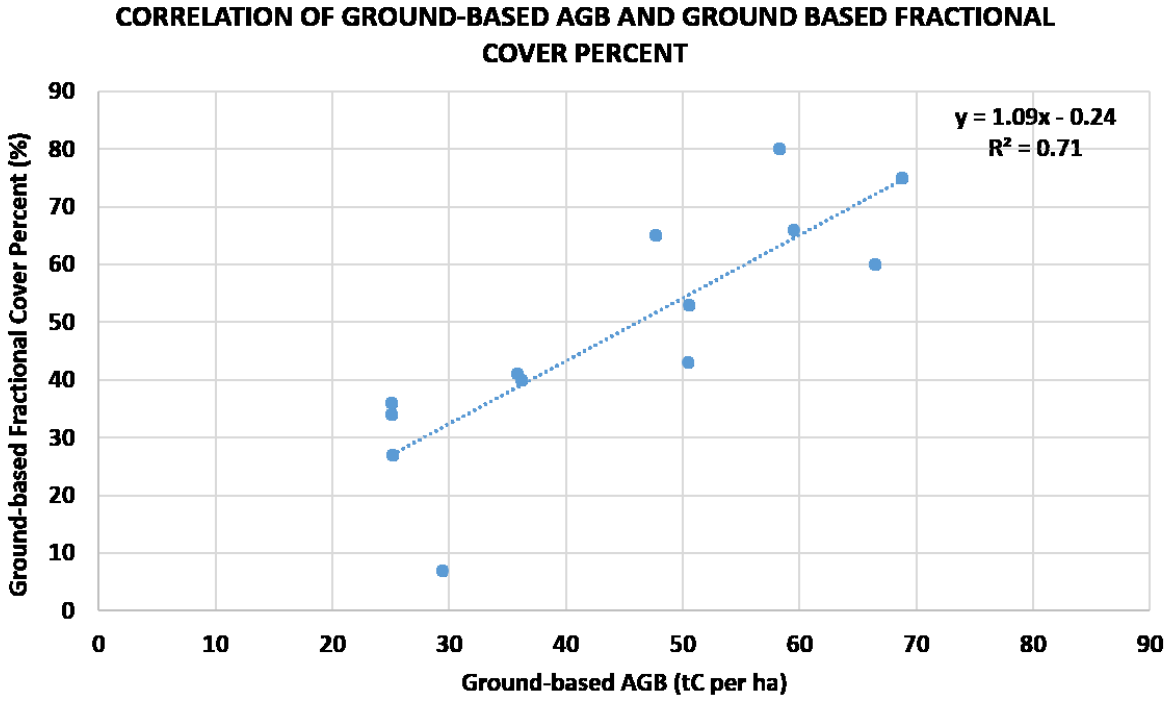

Figure 36. Correlation of ground-based AGB in $tCha^{-1}$ and ground-based Fractional Cover percent (R^2 = 0.7) for each of the 13 ground plots in Ntchisi Forest. An example of how fractional cover is closely related to AGB.

The above graph shows an incredibly positive correlation (R^2 = 0.7) of ground-based AGB ($tCha^{-1}$) and ground-based fractional cover percent. The AGB and fractional cover (FC%) trend displayed sufficiently supports the observations that forest structure

parameters that combine height and gap fraction are closely related to biomass (Ni-Meister et al., 2010). Hence, it implies that the ground-based FC % of Ntchisi Forest is to a significant extent, dependent on its AGB. Alternatively, this implies that the canopy cover in this woodland can be reliably used to explain the AGB pattern.

4.2 Upscaling of Ground-based Measurements using Optical UAV Imagery

This section forms an initial step in establishing whether the low-cost optical 3D CHM derived under S*f*M can be used to estimate AGB in rugged terrain Miombo Woodlands of Malawi. It calibrates and validates the airborne observations (height and canopy cover) using the gb measurements (reference data) while simultaneously scaling them up, thereby directly addressing objective 1.

4.2.1 Correlation of gb individual tree height and airborne based-tree height.

As explained in section 2.4.5 (Caveats in airborne observations and their mitigation), the airborne observations were affected by phenological and seasonality conditions (i.e., leaf-off and fire). This is in addition to the effect of abrupt wind speed change during airborne survey (Fig. 38), fire (Fig. 35 and 42) and steep slopes (Table 6). Despite the efforts to mitigate these which included smoothing filters in ArcMap software, the errors were still inherent in the CHM layers of some of the plots. These were discovered during the preliminary analysis. Hence, for some plots where the UAV predicted heights registered >50% null and underestimated values of ≤1.5m, an average (mean) value was used to normalise the datasets, following the Z-score method.

Ecological studies on biomass have suggested the use of Z-score scaling in regional analyses, especially where fire frequency is high due to long-term human influence (Blarquez et al., 2015; Power et al., 2008; Vannière et al., 2016). Different studies also recommended that where variables do not give equal contribution to the analysis due to known factors, Z-score transformations reduce the influence of outliers while maximising small-scale variation in the dataset (Marlon et al., 2016; Sedgwick, 2014). Therefore, it was fitting for this incumbent study to apply this technique to some of the plots in Ntchisi (Malawi's Miombo Woodlands) where seasonal fire is common and known to highly affect biomass measurements.

The Z-score process involved computing mean (average) height of the plot values using an *a priori* information (the 2019 gb height datasets that were also compared to the 2016 data for the same sites) (Kachamba et al., 2016; USAID PERFORM, 2017). The Z-score method employed the following formula;

$Z = (x\text{-mean})/std.dev$

Where;

Z = Z-score, the standardised value,

x = raw score,

Mean = the average value of the sample,

std.dev = the standard deviation of the sample.

The next figure shows the range of the strength of the correlation of gb individual tree height and airborne-based (predicted) measurements in Ntchisi Forest. The performance trend demonsrated by the four plots represents the general trend for the entire 13 sample plots that ranged from $R^2 = 0.5$ to $R^2 = 0.8$. However, to maximise space, this has been displayed in four figures (instead of displaying all the 13).

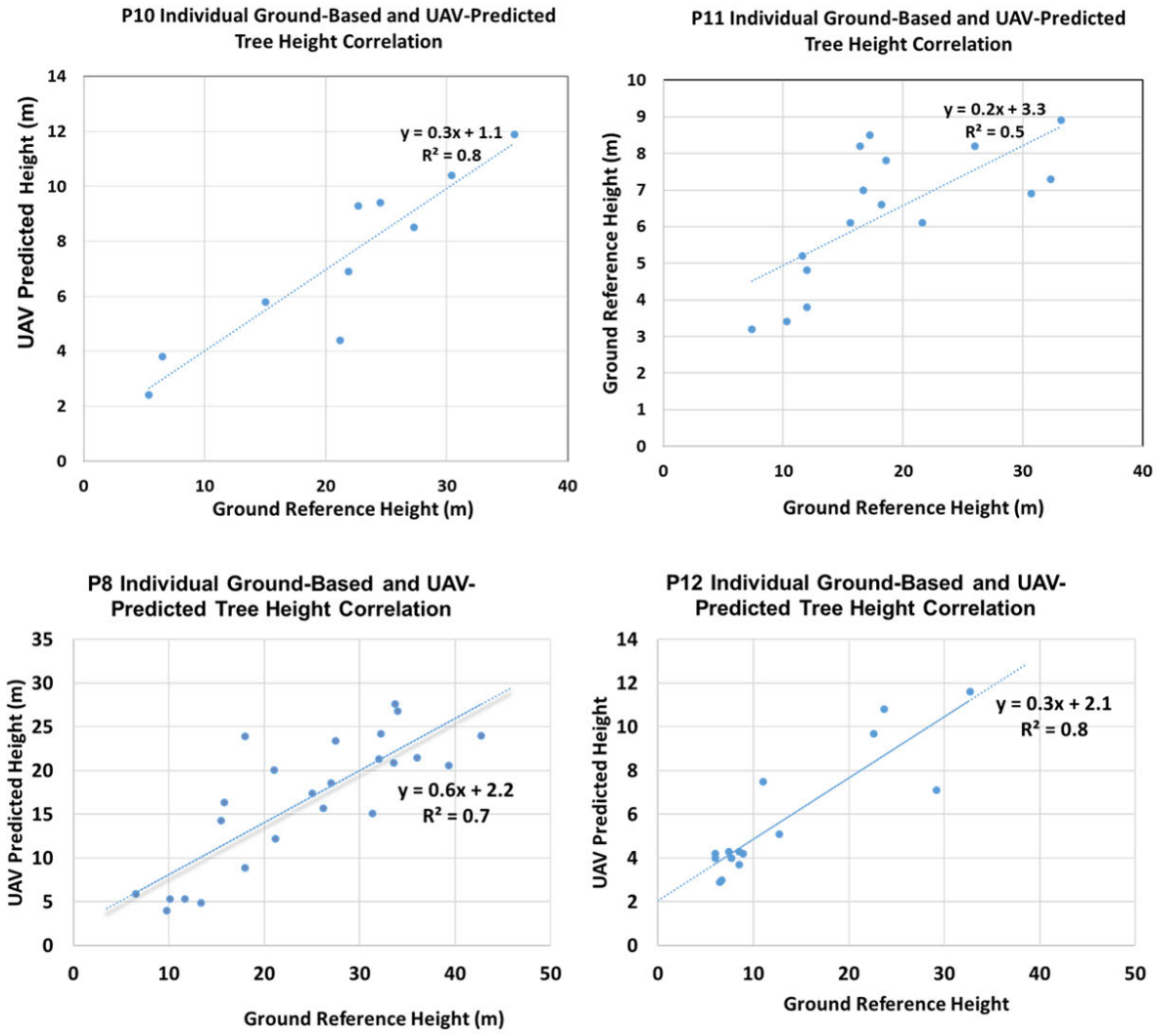

Figure 37. Correlation of ground-based individual tree height and UAV-based tree height: (top-left) P10; R^2 = 0.8, Bias = 5m, RMSE=15m; (top-right) P11; R^2 = 0.5, Bias = 6m, RMSE=14m; (bottom-left) P8; R^2 = 0.7, Bias = 5m, RMSE=10m; and (bottom-right) P12; R^2 = 0.8, Bias = 5m, RMSE=10m. Positive correlation throughout with constant Bias and relatively higher RMSE values, indicative of systematic error associated with the accuracy of the optical drone imagery processed under SfM photogrammetry. Slightly low correlation in P11 signifying the effect of slope and wind speed upsurge.

In Figure 37, the correlation of the gb individual tree height and the predicted airborne height show a positive correlation range of (R^2 = 0.5 to 0.8). A sample mean value of the coefficient of determination (R^2 = 0.70) for P10, P11, P12 and P8 was computed from their R^2 values; 0.84, 0.78, 0.66 and 0.50, respectively. This was used to standardise the predicted values using the *Z*-score method only for the height values that were <1.5m (Blarquez et al., 2015; Power et al., 2008; Vannière et al., 2016). The height threshold was set basing on the fact that the minimum individual tree height value from the 216 trees sampled during this study's ground-based measurements is ≥1.5m. Recent studies have shown that UAV measurements of tree height processed

under S*f*M generally tend to be lower than the actual gb values (Kameyama and Sugiura, 2020; Mohan et al., 2017).

Briefly, the analysis of the ground-based height and the UAV-predicted height has rendered a positive correlation throughout, though the Bias and RMSE values were consistently observed, indicative of a systematic error associated with the accuracy of the optical drone imagery processed under SfM photogrammetry. Some studies have revealed that though individual tree detection using UAV data processed under S*f*M technology can yield an accuracy >85%, the algorithm is capable of missing and/or falsely detecting some trees, despite applying smoothing windows (Mohan et al., 2017).

Besides, the lower predicted height values, (the null/missing values inclusive), and the low height correlation observed in some plots of Ntchisi are not only attributed to the accuracy of the drone imagery processed under S*f*M photogrammetry (Mohan et al., 2017; Zhou et al., 2013); but also, to the environmental factors such as fire. This is even more vivid in P11 where they signify the effect of slope and wind speed upsurge as explained earlier.

Fig. 38 below displays correlational relationships observed between the ground-based AGB (tC/ha) and UAV-based AGB (tC/ha). The AGB calculations were estimated from the dominant trees (10 trees with the largest diameters per plot).

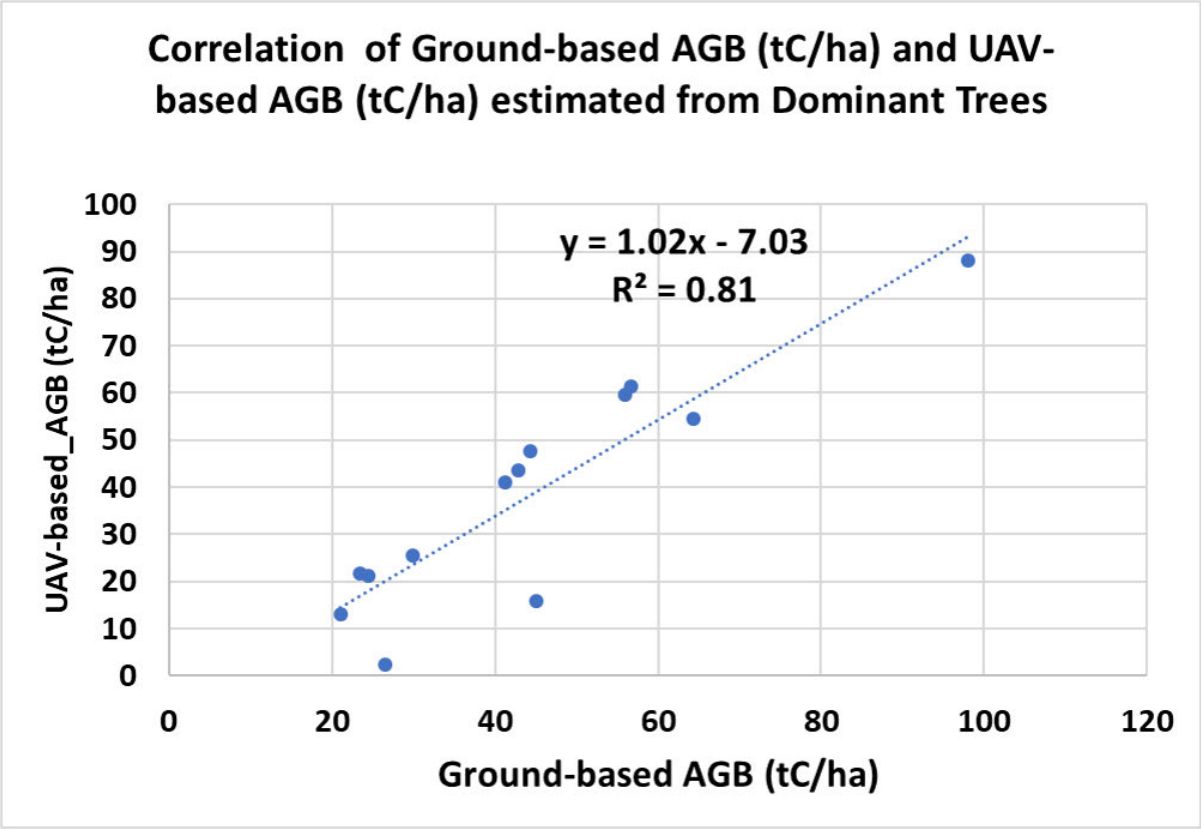

Figure 38. Correlation of ground-based AGB (tCha^{-1}) and UAV-based AGB (tCha^{-1}) estimated from plot dominant trees. Dominant ground-based canopy height and dominant UAV canopy height (R^2 =0.81, RMSE = 12tCha^{-1}, Bias = 8 tCha^{-1}) for all 13 plots. Results show P11 and P3 yielded higher deviations of 24.2tCha^{-1} and 29.8 tCha^{-1} in the correlation, attributable to the effect of slope and wind speed upsurge.

Figure 38 above displays a scatter plot of ground-based AGB (tC/ha) and UAV-based AGB (tCha^{-1}) from all the 13 plots. It shows a strong correlation between the ground-based AGB, and the UAV based AGB (R^2 = 0.81, RMSE=12 tCha^{-1}, Bias = 8tCha^{-1}). The UAV-based estimated height values were derived from the canopy height model (CHM). The AGB datasets were computed using the Malawi local allometry for calculating Miombo AGB (Equation 2) thus; (AGB = 0.104 x dbh^1.921 x ht^0.845).

However, P11 with an extreme slope of 32% (Table 6) registered 26.5tC/ha against 2.3tCha^{-1} for ground-based and UAV based AGB, respectively, yielding a deviation of 24.2tCha^{-1}. P3 which was affected by wind speed upsurge (from 8.4m.s^{-1} thus to 13.1m.s^{-1}) during the airborne survey registered 45.1tCha^{-1} against 15.9tCha^{-1} for ground-based and UAV based AGB, respectively. This bore a deviation of 29.8tCha^{-1} to the correlation. These trends suggest the effect of both the slope and wind speed upsurge on the accuracy of AGB estimation in these Miombo Woodlands. While a tropical woodland study only highlighted that terrain steeper slopes (>35%) affect

biomass predictions though with a small magnitude (Domingo et al., 2019); a different study noted that the accuracy of a DEM (constructed under S*f*M) in a forest is highly dependent on topographic slope (Fayad et al., 2021). Hence, the steepness of the slopes in P11 terrain affected the determination accuracy of the ground (Kadzuwa and Missanjo, 2022b).

Further observations on dominant height revealed that an RMSE increase of 14% can be acquired over slopes >20%, in comparison to slopes between 10% and 20% (Fayad et al., 2021). These findings are in line with the recent Tundra region research outcomes which despite observing a positive correlation between canopy height measured using *in-situ* methods and the drone-photogrammetry based one, the later bore higher biases, comparatively (Cunliffe et al., 2020).

Similarly, the 29.8 $tCha^{-1}$ deviation registered by P3 (between the ground-based and the UAV-based AGB, in contrast, is attributable to the sharp rise of wind speed (south-easterly wind) encountered during the flight mission. Precisely, UAV's back and head wind speed abruptly peaked from an average of 8.4 $m.s^{-1}$ and further beyond the average speed of 10.4 m.s-^{1} to 13.1 m.s-^{1}, rendering considerable degree of mobility to the tree crowns that form the upper canopy height. This resulted to a shift in the *xy* positions, and the maximum and lower limits of the crown as detected by RGB camera sensor aboard the UAV. The repercussions were that the movement affected the feature combination of pixel values in the overlapping images which would have become tie-points during S*f*M photogrammetric process, a condition also observed by several studies (Chen et al., 2022; Uyttendaele et al., 2001; Westoby et al., 2012). Eventually, the shift error was inherent in CHM point-clouds and the extracted values. This contributed to higher deviations between the CHM and the ground/reference height values.

In the same regard, recent forestry research involving S*f*M photogrammetry acknowledged that feature matching algorithms are challenged by the potential movement of branches by wind, an attribute that can induce uncertainty, consequently leading to incomplete reconstruction and/or noisy point-clouds (Iglhaut et al., 2019; Kadzuwa and Missanjo, 2022b). These findings support previous research highlights that wind speed and slope affect biomass estimations in tropical woodlands though the details on how this happens were not neatly divulged (Domingo et al., 2019).

In summary, the strong and positive correlation displayed by the ground reference AGB and the airborne based AGB establishes the feasibility of upscaling the ground based-AGB of Malawi's Miombo Woodlands using the low-cost optical UAV observations obtained under S*f*M. Nevertheless, such an approach should consider the following environmental factors that can hugely compromise accuracy of the results; the topography and the weather changes (wind speed) during the flight missions. Besides, biomass estimations that use S*f*M photogrammetry acquired data should account for systematic errors associated with height measurements of the craft/vehicle used, thus for better accuracy.

4.2.2 Correlation of ground-based and airborne-based estimates

Plot-based AGB and their corresponding airborne-based crown diameter pixel values extracted from the CHM (hereafter renamed UAV canopy cover/fractional cover percentage) covering the 20m radius (0.1ha) plots were regressed. The figure next displays a relationship pattern established from the regression of the datsets.

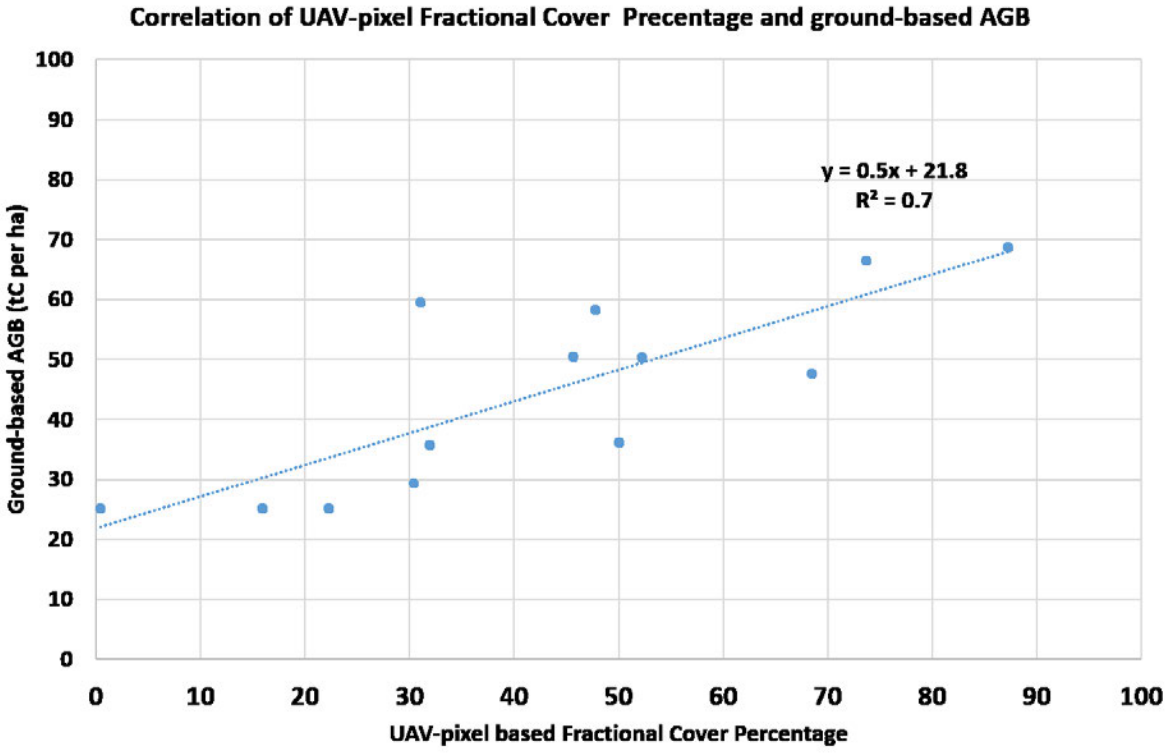

Figure 39. Correlation of UAV Fractional Cover percentage (FC %) and ground-based AGB (tC per ha) at $R^2 = 0.7$, observed from13 sample plots of Ntchisi. P6 shows an exception trend of low ground-based AGB (25.1 $tCha^{-1}$) against 0.5% of the airborne-based fractional cover due to fire that swept the plot after the ground biomass data collection, but prior to the airborne survey, thereby lowering correlational relationship.

Figure 39 shows a high correlation (R^2 = 0.7) observed between the UAV FC % and the gb AGB ($tCha^{-1}$). The general pattern demonstrates that the fractional cover of Ntchisi Forest can be used more reliably to express the AGB pattern of the Miombo Woodland. This is in comparison to the height parameter acquired from CHM of the (UAV datasets) whose correlation has not been consistent enough as it ranged from as low as R^2 = 0.5 (Fig. 37).

However, P6 has shown a unique trend by registering a ground-based AGB stock of 25.1$tCha^{-1}$ against the airborne based 0.5% fractional cover. The variation is attributed to the fire damage that occurred within the lapse period since the ground-based measurements took place (18th September 2019) and the airborne survey (6th October 2019) in the same plot. While fire was physically encountered during both surveys (Fig. 42), studies agree that fire is an environmental factor that reduces both AGB and canopy cover in Miombo Woodlands (Chidumayo and Gumbo, 2010; Nieman et al., 2021; Ribeiro et al., 2012).

In addition to P6, the correlation pattern displayed above (Fig. 39), depicts corresponding and consistent (though low) pattern of values between the UAV–based fractional cover and gb-AGB in Chenche (P5) whereby AGB of 59.5$tCha^{-1}$ is plotted against 31% FC, respectively. This is also ascribable to fire effect in the dry season.

Inversely, the pattern displayed by (P8), whereby high AGB of 68.8$tCha^{-1}$ is plotted against 87.2% FC renders a good example of the impact of better conservation compounded by less exposure to anthropogenic activities such as fire and wood extraction (Munthali, 2013; Munthali and Murayama, 2015). For P8, this is ascribable to less accessibility because of its extremely dangerous terrain (74% slope), in addition to its long distance (less proximity) from villages (~1.8km from the forest boundary, Table 6 and Fig. 43), compared to other plots that are <1km from the plot edge or surrounding villages.

On the whole, the positive and consistent correlation displayed by the UAV fractional cover percentage and the gb AGB above forms the key basis for upscaling the gb-measurement while simultaneously establishing the relationship of the two datasets, thus in reference to the specific objectives 1 and 3 of this study.

In summary, the findings suggest that fractional cover (which is derived from crown diameter measurements) is more reliably correlated to the AGB than the height estimates from the CHM, given the current conditions of Ntchisi Forest. However, the proximity of a plot to the surrounding villages, and topography affect the plot's access and eventually the AGB stock.

The next figure displays correlational relationship between the ground-based fractional cover percentage and Ground-based AGB (tC per ha).

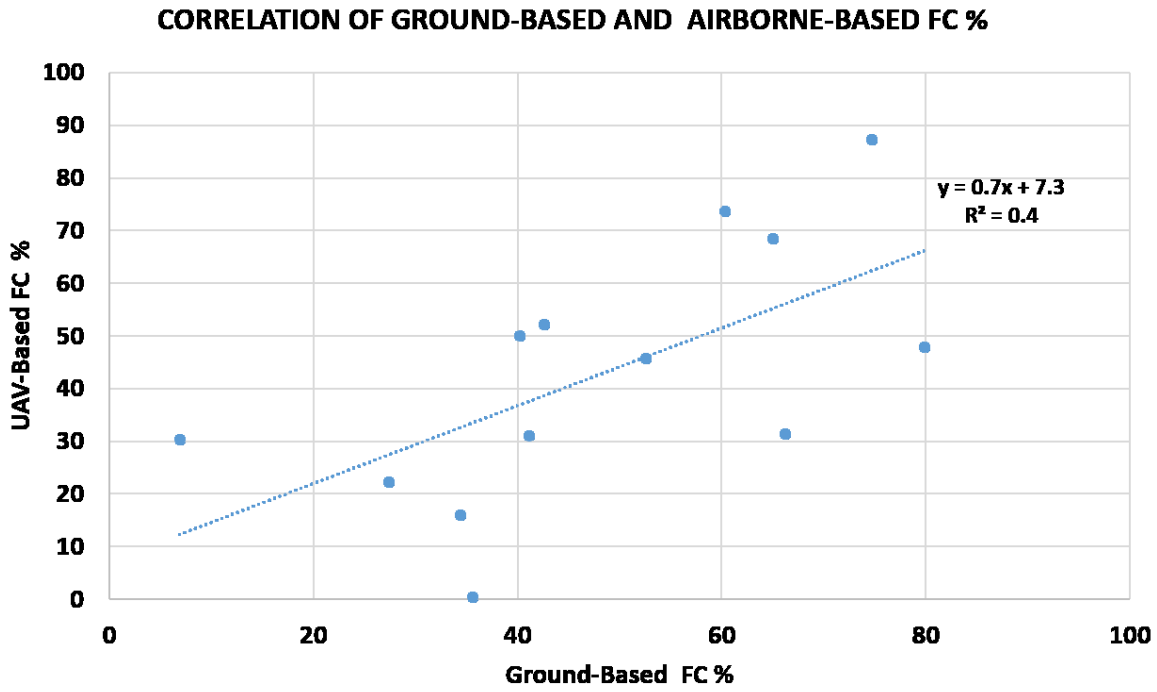

Figure 40. Correlation of UAV-based and ground-based Fractional Cover Percentage (FC %) (R^2 = 0.4) revealing factors affecting fractional cover and woody biomass estimation such as edge-effect, overlapping of tree crowns and clumping of individual trees, fire, leaf-phenology, and topography.

Figure 40 above displays a weak correlation (R^2 = 0.4) observed between the ground-based factional cover percent (gb-FC %) and the UAV-based FC %. Deviations of the values expressed by the UAV-based FC % when regressed against the reference/ground measurements (Fig. 40) are partly attributed to the following factors: (i) edge-effect, (ii) overlapping of tree crowns, (iii) clumping of individual trees and (iv) fire, primarily on part of the ground datasets; and (v) the effect of leaf-phenology (leaf-off and fire, Fig. 42) and (vi) topography and optical sensor data challenges of

underestimations (Cutler et al., 2012; Naidoo et al., 2016), on the part of the UAV based datasets.

While the ground-based FC % values fall within the expected range, as informed by the 2016 Ntchisi Forest inventory (USAID PERFORM, 2017); the current analysis demonstrates that P1, P5, and P6, contributed much to the poor correlation of the airborne and ground-based FC %. This is due to the edge-effect, crown overlaps, clumping of trees and topography attributes observed in these plots. Recent studies revealed that tree crown border effects constitute an important source of uncertainty in estimation of forest biomass by remote sensing due to their nature of not being constrained by plot borders (Knapp et al., 2021; Racine et al., 2021). While remote sensing systems record canopy height within a certain area, ground-based measurement commonly record AGB of inventory trees geolocated at their stem positions, thereby confining them to a given plot (Knapp et al., 2021; Racine et al., 2021). However, the nature of the tree crowns is that they mostly reach out of the given plots into other area/adjacent plots (Fig. 41-left), thereby rendering uncertainty to canopy height-based biomass estimation.

From the same pattern displayed in Fig. 40 above, despite the low airborne-based FC % registered by P6 and P5, their crown diameter, crown area, *dbh* and height per plot, respectively, are above average (Fig. 26 and Table 16), thus suggesting how well correlated to their FC % they ought to be, *ceteris paribus* (Gonzalez-Benecke et al., 2014; Shimano, 1997). In this regard, the underestimations by the UAV-based data are attributable to the effect of crown overlap and overhanging of individual trees, in addition to the systematic error perceived in section 4.2. These elements were observed during the terrestrial measurements (Fig.17 and 41).

A closer examination on the ground datasets also confirms clumping and overlapping of individual trees and their crowns, i.e., tree (ID) number 6 and 7 in P10 growing closely together (i.e., UTM 0824116, 36L 0608109 and UTM 0824115, 36L 0608108). The same scenario was true for P6 where tree ID number 2 and 3 overlapped (UTM 08528 308, 36L 0610894 and UTM 08528 309, 36L 0610893) respectively, just to mention, but a few. More suggesting is Chenche (P5) where besides clumping and overlapping of the crowns, a total of 9 trees shares the same *xy* coordinates. For example, tree ID number 1, 2 and 3 are spatially located on UTM 08529 358, 36L

0616730, while tree ID number 8 and 9 share the coordinates UTM 08529 362, 36L 0616732; and 12 and 13 are on UTM 08529 358, 36L 0616725, respectively. However, these are just a few examples observed from the sampled data.

Despite these two attributes, previous studies observed that S*f*M photogrammetric imagery acquired from UAV particularly, tree height, tend to be lower than the actual ground values (Kameyama and Sugiura, 2020). Another study on fractional cover observed that heterogeneity of Savannahs complicates modelling as areas of remarkably high or low coverage get lost by aggregation to coarser scales (Guerschman et al., 2009; Kadzuwa and Missanjo, 2023). Hence, the low values recorded are attributed to the same aspects.

In brief, these patterns show that estimation of fractional cover of the woodlands is dependent on several environmental factors that include; edge-effect, overlapping of tree crowns and clumping of individual trees and fire. Hence, canopy cover density studies should account for these elements for enhanced accuracy of results.

Figure 41. Crown edge effect, overlapping and clumping trees in Mandwe (P6) (*Left, background*) increase uncertainty in AGB and crown estimations. (Right)-Trees on the plot border have their crowns projecting in the adjacent crop fields affecting AGB and canopy accuracy during remote sensing validation.

The closed gaps of canopy formed by the overlapping and overhanging crowns trees partly contributed to the optical sensor's (aboard the UAV) poor detection of these forest covered areas due to the failure of the signal to penetrate the crown surface through to the ground. A study on forest inventory data and simulations of a tropical rainforest's canopy observed that crown overlap and overhanging of individual trees contribute to uncertainty in canopy height–based biomass estimation (Knapp et al., 2021).

Studies have observed that closed canopy structure of a forest plot contributes to the failure of the S*f*M technique to generate enough below-canopy ground points, leading to errors and eventually poor correlation between S*f*M tree heights and ground measurements (McNicol et al., 2021; Mlambo et al., 2017; Sakai et al., 2021).

Research has further shown that irrespective of the processing method, data acquired from optical sensors possess fundamental limitations for mapping woody environments because, unlike SAR systems, the signal reflectance does not directly correlate to surface structure (Cutler et al., 2012; Naidoo et al., 2016). Hence, the canopy/height underestimates characterise the effect of the failure of the optical sensor to penetrate through closed tree canopies thereby acquiring information from the top canopy surface only, while the lower strata or the ground detection is provided in rare canopy gaps (McNicol et al., 2021; Sakai et al., 2021).

On the other hand, for P11 and P12, it is the effect of terrain that contributed to the canopy underestimates since both plots are extremely located on steep slopes (32% and 48%, respectively, Table 6). The topography rendered difficulties in taking accurate height and crown diameter readings in perpendicular to the ground during the terrestrial measurements, resulting to underestimations. Related studies on the effect of topography and other environmental factors affecting Malawi's Miombo Woodlands estimations, i.e., canopy height and AGB revealed that topographic slopes of >15% can contribute to total 17 to 105% AGB variation errors (Domingo et al., 2019; Kadzuwa and Missanjo, 2022b).

The figure below displays some key factors that contributed to the variation of AGB, and canopy estimates captured in Ntchisi Forest during the September-October 2019 ground based and UAV surveys.

Figure 42. Dry season fire, leaf-fall and its effect on biomass in Ntchisi Forest-October 2019; Airborne ortho-photos depicting parts forest damaged by fire and footpaths caused during wood biomass extraction (bottom-left). Live trees scorched by fire during leaf-off season and a burnt deadwood/tree lying on ground (bottom-right) captured during ground survey.

On the other hand, the effect of the slope and the challenges on lack of penetration of the canopy by the signal of the RGB UAV sensor rendered the need for the integration of data acquired from other bands such as Vis/NIR/SWIR composite combination and more significantly from active sensors such as the SAR that are less challenged by such environmental limitations.

The marginal correlation of the ground-based and airborne FC % displayed by some plots, has already been explained by; the edge effect, crown overlaps and overhanging trees, steep slopes and fire, as stated earlier on. Such a correlation portrays the limitations of the ground-based measurements and simultaneously supports the basis of objectives 1 and 2, thus the need to upscale the ground-based measurements to the remotely sensed datasets using the SfM photogrammetric data acquired from optical small-UAV as a link.

In conclusion, the positive correlation between the airborne-based FC % and the ground-based AGB (R^2 = 0.7) support the premise that the optical S*f*M photogrammetric imagery (fractional cover %) can be used effectively used to inform the AGB and in Malawi's Miombo Woodlands. As far as this study is concerned, no previous efforts on forest biomass studies in the Malawi's Miombo Woodlands had explicitly established the correlational relationship between the crown area (canopy cover/canopy fractional cover percentage) and the AGB and C patterns using a statistical regression predictive factor (Government of Malawi, 2019a; Tetra Tec and Winrock International, 2022, 2021).

4.3 Validation and Estimation SAR AGB Datasets

This section analyses the AGB, and fractional canopy cover correlational relationships observed between the ground-based measurements, the UAV datasets and the satellite Earth Observations acquired over Ntchisi Forest. It also further provides an account of their causes and effects. Structurally, the aerial observations (acquired through low-cost S*f*M photogrammetric process) i.e., canopy height and crown cover were used as a bridge to scale-up the gb AGB and FC measurements (objectives 2, 3 and 4) as follows;

(i) initially from 0.1ha terrestrial plots to 50ha UAV plots, and
(ii) from 50 ha airborne observations to wall-to-wall coverage of the unrestricted source global observations from; (a) ALOS-2 PALSAR-2-L-band, (b) ESA-CCI BIOMASS Map, and (c) Sentinel-1-C-band.

4.3.1 Calibration of ALOS-2 PALSAR-2 2019 data

ALOS-PALSAR-2 imagery mosaics are acquired as integers (whole numbers) for efficient data storage, nevertheless, for the sake of interpretation and comparisons in this study, they were pre-processes/calibrated using QGIS (3.10.10) software. The initial step involved transforming the integer datasets into decibels, which are the standard units of radar backscatter measurements. This was carried out using the following equation, supplied together with the datasets from the JAXA website (as explained in section 3.4.1);

$\gamma^{0(\text{decibels})}=10log_{10}(DN^2)-83.0dB$ (Shimada et al., 2009),

Where:

γ^0 =backscattering coefficient (sigma naught or sigma zero) in unit decibels (*dB*),

DN=Digital number (or raw pixel value),

-83=Calibration factor in *dB* units.

The unit result obtained in the imagery datasets are decibels (*dB)* which is a logarithmic measure of the radar backscatter and for this study the values ranged from -43 to 8.7*dB*.

The second step involved calibration of the decibels into the natural units to portray a linear relationship. This process employed the following allometry for HV polarisation;

$\gamma^0(\text{natural})=10^{(\gamma 0(\textit{decibels})/10)}$

The third step involved converting the natural values to units of AGB in $tCha^{-1}$. This process entailed the application of a generic equation derived from Miombo Woodlands (tested in Southern Africa, Malawi inclusive) by (McNicol et al., 2018) as follows;

$AGB=715.667*\gamma^0(\text{natural})-5.967$

Where AGB=Above Ground Biomass

Computation of this process generated an AGB map layer whose visualisation colour ramp were changed to ‘red-yellow-green and pseudocolour’ where; red and green colours denote low and high biomass, respectively, thus for easy visibility and interpretation.

Initially, the AGB propagated included speckle and with values ranging from -5 to $463tCha^{-1}$. Speckle refers to some random constructive and destructive interference from the multiple scattering returns that occur within each resolution cell and render false readings (Woodhouse, 2006). This challenge was resolved by applying a 5 x 5 filter size under the lee technique (low pass) in Sentinel Application Platform (SNAP) 7.0 software. The Lee technique was preferred due to its efficiency in preserving and

smoothening the edges of an image while preserving its details, i.e., pixel values in heterogeneous areas (Sameen et al., 2016).

The next figure shows a 2019 Ntchisi AGB map generated from ALOS-PALSAR-2 datasets in $tCha^{-1}$units.

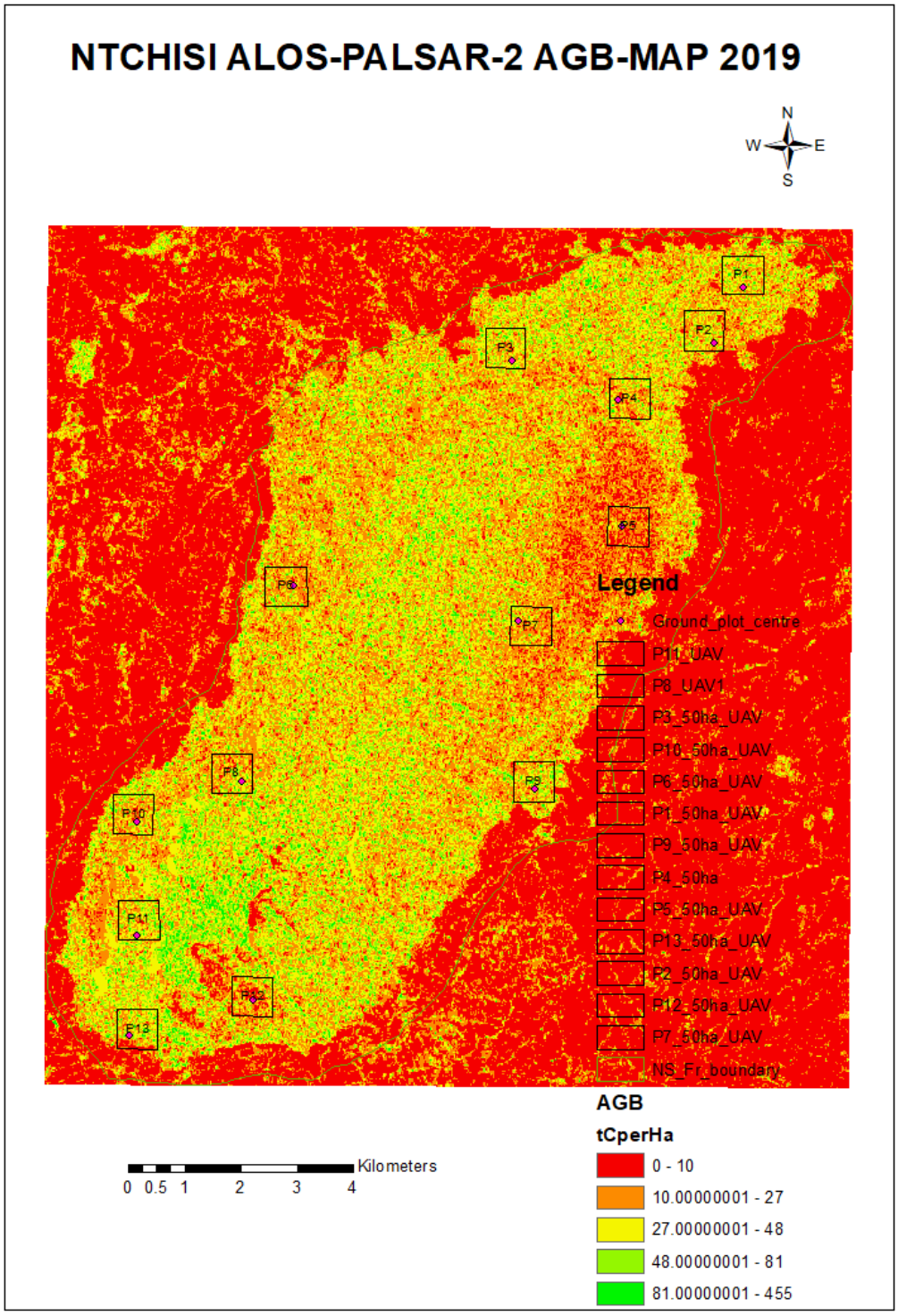

Figure 43. Ntchisi Forest AGB (0-81tCha^{-1}) Map generated from ALOS-PALSAR-2 2019 imagery.13 sampling plot units of 50ha each (size of UAV plots, represented in black square boxes) overlaid on the 0.1ha ground plots, represented in magenta circular boxes.

Figure 43 above shows AGB (tCha^{-1}) map of Ntchisi Forest generated from the 2019 ALOS-PALSAR-2019 imagery with a focus on the 13 sampling plot units. The imagery

overlaid both the 50ha UAV plots as well as the 0.1ha ground plots. The AGB pixel values covering 0.1ha followed by 50ha plots were extracted and from each of the 13 plots by in ArcMap 10.8. These were regressed against their corresponding gb AGB measurements (Tables 15 and 16 and Fig.44). Full analysis details have been captured in the subsequent sections.

4.3.2 Correlation of ground-based AGB and ALOS PALSAR-2 AGB

The scatter plot below displays a relationship between gb AGB and ALOS PALSAR-2 AGB in $tCha^{-1}$ analysed from the 0.1ha plot dimension of Ntchisi Forest.

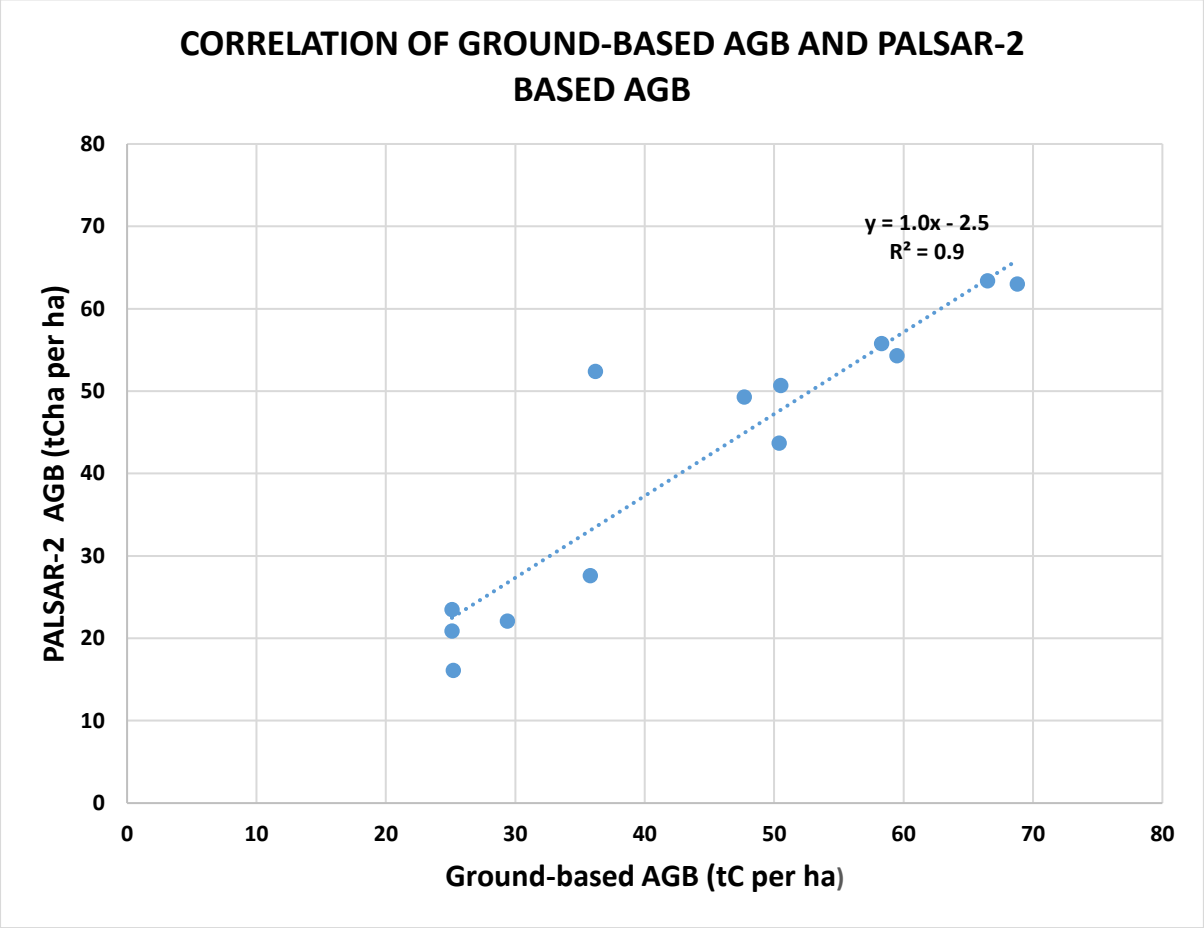

Figure 44. Correlation of ground-based AGB and ALOS PALSAR-2 AGB in $tCha^{-1}$ (R^2 = 0.9, RMSE = 7$tCha^{-1}$, Bias = 3$tCha^{-1}$); a very strong relationship signifying the suitability of the PALSAR-2 datasets in estimating AGB and C in Miombo Woodlands of Malawi.

The above figure shows a very strong relationship (R^2 = 0.9, RMSE = 7$tCha^{-1}$, Bias = 3$tCha^{-1}$) for ground-based AGB and ALOS-PALSAR-2 AGB attained through Linear Regression (LR). The correlation implies that the distribution of the ground-based AGB is highly correlated to the PALSAR-2 AGB in these Miombo Woodlands.

In comparison to the other plots, the analysis further shows a higher bias contribution in P8 (68.8tCha^{-1} for ground-based AGB against 63.0tCha^{-1} from PALSAR-2 AGB) and P11 (36.2tCha^{-1} for ground-based AGB against 54.2tCha^{-1} from PALSAR-2 AGB) whose ground slopes are very steep, thus, 74% and 32%, respectively (Table 6). Therefore, the biases are attributed to the effect of overshadowing and lay-over distortions associated with SAR datasets, especially in the mountainous slopes (Chen and Wang, 2008; Woodhouse, 2006).

The lay-over effect is caused by the look angle of a SAR sensor, especially in mountainous area and results to shortening distance of the imagery for the target features observed (Woodhouse, 2006). Practically, P8 (Fig. 55) has exhibited a pattern of trees' crown growing along the north-south riverine that might have not been conspicuous enough in the PALSAR- backscatter thereby contributing to the lay-over condition.

Furthermore, these observations agree with the findings of a previous study conducted in Malawi's Miombo Woodlands which used ALOS PALSAR-1 backscatter measurements and revealed that their sensitivity was highly attenuated by the topography of the forest site, besides other environmental factors (Cassells, 2012).

Overall, the correlation between the gb AGB and the ALOS-PALSAR AGB implies that the terrestrial AGB inventory measurements in this site can be effectively estimated using the free/unrestricted, but moderate spatial resolution ALOS-PALSAR-backscatter imagery. In this particular case, the use of the low-cost imagery mitigates the inventory costs while at the same time expanding the scope of measurements from the 0.1ha to national wide (wall-to-wall) expanse in these Miombo Woodlands.

The next figure shows the relationship between the UAV-based fractional cover and the ALOS-PALSAR–based AGB.

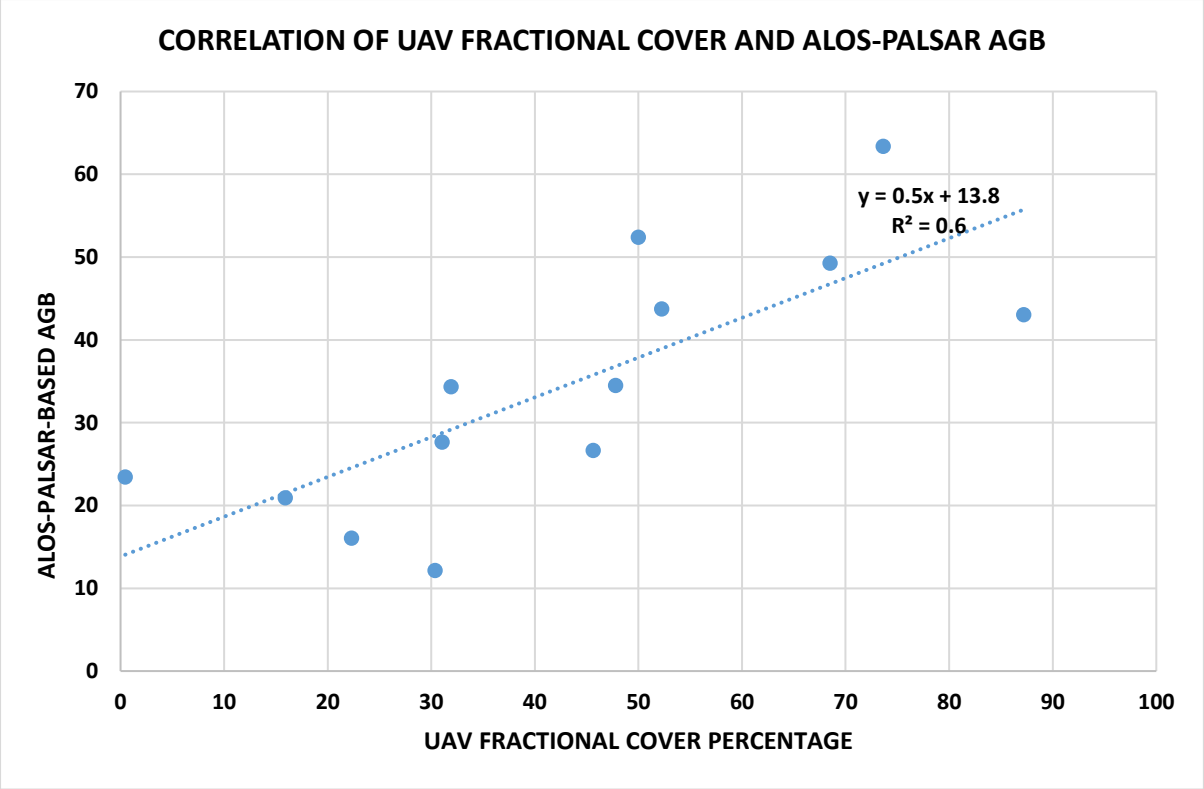

Figure 45. Correlation of UAV Fractional Cover Percentage and ALOS-PALSAR-2 AGB ($tCha^{-1}$) covering the 13 ground sampling units (0.1ha) computed as a total sum of each plot, yielded a positive correlation ($R^2 = 0.6$); characterising the suitability of the optical UAV imagery in linking the ground data with the PALSAR datasets while underscoring the challenge of optical sensors associated with the SfM photogrammetry datasets in underestimating biomass of Miombo.

Figure 45 shows a positive correlation ($R^2 = 0.6$) of the optical airborne FC% and the ALOS-PALSAR-2 AGB. Among others, the scatterplot displays low 30% FC plotted against $12.1tCha^{-1}$ AGB for P12. Inference from the gb parametric trends of the same plot reveals a pattern characterised by; a wide range of *dbh* classes within the 10 dominant trees ranging from 7.7-32.7cm, and a relatively high stand density (15 stems $plot^{-1}$), though bearing one of the 3 least ground-based AGB ($29.4tCha^{-1}$). Similarly, the P6 values extracted from an intercept of airborne 0.5 % FC and $23.5tCha^{-1}$ AGB from ALOS-2 PALSAR-2 observed were the least of all. In the same pattern, the plot also registered low ground-based AGB ($25.1tCha^{-1}$) and a corresponding low stem density (10 stems $plot^{-1}$).

In Fig 45 above, the variation (underestimation) displayed by P1 (68.5% FC from the UAV imagery versus $49.3tCha^{-1}$ AGB from the ALOS PALSAR imagery) is primarily attributable to the effect leaf-off and fire conditions which were observed during both

the ground and airborne surveys in September and October 2019 (Fig. 5). While ~ 70% of the trees had leafed-off, fire erased ~30% of the sample plots immediately after the ground-based measurements, but prior to the airborne surveys of the same study site (Fig. 42). This caused significant AGB estimation variations in the two datasets, i.e., very low values in the airborne observations compared to the ALOS-PALSAR datasets and eventually affected the correlational relationships.

The predicament was also exacerbated by the semi-arid conditions of the study site, which were at peak during the UAV imagery acquisition. Key tropical biomass studies in the African Savannahs reveal that fire is an environmental factor that reduces both AGB and canopy cover in Miombo Woodlands (Chidumayo and Gumbo, 2010; Nieman et al., 2021; Ribeiro et al., 2012). Furthermore, a previous study that focused on the study site noted that Ntchisi Forest, like many Miombo Woodlands is associated with dry season fires that potentially damage the woody biomass (Chinangwa et al., 2016)

From the point of optical remote sensing view (affecting the UAV FC, in this case), the previously mentioned *rara-avis* were sufficient to induce low signal detection of tree AGB (Fig. 40 and 41). Recent comprehensive study on remote sensing of phenology among plant communities revealed that foliar senescence and dry conditions exacerbated during fire occurrences lead to low biomass detection by optical sensors (Vrieling et al., 2018; Zhu et al., 2021). Studies observed further that optical imagery collected during dry season lack phenological information useful for discriminating deciduous formations because their spectral reflectance is sensitive to vegetation structure (leaf area index, crown size and tree density), texture and shadows which may be affected by the arid conditions (Nunes et al., 2022; Zhang and Ni-meister, 2014).

Unlike the EO acquired from active sensors, i.e., SAR backscatter measurements whose signal detection is based on direct correlation to surface structure, the optical datasets render fundamental limitations for mapping woody environments because they lack this aspect (Cutler et al., 2012; Naidoo et al., 2016).

Inversely, it is not a surprise to observe the ground-based AGB measurements and the ALOS-PALSAR-based (measurements from active sensor), i.e., in P1 (25.1tCha-

^{1}) from the gb-measurements and 23.5tCha^{-1} from the ALOS-PALSAR imagery rendered a higher correlation in contrast to the ones from the optical datasets (UAV imagery) (Table 15 and Fig. 44 and 45). This because despite the leaf-off condition and fire-season (hazy and clouds conditions, inclusive); the SAR dual-cross polarised (HH+HV) PALSAR-L-band datasets employed operated well, regardless of the weather conditions and they are more correlated to the stems and trunks than just the leaf biomass, due to their longer wavelength (~23cm) penetration (Cassells et al., 2009; Cutler et al., 2012; McNicol et al., 2018; Naidoo et al., 2016).

These correlated values of earth observations (FC % and AGB) acquired from both optical and active sensors discernibly corroborate with the earlier assertions established by this very same study (from ground measurements, though) that the AGB of Ntchisi Forest is not merely expressed by stem density, but its canopy cover. More than anything else, the consistent trend of (low values) attained particularly by these two plots thus P12 and P1 pertaining to the optical airborne and radar backscatter measurements suggest the high predictive power that the two selected datasets rendered in estimating AGB of the Miombo Woodlands.

Briefly, these findings support the premise that the low-cost UAV orthomosaics acquired through S*f*M (the FC% in this case) can be effectively used as the bridge to scale-up the terrestrial *in-situ* measurements (that are deemed expensive yet, cover limited area) to the EO from ALOS–PALSAR from unrestricted source, but have got better resolution in estimating AGB. However, critical considerations should be made on the accuracy challenges that the optical imagery are associated with during AGB estimations as encountered in this study.

4.3.3 Determination of ESA CCI Biomass Map AGB for Ntchisi Forest

Another set of analysis involved AGB pixel values covering both the 0.1ha ground plots and the 50ha UAV plots were extracted from the ESA CCI Biomass Map 2018 datasets acquired over Ntchisi. These were processed in ArcMap 10.8 software. The ESA-CCI datasets comprised the SAR backscatter measurements from ALOS-PALSAR and Sentinel-1 *inter alia*. From these datasets, an AGB map was generated as displayed in the next figure.

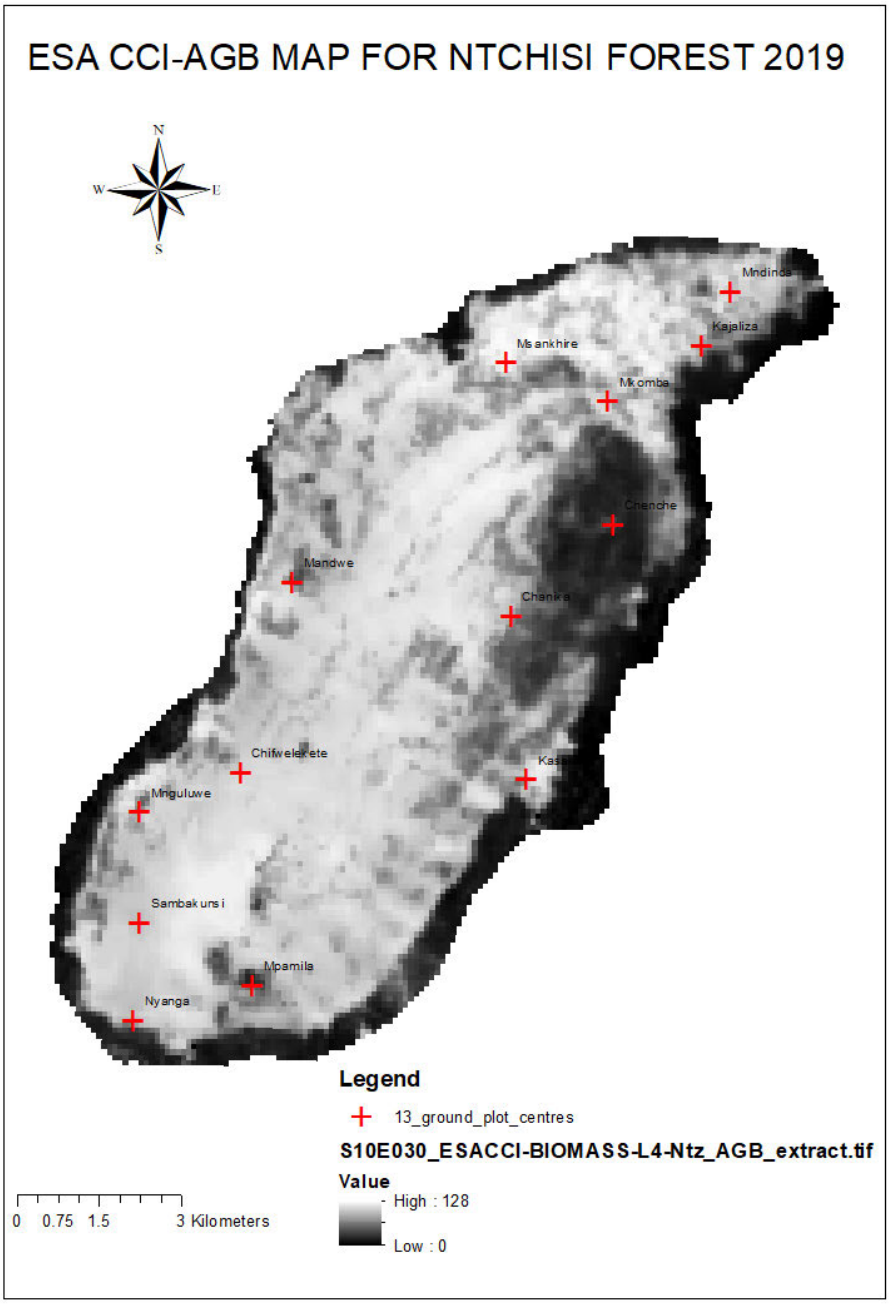

Figure 46. Map of Ntchisi Forest ESA-CCI AGB 2018 (0-128tCha^{-1}) estimated from the 13 plots overlaying both the 0.1ha ground plots and the 50ha airborne plots. The red plus sign represents the ground plot centres. While the scale of the AGB ranged from 0-128 (tCha^{-1}) throughout the forest. The specific 13 plots estimates analysed ranged from 16-50.8tCha^{-1}. They fairly compare with the 25.1-68.8tCha^{-1} estimated from ground-based datasets. S10E30_ESACCI-BIOMASS-L4-Ntz_AGB_extract.tif represents the imagery layer of ESA-CCI Map AGB dataset covering Ntchisi in GeoTiff.

The 2018 ESA–CCI AGB plot estimations ranged from 16-50.8tCha^{-1}. They fairly compare against the ground-based AGB which range from 25.1 - 68.8tCha^{-1} (Table

15), suggesting their suitability when used for assessing AGB in the Miombo Woodlands.

The next diagram (Fig. 47) depicts correlational patterns between the ground-based AGB and ESA-CCI above ground biomass, both in $tCha^{-1}$ units.

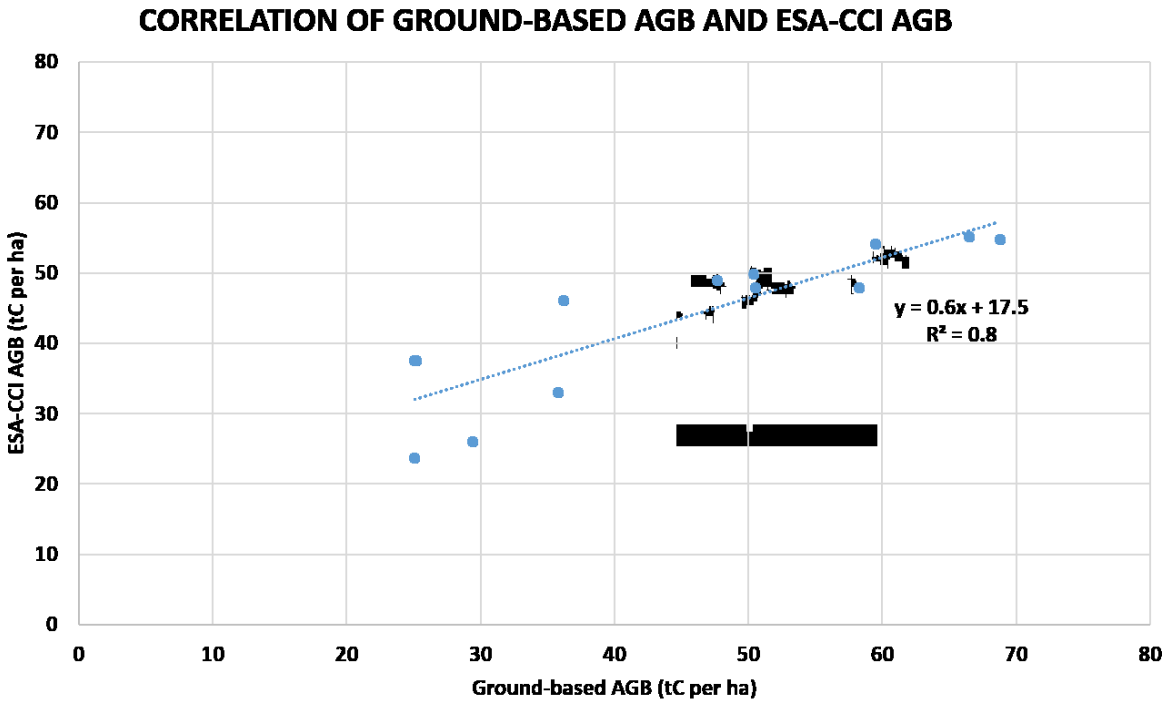

Figure 47. Correlation of ground-based AGB in $3tCha^{-1}$ and ESA-CCI AGB in $tCha^{-1}$ $R^2 = 0.8$, RMSE = $8tCha^{-1}$, and Bias = $1tCha^{-1}$, an extraordinarily strong relationship signifying the suitability of the ESA-CCI BIOMASS Map imagery dataset in estimating AGB and C in Malawi's Miombo Woodlands. A clear saturation pattern observed as the AGB reaches ~$50tCha^{-1}$ on the part of the ESA CCI AGB.

In the above figure, another strong correlation ($R^2 = 0.8$, RMSE = $8tCha^{-1}$, and Bias =$1tCha^{-1}$), has been observed between the ground-based AGB and ESA CCI above ground biomass. Two plots bear similar AGB stocks ($25.1tCha^{-1}$ and $25.2\ tCha^{-1}$ for the ground based P2 and P10) and $36tCha^{-1}$ each for both P11 and P7 ESA-CCI datasets, as a result these points have coincided as one point in the scatter plot above.

However, the ESA CCI AGB pattern shows a vivid saturation condition as the AGB reaches ~$50tCha^{-1}$. Studies in Savannah woodlands, some of which were conducted in the Miombo observed that (L-band radar) is sensitive to woody carbon stocks up to a saturation range of 40-$180tCha^{-1}$, a range which varies across vegetation classes and moisture, phenological and seasonal conditions (McNicol et al., 2018; Mitchard et al., 2009; Wingate et al., 2018).

Notwithstanding the saturation challenge, the strong correlation displayed by the ESA-CCI AGB is significantly closer to the one displayed by the gb and ALOS-PALSAR AGB datasets (R^2 = 0.9) (Fig. 44, Table 17). This further demonstrates that the distribution of the gb AGB in Malawi's Miombo Woodlands is highly correlated to the both the ESA-CCI-Biomass Map and the ALOS-PALSAR imagery datasets. This renders the suitability of using these two datasets in the woodlands. Nevertheless, the 8tCha^{-1} RMSE and the saturation trend at relatively higher biomass (i.e., ≥40tCha^{-1}) demonstrates the limitations of the ESA-CCI Biomass Map datasets. Assessment on these 2018 ESA CCI Biomass Map datasets show that they yield a relative error of <20% where AGB exceeds 50tCha^{-1} and an error of 10tCha^{-1} where the AGB is <50tCha^{-1} (Santoro et al., 2021).

Inversely, the strong relationship (R^2=0.9) by the same datasets further shows the risk of basing predictive power on the coefficient of determination values only, hence it is always ideal to infer both the R^2 and the RMSE for better accuracy of results.

Overall, the values of the R^2, RMSE and Bias accrued provide sufficient evidence to conclude that the gb AGB measurements from these woodlands can be effectively up scaled with the open-access, but medium resolution backscatter measurements of ALOS-PALSAR and/or ESA-CCI-Biomass Map. However, the effect of fire and the saturation challenges, particularly exhibited by the EAS-CCI Biomass Map datasets should be accounted for to enhance accuracy.

4.3.4 Correlation of ground-based AGB and Sentinel 1-C-band radar backscatter

This study also analysed the correlation between the Sentinel-1(S1)-C-band radar backscatter measurements (in decibel units*)* and the ground based AGB (tCha^{-1}). The S1-C band measurements were not converted to AGB because there is no allometry that has been generated and specifically tested for Malawi's Miombo Woodlands using these datasets to date, at least from the author's knowledge.

The next figure shows a correlation of gb AGB (in tCha^{-1}) and S1-C-radar backscatter (*dB*).

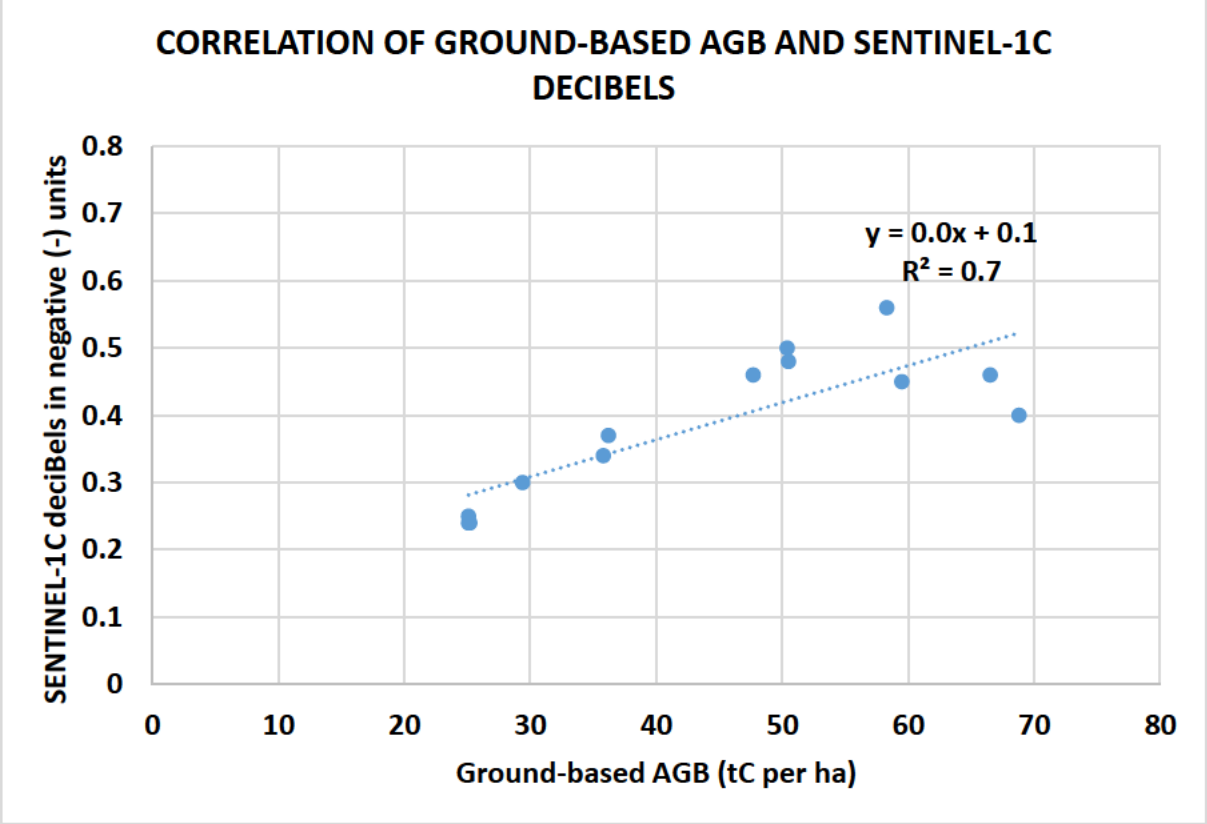

Figure 48. Correlation of ground-based AGB in $tCha^{-1}$ and Sentinel-1 C-radar backscatter *decibels* (in negative units) shows a strong relationship (R^2 = 0.7), signifying the suitability of using of the S1-C datasets in estimating AGB and C in Miombo Woodlands of Malawi.

The above figure shows another strong relationship (R^2 = 0.7) between ground-based AGB and Sentinel-1C-band radar backscatter measurements (*dB*) in negative (-) units. Much as the Miombo, like any other broad-leaved trees exhibit different backscatter responses throughout the year, studies have observed that the total backscatter signal of an imaging radar is also dependent on the following;

(i) structural and dielectric characteristics of forest canopies,
(ii) relative contribution of volume, surface–volume interactions, and
(iii) surface scattering on the target (Freeman and Durden, 1998; Laurin et al., 2018; Saatchi, 1997).

Therefore, the variation in the correlation values registered by the S1-C-band (R^2 = 0.7) in comparison to the ESA-CCI (R^2 = 0.8) and/or the ALOS-PALSAR-2 (R^2 = 0.9) is attributable to the weaker penetration of the C-band (λ = 5.6cm) through thicker surfaces i.e. the branches and trunks of the Miombo, in contrast to the L- band performance on the same surface. These observations were also influenced by the leaf-off condition during the dry season of this semi-arid region study site. Models on

performance of radar backscatter measurements have demonstrated that P- and L-bands provide stronger backscatter from branches and trunks with respect to X- and C-bands, respectively, which collect most of the energy from leaves and needles (Beaudoin et al., 1994; Brolly and Woodhouse, 2013; Cutler et al., 2012; Laurin et al., 2018; Le Toan et al., 2004). The studies have further ascertained that C- or X-bands wavelength are more sensitive to surface moisture (Mahdavi, 2017). Hence, the dry conditions of the leaf-off season in the Miombo Woodlands contributed to the weakening of the correlation.

Analysis of the Residual Error analysis based on the correlational pattern shows that P5 values (59.5tCha^{-1} and -0.45tCha^{-1} for the ground-based AGB and S1-C decibels, respectively) contributed significantly to the weakening of the relationship. Inference on gb measurements reveals that P5 comprises of uneven/diverse tree height and crown ranges that have given rise to interspaces of bare land, tree cover and rock outcrops (Table 14 and Fig. 53). Such spatial arrangement affects the surface roughness and dielectric constant properties (surface moisture) by providing heterogeneous roughness with low surface reflectance (Woodhouse and Hoekman, 2000).

In the same regard, forest studies on retrieval of vegetation and bare surfaces parameters from microwave backscatter in different climatic regions have observed that bare land spaces (soil) among the tree cover (vegetation) lead to low backscatter values (Brolly and Woodhouse, 2012; Grippa and Woodhouse, 2003; Woodhouse and Hoekman, 2000). Therefore, in P5, the biomass energy density (backscatter) directed to the sensor was relatively low, thereby yielding low AGB estimates.

To crown it all, the correlation displayed in Fig. 48 cements the premise assumed from a series of analyses conducted earlier by this study that the terrestrial AGB distribution of Ntchisi is highly correlated to the SAR datasets and the recent analysis includes the Sentinel1-C-band datasets as well.

However, while, the gb AGB measurements have demonstrated the potential to be effectively up-scaled with the unrestricted S1-C backscatter measurements, the weak penetration limitations of the C-band signal were apparent in the broadleaved Miombo. In addition, the effect of fire compounded by the dry conditions in affecting the surface

roughness and surface moisture of the backscatter signal were vivid as well. Hence, these aforementioned factors should be considered when using S1-C imagery in the Miombo Woodlands.

Since there is no specific allometry locally tested to estimate AGB of Malawi's Miombo Woodland, to date, as it is the case with ALOS PALSAR (McNicol et al., 2018), at least to the knowledge of the author; this study encourages further research on its development to enhance accuracy of the estimates, especially for the REDD+ purposes.

Table 17 below display a summary of correlational relationship statistics observed between AGB and fractional cover estimates for the ground-based, optical UAV based and SAR datasets of Ntchisi Forest discussed in the preceding sections.

Table 17. Summary Statistics for Bias, RMSE and R-Squared Observed on AGB Estimates

Parametric Variable					
No.	**Explanatory Variable**	**Independent Variable**	**R^2**	**RMSE ($tCha^{-1}$)**	**Bias ($tCha^{-1}$)**
1	Gb AGB	Gb FC %	0.7	11	-4
2	Gb AGB	PALSAR-2 AGB	0.9	7	3
3	Gb AGB	ESA-CCI Map AGB	0.8	8	1
4	Gb AGB	Optical UAV FC%	0.7	-	-
5	Gb AGB	S1-C band (*dB*)	0.7	-	-

Key: GB = ground-based, R^2 = R-squared (Pearson's coefficient of determination), RMSE = Root Mean Square Error, AGB = Aboveground Biomass, FC% = Fractional Cover Percentage, $tCha^{-1}$ = tonnes of carbon per hectare.

NB: RMSE and Bias for variables 4 and 5 in Table 17 above have not been included since their units under comparison (regressed) are different and they would not give any meaningful interpretation in these two different parametric relationships under test.

4.3.5 Correlation of resampled UAV and SAR imagery AGB at 25m resolution

The different imagery spatial resolution of; (i) UAV, (ii) ALOS-PALSAR, (iii) S1, and (iv) S2 datasets were downscaled to render a geometric unification. The imagery were coarsened to; 25m, 50m and 100m pixel spatial resolution, thus prior to evaluating their performance on AGB biomass and canopy cover accuracy. The first and the last are the original scales of ALOS-PALSAR and ESA-CCI Biomass Map datasets,

respectively (Liao et al., 2020; Santoro et al., 2021). The 50m (0.25ha or ~0.3ha) is the unit size for ground sample-plot otherwise known as the 3-T cluster used during the REDD+ forest inventories in Malawi (Government of Malawi, 2019a; Mueller, 2012).

Studies have observed that coarsening an imagery dataset is relied for better accuracy, thus in addition to utilising the detailed information obtained by its fine resolution bands (Atkinson, 2013; Zheng et al., 2017). Furthermore, downscaling of EO is essential for not only comparing and integrating disparate datasets, but more importantly for calibration and validation of models in a range of applications (Atkinson, 2013).

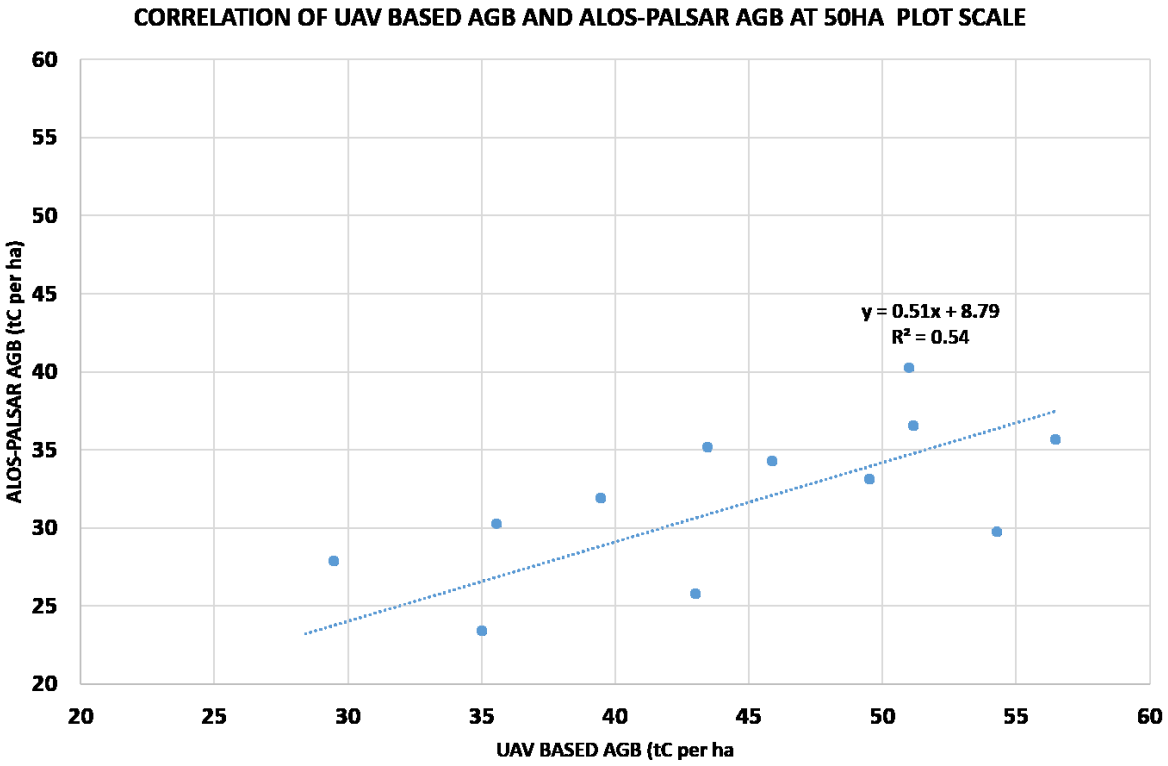

Figure 49. Correlation of UAV-based and ALOS-PALSAR AGB ($tCha^{-1}$) at 50ha plot scale. UAV imagery coarsened from 0.7m to 25m pixel resolution to enhance accuracy of the AGB estimates. Positive correlation (R^2=0.54), depicting the reliability of the UAV datasets in upscaling the measurements. However, the accuracy range of the estimates was affected by the leaf-off condition that was exacerbated by the dry season fire during in this Miombo Woodland.

The resampled imagery analysis was conducted on pixel-by-pixel basis. This employed an equation determined from the correlation between fractional cover percentage (FC %) and ground-based AGB ($tCha^{-1}$), thus y=0.5x+21.8 (Figure 39).

In Figure 49, the UAV-based AGB and ALOS-PALSAR AGB ($tCha^{-1}$) resampled at 25m pixel spatial resolution yielded a positive correlation ($R^2 = 0.54$). In the analysis, P11 and P7 were excluded due to poor construction of some parts of their DSM, DTM mesh. This was due to the abrupt change of wind speed encountered during the plot's flight missions, as previously explained (Chapter 3.3.5.5). Despite the positive correlation, the range of the accuracy of the estimates displayed in the scatter plot was still affected by the leaf-off condition that was exacerbated by fire during the dry season.

The downscaling process has though exposed another significant trend (displayed by closeness of the scatter points and the trend line) suggesting that; as the ground-based AGB (0.1ha measurements) are scaled to 50ha plot (by the UAV), the mean stock ha^{-1} decreases slightly. This depicts the AGB stock plot-based variations, thus under the given leaf-off and fire conditions. For instance, the range of the entire ground-based AGB fell between 29.4 to 68.8$tCha^{-1}$, yielding a variation of 39.4$tCha^{-1}$. On the other hand, the ALOS–PALSAR AGB stock ranged between 16.1$tCha^{-1}$ and 40.2$tCha^{-1}$, recording a comparatively low variation of 24.1$tCha^{-1}$. This typifies the limitations of the field measurements whose small-sized (0.1ha) plots fail to adequately account for the spatial variability of their surrounding areas by either overestimating or underestimating (Réjou-Méchain et al., 2014). These findings further expose the disadvantage of estimating AGB during the period when the tree leaves have been shed off, thus during the dry season.

4.3.6 Correlation of resampled UAV and SAR imagery (50m/100m resolution)

Coarser spatial resolutions are preferred for their ability to reduce noise and variability in the data, thereby facilitating detection of large-scale patterns which ultimately render better accuracy and precision, compared to individual full spatial resolution pixels (Atkinson, 2013; Zheng et al., 2017). Nevertheless, the UAV and ALOS-PALSAR rescaled imagery at 50m and 100m spatial pixel resolution yielded poor correlations in this study. This is attributed to the effect of the leaf-off and dry season conditions most of which yielded underestimates. Partly, this emphasises preference of the leaf-on season datasets (especially for imagery by acquired by optical sensors) over the leaf-off season imagery, thus for enhanced estimations' accuracy.

In addition, the ALOS-PALSAR findings have also demonstrated that higher biomass areas/plots e.g., ≥50tCha^{-1} display better correlation than those with lower/without biomass. As explained earlier on, this is attributed to the premise that higher biomass stocks have a better correlation with SAR L-band (Meyer et al., 2018; Santoro et al., 2021, 2013), since both the ALOS-PALSAR and ESA-CCI-Biomass Map imagery comprise datasets acquired from the L-band sensor, known to be better at penetrating broader/thicker surfaces (Santoro et al., 2021).

In Miombo Woodlands, optical imagery acquired during the post-rainy season tend to derive the same spectral reflectance between the closed and open woodland classes as well as the grassland classes, thereby compromising the accuracy of land cover results (Kamusoko et al., 2014). The increase in greenness during the rainy season is associated with the peak of the woodland's phenological cycle (*ibid*).

Therefore, this study urges that caution should be taken against collecting AGB datasets during the leaf-off season (peak of dry season) only, especially when using the optical imagery in these deciduous Miombo Woodlands of Malawi. It precisely, encourages researchers using optical datasets to undertake AGB and C assessments, preferably 2-3 weeks after the rainy season has stopped. This widow renders an opportunity to capture trees while they are in leaf (with sufficient canopy cover) critical for the optical spectral interpretation (Kamusoko et al., 2014). The period also serves to render an advantage of providing the spectral signature difference (during imagery classification) between the trees and the lower vegetation (grass, shrubs and herb) that wither soon after the rains (Chidumayo, 2001; Kamusoko et al., 2014).

4.4 Validation of S*F*M Photogrammetry Acquired Imagery

This section provides the visual inference (qualitative analysis) of the ground-based and the airborne (RGB) based imagery observations of the sampled Ntchisi Forest plots. It begins by providing the justification for the employment of the qualitative analysis, thus in addition to the point-to-point analysis.

The use of the visual interpretation in this study was to augment the quantitative data analysis efforts because of the following the challenges that were encountered during data acquisition (as previously mentioned in sections 3.2.5 and 3.3.5) and affected the point-to-point analysis.

Since both the ground and airborne based-datasets were collected during the dry season (when the trees had leafed-off and their biomass affected by fire as well), the point-to-point correlational analyses of some plots did not work as expected (Section 4.2.1, Figures 37 (P10), 40 and 42). This is despite the observations that the point-to-point method remains an ideal means of validating the ground and the imagery datasets (Gao and Mas, 2008; Solberg et al., 2015). Hence, due to insufficient funding and time resource, compounded by the global lockdown effected to curtail the Covid-19 pandemic for more than one full year, it was not possible for the researcher to travel back to Malawi (Ntchisi Forest) and collect data again during the next leaf-on seasons (2020 to mid 2021). As a result, it was imperative for this study to include the visual (qualitative) interpretations to aid explanations presented under the quantitative assay.

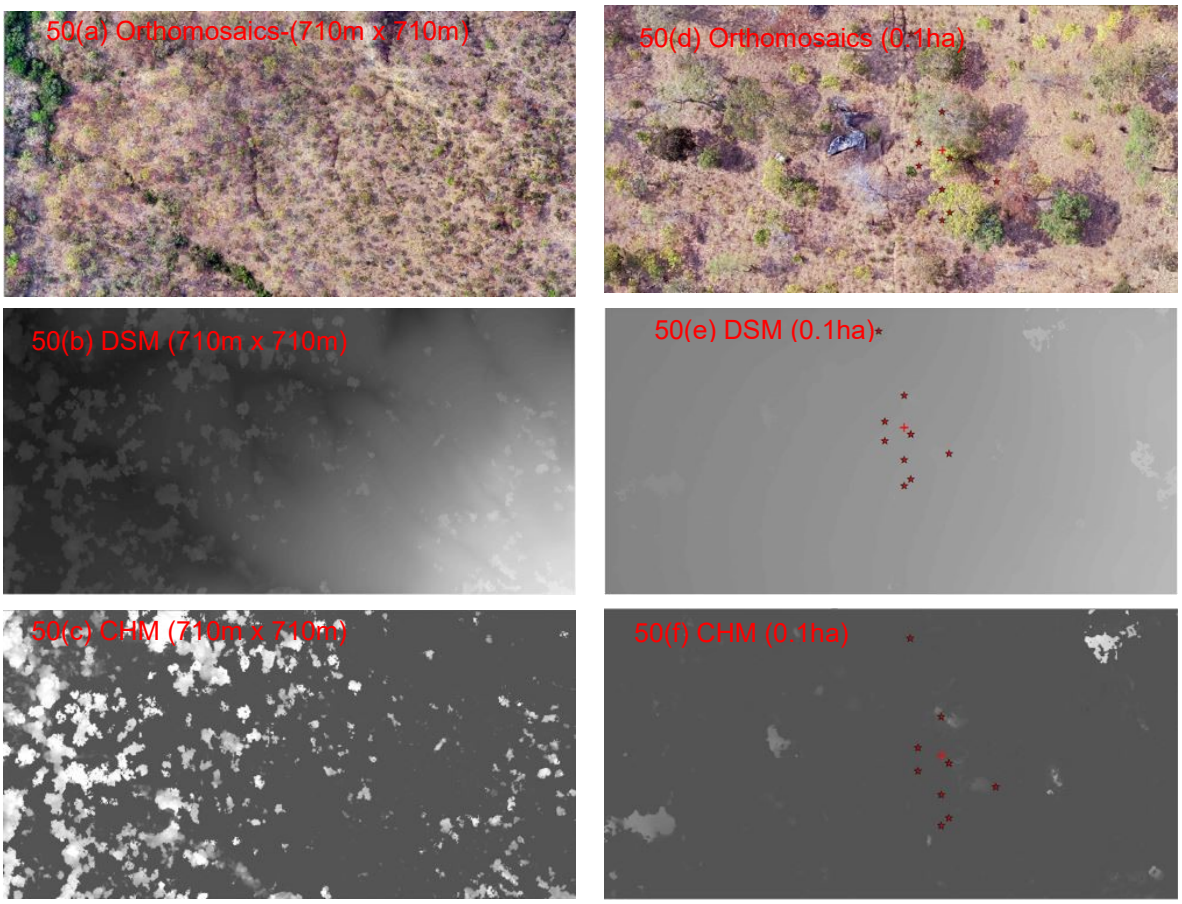

Figure 50. Effect of tree leaf-off, dry season, fire and other environmental conditions on AGB detection: P10, (a)-Orthomosaics, (b)-DSM and (c)-CHM, respectively (all at 710m x 710m, scale of 50ha UAV boxes); P2 (d)-Orthomosaics, (e)-DSM and (f)-CHM respectively (all at 0.1ha or 20m radius ground plot size). In ground plots, the red plus sign and red stars denote the plot centroids and trees sampled, respectively.

Figure 50 above displays a comparison of optical airborne layers acquired through S*f*M photogrammetry (orthomosaics, DSM and CHM) at different scales of 50ha (710m

x 710m, *left*) and at 0.1ha ground plot level *(right*), respectively. It displays key environmental conditions that affect the crown and AGB estimations which include tree leaf-off condition and dry season. The airborne plot boxes were deliberately overlaid on the terrestrial plots for reference's sake. The centroids of the gb plots marked by the red-cross (plus sign) plots acted as the reference points while the individual trees sampled during the terrestrial inventory are marked by the red stars.

The spatial distribution of the ground and the UAV datasets in the orthomosaics, DSM and CHM show identical patterns. However, detection of the woody biomass (crown pattern and AGB estimation) using the optical UAV sensor operating in RGB electromagnetic spectrum in the figure above was affected by the following factors;

(i) Fire (also in Fig. 51),
(ii) Seasonality-dry season condition, and
(iii) Tree morphology (leaf-off and leafless thorny foliar condition of *Acacia species* dominating the plots).

Current research on plant communities' phenology indicates that leaf-on and broad-leaf conditions in contrast to foliar senescence provide the edge for biomass detection by optical sensors (Vrieling et al., 2018; Zhu et al., 2021). Hence, the fairly leaf-on and broad-leaf shape conditions (as opposed to the leaf–off and small thorny leaves- Fig. 51) of some of the trees observed during the terrestrial inventory period, particularly in P10 contributed to the better detection of canopy and biomass by the UAV (RGB) sensor.

Below is a figure further depicting the effect of fire, leaf-off and small thorny leaves conditions in detection crown distribution and AGB estimations as encountered in P2.

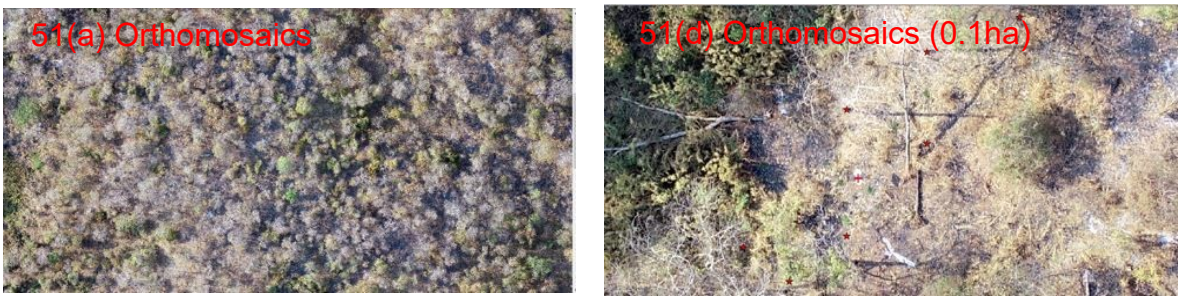

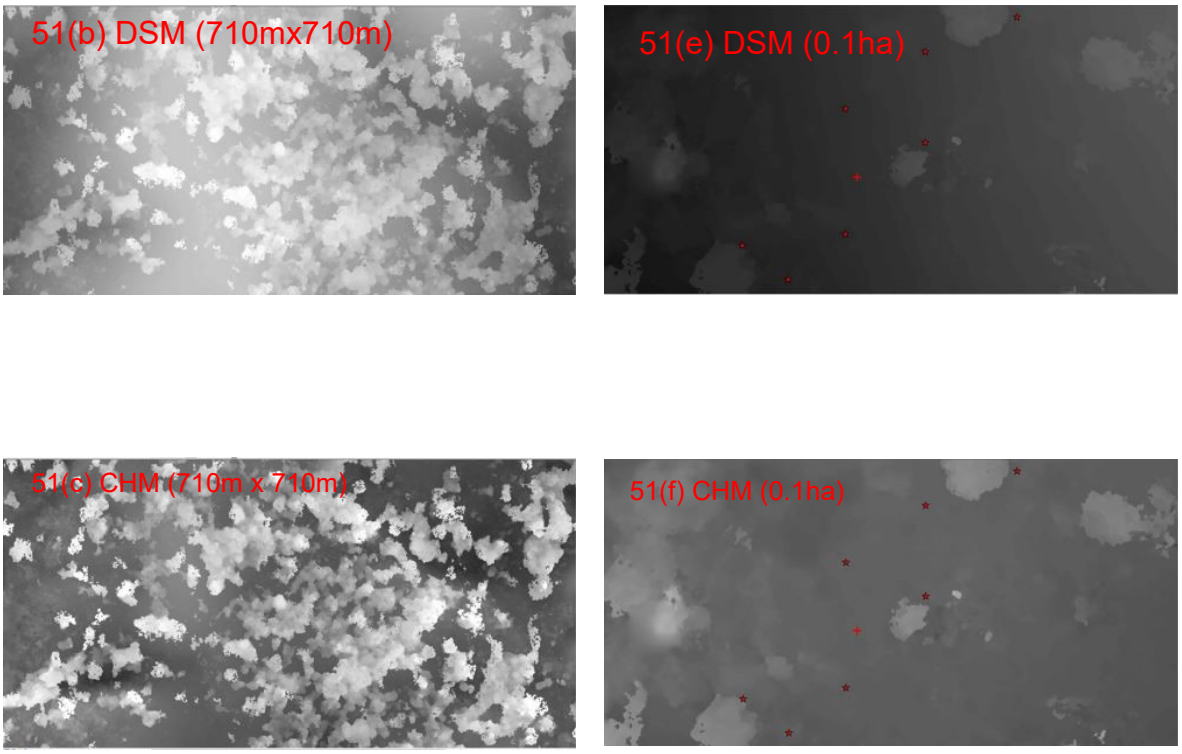

Figure 51. Effect of tree leaf-off, dry season and fire on AGB estimations in P2: (a)-Orthomosaics (b)-DSM and (c)-CHM (all at 710m x 710m-scale of 50ha UAV plot-boxes); (d)-Orthomosaics, (e)-DSM and (f)-CHM, (all at 0.1ha or 20m radius of ground plot size). In ground plots, the red plus sign and reds stars denote the plot centroids and trees sampled, respectively.

Inferring from Figure 51, thus in addition to the gb based observations period (September and October 2019), fire erased P2 and other plots, leaving most of the trees in leafless and dry. The plot was dominated by the *Acacia species* (Figures 51(a and d) characterised by short stipulate thorns and small bi-pinnate leaves that were shed-off during the 2019 survey. The DSM and CHM observations at ground plot level do not show a consistent and clear pattern of the crown and AGB spatial distribution due to the effect of fire and the nature of the thorny and leafless Acacia species dominating the plot. Studies that focused on optical imagery collected during dry season indicate that observations may be affected by the arid conditions since their spectral reflectance is sensitive to vegetation structure (Nunes et al., 2022; Zhang and Ni-meister, 2014).

Research further observed that data acquired from optical sensors possess fundamental limitations for mapping wood biomass as their signal reflectance does not directly correlate to surface structure (Cutler et al., 2012; Naidoo et al., 2016). Hence,

the aspects of fire, leafless and dry conditions contributed to the loss of trees leaves that resulted to weak signal reflectance and eventually yielded lower/underestimates. In summary, these leaf morphological environment and attributes hugely affected detection of the tree crowns by the optical UAV sensor and consequently underestimated the AGB stock as explained in the quantitative correlations earlier.

Therefore, this study has tried to determine the ideal timing for conducting biomass studies using optical RS in Malawi's Miombo Woodlands as the period soon after the rainy season has stopped, thus when the trees still have got leaves and there is little or no cloud cover (thus April-May, or precisely, 2-3 weeks after the last rains).

4.4.1 Validation of UAV and ALOS-PALSAR crown and AGB spatial pattern by lacunarity analysis

Lacunarity analysis refers to a simple technique for characterising texture in binary images and principally focuses on distribution of gap sizes in a geometric object or the complex intermingling of the shapes and distribution of gaps within an image (Henebry and Kux, 1995; Mandelbrot and Wheeler, 1983; Plotnick et al., 1993). Highly lacunar image exhibits gaps distributed across a broad range of sizes while the low lacunar is expressed by being homogeneous and translationally invariant (Plotnick et al., 1993). The technology has been identified as suitable for analysing imagery for pattern recognition in tree structure (Frazer et al., 2005; Zheng et al., 1995).

In this study, the initial lacunarity analysis involved visual inspection of spatial texture patterns of homogeneity and heterogeneity displayed by the tree crown/canopy in the optical UAV imagery and the ALOS-2 PALSAR-2 (L-band) backscattering intensity. The comparison focused on the following key elements; (i) forest woody structure (tree crown/canopy and AGB distribution i.e., spectral reflectance for both leaf-on and leaf-off trees), (ii) non-tree vegetation (grasses, shrubs), and (iii) gap features i.e., bare-land/soils, cultivated land, rocks, burned area, streams, ponds etc.

Lacunarity image analysis is on the other hand recommended for pattern recognition in tree structures (i.e., for expressing features of the size and distribution of holes, complex spatial distributions, or other morphologic features (Frazer et al., 2005; Zheng et al., 1995).

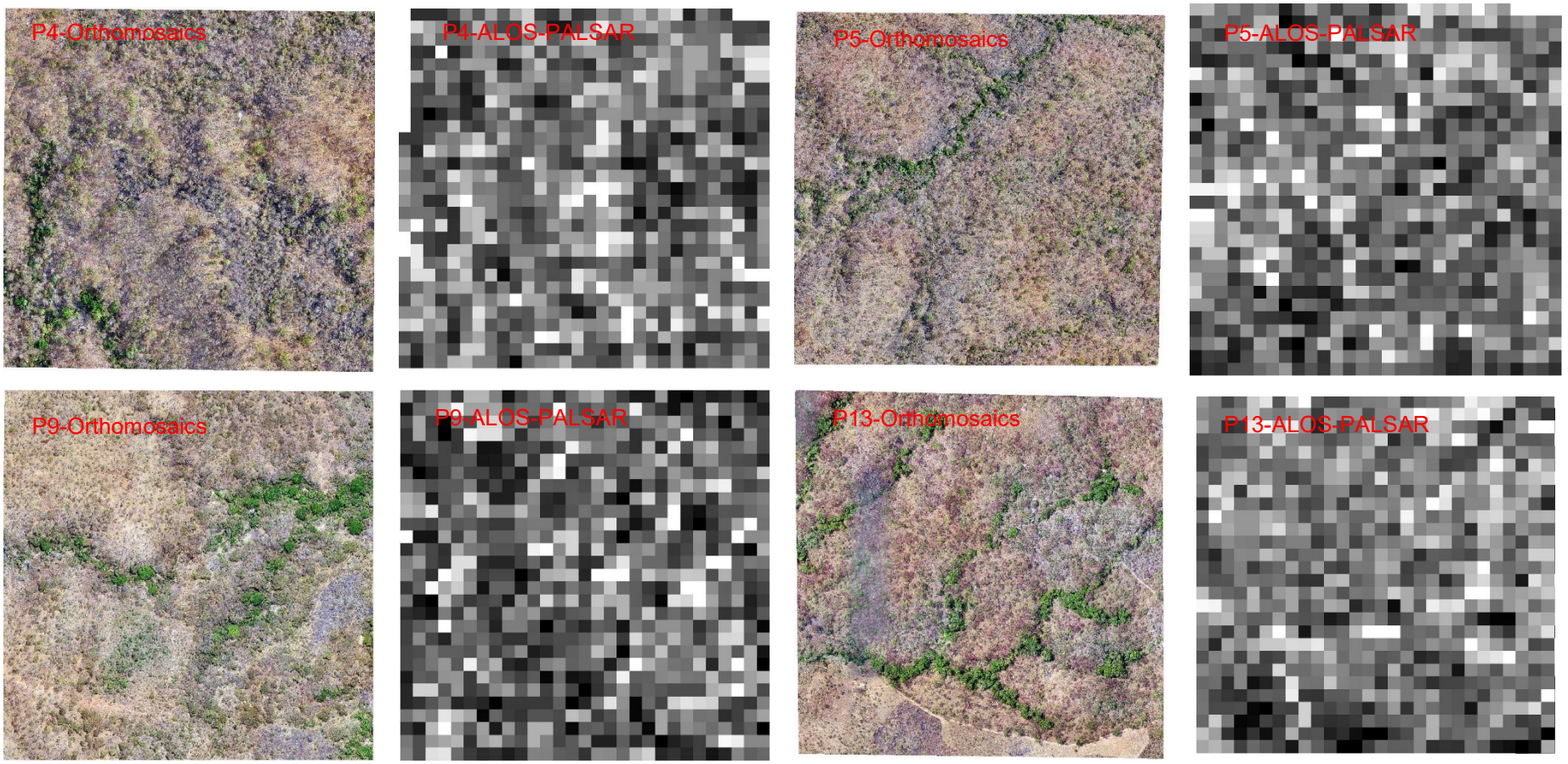

Figure 52. Visual spatial pattern comparison of P4, P5, P9 and P13 50ha UAV-RGB Orthomosaics (7cm pixel spatial resolution) and 50ha ALOS-2-PALSAR-2 L-band Radar Backscatter (25m pixel resolution) acquired over Ntchisi Forest Reserve in 2019. Strong homogenous spatial pattern displayed by vegetation and weak trend by non-vegetation features. Remarkably high reflectance from green trees (especially leaf-on evergreen tree crowns growing along the riverine) in contrast to non-green or bare areas. The SAR imagery ascertains the strong correlation of HV-L-band polarisation and high backscatter.

Studies have observed that in ALOS-2-PALSAR-2 imagery, the mosaics classify backscattering in HH+HV polarisation in the following manner (Woodhouse, 2006);

(i) Strong backscatter intensity (i.e., bright/white colour pixels) in Fig. 52 has corresponded to the high reflectance of the green crowns in the optical orthomosaics, in contrast to,

(ii) Weak backscatter intensity (i.e., grey/dark/black colour pixels) which have corresponded to low reflectance of the leaf-off, dry and lower vegetation and bare ground areas.

Detailed studies on forest biomass and SAR backscatter have observed that radar reflection intensity is depended on surface roughness of the target features (Woodhouse, 2006; Woodhouse and Hoekman, 2000). In this case, the green Miombo tree crowns, especially along the streams rendered this property and highly yielded reflectance (brighter pixels) i.e., they reflected the radar in all directions, thereby scattering more energy back to the antenna sensor than the backscatter intensity from bare, dry land/ soil and/or the scotched vegetation.

The ground reference plot (0.1ha) tree metrics in addition to the UAV orthomosaics observations characterise P9, P5 and P13 as having overlapping tree crowns while also growing in cohorts and some even constituting belts along riverine (Fig. 52). Although these ground plots constitute only a fraction of the UAV plot boxes (0.1ha each of 50ha), the very high spatial resolution orthomosaics visibly depict the tree cohorts (evergreen in RGB band combination) i.e., in P13, forming a riparian belt whose pattern has been homogeneous and reflected high radar backscatter intensity.

Granting that the overlaps and the cohort attributes rendered difficulties in sighting individual tree tips and crowns during height and crown ground measurements, they have contrastingly provided the advantage for the ALOS-PALSAR-2 backscattering dataset to highly detect biomass. Studies indicate that signal reflectance captured by the SAR systems directly correlates to surface structure (Cutler et al., 2012; Naidoo et al., 2016; Sun and Ranson, 1998). Hence, the high radar backscatter intensity is attributed to the fact that the canopy belt forms a greater average diameter of the surface roughness, thereby giving rise to greater backscatter (Cassells et al., 2009). This is further attributed to aspect of the long-wave operation of HH+HV polarisation

of the L-band ALOS-PALSAR-2 (ʎ=23 cm) which penetrates deeper through the broad and thick leaves and branches. Miombo trees are broadleaved vegetation, therefore, the ALOS-PALSAR-2's longwave provided sufficient backscatter signal/information on the form and orientation of scattering elements that compose the surface of the tree crown morphology/belt.

Albeit displaying a discernible homogeneous pattern, the leaf-off crowns of the Miombo trees with sparse density have, on the other hand, rendered a heterogeneous pattern in contrast to the leaf-on green belts. This is ascribable to the leaf-fall, the dry conditions that resulted in exposure of more bare land and soil, which in turn affected surface roughness and dielectric properties in the ALOS-2 PALSAR-2 imagery.

The next figure shows the effect of the environmental conditions on detection of AGB, and crown spatial pattern displayed by the ALOS-2-PALSAR-2 radar backscatter imagery in reference to the optical airborne orthomosaics.

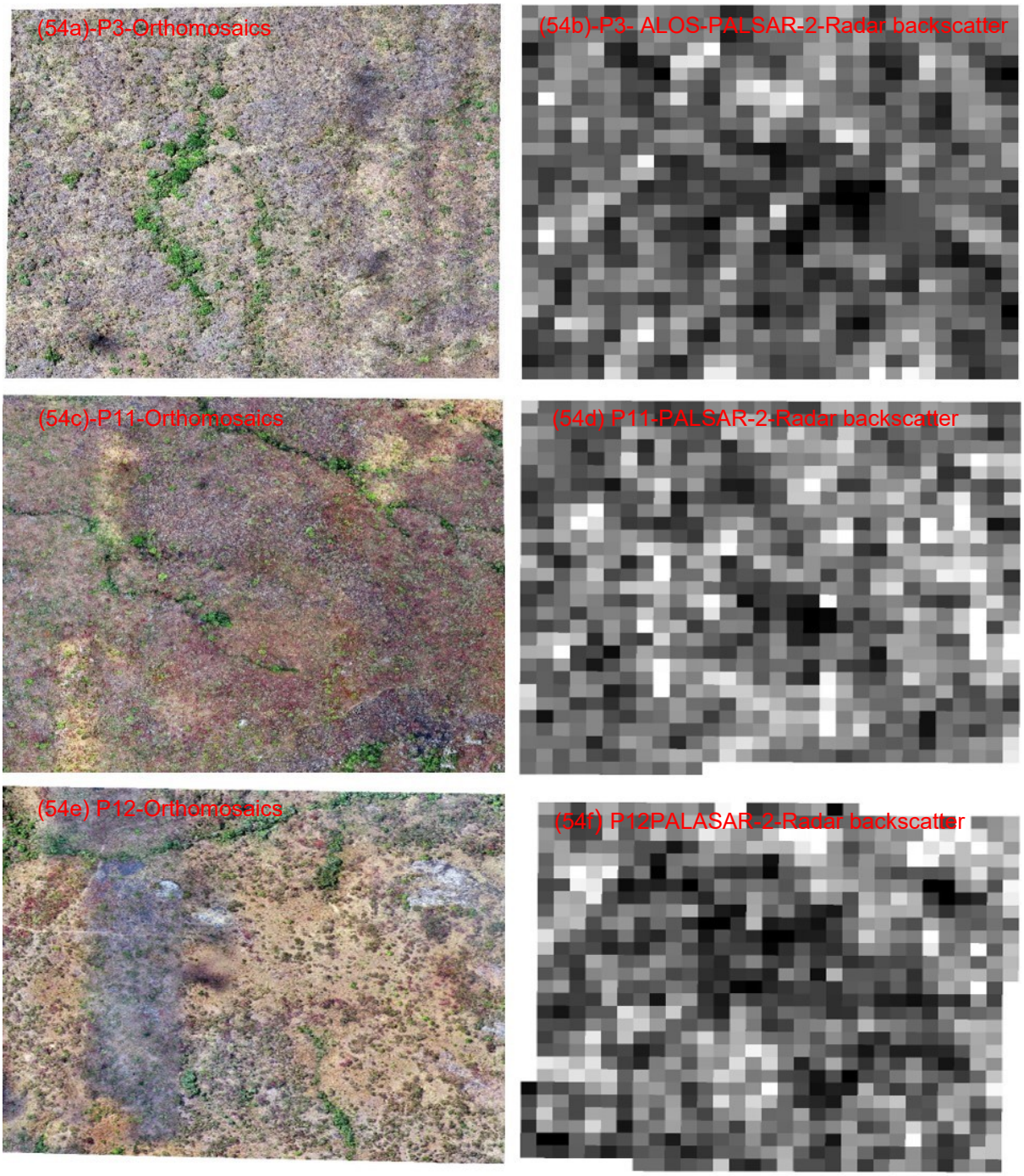

Figure 53. Interplay of fire and rock outcrop on intermediate heterogeneous spatial pattern displayed by UAV-RGB orthomosaics (*left*) and ALOS-2-PALSAR-2 L-band radar backscatter (*right*) in P3, P11 and P12 of Ntchisi Forest.

Figure 53 (above) demonstrates a rather inconsistent and unclear pattern of crown distribution and AGB displayed by P3, P11 and P12 radar backscattering measurements (right) compared to the UAV Orthomosaics (left). Unlike the ground-based datasets, which have displayed a strong-positive correlation with the predicted

tree heights on UAV Orthomosaic datasets, the bare land and burnt areas have demonstrated a definite heterogenous pattern (black and sharply defined low backscatter areas). The poor pattern displayed by the woody biomass is attributed to fire which reduced surface moisture, thereby resulting to the radar shadow effect propagated from target area where there has been exceptionally low or complete lack of received information (Woodhouse, 2006). In this regard, the bare and burnt areas did not return enough echo/backscatter due to reduced surface moisture caused by to fire.

In addition, the interplay of the phenological/seasonal and environmental conditions of the Miombo woodlands of Ntchisi Forest have contributed to the heterogeneous pattern. First, notwithstanding the long hot and dry season that Malawi experiences each year, October 2019 (the period for the data collection) was recorded as the extremely hot and dry month with mean daily temperatures ranging from 29.2 - 42.1^{o}C (Government of Malawi, 2019b). Research has shown that in all land cover classes of Southern Africa Tropics, dry periods lead to additional decrease in surface moisture (Urban et al., 2018). Therefore, the severe hot weather condition in Ntchisi enhanced evapotranspiration rate, which consequently induced leaf senescence among the deciduous Miombo trees (Fig. 5). Since radar backscatter intensity is partially a function of surface moisture (Belenguer-Plomer et al., 2019; Woodhouse, 2006); the evapotranspiration drastically contributed to the reduction of the branches and leaf-relative water content of the Miombo tree crown biomass. This lowered the dielectric constant value and alternatively influenced direct ground-backscatter (together with the leaf-fall), yielding low intensity that dominated the spectral reflectance.

Second, Ntchisi Forest, like many Miombo woodlands is associated with dry season fires (Chinangwa et al., 2016) and these were also captured during terrestrial and UAV data collection (Fig. 53). Research has shown that combustion of vegetation due to fire may result in reduction of scattering elements that induces low post-fire backscatter coefficient (sigma) (Belenguer-Plomer et al., 2019). Inversely, it is the ground surface scattering (signal attenuation by the vegetation) that is more recorded in SAR microwave spectrum (*ibid*). In this regard, the heat generated by the fire highly reduced both the internal and surface moisture of crown biomass, thereby minimising the dielectric constant value extremely. This resulted in low backscatter intensity from

the tree biomass while the exposing the ground surface, whose scattering eventually dominated the spectral signature.

Differently, the existence of bare rock outcrops in some parts of P11 and P12 (Fig. 53) also contributed much to the low radar backscatter intensity from the crown biomass. Bare rock backscattering occurs at the rock-air boundary, and it is renowned for its influence on surface roughness signal reflectance (Kamusoko et al., 2014; Woodhouse, 2006).

A study on performance of SAR L- and C- bands in Kenya's arid terrain, thus in the Savanah vegetation of Marsabit, observed that the presence of large rocks contributed to multiple scattering and yielded moderate backscatter under HV polarisation (Rosenqvist, 2018). Therefore, the smooth bedrock outcrops observed in P11 and P12 (Fig. 53) provided the moderate surface roughness for the backscatter (in contrast to the rough surface i.e., sharp edged rock fragments) and yielded low surface scattering. This eventually, dominated the spectral reflectance pattern of the tree biomass that appeared heterogeneous in these plots.

The next figure demonstrates the effect of topography/slope in assessing tree crown and AGB spatial distribution.

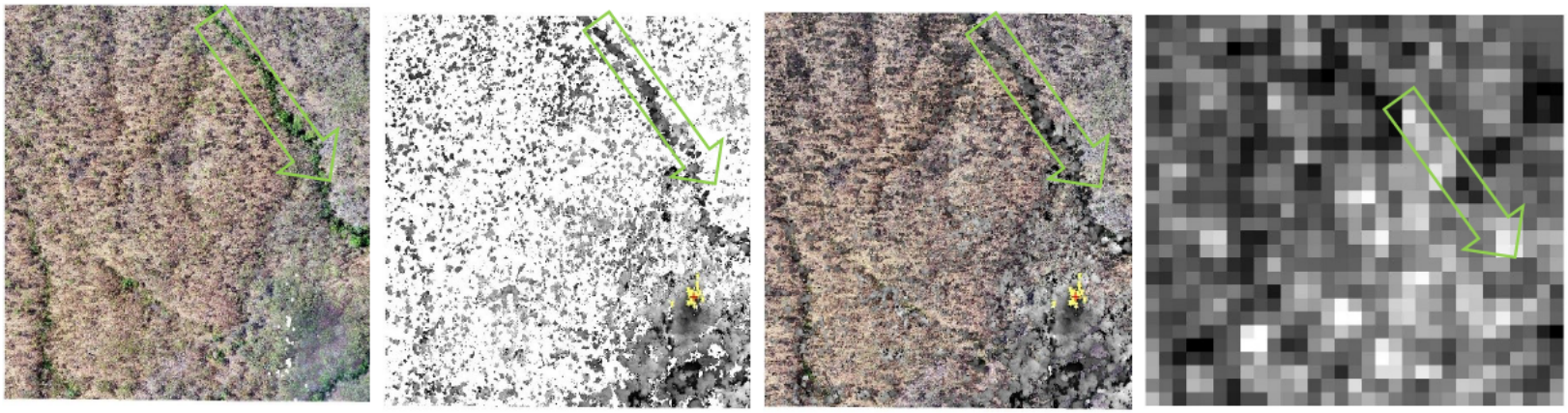

Figure 54. Effect of slope on canopy and AGB determination-P8 (50ha plot); (i) UAV orthomosaics (*left*), (ii) CHM (*second-left*), (iii) Orthomosaics overlaid by CHM (*third-left*) all at 7cm pixel spatial resolution, and (iv) ALOS-PALSAR-2 radar backscatter (*right*) at 25m pixel spatial resolution. Green arrows inside the imagery boxes drawn using free hand and not to scale denote leaf-on tree crown belts along a riverine north-south slope. In the PALSAR imagery, backscatter intensity along the slope appears to have been shifted and cut short, characterising layover and foreshortening distortions associated with SAR imagery.

The SAR backscatter distortions indicate that layover effect is caused by the look angle of a sensor in the mountainous sites resulting to shortening distance of an imagery target features (Chen and Wang, 2008; Woodhouse, 2006). As observed in Fig 54, P8 sits on dangerously sharp steep terrain with a slope estimate 74% (Table 6), hence, the slight upward (north-ward) shift of the tree crown biomass pattern in the PALSAR image ascertains this distortion. In addition, the P8 ALOS-PALSAR-2 observations support the findings of a previous study on ALOS PALSAR-1 measurements conducted in Malawi whose findings revealed that the backscatter sensitivity was highly attenuated by the topography the forest site, besides other factors (Cassells, 2012).

In closing, the overall homogenous pattern displayed by the spatial crown distribution in the optical orthomosaics and ALOS-2 PALSAR-2 backscatter measurements establishes the high degree of correspondence that the employment of the two datasets render in determining the crown distribution and AGB pattern of the Miombo Woodlands. This demonstrates that the optical airborne data can be effectively used as a bridge to scale-up the ground observations to a wall-to-wall coverage using the PALSAR backscatter datasets.

Nonetheless, the study has significantly exposed the effect leaf-off (foliar morphology), fire, rock outcrop and topography as pivotal factors influencing the determination of the woody canopy and AGB. In addition, the analysis has also shown the effect of the layover distortion in determining the crown and AGB patterns on the ALOS-PALSAR imagery.

4.5 Validation of Sentinel-1C Band Radar Observations

This section presents observations drawn from the spatial crown patterns inferred from Sentinel-1-C-(S1-C) band radar backscatter measurements using the optical orthomosaics as reference data. The comparisons involved both wet and dry season S1-C imagery.

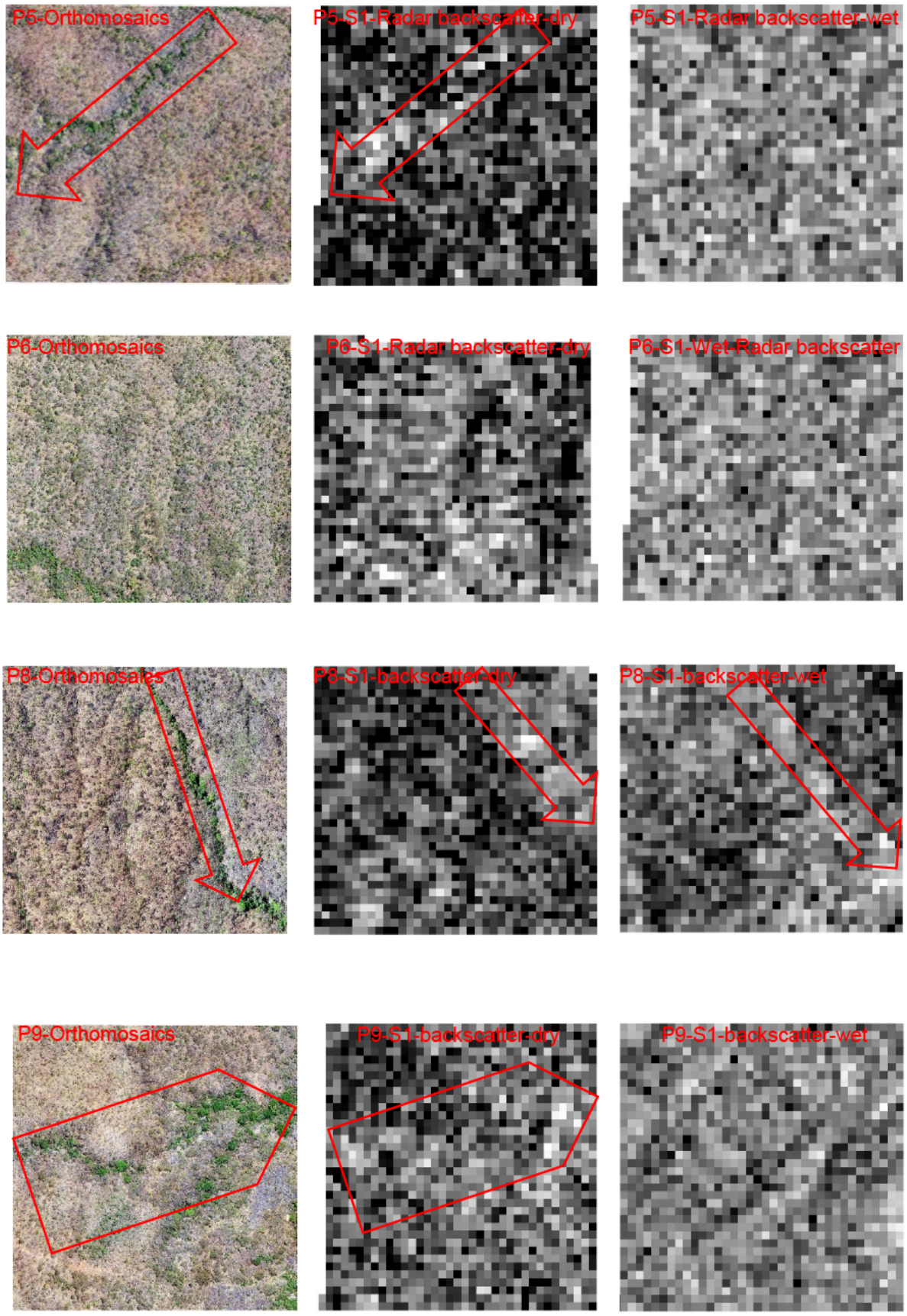

Figure 55. Visual spatial pattern comparison of 2019 UAV-RGB Orthomosaics and Sentinel1-C-band radar backscatter wet and dry season imagery acquired over P5, P6, P8 and P5 in Ntchisi Forest. Dry

season scenes portraying homogenous correspondence, especially leaf-on (green) tree belt in contrast to wet season scenes, attributed to double-bounce scattering induced by moisture/rains-tree biomass interaction on the part of the C-band imagery. Imagery distortions observed in south-west direction in the SAR scenes attributed to shadowing effect. Red polygons inside the imagery boxes drawn using free hand and not to scale.

The dry season plot scenes demonstrate a conspicuous homogenous spatial pattern whereby; high backscattering intensity is portrayed by a belt of tree cover with green leaves (leaf-on) while the low intensity values (grey/dark to black) in the radar imagery is characterised by the leaf–off trees and/or non-tree features. In contrast, the wet season imagery, except P8, have shown neither a distinct nor reliable tree crown distribution, but rather they have demonstrated a more-less evenly distributed backscattering throughout the plots.

The even distribution of the pixel reflectance in rest of the plots is attributed to double-bounce scattering which was induced by moisture/rains-tree biomass interaction during the wet season (Rosenqvist, 2018). These observations confirm the previous findings that radar response to forest biomass is more sensitive to changes in temporally varying parameters at C-band than at L-band (Pulliainen et al., 1999). Precisely, the study observed that the effect of seasonal and weather conditions affects the sensitivity of C-band (*ibid*). In contrast, the P8 wet season correspondence of tree crown distribution (homogeneity pattern of the tree canopy and of non-vegetation features) is ascribable to the effect of the steep slope of a ridge, which facilitates drainage, and evapotranspiration of water/moisture in the plot.

Imagery shifts distortions in the south-west direction and more vividly in the northern direction were noticed in P6 and P8 S1-C radar backscatter, respectively, thus in reference to the optical orthomosaics (Fig, 55). These typify the shadow effect (an advanced stage of layer over) which is known to cause the other sides of the mountain where the radar beams cannot illuminate appear dark on the image (Chen and Wang, 2008; Laurin et al., 2018; Woodhouse, 2006). Ntchisi Forest being mountainous, the shadow effect of the radar beam is sufficiently considered to have affected the crown and AGB reflectance pattern, precisely in P6 and P8 (with a portion beneath a ridge) which are steep, bearing 18% and 74% slopes, respectively (Table 6).

A study on SAR imagery geometric distortions observed that though these may vary between scenes, technically the displacements are dependent on the angle of incidence acquired during imaging and on local relief (Chen and Wang, 2008). The shadowing patterns demonstrated in the three plots are comparatively more pronounced in the dry season imagery than the wet season. The same is true for the heterogeneity pattern of the crown cover distribution. This is because radar backscatter biomass reflectance attenuates more with higher soil moisture, especially in these low vegetation cover sites (Laurin et al., 2018; Woodhouse and Hoekman, 2000).

During the wet season, high volumetric water content of the ground influences the dielectric constant value by raising it, thereby affecting the direct ground backscatter which eventually attenuates, resulting to low backscatter measurements (Brolly and Woodhouse, 2012). These plot observations support the previous findings that that any changes in moisture pattern within Miombo Woodlands (i.e., early rains or late rains and/or reduced and even prolonged dry season) are likely to affect the pattern of the radar backscattering intensity (Cassells, 2012).

Comparatively, these findings demonstrate that the SAR L-band observations have produced better spatial crown and AGB distribution patterns than the C-band observations. They support the findings of a study that investigated the increase of accuracy in forest AGB estimates when using HV polarization which showed that the dynamic range appears much greater at L-band than at C-band (Picard et al. 2004).

In summary, the tree crown pattern observations demonstrate the positive correlation of the Miombo tree AGB of the rugged terrain of Malawi analysed between the optical airborne observations and the radar backscattering measurements. Nevertheless, the S1-C-band reflectance has been highly affected by the wet season compared to the dry season condition. Despite the effect of shadowing distortion being apparent in the SAR backscatter measurements of the rugged terrain plots, uniquely, the steep slopes have facilitated detection of crown distribution for the S1-C band wet season dataset by apparently, aiding drainage the moisture in the plot.

This study, therefore, suggests that the potential of S1-C-data in predicting AGB specifically for Miombo Woodlands could be enhanced if;

(i) both the wet and dry season scenes are comparatively used,

(ii) the effect of water/moisture drainage on plots sampled from steep slopes could be explored more,

(iii) local allometric models are developed using the deciduous Miombo trees of Malawi as it is the case with ALOS-PALSAR's i.e., the one developed by (McNicol et al., 2018), and

(iv) modelling/estimating of the AGB and crown distribution are conducted using Machine Learning techniques, such as *randomforest* algorithm in contrast to the traditional methods i.e., simple linear regression as established by (Kadzuwa and Missanjo, 2023)

4.6 Crown Distribution Comparisons using Resampled Imagery

The Digital Terrain Model and Fractional Cover datasets of PALSAR-2 and S1-C-imagery were rescaled to 50m and 100m pixel spatial resolutions to compare and determine crown distribution pattern in Miombo Woodlands of Ntchisi (Figure 56-69).

The next set of figures show comparisons of the crown spatial distribution patterns from the optical UAV and the ALOS-PALSAR-2 resampled imagery.

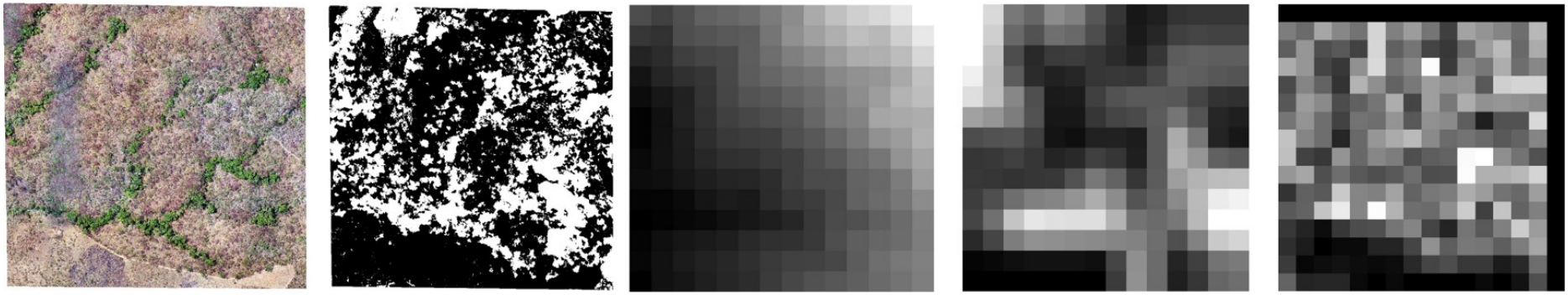

Figure 56. Comparison of crown distribution measured at 50ha scale in P13, (*Left – Right*): (i) UAV orthophoto-7cm pixel spatial resolution, 0-255 scale; (ii) FC-7cm pixel spatial resolution, 0-100% scale; (iii) DTM-50m pixel spatial resolution, 634-708 scale; (iv) CHM-50m pixel spatial resolution, 0-55m scale; and (v) ALOS-PALSAR-2 AGB mosaics-50m pixel spatial resolution, 0-83tCha^{-1} scale.

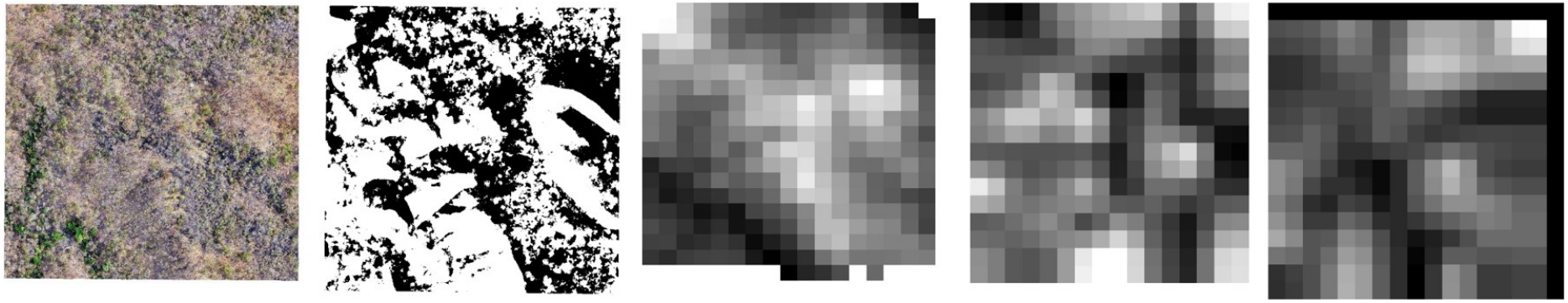

Figure 57. Comparison of crown distribution measured at 50ha scale in P4, (*Left – Right*): (i) UAV orthophoto-7cm pixel spatial resolution, 0-255 scale; (ii) FC-7cm pixel spatial resolution, 0-100% scale; (iii) DTM-50m pixel spatial resolution, 634-708 scale; (iv) CHM-50m pixel spatial resolution, 0-55 scale; and (v) ALOS-PALSAR-2 AGB mosaics-50m pixel spatial resolution, 0-68tCha^{-1} scale.

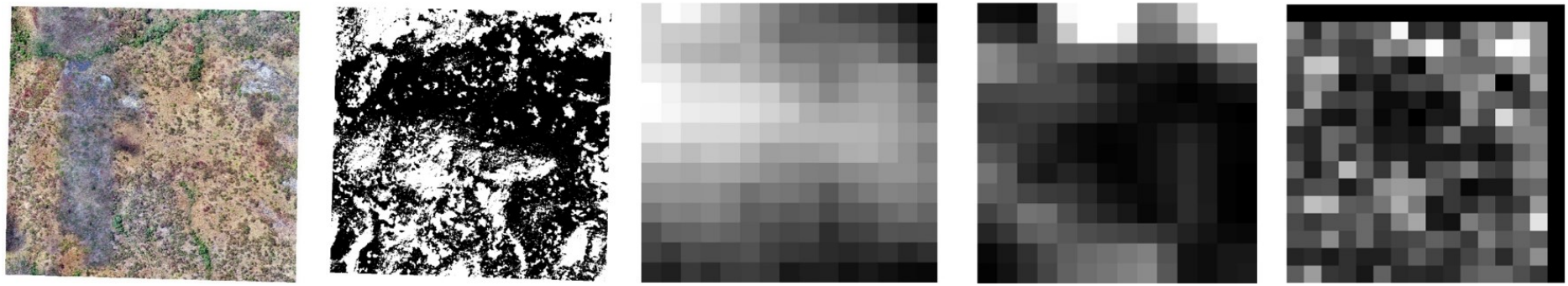

Figure 58. Comparison of crown distribution measured at 50ha scale in P12, (*Left – Right*) (i) UAV orthophoto-7cm pixel spatial resolution, 0-255 scale; (ii) FC-7cm pixel spatial resolution, 0-100% scale; DTM-50m pixel spatial resolution, 634-708 scale; (iii) CHM-50m pixel spatial resolution, 0-55m scale; and (v) ALOS-PALSAR-2 AGB mosaics-50m pixel spatial resolution, 0-75tCha^{-1} scale.

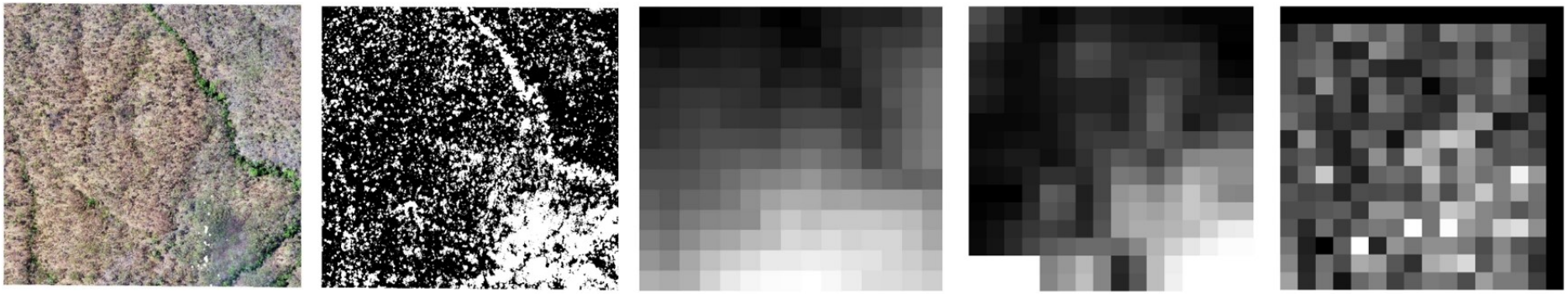

Figure 59. Comparison of crown distribution measured at 50ha scale in P8, (*Left – Right*): (i) UAV Orthophoto-7cm pixel spatial resolution, 0-255 scale; (ii) FC-7cm pixel spatial resolution, 0-100% scale; (iii) DTM -50m pixel spatial resolution, 634-708 scale; (iv) CHM 50m pixel spatial resolution, 0-55m scale; and (v) ALOS-PALSAR-2 AGB mosaics-50m pixel spatial resolution, 0-106tCha^{-1} scale**.**

The trend of crown spatial distribution patterns in P13, P4, P12, P8 (Figures 56-59 above) demonstrated that as the pixel spatial resolution is downsized from 7cm-50m, spectral reflectance gets attenuated highly (~30%) and worsens at 100m pixel spatial resolution. As result, the resampled imagery at this scale have not been included.

P12 clearly displays areas affected by fire and dominated by rock-outcrop, showing low backscatter pixels (greyish-to-black) correspondingly, suggesting bare/low vegetation surfaces (except dry snow and dry sandy-soils) attenuate microwave penetration while influencing surface scatter.

Nevertheless, at 50m pixel spatial resolution for instance, some high degree of correspondence in the patterns were observed on bare land, i.e., P13, bottom/southern part with footpaths) and other areas covered by green vegetation (Fig. 56). This is in addition, to P8 (Fig. 59) where spectral reflectance on vegetation cover displayed by bright pixels while low or no tree vegetation cover in the optical UAV FC % image; and correspondingly shown by the dark pixels of the DTM, CHM and ALOS-PALSAR imagery.

However, P12 orthomosaics (Fig. 58-left) clearly indicate areas affected by fire and dominated by rock outcrop, which have correspondingly displayed low backscatter pixels (greyish to black areas) in the ALOS-PALSAR scene. The low values are attributed to the effect of surface roughness & dielectric properties (moisture) attenuated by the fire and rock outcrops. These PALSAR scene observations support the premise uncovered by studies that most bare or low vegetation surfaces (except dry snow and dry sandy soils) allow extraordinarily little penetration of microwave, thereby allowing surface scatter to dominate the measured intensity (Meyer, 2019; Sinha et al., 2015; Woodhouse, 2006).

The next figures demonstrate comparisons of the spatial crown distribution in Sentinel-1–C band resampled imagery and the UAV orthomosaics.

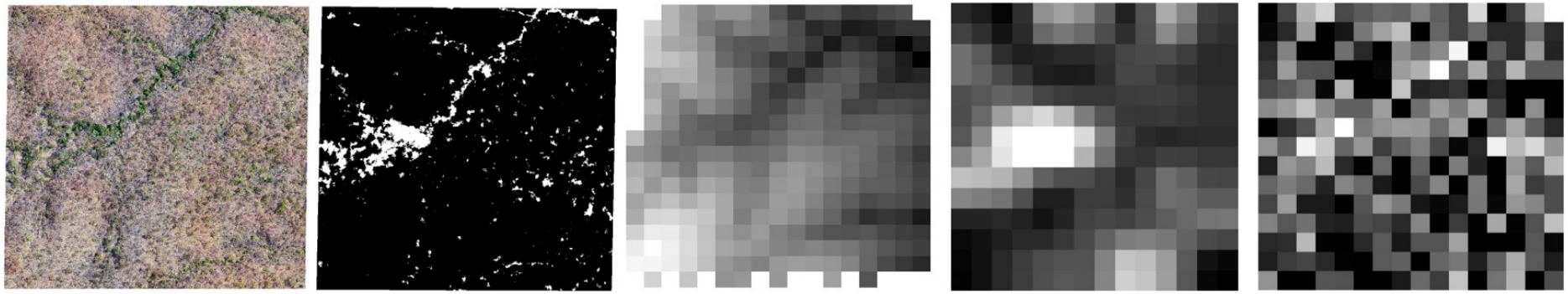

Figure 60. Comparison of crown distribution measured at 50ha scale in P5, (*Left – Right*): (i) UAV Orthophoto-7cm pixel spatial resolution, 0-255 scale; (ii) FC-7cm pixel spatial resolution, 0-100% scale;(iii) DTM -50m pixel spatial resolution, 634-708 scale; (iv) CHM 50m pixel spatial resolution, 0-55m scale; and (v) Sentinel-1-C -50m pixel spatial resolution, 0 to -0.6 *decibels* scale.

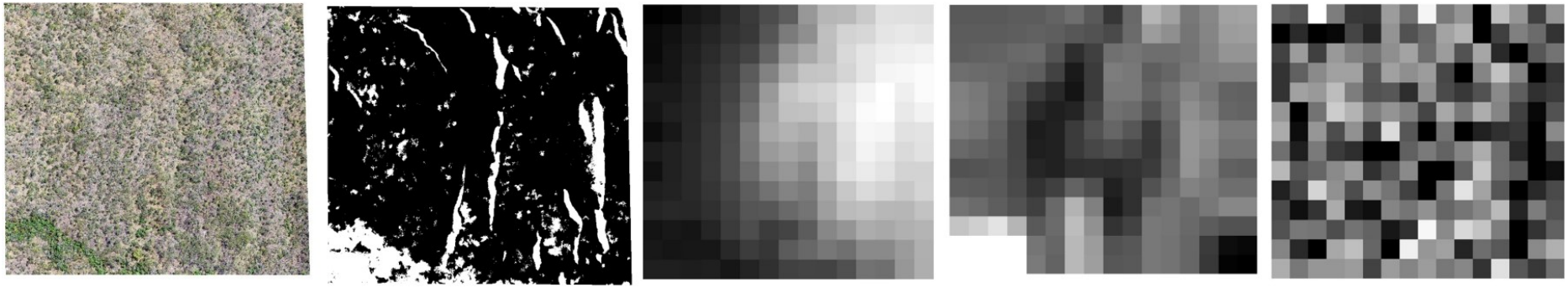

Figure 61. Comparison of crown distribution measured at 50ha scale in P6, (*Left – Right*):(i) UAV Orthophoto-7cm pixel spatial resolution, 0-255 scale; (ii) FC-7cm pixel spatial resolution, 0-100% scale; (iii) DTM -50m pixel spatial resolution, 634-708 scale; (iv) CHM 50m pixel spatial resolution, 0-55m scale; and (v) Sentinel-1-C -50m pixel spatial resolution, 0 to -0.6 *decibels* scale.

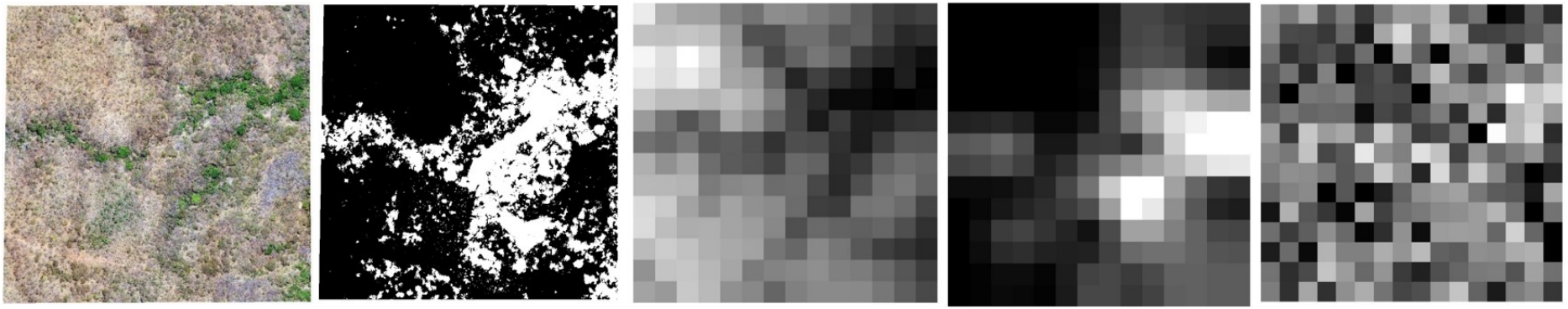

Figure 62. Comparison of crown distribution measured at 50ha scale in P9, (*Left* – *Right*): (i) UAV Orthophoto-7cm pixel spatial resolution, 0-255 scale; (ii) FC-7cm pixel spatial resolution, 0-100% scale; (iii) DTM -50m pixel spatial resolution, 634-708 scale; (iv) CHM -50m pixel spatial resolution, 0-55m scale; and (v) Sentinel-1-C -50m pixel spatial resolution, 0 to -0.6 *decibels* scale.

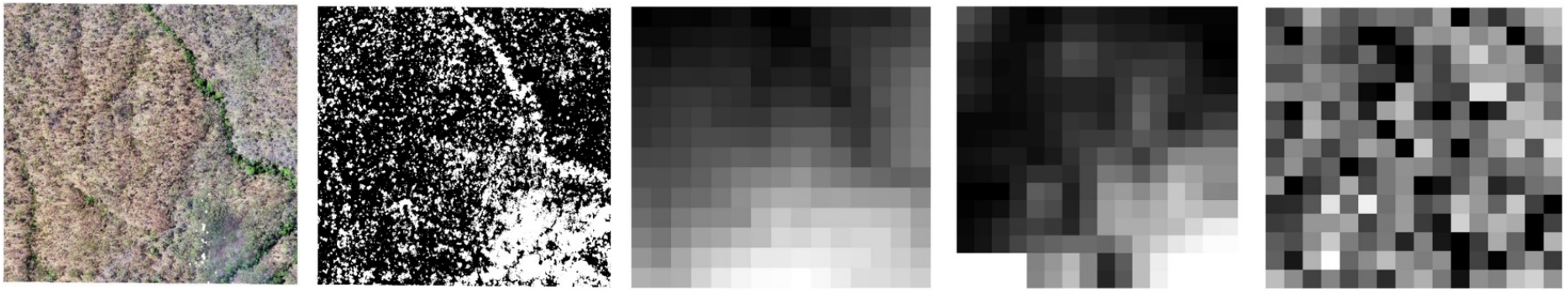

Figure 63. Comparison of crown distribution measured at 50ha scale in P8; (*Left* – *Right*) (i) UAV Orthophoto-7cm pixel spatial resolution, 0-255 scale; (ii) FC-7cm pixel spatial resolution, 0-100% scale; (iii) DTM -50m pixel spatial resolution, 634-708 scale; (iv) CHM -50m pixel spatial resolution, 0-55m scale; and (v) Sentinel-1-C -50m pixel spatial resolution, 0 to -0.6 *decibels* scale.

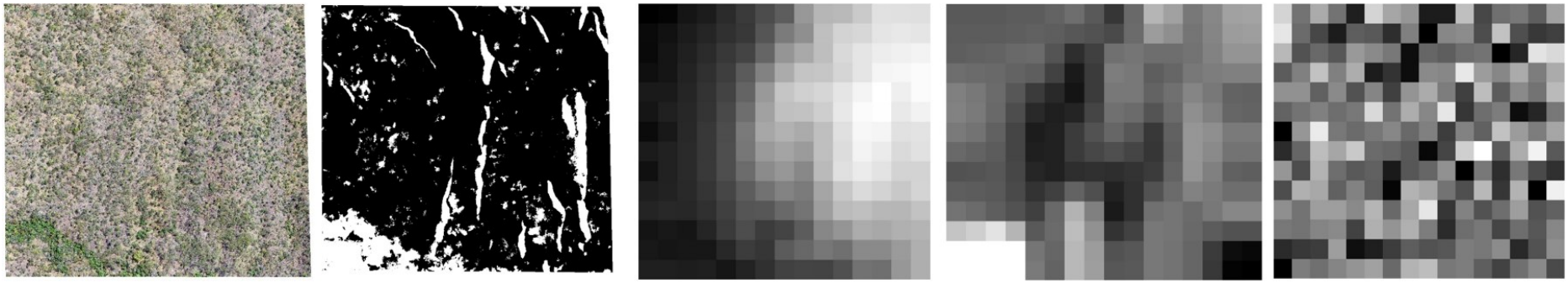

Figure 64. Comparison of Crown Distribution measured at 50ha scale in P1; (*Left* – *Right*): (i) UAV Orthophoto-7cm pixel spatial resolution, 0-255 scale; (ii) FC-7cm pixel spatial resolution, 0-100% scale; (iii) DTM -50m pixel spatial resolution., 634-708 scale; (iv) CHM -50m pixel spatial resolution, 0-55m scale; and (v) Sentinel-1-C -50m pixel spatial resolution, 0 to -0.6 *decibels* scale.

Figure 65. Comparison of Crown Distribution measured at 50ha in P2; (*Left* – *Right*): (i) UAV Orthophoto-7cm pixel spatial resolution, 0-255 scale; (ii) FC-7cm pixel spatial resolution, 0-100% scale; (iii) DTM -50m pixel spatial resolution, 634-708 scale; (iv) CHM -50m pixel spatial resolution, 0-55m scale; and (v) Sentinel-1-C -50m pixel spatial resolution, 0 to -0.6 *decibels* scale.

Similarly, in the above figures, the trend of crown spatial distribution patterns in P5, P6, P9, P8, P1 and P2 have demonstrated that as the pixel spatial resolution is downsized from 7cm-50m, spectral reflectance gets attenuated highly (~30%) and worsens at 100m pixel spatial resolution. Heterogeneous spatial crown arrangement displayed by P1 and P2 confirms the effect of fire on woody biomass in Miombo. Overall, S1-C observations (demonstrate less conspicuous and consistent crown spatial patterns compared to the one from the ALOS-PALSAR-2 (Fig. 56-59).

Notably, both P1 and P2 (Fig. 64 and 65) have not rendered a vivid pattern of the spatial tree crown reflectance due to the fire that swept these plots.

In comparison, the S1-C observations (demonstrate less conspicuous and consistent crown spatial patterns compared to one from ALOS-PALSAR-2 (Fig. 56-59). This is attributable to the SAR-C band's (λ = 5.6cm) weaker penetration than the PALSAR'S L-band (λ= 23 cm), thus through thicker surfaces such as branches and trunks of the Miombo trees. This is in addition to the observation that most of the trees lost their leaves due to the fire as well their deciduous nature during the dry season (Carreiras et al., 2013; Ghosh and Behera, 2018; Pulliainen et al., 1999; Santoro et al., 2013).

Overall, inference made on the ALOS-PALSAR-2 and Sentinel-1-C-band resampled imagery indicates that <50m pixel spatial resolution is the ideal scale with which spatial crown pattern distribution for the AGB and C can be estimated for better accuracy, thus under the given conditions of Malawi's Miombo Woodlands.

However, this study encourages employment of multiple seasonal datasets (wet and dry season) due to their advantage of averaging out the extreme conditions of a single season that affect woody biomass detection as observed in P8 imagery for Sentinel-1-C datasets. This ultimately enhances accuracy of the estimates.

4.7 Validation of Sentinel-2-L2A SWIR Band Combination Observations

The next figures portray Sentinel-2 L2A-SWIR band combination scene covering wet and dry season that have been reference against the optical UAV based orthomosaics acquired over Ntchisi Forest in 2019.

(66a) P13-Orthomosaics

(66b) P13-S2-SWIR-dry

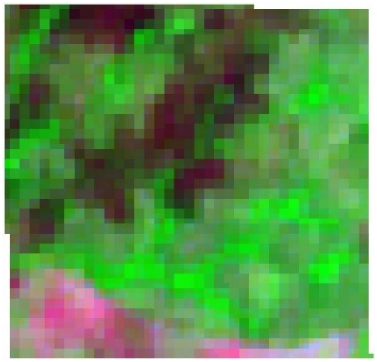

(66c) P13-S2-SWIR-wet

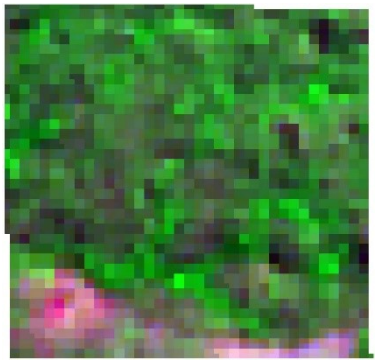

(66d) P12-Orthomosaics

(66e) P12-S2-SWIR-dry

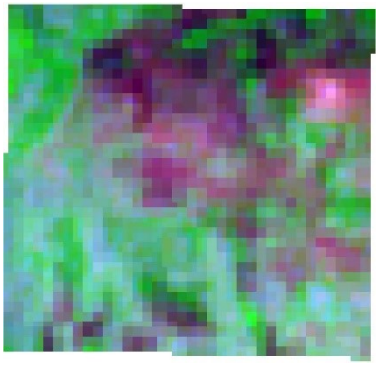

(66f) P12-S2-SWIR-wet

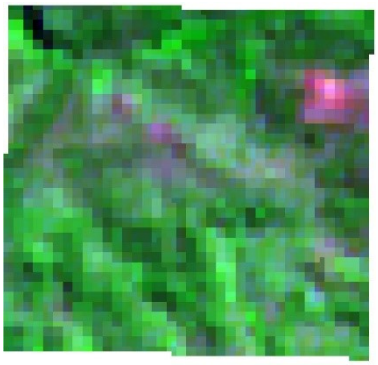

(66g) P10-Orthomosaics

(66h) P10-S2-SWIR-dry

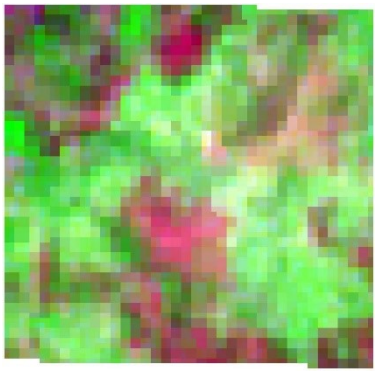

(66i) P10-S2-SWIR-wet

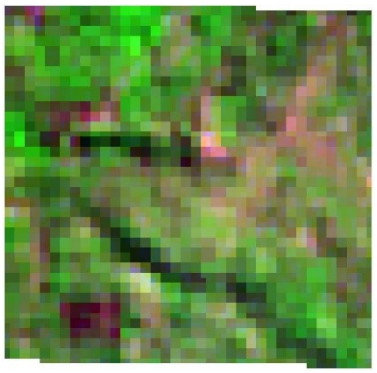

(66j) P9-Orthomosaics

(66k) P9-S2-SWIR-dry

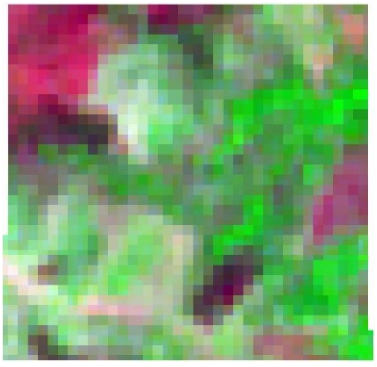

(66l) P9-S2-SWIR-wet

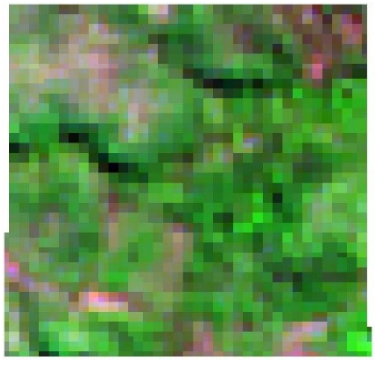

Figure 66. Comparison of crown distribution pattern at 50ha scale in P13, P12, P10 and P9, Crown Distribution, (*Left – Right*) (i) UAV Orthophoto (7cm pixel spatial resolution), (ii) S2-SWIR-dry season (20m pixel spatial resolution), and (iii) S2-SWIR-wet season (20m pixel spatial resolution). High spectral reflectance by tree crown cover and AGB from leaf-on conditions (tree belts) and low reflectance on leaf-off trees and contrastingly exceptionally low from non-vegetation/biomass features i.e., bare earth, soil, or rocks.

In Figure 66 above, both the wet (right) and dry season's (middle) imagery scenes are compared against the optical airborne orthomosaics (left), for crown spatial distribution. The S2 SWIR observations show a consistent pattern with the corresponding optical orthomosaics for the spatial crown distribution, i.e., high spectral reflectance intensity (greener pixels values) displayed by tree cover and AGB especially, in leaf-on condition (tree belts) and low intensity values (pale-green to yellowish) for leaf-off trees and contrastingly, brown to light-tan on non-tree-features such as bare earth, soil, or rocks (P13, 12,10 and P9).

The clear distinction of the non-biomass features; bare land (P13 and P9, Figures 66a and 66j) and conspicuously the rock out crops in P10 (Fig.66g) is due to the high reflectance of the SWIR band combination, thus in contrast to the L-band's ALOS-2 PALSAR-2 and or S1-C- bands radar backscatter measurements on rocks. A study on vegetation indices of African arid steppes observed that SWIR is moderately and strongly reflected by the vegetation canopy and soil, respectively, within the corresponding 1600–1800nm and 2200–2300nm regions (Benseghir and Bachari, 2021). Similarly, this attribute in the Malawi's Miombo Woodland under study influenced the overall spectral reflectance of the (P13, P9 and P10), resulting to clear-cut pattern demarcations of soil and rock outcrops that are lucidly separated from tree biomass in the S2 SWIR band combination imagery scene.

On the other hand, a clear pattern displayed by the vivid distinction of the burnt area and bare land/soils in P12 and the lower part of P13 can be highly attributed to the fact that newly burnt land reflects highly in SWIR (Guerschman et al., 2009; Nyasulu et al., 2020).

The next figure shows a comparison of tree spatial crown and AGB distribution pattern in plots that were highly affected by fire, in contrast to the wet season conditions.

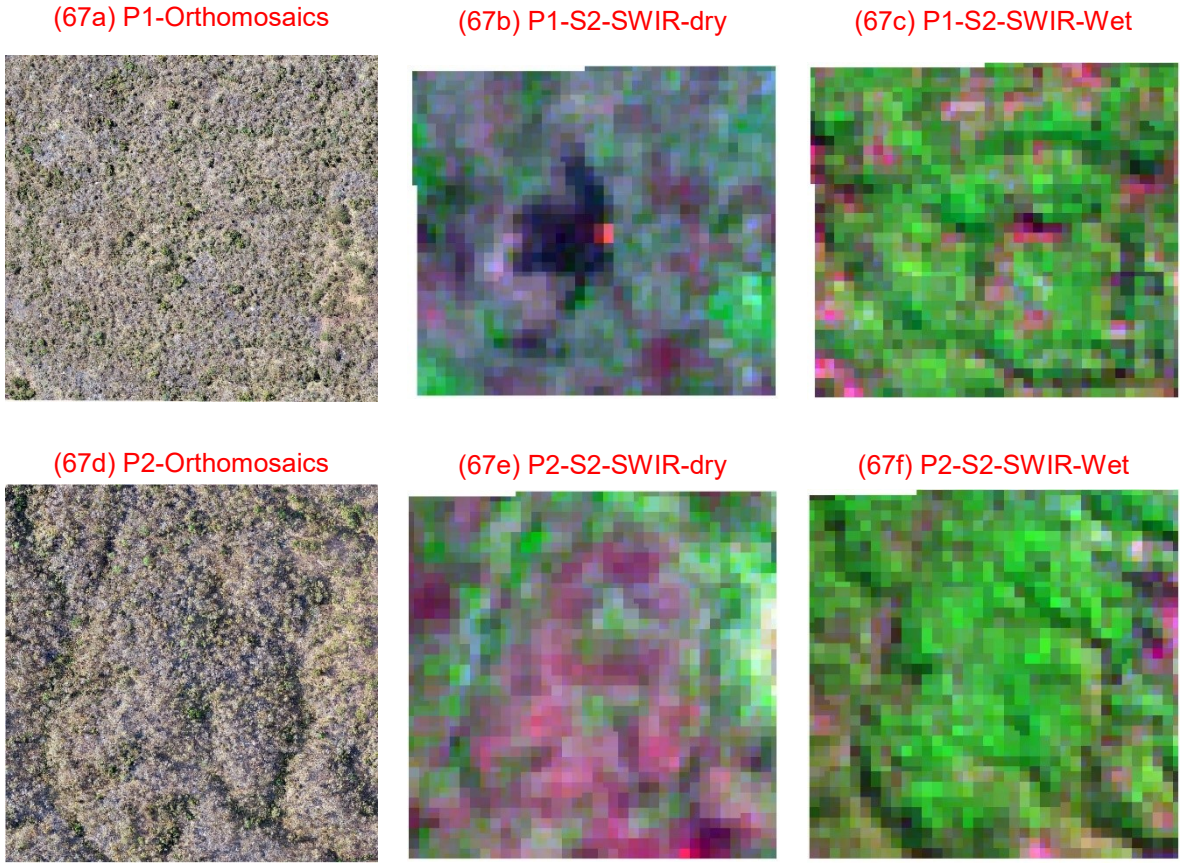

Figure 67. Comparison of crown distribution pattern at 50ha scale in P1 and P2. (*Left – Right*): (i) UAV Orthophoto (7cm pixel spatial resolution), (ii) S2-SWIR-dry season scene (20m pixel spatial resolution), and (iii) S2-SWIR-wet season scene (20m pixel spatial resolution). Heterogenous spatial crown and AGB distribution pattern in dry season is attributed to the effect fire while the homogeneous pattern in the wet season is attributed to the vegetation greenness that is induced by abundant moisture.

The crown spatial arrangement displayed in both P1 and P2 (Fig. 67) is heterogeneous, dominating with pale red to brownish colours in the dry season imagery (67b and 67e), in contrast to the wet season which is homogeneous. The evenly, pattern of the crown arrangement in the S2-SWIR wet season is attributed to the sufficient moisture that induces vegetation to develop green leaves.

On the other hand, the non-distinct pattern is attributable to fire (besides the leaf-off condition) and it was exacerbated by the dry period experienced during the survey period, thus September and October 2019. Studies observed that that newly burned land reflects strongly in SWIR, an aspect that makes the band combination valuable for mapping fire damaged area (Guerschman et al., 2009; Nyasulu et al., 2020).

To crown it all, both wet and dry season Vis/NIR/SWIR band combination scenes should be employed in the Miombo Woodlands for enhanced accuracy when assessing crown spatial distribution and AGB cover, given the conditions of the study site. These band combination datasets have also proven useful in detecting the areas affected by fire, and the bare land/open soils and even rock-outcrops as they reflect highly.

CHAPTER-5

5.0 CONCLUSION

This study explored the effectiveness of low-cost optical S*f*M photogrammetric orthomosaics acquired from UAV in upscaling the ground-based (gb) measurements of forest biomass in Miombo Woodlands of Malawi. The results were compared to open-sourced radar and optical satellite EO to assess their relative suitability. In brief, UAV data has an increasing role in tackling the problem of using open satellite data for supporting the sustainability of Malawi's National Forest Monitoring System (NFMS), thus regarding the financial constraints of the country.

The aim of the study was to establish the effectiveness by considering costs, assess spatial and temporal coverage and the associated accuracy of the optical airborne and freely/unrestricted Earth Observations datasets for Malawi's NFMS to help the Government attain the level required for global standards of REDD+ mechanism and more significant, carbon-based (C) payments. The specific objectives were;

(i) To investigate the effectiveness of low-cost optical UAV orthomosaics in geo-locating individual trees and estimating above ground biomass (AGB) and C and crown diameter that yields fractional cover (FC);
(ii) To scale-up the plot-based AGB measurements using height and crown diameter/(FC) parameters extracted from the UAV survey (objective 1) to evaluate the use of EO from ALOS-PALSAR-2 and Sentinel1 and 2, and ESA-CCI Biomass Map missions in estimating AGB and C on wall-to wall basis,
(iii) To compare AGB and crown diameter results from objective ii, thus between ALOS-PALSAR-2 and Sentinel1 backscatter, and the ESA-CCI Biomass Map measurements in terms of (a) accuracy, (b) extent and frequency of coverage, (c) costs, and (d) reliability of operation in the study site's environment, and
(iv) To explore the relationship among the ground-based, airborne-based and satellite-based AGB, C and fractional cover (achieved simultaneously through undertaking the first two objectives).

The undertaking of the four objectives provided insights into where these datasets are more/less successful in mapping biomass in Malawi. Data were acquired in 2019 from 13 plots over Ntchisi Forest in 3-fold, *vis-a-vis*; (i) individual tree measurements from

0.1ha gb plots, (ii) 3-7cm pixel resolution optical airborne imagery from 50ha plots, and (iii) SAR backscatter and Vis/NIR/SWIR band combination imagery.

5.1 Ground Based Measurements Analysis

The AGB mean stock of 44.5tCha^{-1} revealed the effect of escalated anthropogenic environmental threats affecting woody biomass that include; wood extraction (firewood, charcoal, poles, and timber), dry season fire and grazing. They further demonstrate how these attributes have contributed to diverse range of the plot-based AGB stock (25.1 to 68.8 tCha^{-1}) and a density of 7-24 stems per plot.

The findings from the ground-based measurements have demonstrated a positive relationship between the individual tree diameter at breast (*dbh*) and height parameters, supporting the premise that positive parametric correlations exist between the former and crown size, especially from the field-based measurements. The correlation of *dbh* and crown diameter of the dominant individual trees (R^2 = 0.6) suggests that the crown cover or better still the Fractional Cover (which is extracted from crown diameter) is dependent on the stem form *(dbh*) of the trees in Ntchisi Forest. On the other hand, the strong correlation (R^2 = 0.7) between the ground-based AGB (tCha^{-1}) and the ground-based Fractional Cover percent (FC %) has demonstrated reliably that FC % can be used to determine AGB stocks in the Miombo Woodland.

The study has however, observed that individual tree crown overlapping and overhanging observed in some plots rendering difficulties in sighting the tree tips also hampered crown delineation, thereby inherently affecting height and crown diameter measurements, and more importantly, AGB estimation accuracy.

5.2 UAV Imagery Analysis

The key results from the UAV imagery analysis demonstrate a strong correlational relationship (R^2 = 0.7) between ground-based AGB and UAV-based fractional cover percentage (FC %) considering the site conditional challenges associated with both datasets; i.e., tree leaf-off condition exacerbated by fire, overlapping and overhanging of individuals trees, non-use of Differential GPS and the wind upsurge. Hence, the 70% correlation consistently established on estimation of AGB across the entire Ntchisi Forest is by far, a better predictive power compared to the ground-based

individual tree height and Canopy Height Model (CHM) correlation whose values ranged from as low as R^2=0.5 and generated a wide range of Bias (5-15m). Despite the relatively weak correlation observed from the height parametric relationship, this study still encourages employment of the UAV orthomosaics (CHM, thus as a supplement to the EO) due to;

(i) the 3D aspect which under normal conditions has proven to yield better accuracy in estimations of AGB in other Tropical woodland studies, an aspect not available in 2-dimensional satellite imagery, and

(ii) the higher repetitive frequency and very fine spatial resolution of AGB observations that a drone can provide in contrast to the most satellite Earth Observations (i.e., ≥ 30m for Landsat Missions). However, the UAV imagery must be acquired during the leaf-on season, in contrast to the leaf-off (dry) season.

The UAV survey findings further show that a low-budget UAV system can collect optical/RGB data of very high resolution (3-7cm resolution), with a spatial horizontal geolocation uncertainty of ±13m in the rugged terrain Miombo Woodlands of Malawi. In view of the high expenses of ground-based forest inventories, plus their limited coverage (estimated in this study as £30 per ha, per person), the UAV provides a cost-effective means of bridging the ground datasets to the wall-to-wall satellite EO data, with an estimated cost of £7 per ha.

These findings reveal that the consumer grade UAV employed, and the optical observations acquired (collectively categorised under low-cost Structure-*from*-Motion photogrammetry), as used in this study is straightforward and cheap to operate compared to data acquired from commercial RADAR/LiDAR/ALS platforms, thus for Malawi's REDD+ purposes. The outcomes further establish that airborne FC is a more reliable indicator of the AGB stock distribution pattern in contrast to the airborne canopy height model (CHM), thus under the measurement conditions encountered in this work. Hence, for enhanced accuracy during estimation of AGB and C in the Miombo Woodlands, this study encourages incorporation of FC measurements as a key parameter.

The poor correlation of the UAV orthomosaics derived tree height and the ground-based height datasets (R^2 = 0.4) is attributed to the environmental factors outwith the control of the drone operators (at the time of the survey) i.e., leaf-off condition (which meant tree top canopy surfaces were unobserved due to the loss of the leaves), forest fires that also caused loss of woody biomass, topography (slope variation of 18-74% that impacted on the geo-correction) and wind squalls (>10.4 $m.s^{-1}$ to 13.1 $m.s^{-1}$) encountered during the UAV flight missions (which reduced the quality of the orthomosaics).

Additionally, these results signify the influence of, (i) individual tree crown overlaps, (ii) tree clumping, and (iii) plot-edge effect that rendered height and other parameters difficult to measure. These consequently, led to either underestimations or overestimations of AGB, C stocks and/or crown distribution. Furthermore, the poor correlation further exemplifies the limitations of ground-based inventory, i.e., the size of 0.1ha ground sampling plot units not being fully representative of forest biomass conditions, thereby resulting to spatial inexplicitness and weak correlation. The low correlation is further attributed to the UAV's systematic error associated with Structure-*from*-Motion photogrammetry.

On the other hand, the outcomes illustrate the limits of optical sensors and S*f*M photogrammetry in detecting tree biomass under challenging weather conditions (wind and hazy/fire) and the topography of Malawi's Miombo Woodlands. Nevertheless, this study encourages the Malawi Government to engage the optical low-cost UAV datasets as a bridging and cost-effective means of upscaling the ground-based measurements through incorporating the FC parameter in estimating AGB and C.

For most reliable results, this study recommends researchers to undertake UAV flight surveys in the dry tropics during the leaf-on season, at least within 2-3 weeks after the rainy season has stopped, thus when tree canopy cover still abundant.

5.3 SAR Imagery Analysis

The fundamental results observed between the gb AGB (tested at 0.1ha ground plot scale) and AGB from ALOS-PALSAR-2, ESA CCI-Biomass Map, and S1-C-band (at their original pixel resolutions) show strong correlational relationships: R^2 = 0.9, RMSE = 7$tCha^{-1}$; R^2 = 0.8, RMSE = 8$tCha^{-1}$; and R^2 = 0.7, respectively. The overall better

performance range of the SAR backscatter (R^2 = 0.7 to 0.9) demonstrate that SAR measurements can be suitably used to infer the Miombo AGB with better accuracy. Nevertheless, the RMSE range of 7-8tCha^{-1} can be attributed partly to the effect of sensing angle, canopy heterogeneity, and topographical distortions apparent in some of the plots, especially those with steep terrain and topographic ridges. While effect of these was apparent in the SAR imagery scene, as displayed by the layover and foreshortening distortions, their encounter reaffirms the need to cautiously consider the contribution of these geometric effects to the accuracy of the AGB and C estimates especially in these Miombo Woodlands.

The correlation of the UAV-based AGB and ALOS-PALSAR AGB showed a decline (R^2= 0.54) as the estimates were scaled from 0.1ha ground-based (gb) plot to 50ha (by coarsening the imagery to 50m pixel spatial resolution). This is attributed to the effect of leaf-off condition. However, results from the following 3 datasets, (i) gb AGB reference measurements (0.1ha plot), (ii) UAV-based 50ha plot AGB and the ALOS-PALSAR based AGB at 50ha plot show closely related mean stocks of 44.5tCha^{-1}, 43tCha^{-1} and 30.8tCha^{-1}, respectively, in which Fractional Cover percentage was used as the measurement parameter. This indicates that the gb datasets can be reliably scaled up to the wall-to-wall remotely sensed datasets using the fractional cover estimates. While the RMSE and the Bias ranges slightly improved when the datasets were coarsened to 100m pixel spatial resolution (the scale of ESA-CCI-Biomass Map data), the effect of the seasonal loss of leaves was still inherent, worse-still significant information on spatial distribution crown diameter were lost. Hence, this scale resulted in very low correlation and is discouraged by this research, thus under the conditions of the study encountered.

To conclude, while this study recommends scaling up of AGB and C estimates using the ALOS-PALSAR-2 datasets as a cost-effective means under the REDD+ mechanism, it cautiously emphasises the need to calibrate the AGB during the leaf-on season and use a scale of <50m, preferably 25m pixel spatial resolution for better accuracy. The leaf-on season datasets would minimise the effect of phenological and seasonal conditions that contributed to underestimation of AGB and C estimations.

5.4 Visual Imagery Analysis

The findings on visual qualitative analysis show that the optical UAV orthomosaics, S2-Vis/NIR/SWIR band combination and SAR (S1-C band) backscatter measurements mostly show a correspondence of crown diameter spatial distribution patterns i.e., consistent, and homogenous patterns exhibited particularly by the leaf-on tree canopies growing along the riverine tree belts and cohorts in each imagery. However, to yield robust results, the crown spatial distribution data must be collected at the right season, i.e., during the leaf-on season, preferably soon after the rains have stopped, in contrast to the dry season (leaf-off condition).

While the high relationship observed echoes the significance of the leaf-on condition as a pre-requisite for accurate AGB and crown diameter spatial distribution estimation, these outcomes further expose the effect of fire, rock outcrops and bare land/soil as some of the key factors affecting the estimates in the Miombo Woodlands. These factors are better detected by the SWIR band combination while vegetation cover (crown and other biomass) are well estimated using the Vis/NIR (Red-Edge) of the Sentinel-2 imagery. The entire results, however, prominently uncover the potential of the Vis/NIR/SWIR band combination in detecting the effect of newly burnt areas and rock outcrops affecting mapping of AGB and crown diameter spatial distribution.

In conclusion, the findings reveal that the ground-based datasets can be cost-effectively scaled-up with the freely available and unrestricted EO (SAR and/or Vis/NIR/SWIR band combination) datasets by using optical UAV datasets as a link in estimating AGB and C in Malawi's Miombo Woodlands. However, scaling up the AGB from height was not robust enough due to leaf-off condition of the trees; instead, the canopy (fractional) cover parameter was considered more reliable. The choice of appropriate scale of measurement i.e., <50m spatial resolution scale for coarsening imagery to enhance mapping accuracy of AGB, C and crown diameter spatial distribution is quite significant while also considering the environmental conditions of the Miombo Woodlands under study. These attributes are envisaged to go a long way in supporting the Malawi's NFMS standards to yield carbon-offset payments under the global REDD+ mechanism.

5.5 Areas Suggested for Further Research

As a way forward, the study encourages further exploration on;

(i) The suitability of the Vis/NIR/SWIR band combination band combination in evaluating dry season fire, bare-lands and presence of rock outcrops during woody biomass assessments, given the conditions of the Miombo Woodlands,

(ii) The effectiveness of other vegetation indices such as Modified Soil Adjusted Vegetation Index (MSAVI), Transformed Vegetation Index (TVI), Soil Adjusted Vegetation Index (SAVI), just to mention, but a few, in estimating woody components of the Miombo given the woodlands' conditions encountered during the study,

(iii) Generation of local allometry that can be used to calculate woody biomass from the SAR S1-C band datasets with enhanced accuracy, and

(iv) Modelling of the AGB and crown distribution using other Machine Learning techniques that have proven to render better accuracy, in contrast to the traditional methods i.e., simple linear regression as recommended by (Kadzuwa and Missanjo, 2023).

6.0 REFERENCES

Accadia, C., Mariani, S., Casaioli, M., Lavagnini, A., Speranza, A., 2003. Sensitivity of precipitation forecast skill scores to bilinear interpolation and a simple nearest-neighbor average method on high-resolution verification grids. Weather Forecast. 18, 918–932. https://doi.org/10.1175/1520-0434(2003)018<0918:SOPFSS>2.0.CO;2

Adame-Campos, R.L., Ghilardi, A., Gao, Y., Paneque-Gálvez, J., Mas, J.F., 2019. Variables selection for aboveground biomass estimations using satellite data: A comparison between relative importance approach and stepwise Akaike's information criterion. ISPRS Int. J. Geo-Inf. 8. https://doi.org/10.3390/ijgi8060245

Ahrends, A., Bulling, M.T., Platts, P.J., Swetnam, R., Ryan, C., Doggart, N., Hollingsworth, P.M., Marchant, R., Balmford, A., Harris, D.J., Gross-Camp, N., Sumbi, P., Munishi, P., Madoffe, S., Mhoro, B., Leonard, C., Bracebridge, C., Doody, K., Wilkins, V., Owen, N., Marshall, A.R., Schaafsma, M., Pfliegner, K., Jones, T., Robinson, J., Topp-Jørgensen, E., Brink, H., Burgess, N.D., 2021. Detecting and predicting forest degradation: A comparison of ground surveys and remote sensing in Tanzanian forests. Plants People Planet 3, 268–281. https://doi.org/10.1002/ppp3.10189

Alegria, J., Matthews, B., 2014. Malawi REDD+ Readiness Program: USFS GIS/RS Technical Detail Final Report. USDA Forest Service, Washington, USA.

Ali, A., Lin, S.L., He, J.K., Kong, F.M., Yu, J.H., Jiang, H.S., 2019. Big-sized trees overrule remaining trees' attributes and species richness as determinants of aboveground biomass in tropical forests. Glob. Change Biol. 25, 2810–2824. https://doi.org/10.1111/gcb.14707

Ali, T., Ahmad, M., Shahbaz, B., Suleri, A., 2007. Impact of participatory forest management on vulnerability and livelihood assets of forest-dependent communities in northern Pakistan. Int. J. Sustain. Dev. World Ecol. 14, 211–223. https://doi.org/10.1080/13504500709469721

Alleaume, S., Dusseux, P., Thierion, V., Commagnac, L., Laventure, S., Lang, M., Féret, J.B., Hubert-Moy, L., Luque, S., 2018. A generic remote sensing approach to derive operational essential biodiversity variables (EBVs) for conservation planning. Methods Ecol. Evol. 9, 1822–1836. https://doi.org/10.1111/2041-210X.13033

Angelsen, A., 2008. Moving ahead with REDD: Issues, options and implications. Center for International Forestry Research Jl. CIFOR, Situ Gede, Bogor, Indonesia.

Atkinson, P.M., 2013. Downscaling in remote sensing. Int. J. Appl. Earth Obs. Geoinformation 22, 106–114. https://doi.org/10.1016/j.jag.2012.04.012

Avitabile, V., Herold, M., Henry, M., Schmullius, C., 2011. Mapping biomass with remote sensing: a comparison of methods for the case study of Uganda. Carbon Balance Manag. 6. https://doi.org/10.1186/1750-0680-6-7

Avitabile, V., Herold, M., Heuvelink, G.B.M., Lewis, S.L., Phillips, O.L., Asner, G.P., Armston, J., Ashton, P.S., Banin, L., Bayol, N., Berry, N.J., Boeckx, P., de Jong, B.H.J., Devries, B., Girardin, C.A.J., Kearsley, E., Lindsell, J.A., Lopez-Gonzalez, G., Lucas, R., Malhi, Y., Morel, A., Mitchard, E.T.A., Nagy, L., Qie, L., Quinones, M.J., Ryan, C.M., Ferry, S.J.W., Sunderland, T., Laurin, G.V., Gatti, R.C., Valentini, R., Verbeeck, H., Wijaya, A., Willcock, S., 2016. An

integrated pan-tropical biomass map using multiple reference datasets. Glob. Change Biol. 22, 1406–1420. https://doi.org/10.1111/gcb.13139

Baboo, S.S., Devi, M.R., 2010. An Analysis of Different Resampling Methods in Coimbatore, District. Glob. J. Comput. Sci. Technol. 10, 61–66.

Baccini, A., Goetz, S.J., Walker, W.S., Laporte, N.T., Sun, M., Sulla-Menashe, D., Hackler, J., Beck, P.S.A., Dubayah, R., Friedl, M.A., Samanta, S., Houghton, R.A., 2012. Estimated carbon dioxide emissions from tropical deforestation improved by carbon-density maps. Nat. Clim. Change 2, 182–185. https://doi.org/10.1038/nclimate1354

Baccini, A., Laporte, N., Goetz, S.J., Sun, M., Dong, H., 2008. A first map of tropical Africa's above-ground biomass derived from satellite imagery. Environ. Res. Lett. 3. https://doi.org/10.1088/1748-9326/3/4/045011

Baccini, A., Walker, W., Carvalho, L., Farina, M., Houghton, R.A., 2019. Response to Comment on "Tropical forests are a net carbon source based on aboveground measurements of gain and loss." Science 363, 1–4. https://doi.org/10.1126/science.aat1205

Beaudoin, A., Le Toan, T., Goze, S., Nezry, E., Lopes, A., Mougin, E., Hsu, C.C., Han, H.C., Kong, J.A., Shin, R.T., 1994. Retrieval of forest biomass from SAR data. Int. J. Remote Sens. 15, 2777–2796. https://doi.org/10.1080/01431169408954284

Belenguer-Plomer, M.A., Chuvieco, E., Tanase, M.A., 2019. Evaluation of Backscatter Coefficient Temporal Indices for Burned Area Mapping. Presented at the Proc.SPIE, p. 111540D. https://doi.org/10.1117/12.2532832

Benseghir, L., Bachari, N.E.I., 2021. Shortwave infrared vegetation index-based modelling for aboveground vegetation biomass assessment in the arid steppes of Algeria. Afr. J. Range Forage Sci. https://doi.org/10.2989/10220119.2021.1882575

Berry, N., Utila, H., Clunas, C., Viergever, K., Tipper, R., 2009. Avoiding Unplanned Mosaic Deforestation and Degradation in Malawi Plan Vivo Technical Specification (No. Version 1.0). Malawi Environmental Endowment Trust, Blantyre, Malawi.

Berry, N.J., Catriona, C.J., Richard, T., 2008. Estimating Carbon Stocks: Toward Forest Conservation in Mkuwazi Forest Reserve and Thazima of Nyika Park in Malawi. COMPASS II and Ecometrica Ltd., Blantyre, Malawi.

Bhattarai, T., Skutsch, M., Midmore, D., Shrestha, H.L., 2016. Carbon Measurement: An Overview of Forest Carbon Estimation Methods and the Role of Geographical Information System and Remote Sensing Techniques for REDD+ Implementation. J. For. Livelihood 13, 69–86. https://doi.org/10.3126/jfl.v13i1.15367

Blarquez, O., Ali, A.A., Girardin, M.P., Grondin, P., Fréchette, B., Bergeron, Y., Hély, C., 2015. Regional paleofire regimes affected by non-uniform climate, vegetation and human drivers. Sci. Rep. 5, 1–13. https://doi.org/10.1038/srep13356

Bond, I., Chambwera, M., Jones, B., Chundama, M., Nhantumbo, I., 2010. REDD + in dryland forests: Issues and Prospects for Pro-poor REDD in the Miombo Woodlands of Southern Africa, Design. https://doi.org/10.1046/j.1420-9101.1995.8030301.x

Booysen, R., Gloaguen, R., Lorenz, S., Zimmermann, R., Nex, P.A.M., 2021. Geological Remote Sensing, 2nd ed, Encyclopedia of Geology. Elsevier Ltd. https://doi.org/10.1016/b978-0-12-409548-9.12127-x

Böttcher, H., Eisbrenner, K., Fritz, S., Kindermann, G., Kraxner, F., McCallum, I., Obersteiner, M., 2009. An assessment of monitoring requirements and costs of “Reduced Emissions from Deforestation and Degradation.” Carbon Balance Manag. 4, 7–7. https://doi.org/10.1186/1750-0680-4-7

Bouriaud, O., Don, A., Janssens, I.A., Marin, G., Schulze, E.D., 2019. Effects of forest management on biomass stocks in Romanian beech forests. For. Ecosyst. 6. https://doi.org/10.1186/s40663-019-0180-4

Bouvet, A., Mermoz, S., Le Toan, T., Villard, L., Mathieu, R., Naidoo, L., Asner, G.P., 2018. An above-ground biomass map of African savannahs and woodlands at 25 m resolution derived from ALOS PALSAR. Remote Sens. Environ. 206, 156–173. https://doi.org/10.1016/j.rse.2017.12.030

Brolly, M., Woodhouse, I.H., 2013. Vertical backscatter profile of forests predicted by a macroecological plant model. Int. J. Remote Sens. 34, 1026–1040. https://doi.org/10.1080/01431161.2012.715777

Brolly, M., Woodhouse, I.H., 2012. A “Matchstick Model” of microwave backscatter from a forest. Ecol. Model. 237–238, 74–87. https://doi.org/10.1016/j.ecolmodel.2012.04.014

Cairns, M.A., Helmer, E.H., Baumgardner, G.A., 1997. Root Biomass Allocation in the World’s Upland Forests: A Literature Review. J. Trop. Ethnobiol. 111, 1–11. https://www.academia.edu/26144290/Root_biomass_allocation_in_the_worlds_upland_forests

Campbell, B., 1996. The Ecology of Miombo Woodlands, The Miombo in Transition: Woodlands and Welfare in Africa. Centre for International Forestry Research, Bogor, Indonesia.

Campbell, B.M., Angelsen, A., Cunningham, A.B., Katerere, Y., Sitoe, A.A., Wunder, S., 2007. Miombo woodlands – opportunities and barriers to sustainable forest management. CIFOR Miombo Proj. 41–41.

Carreiras, J.M.B., Melo, J.B., Vasconcelos, M.J., 2013. Estimating the above-ground biomass in miombo savanna woodlands (Mozambique, East Africa) using L-band synthetic aperture radar data. Remote Sens. 5, 1524–1548. https://doi.org/10.3390/rs5041524

Cassells, G., 2012. Can remote sensing be used to support sustainable forestry in Malawi? University of Edinburgh, Edinburgh, United Kingdom.

Cassells, G.F., Woodhouse, I.H., Mitchard, E.T.A., Tembo, M.D., 2009. The Use of ALOS PALSAR for Supporting Sustainable Forest Use in Southern Africa: A Case Study in Malawi. Int. Geosci. Remote Sens. Symp. IGARSS 2, 206–209. https://doi.org/10.1109/IGARSS.2009.5418042

Cauldwell, A.E., Zieger, U., 2000. A reassessment of the fire-tolerance of some miombo woody species in the Central Province, Zambia. Afr. J. Ecol. 38, 138-146>. https://doi.org/10.1046/j.1365-2028.2000.00232.x

Chave, J., Andalo, C., Brown, S., Cairns, M.A., Chambers, J.Q., Eamus, D., Fölster, H., Fromard, F., Higuchi, N., Kira, T., Lescure, J.P., Nelson, B.W., Ogawa, H., Puig, H., Riéra, B., Yamakura, T., 2005. Tree allometry and improved estimation of carbon stocks and balance in tropical forests. Oecologia 145, 87–99. https://doi.org/10.1007/s00442-005-0100-x

Chen, J., Li, Z., Peng, C., Wang, Y., Gong, W., 2022. UAV Image Stitching Based on Optimal Seam and Half-Projective Warp. Remote Sens. 14, 1068–1068. https://doi.org/10.3390/rs14051068

Chen, L., Ren, C., Zhang, B., Wang, Z., Xi, Y., 2018. Estimation of Forest Above-Ground Biomass by Geographically Weighted Regression and Machine Learning with Sentinel Imagery. Forests 9, 1–20. https://doi.org/10.3390/f9100582

Chen, Z., Wang, J., 2008. A new method for minimizing topographic effects on RADARSAT-1 images: An application in mapping human settlements in the mountainous Three Gorges Area, China. Can. J. Remote Sens. 34, 13–25. https://doi.org/10.5589/m08-005

Chidumayo, E., 2015. Dry season watering alters the significance of climate factors influencing phenology and growth of saplings of savanna woody species in central Zambia, southern Africa. Austral Ecol. 40, 794–805. https://doi.org/10.1111/aec.12254

Chidumayo, E.N., 2019. Management implications of tree growth patterns in miombo woodlands of Zambia. For. Ecol. Manag. 436, 105–116. https://doi.org/10.1016/j.foreco.2019.01.018

Chidumayo, E.N., 2001. Climate and Phenology of Savanna Vegetation in Southern Africa. J. Veg. Sci. 12, 347–347. https://doi.org/10.2307/3236848

Chidumayo, E.N., 1997. Miombo Ecology and Management : An Introduction, 1st ed. Practical Action Publishing, United Kingdom.

Chidumayo, E.N., 1994. Phenology and nutrition of miombo woodland trees in Zambia. Trees 9, 67–72. https://doi.org/10.1007/BF00202124

Chidumayo, E.N., 1991. Woody biomass structure and utilisation for charcoal production in a Zambian Miombo woodland. Bioresour. Technol. 37, 43–52. https://doi.org/10.1016/0960-8524(91)90110-6

Chidumayo, E.N., 1987. Species Structure in Zambian Miombo Woodland. J. Trop. Ecol. 3, 109–118. https://www.jstor.org/stable/2559782

Chidumayo, E.N., Gumbo, D.J., 2010. The dry forests and woodlands of Africa: Managing for products and services, The Dry Forests and Woodlands of Africa: Managing for Products and Services. https://doi.org/10.4324/9781849776547

Chinangwa, L., Pullin, A.S., Hockley, N., 2016. Livelihoods and Welfare Impacts of Forest Comanagement. Int. J. For. Res. 2016. https://doi.org/10.1155/2016/5847068

Chiteculo, V., Lojka, B., Surový, P., Verner, V., Panagiotidis, D., Woitsch, J., 2018. Value chain of charcoal production and implications for forest degradation: Case study of Bié Province, Angola. Environ. - MDPI 5, 1–13. https://doi.org/10.3390/environments5110113

Chu, T., Starek, M.J., Brewer, M.J., Murray, S.C., Pruter, L.S., 2018. Characterizing canopy height with UAS structure-from-motion photogrammetry—results analysis of a maize field trial with respect to multiple factors. Remote Sens. Lett. 9, 753–762. https://doi.org/10.1080/2150704x.2018.1475771

Cunliffe, A.M., J Assmann, J., N Daskalova, G., Kerby, J.T., Myers-Smith, I.H., 2020. Aboveground biomass corresponds strongly with drone-derived canopy height but weakly with greenness (NDVI) in a shrub tundra landscape. Environ. Res. Lett. 15. https://doi.org/10.1088/1748-9326/aba470

Cutler, M.E.J., Boyd, D.S., Foody, G.M., Vetrivel, A., 2012. Estimating tropical forest biomass with a combination of SAR image texture and Landsat TM data: An assessment of predictions between regions. ISPRS J. Photogramm. Remote Sens. 70, 66–77. https://doi.org/10.1016/j.isprsjprs.2012.03.011

DeFries, R., Achard, F., Brown, S., Herold, M., Murdiyarso, D., Schlamadinger, B., de Souza, C., 2007. Earth observations for estimating greenhouse gas emissions from deforestation in developing countries. Environ. Sci. Policy 10, 385–394. https://doi.org/10.1016/j.envsci.2007.01.010

Department of Forestry, 2015. MALAWI REDD + LAUNCH OF UN-REDD SUPPORT. Department of Forestry-Malawi, Lilongwe, Malawi.

Department of Forestry, 2012. Forest Resource Mapping Final Report for Implementation Phase. Department of Forestry-Malawi, Lilongwe, Malawi.

Desanker, P.V., Frost, P.G.H., Justice, C.O., Scholes, R.J., 1997. The Miombo Network : Framework for a Terrestrial Transect Study of Land-Use and Land-Cover Change in the Miombo Ecosystems of Central Africa. Stockholm, Sweden.

Dixon, R.K., Brown, S., Houghton, R.A., Solomon, A.M., Trexler, M.C., Wisniewski, J., 2011. Carbon pools and flux of global forest ecosystems. Science 263, 185–190. https://doi.org/10.1126/science.263.5144.185

Domingo, D., Ørka, H.O., Næsset, E., Kachamba, D., Gobakken, T., 2019. Effects of UAV image resolution, camera type, and image overlap on accuracy of biomass predictions in a tropical woodland. Remote Sens. 11. https://doi.org/10.3390/rs11080935

Drigo, R., 2019. Woodfuel Integrated Supply/Demand Overview Mapping (WISDOM) Malawi: Analysis of Woodfuel Demand, Supply, and Harvesting Sustainability. Winrock International, Poggibonsi, Italy.

Dube, T., Mutanga, O., 2015. Evaluating the utility of the medium-spatial resolution Landsat 8 multispectral sensor in quantifying aboveground biomass in uMgeni catchment, South Africa. ISPRS J. Photogramm. Remote Sens. 101, 36–46. https://doi.org/10.1016/j.isprsjprs.2014.11.001

Duncanson, L.I., Cook, B.D., Hurtt, G.C., Dubayah, R.O., 2014. An efficient, multi-layered crown delineation algorithm for mapping individual tree structure across multiple ecosystems. Remote Sens. Environ. 154, 378–386. https://doi.org/10.1016/j.rse.2013.07.044

Ene, L.T., Næsset, E., Gobakken, T., Mauya, E.W., Bollandsås, O.M., Gregoire, T.G., Ståhl, G., Zahabu, E., 2016. Large-scale estimation of aboveground biomass in miombo woodlands using airborne laser scanning and national forest inventory data. Remote Sens. Environ. 186, 626–636. https://doi.org/10.1016/j.rse.2016.09.006

Fankhauser, K., Strigul, N., Gatziolis, D., 2018. Augmentation of Traditional Forest Inventory and Airborne Laser Scanning with Unmanned Aerial Systems and Photogrammetry for Forest Monitoring. Remote Sens. 10. https://doi.org/10.3390/rs10101562

[FAO] Food and Agriculture Organization, 2020. Global Forest Resources Assessment 2020 Main Report. https://doi.org/10.4324/9781315184487-1

Fayad, I., Baghdadi, N., Alvares, C.A., Stape, J.L., Bailly, J.S., Scolforo, H.F., Cegatta, I.R., Zribi, M., Le Maire, G., 2021. Terrain Slope Effect on Forest Height and Wood Volume Estimation from GEDI Data. Remote Sens. 13. https://doi.org/10.3390/rs13112136

Fitzgerald, G.J., 2010. Characterizing vegetation indices derived from active and passive sensors. Int. J. Remote Sens. 31, 4335–4348. https://doi.org/10.1080/01431160903258217

Frazer, G.W., Wulder, M.A., Niemann, K.O., 2005. Simulation and quantification of the fine-scale spatial pattern and heterogeneity of forest canopy structure: A

lacunarity-based method designed for analysis of continuous canopy heights. For. Ecol. Manag. 214, 65–90. https://doi.org/10.1016/j.foreco.2005.03.056
Freeman, A., Durden, S.L., 1998. A three-component scattering model for polarimetric SAR data. IEEE Trans. Geosci. Remote Sens. 36, 963–973. https://doi.org/10.1109/36.673687
Frost, P., 1996. The ecology of miombo woodlands. In: Campbell, B.M. (Ed.), The Miombo in Transition: Woodlands and Welfare in Africa. Centre for International Forestry Research, Bogor, Indonesia.
Gao, Y., Mas, J., 2008. A comparison of the Performance of Pixel based and Object Based Classifications over Images with various Spatial Resolutions. Online J. Earth Sci. 2, 27–35.
Gaucher, C., Domingues-Hamdi, É., Prin-Mathieu, C., Menu, P., Baudin-Creuza, V., 2015. Good Practice Guidance for Land Use, Land-Use Change and Forestry, Comptes Rendus - Biologies. https://doi.org/10.1016/j.crvi.2014.11.004
Ghosh, S.M., Behera, M.D., 2018. Aboveground biomass estimation using multi-sensor data synergy and machine learning algorithms in a dense tropical forest. Appl. Geogr. 96, 29–40. https://doi.org/10.1016/j.apgeog.2018.05.011
Goetz, S., Dubayah, R., 2011. Advances in remote sensing technology and implications for measuring and monitoring forest carbon stocks and change. Carbon Manag. 2, 231–244. https://doi.org/10.4155/cmt.11.18
Goetz, S.J., Hansen, M., Houghton, R.A., Walker, W., Laporte, N., Busch, J., 2015. Measurement and monitoring needs, capabilities and potential for addressing reduced emissions from deforestation and forest degradation under REDD+. Environ. Res. Lett. 10. https://doi.org/10.1088/1748-9326/10/12/123001
Gonçalves, F.M.P., Revermann, R., Gomes, A.L., Aidar, M.P.M., Finckh, M., Juergens, N., 2017. Tree Species Diversity and Composition of Miombo Woodlands in South-Central Angola: A Chronosequence of Forest Recovery after Shifting Cultivation. Int. J. For. Res. 2017. https://doi.org/10.1155/2017/6202093
Gonsamo, A., Chen, J.M., Colombo, S.J., Ter-Mikaelian, M.T., Chen, J., 2017. Global change induced biomass growth offsets carbon released via increased forest fire and respiration of the central Canadian boreal forest. J. Geophys. Res. Biogeosciences 122, 1275–1293. https://doi.org/10.1002/2016JG003627
Gonsamo, A., D'odorico, P., Pellikka, P., 2013. Measuring fractional forest canopy element cover and openness - definitions and methodologies revisited. Oikos 122, 1283–1291. https://doi.org/10.1111/j.1600-0706.2013.00369.x
Gonzalez-Benecke, C.A., Gezan, S.A., Samuelson, L.J., Cropper, W.P., Leduc, D.J., Martin, T.A., 2014. Estimating Pinus palustris tree diameter and stem volume from tree height, crown area and stand-level parameters. J. For. Res. 25, 43–52. https://doi.org/10.1007/s11676-014-0427-4
González-Jaramillo, V., Fries, A., Bendix, J., 2019. AGB estimation in a tropical mountain forest (TMF) by means of RGB and multispectral images using an unmanned aerial vehicle (UAV). Remote Sens. 11. https://doi.org/10.3390/rs11121413
Goodbody, T.R.H., Coops, N.C., Marshall, P.L., Tompalski, P., Crawford, P., 2017. Unmanned aerial systems for precision forest inventory purposes: A review and case study. For. Chron. 93, 71–81. https://doi.org/10.5558/tfc2017-012
Government of Malawi, 2019a. Malawi National Forest Inventory 2018 Analysis Report. Winrock International, Arling, USA.

Government of Malawi, 2019b. Malawi 10-day Weather and Agrometeorological Bulletin (Weather and Agrometerological Bulletin No. Issue No. 03), Period: 21-31 October 2019. Department of Climate Change and Meterogical Services, Lilongwe, Malawi.

Government of Malawi, 2017. The Malawi Growth and Development Strategy (MGDS) III Building a Productive, Competitive and Resilient Nation. Ministry of Finance, Economic Planning and Development, Lilongwe.

Government of Malawi, 2011. The Second National Communication of the Republic of Malawi to the Conference of the Parties (COP) of the United Nations Framework Convention on Climate Change. Environmental Affairs Department, Lilongwe, Malawi.

Grippa, M., Woodhouse, I.H., 2003. Retrieval of bare soil and vegetation parameters from wind scatterometer measurements over three different climatic regions. Remote Sens. Environ. 84, 16–24. https://doi.org/10.1016/S0034-4257(02)00067-6

Guerschman, J.P., Hill, M.J., Renzullo, L.J., Barrett, D.J., Marks, A.S., Botha, E.J., 2009. Estimating fractional cover of photosynthetic vegetation, non-photosynthetic vegetation and bare soil in the Australian tropical savanna region upscaling the EO-1 Hyperion and MODIS sensors. Remote Sens. Environ. 113, 928–945. https://www.sciencedirect.com/science/article/pii/S0034425709000121

Gumbo, D., Clendenning, J., Martius, C., Moombe, K., Grundy, I., Nasi, R., Mumba, K.Y., Ribeiro, N., Kabwe, G., Petrokofsky, G., 2018. How have carbon stocks in central and southern Africa's miombo woodlands changed over the last 50 years? A systematic map of the evidence. Environ. Evid. 7, 1–19. https://doi.org/10.1186/s13750-018-0128-0

Haack, B., Mahabir, R., Kerkering, J., 2015. Remote sensing-derived national Land over Land use maps: A comparison for Malawi. Geocarto Int. 30, 270–292. https://doi.org/10.1080/10106049.2014.952355

Hancock, S., Armston, J., Hofton, M., Sun, X., Tang, H., Duncanson, L.I., Kellner, J.R., Dubayah, R., 2019. The GEDI Simulator: A Large-Footprint Waveform Lidar Simulator for Calibration and Validation of Spaceborne Missions. Earth Space Sci. 6, 294–310. https://doi.org/10.1029/2018EA000506

Hancock, S., McGrath, C., Lowe, C., Davenport, I., Woodhouse, I., 2021. Requirements for a global lidar system: spaceborne lidar with wall-to-wall coverage. R. Soc. Open Sci. 8. https://doi.org/10.1098/rsos.211166

Hansen, M.C., 2013. High-Resolution Global Maps of 21st-Century Forest Cover Change. SCIENCE 850, 850–854. https://doi.org/10.1126/science.1244693

Hariyanto, T., Kurniawan, A., Pribadi, C.B., Amin, R.A., 2019. Optimization of Ground Control Point (GCP) and Independent Control Point (ICP) on Orthorectification of High Resolution Satellite Imagery. E3S Web Conf. 94, 1–5. https://doi.org/10.1051/e3sconf/20199402008

Henebry, G.M., Kux, H.J., 1995. Lacunarity as a texture measure for SAR imagery. Int. J. Remote Sens. 16, 565–571. https://doi.org/10.1080/01431169508954422

Heo, H.K., Lee, D.K., Park, J.H., Thorne, J.H., 2019. Estimating the heights and diameters at breast height of trees in an urban park and along a street using mobile LiDAR. Landsc. Ecol. Eng. 15, 253–263. https://doi.org/10.1007/s11355-019-00379-6

Hilker, T., Wulder, M.A., Coops, N.C., 2008. Update of forest inventory data with lidar and high spatial resolution satellite imagery. Can. J. Remote Sens. 34, 5–12. https://doi.org/10.5589/m08-004

Hugel, Bruno., Hicks, Charlotte., Guedez, P.-Yves., Vaananen, Elina., Chiu, Marco., Scriven, Joel., Eggerts, Elizabeth., 2018. REDD+ Academy Learning Journals, Policies and Measures for Redd+ Implementation. REDD Acad. Learn. J. Edition 3, 1–36. http://bit.ly/REDD_Academy

Hummel, S., Hudak, A.T., Uebler, E.H., Falkowski, M.J., Megown, K.A., 2011. A comparison of accuracy and cost of LiDAR versus stand exam data for landscape management on the Malheur National Forest. J. For. 109, 267–273. https://doi.org/10.1093/jof/109.5.267

Iglhaut, J., Cabo, C., Puliti, S., Piermattei, L., O'Connor, J., Rosette, J., 2019. Structure from Motion Photogrammetry in Forestry: a Review. Curr. For. Rep. 5, 155–168. https://doi.org/10.1007/s40725-019-00094-3

Iman, G., Boyemba, F., Lewis, S., Nabahungu, N.L., Calders, K., Zapfack, L., Riera, B., Balegamire, C., Cuni-sanchez, A., 2017. Height-diameter allometry and above ground biomass in tropical montane forests : Insights from the Albertine Rift in Africa. Plos One 1–20. https://journals.plos.org/plosone/article?id=10.1371/journal.pone.0179653

Isango, J.A., 2007. Stand Structure and Tree Species Composition of Tanzania Miombo Woodlands : A Case Study from Miombo Woodlands of Community Based Forest Management in Iringa District 50, 43–56. http://www.metla.fi/julkaisut/workingpapers/2007/mwp050.htm

Kachamba, D.J., 2016. Biomass Estimation Models and Methods for Miombo woodlands of Malawi Using Field and Remotely Sensed Data. Norwegian University of Life Sciences, Norway. https://doi.org/10.3390/rs8110968

Kachamba, Ørka, H.O., Gobakken, T., Eid, T., Mwase, W., 2016. Biomass Estimation Using 3D Data from Unmanned Aerial Vehicle Imagery in a Tropical Woodland. Remote Sens. 8, 1–18. https://doi.org/10.3390/rs8110968

Kadzuwa, H., Missanjo, E., 2023. Modelling Above-ground Biomass Using Machine Learning Algorithm : Case Study Miombo Woodlands of Malawi. J. Glob. Ecol. Environ. 17, 1–15. https://doi.org/10.56557/JOGEE/2023/v17i38178

Kadzuwa, H., Missanjo, E., 2022a. Comparison of Varied Forest Inventory Methods and Operating Procedures for Estimating Above-Ground Biomass in Malawi's Miombo Woodlands. J. Glob. Ecol. Environ. 16, 7–27. https://www.ikprress.org/index.php/JOGEE/article/view/7675

Kadzuwa, H., Missanjo, E., 2022b. Effect of Leaf Phenology, Topography and Wind speed on Forest Canopy Height and Above Ground Biomass Estimation using Optical UAV Data in Malawi's Miombo Woodlands. J. Glob. Ecol. Environ. 16, 28–42. https://doi.org/ikprress.org/index.php/JOGEE/article/view/7720

Kalaba, F.K., Quinn, C.H., Dougill, A.J., Vinya, R., 2013. Floristic composition, species diversity and carbon storage in charcoal and agriculture fallows and management implications in Miombo woodlands of Zambia. For. Ecol. Manag. 304, 99–109. https://doi.org/10.1016/j.foreco.2013.04.024

Kambewa, P., Mataya, B., Sichinga, K., Johnson, T., 2007. Charcoal The Reality: A case study of charcoal consumption, trade and production in Malawi, 1st ed, Small and Medium Forestry Enterprise. International Institute for Environment and Development (IIED), London,United Kingdom.

Kameyama, S., Sugiura, K., 2020. Estimating Tree Height and Volume Using Unmanned Aerial Vehicle Photography and SfM Technology, with Verification of Result Accuracy. Drones 4, 1–21. https://doi.org/10.3390/drones4020019

Kamusoko, C., Gamba, J., Murakami, H., 2014. Mapping Woodland Cover in the Miombo Ecosystem: A Comparison of Machine Learning Classifiers. Land 3, 524–540. https://doi.org/10.3390/land3020524

Kayambazinthu, D., Barany, M., Mumba, R., Anyonge, C.H., 2005. Miombo woodlands and HIV/AIDS interactions : Malawi Country Report. Food and Organization of the United Nations, Rome, Italy.

Kellndorfer, J., Cartus, O., Bishop, J., Walker, W., Holecz, F., 2014. Large Scale Mapping of Forests and Land Cover with Synthetic Aperture Radar Data. Land Appl. Radar Remote Sens. https://doi.org/10.5772/58220

Kerr, A., 2005. Disappearing forests in Malawi Causes and solutions. University of California, Berkeley, USA.

Kim, K.H., Shim, P.S., Shin, S., 2019. An alternative bilinear interpolation method between spherical grids. Atmosphere 10. https://doi.org/10.3390/atmos10030123

Knapp, N., Huth, A., Fischer, R., 2021. Tree crowns cause border effects in area-based biomass estimations from remote sensing. Remote Sens. 13. https://doi.org/10.3390/rs13081592

Köhl, M., Neupane, P.R., Mundhenk, P., 2020. REDD+ measurement, reporting and verification – A cost trap? Implications for financing REDD+MRV costs by result-based payments. Ecol. Econ. 168, 106513–106513. https://doi.org/10.1016/j.ecolecon.2019.106513

Kondratyev, K.Y.A., Vassilyev, O.B., Grigoryev, A.A., Ivanian, G.A., 1973. An Analysis of the Earth's Resources Satellite (ERTS-1) Data Pictures of the Earth. Remote Sens. Environ. 2, 273–283. https://doi-org.ezproxy.is.ed.ac.uk/10.1016/0034-4257(71)90100-3

Kronseder, K., Ballhorn, U., Böhmc, V., Siegert, F., 2012. Above ground biomass estimation across forest types at different degradation levels in central kalimantan using lidar data. Int. J. Appl. Earth Obs. Geoinformation 18, 37–48. https://doi.org/10.1016/j.jag.2012.01.010

Krug, J.H.A., 2018. Accounting of GHG emissions and removals from forest management: A long road from Kyoto to Paris. Carbon Balance Manag. 13, 1–11. https://doi.org/10.1186/s13021-017-0089-6

Kuyah, S., Sileshi, G.W., Njoloma, J., Mng'omba, S., Neufeldt, H., 2014. Estimating aboveground tree biomass in three different miombo woodlands and associated land use systems in Malawi. Biomass Bioenergy 66, 214–222. https://doi.org/10.1016/j.biombioe.2014.02.005

Laurin, G.V., Balling, J., Corona, P., Mattioli, W., Papale, D., Puletti, N., Rizzo, M., Truckenbrodt, J., Urban, M., 2018. Above-ground biomass prediction by Sentinel-1 multitemporal data in central Italy with integration of ALOS2 and Sentinel-2 data. J. Appl. Remote Sens. 12, 1–1. https://doi.org/10.1117/1.jrs.12.016008

Lawton, R.M., 1964. The Ecology of the Marquesia Acuminata (Gilg) R.E.FR. Evergreen Forest and the Related Chipya Vegetation Types of North-Eastern Rhodesia. Br. Ecol. Soc. 52, 467–479.

Le Toan, T., Quegan, S., Woodward, I., Lomas, M., Delbart, N., Picard, G., 2004. Relating Radar Remote Sensing of Biomass to Modelling of Forest Carbon

Budgets. Clim. Change 67, 379–402. https://doi.org/10.1007/s10584-004-3155-5

Lechner, A.M., Foody, G.M., Boyd, D.S., 2020. Applications in Remote Sensing to Forest Ecology and Management. One Earth 2, 405–412. https://doi.org/10.1016/j.oneear.2020.05.001

Li, B., Good, S.P., URycki, D.R., 2021. The value of L-band soil moisture and vegetation optical depth estimates in the prediction of vegetation phenology. Remote Sens. 13. https://doi.org/10.3390/rs13071343

Li, C., Zhou, L., Xu, W., 2021. Estimating Aboveground Biomass Using Sentinel-2 MSI Data and Ensemble Algorithms for Grassland in the Shengjin Lake Wetland, China. Remote Sens. 13, 1–18. https://doi.org/10.3390/rs13081595

Li, Y., Li, M., Li, C., Liu, Z., 2020. Forest aboveground biomass estimation using Landsat 8 and Sentinel-1A data with machine learning algorithms. Sci. Rep. 10, 1–12. https://doi.org/10.1038/s41598-020-67024-3

Liao, Z., Van Dijk, A.I.J.M., He, B., Larraondo, P.R., Scarth, P.F., 2020. Woody vegetation cover, height and biomass at 25-m resolution across Australia derived from multiple site, airborne and satellite observations. Int. J. Appl. Earth Obs. Geoinformation 93, 102209–102209. https://doi.org/10.1016/j.jag.2020.102209

Lindsay, J.B., Francioni, A., Cockburn, J.M.H., 2019. LiDAR DEM smoothing and the preservation of drainage features. Remote Sens. 11, 17–19. https://doi.org/10.3390/rs11161926

Liu, A., Cheng, X., Chen, Z., 2021. Performance evaluation of GEDI and ICESat-2 laser altimeter data for terrain and canopy height retrievals. Remote Sens. Environ. 264, 112571. https://doi.org/10.1016/j.rse.2021.112571

Liu, K., Wang, J., Zeng, W., Song, J., 2017. Comparison and Evaluation of Three Methods for Estimating Forest above Ground Biomass Using TM and GLAS Data. Remote Sens. 9. https://doi.org/10.3390/rs9040341

Liu, M., Feng, Z., Zhang, Z., Ma, C., Wang, M., ling Lian, B., Sun, R., Zhang, L., 2017. Development and evaluation of height diameter at breast models for native Chinese Metasequoia. PLoS ONE 12, 1–16. https://doi.org/10.1371/journal.pone.0182170

Loubota Panzou, G.J., Fayolle, A., Jucker, T., Phillips, O.L., Bohlman, S., Banin, L.F., Lewis, S.L., Affum-Baffoe, K., Alves, L.F., Antin, C., Arets, E., Arroyo, L., Baker, T.R., Barbier, N., Beeckman, H., Berger, U., Bocko, Y.E., Bongers, F., Bowers, S., Brade, T., Brondizio, E.S., Chantrain, A., Chave, J., Compaore, H., Coomes, D., Diallo, A., Dias, A.S., Dimobe, K., Djagbletey, G.D., Domingues, T., Doucet, J.L., Drouet, T., Forni, E., Godlee, J.L., Goodman, R.C., Gourlet-Fleury, S., Hien, F., Iida, Y., Ilondea, B.A., Ilunga Muledi, J., Jacques, P., Kuyah, S., López-Portillo, J., Loumeto, J.J., Marimon-Junior, B.H., Marimon, B.S., Mensah, S., Mitchard, E.T.A., Moncrieff, G.R., Narayanan, A., O'Brien, S.T., Ouedraogo, K., Palace, M.W., Pelissier, R., Ploton, P., Poorter, L., Ryan, C.M., Saiz, G., dos Santos, K., Schlund, M., Sellan, G., Sonke, B., Sterck, F., Thibaut, Q., Van Hoef, Y., Veenendaal, E., Vovides, A.G., Xu, Y., Yao, T.L., Feldpausch, T.R., 2020. Pantropical variability in tree crown allometry. Glob. Ecol. Biogeogr. 1–17. https://doi.org/10.1111/geb.13231

Lupala, Z.J., Lusambo, L.P., Ngaga, Y.M., Makatta, A.A., 2015. The Land Use and Cover Change in Miombo Woodlands under Community Based Forest Management and Its Implication to Climate Change Mitigation: A Case of

Southern Highlands of Tanzania. Int. J. For. Res. 2015, 1–11. https://doi.org/10.1155/2015/459102

Magrath, J., Sukali, E., 2009. The winds of change: Climate change, poverty and the environment in Malawi. Oxfarm International, Lilongwe, Malawi.

Mahdavi, S., 2017. Effects of changing environmental conditions on synthetic aperture radar backscattering coefficient, scattering mechanisms, and class separability in a forest area. J. Appl. Remote Sens. 11, 1. https://doi.org/10.1117/1.jrs.11.036015

Malawi Redd+ Programme, 2015. Malawi REDD+ Readiness Program: Final Report on Carbon Inventory in Malawi's Forests Capacity to Support REDD+ and National forest Inventory Activities (Forestry). US Forest Service, Department of Agriculture, USA.

Mandelbrot, B.B., Wheeler, J.A., 1983. The Fractal Geometry of Nature. Am. J. Phys. 51, 286–287. https://doi.org/10.1119/1.13295

Manyanda, B.J., Nzunda, E.F., Mugasha, W.A., Malimbwi, R.E., 2021. Effects of drivers and their variations on the number of stems and aboveground carbon removals in miombo woodlands of mainland Tanzania. Carbon Balance Manag. 16, 1–15. https://doi.org/10.1186/s13021-021-00180-9

Maquia, I., Ribeiro, N.S., Silva, V., Bessa, F., Goulao, L.F., Ribeiro, A.I., 2013. Genetic diversity of Brachystegia boehmii Taub. and Burkea africana Hook. f. across a fire gradient in Niassa National Reserve, Northern Mozambique. Biochem. Syst. Ecol. 48, 238–247. https://doi.org/10.1016/j.bse.2012.12.020

Marlon, J.R., Kelly, R., Daniau, A.L., Vannière, B., Power, M.J., Bartlein, P., Higuera, P., Blarquez, O., Brewer, S., Brücher, T., Feurdean, A., Romera, G.G., Iglesias, V., Yoshi Maezumi, S., Magi, B., Mustaphi, C.J.C., Zhihai, T., 2016. Reconstructions of biomass burning from sediment-charcoal records to improve data-model comparisons. Biogeosciences 13, 3225–3244. https://doi.org/10.5194/bg-13-3225-2016

Matsuoka, M., Yoshioka, H., Obata, K., Tadono, T., 2013. Effect of bandwidth of panchromatic image on the quality of pansharpened multispectral image. Int. Geosci. Remote Sens. Symp. IGARSS 3602–3605. https://doi.org/10.1109/IGARSS.2013.6723609

McGann, M., 2015. Final Report on Developing a Recommended Suite of Land Use/Land Cover Standards for the Government of Malawi. USDA Forest Service, USA.

McKee, M., Nassar, A., Torres-Rua, A., Aboutalebi, M., Kustas, W., 2019. Implications of sensor inconsistencies and remote sensing error in the use of small unmanned aerial systems for generation of information products for agricultural management. NASA Public Access 3, 163–186. https://doi.org/10.1117/12.2305826.Implications

McNicol, I.M., Mitchard, E.T.A., Aquino, C., Burt, A., Carstairs, H., Dassi, C., Modinga Dikongo, A., Disney, M.I., 2021. To What Extent Can UAV Photogrammetry Replicate UAV LiDAR to Determine Forest Structure? A Test in Two Contrasting Tropical Forests. J. Geophys. Res. Biogeosciences 126, 1–17. https://doi.org/10.1029/2021JG006586

McNicol, I.M., Ryan, C.M., Mitchard, E.T.A., 2018. Carbon losses from deforestation and widespread degradation offset by extensive growth in African woodlands. Nat. Commun. 9. https://doi.org/10.1038/s41467-018-05386-z

McRoberts, R.E., Næsset, E., Gobakken, T., Bollandsås, O.M., 2015. Indirect and direct estimation of forest biomass change using forest inventory and airborne

laser scanning data. Remote Sens. Environ. 164, 36–42. https://doi.org/10.1016/j.rse.2015.02.018

Mendes, F. de S., Baron, D., Gerold, G., Liesenberg, V., Erasmi, S., 2019. Optical and SAR remote sensing synergism for mapping vegetation types in the endangered Cerrado/Amazon ecotone of Nova Mutum-Mato Grosso. Remote Sens. 11. https://doi.org/10.3390/rs11101161

Meyer, F., 2019. Spaceborne Synthetic Aperture Radar : Principles, Data Access, and Basic Processing Techniques, 1st ed. Alaska Satellite Facility, NASA Prime Data Centre, Alaska, USA.

Meyer, V., Saatchi, S., Clark, D.B., Keller, M., Vincent, G., Ferraz, A., Espírito-Santo, F., D'Oliveira, M.V.N., Kaki, D., Chave, J., 2018. Canopy area of large trees explains aboveground biomass variations across neotropical forest landscapes. Biogeosciences 15, 3377–3390. https://doi.org/10.5194/bg-15-3377-2018

Michelakis, D., Stuart, N., Brolly, M., Woodhouse, I.H., Lopez, G., Linares, V., 2015. Estimation of woody biomass of pine savanna woodlands from ALOS PALSAR imagery. IEEE J. Sel. Top. Appl. Earth Obs. Remote Sens. 8, 244–254. https://doi.org/10.1109/JSTARS.2014.2365253

Miewald, T., Oduor, P., 2014. Assessment of Land Cover Mapping in Malawi Existing Data and Institutional Factors. US Department of the Interior Technical Assistance Program, USA.

Ministry of Forestry and Natural Resources, 2021. The Third National Communication of the Republic of Malawi to the Conference of the Parties (COP) of the United Nations Framework Convention on Climate Change (UNFCCC). Ministry of Forestry and Natural Resources, Lilongwe, Malawi.

Ministry of Natural Resouces Energy and Mining, 2019. Malawi Redd+ National Forest Reference Level. Department of Forestry-Malawi, Lilongwe, Malawi.

Ministry of Natural Resources, Energy and Mining, 2017. National Forest Landscape Restoration Strategy. Ministry of Natural Resources, Energy and Mining, Lilongwe, Malawi.

Ministry of Natural Resources Energy and Mining, 2016. Forest Carbon Inventory Standard Operating Procedures Vol 3. Ministry of Natural Resources, Energy and Mining, Lilongwe, Malawi.

Mitchard, E, Meir, P., Ryan, C.M., Woollen, E.S., Williams, M., Goodman, L.E., Mucavele, J.A., Watts, P., Woodhouse, I.H., Saatchi, S.S., 2013. A novel application of satellite radar data: Measuring carbon sequestration and detecting degradation in a community forestry project in Mozambique. Plant Ecol. Divers. 6, 159–170. https://www.pure.ed.ac.uk/ws/portalfiles/portal/10769606/PDF_NovelApplication2013.pdf

Mitchard, Edward, Meir, P., Ryan, C.M., Woollen, E.S., Williams, M., Goodman, L.E., Mucavele, J.A., Watts, P., Woodhouse, I.H., Saatchi, S.S., 2013. A novel application of satellite radar data: Measuring carbon sequestration and detecting degradation in a community forestry project in Mozambique. Plant Ecol. Divers. 6, 159–170. https://www.pure.ed.ac.uk/ws/portalfiles/portal/10769606/PDF_NovelApplication2013.pdf

Mitchard, E.T.A., Feldpausch, T.R., Brienen, R.J.W., Lopez-Gonzalez, G., Monteagudo, A., Baker, T.R., Lewis, S.L., Lloyd, J., Quesada, C.A., Gloor, M., ter Steege, H., Meir, P., Alvarez, E., Araujo-Murakami, A., Aragão, L.E.O.C.,

Arroyo, L., Aymard, G., Banki, O., Bonal, D., Brown, S., Brown, F.I., Cerón, C.E., Chama Moscoso, V., Chave, J., Comiskey, J.A., Cornejo, F., Corrales Medina, M., Da Costa, L., Costa, F.R.C., Di Fiore, A., Domingues, T.F., Erwin, T.L., Frederickson, T., Higuchi, N., Honorio Coronado, E.N., Killeen, T.J., Laurance, W.F., Levis, C., Magnusson, W.E., Marimon, B.S., Marimon Junior, B.H., Mendoza Polo, I., Mishra, P., Nascimento, M.T., Neill, D., Núñez Vargas, M.P., Palacios, W.A., Parada, A., Pardo Molina, G., Peña-Claros, M., Pitman, N., Peres, C.A., Poorter, L., Prieto, A., Ramirez-Angulo, H., Restrepo Correa, Z., Roopsind, A., Roucoux, K.H., Rudas, A., Salomão, R.P., Schietti, J., Silveira, M., de Souza, P.F., Steininger, M.K., Stropp, J., Terborgh, J., Thomas, R., Toledo, M., Torres-Lezama, A., Van Andel, T.R., van der Heijden, G.M.F., Vieira, I.C.G., Vieira, S., Vilanova-Torre, E., Vos, V.A., Wang, O., Zartman, C.E., Malhi, Y., Phillips, O.L., 2014. Markedly divergent estimates of Amazon forest carbon density from ground plots and satellites. Glob. Ecol. Biogeogr. 23, 935–946. https://doi.org/10.1111/geb.12168

Mitchard, E.T.A., Saatchi, S.S., Baccini, A., Asner, G.P., Goetz, S.J., Harris, N.L., Brown, S., 2013. Uncertainty in the spatial distribution of tropical forest biomass: A comparison of pan-tropical maps. Carbon Balance Manag. 8, 1–13. https://doi.org/10.1186/1750-0680-8-10

Mitchard, E.T.A., Saatchi, S.S., Woodhouse, I.H., Nangendo, G., Ribeiro, N.S., Williams, M., Ryan, C.M., Lewis, S.L., Feldpausch, T.R., Meir, P., 2009. Using satellite radar backscatter to predict above-ground woody biomass: A consistent relationship across four different African landscapes. Geophys. Res. Lett. 36, 1–6. https://doi.org/10.1029/2009GL040692

Mitchell, A.L., Rosenqvist, A., Mora, B., 2017. Current remote sensing approaches to monitoring forest degradation in support of countries measurement, reporting and verification (MRV) systems for REDD+. Carbon Balance Manag. 12. https://doi.org/10.1186/s13021-017-0078-9

Mladenova, I., Lakshmi, V., 2009. Terrain: Slope influence on QuikSCAT backscatter. IEEE Trans. Geosci. Remote Sens. 47, 2722–2732. https://doi.org/10.1109/TGRS.2009.2016652

Mlambo, R., Woodhouse, I.H., Gerard, F., Anderson, K., 2017. Structure from motion (SfM) photogrammetry with drone data: A low cost method for monitoring greenhouse gas emissions from forests in developing countries. Forests 8. https://doi.org/10.3390/f8030068

Moesinger, L., Zotta, R.-M., van der Schalie, R., Scanlon, T., de Jeu, R., Dorigo, W., 2022. Monitoring vegetation condition using microwave remote sensing: the standardized vegetation optical depth index (SVODI). Biogeosciences 19, 5107–5123. https://doi.org/10.5194/bg-19-5107-2022

Mohan, M., Silva, C.A., Klauberg, C., Jat, P., Catts, G., Cardil, A., Hudak, A.T., Dia, M., 2017. Individual tree detection from unmanned aerial vehicle (UAV) derived canopy height model in an open canopy mixed conifer forest. Forests 8. https://doi.org/10.3390/f8090340

Moreno, A., Neumann, M., Hasenauer, H., 2016. Optimal resolution for linking remotely sensed and forest inventory data in Europe. Remote Sens. Environ. 183, 109–119. https://doi.org/10.1016/j.rse.2016.05.021

Morsdorf, F., Nichol, C., Malthus, T., Woodhouse, I.H., 2009. Assessing forest structural and physiological information content of multi-spectral LiDAR waveforms by radiative transfer modelling. Remote Sens. Environ. 113, 2152–2163. https://doi.org/10.1016/j.rse.2009.05.019

Mueller, A., 2012. Development of Integrated Monitoring Systems for REDD + in the Southern African Development Community (SADC) Field Inventory Results: Transboundary Test Area (Malawi-Zambia) (No. 1.0). Deutsche Gesellschaft fuer Internationale Zusammenarbeit (GIZ) GmbH, Bonn and Eschborn, Germany.

Mulvaney, D., Robbins, P., Kte'pi, B., 2011. UN Framework Convention on Climate Change. Green Polit. --Z Guide 1–31. https://doi.org/10.4135/9781412971867.n129

Munthali, K.G., 2013. Modelling Deforestation in Dzalanyama Forest Reserve, Lilongwe, Malawi: Using Multi-agent Simulation Approach. University of Tsukuba, Ibarak, Japan.

Munthali, K.G., Murayama, Y., 2015. Modeling deforestation in Dzalanyama Forest Reserve, Lilongwe, Malawi: a multi-agent simulation approach. GeoJournal 80, 743–757. https://doi.org/10.1007/s10708-014-9592-4

Næsset, E., 2015. Forest monitoring with airborne laser scanning in Tanzania (No. 31). Norwegian University of Life Sciences, Norway.

Naidoo, L., Mathieu, R., Main, R., Wessels, K., Asner, G.P., 2016. L-band Synthetic Aperture Radar imagery performs better than optical datasets at retrieving woody fractional cover in deciduous, dry savannahs. Int. J. Appl. Earth Obs. Geoinformation 52, 54–64. https://doi.org/10.1016/j.jag.2016.05.006

Neeff, T., Kadzuwa, Henry, Mataya, Bennet, B., 2015. A Roadmap for Developing Malawi's National Forest Monitoring System. Department of Forestry- Malawi, Lilongwe, Malawi.

Neuwirthová, E., Lhotáková, Z., Albrechtová, J., 2017. The effect of leaf stacking on leaf reflectance and vegetation indices measured by contact probe during the season. Sens. Switz. 17. https://doi.org/10.3390/s17061202

Ngulube, Mwabumba, L., Chirwa, P., 1999. Community-based management of Miombo Woodlands in Malawi. Proceedings of a National Workshop, Sun and Sand Holiday Resort, Mangochi, Malawi, 27-29 September 1999., in: Community-Based Management of Miombo Woodlands in Malawi. Proceedings of a National Workshop, Sun and Sand Holiday Resort, Mangochi, Malawi, 27-29 September 1999 1999 Pp.Viii + 251 Pp. Ref.Many. Presented at the Community-based management of Miombo Woodlands in Malawi. Proceedings of a National Workshop, Sun and Sand Holiday Resort, Mangochi, Malawi, 27-29 September 1999., Foestry Research Institute of Malawi, Zomba, Malawi., pp. 1–0. https://www.cabdirect.org/cabdirect/FullTextPDF/2010/20103041299.pdf

Nieman, W.A., van Wilgen, B.W., Leslie, A.J., 2021. Correction to: A reconstruction of the recent fire regimes of Majete Wildlife Reserve, Malawi, using remote sensing (Fire Ecology, (2021), 17, 1, (4), 10.1186/s42408-020-00090-0). Fire Ecol. 17. https://doi.org/10.1186/s42408-021-00122-3

Ni-Meister, W., Lee, S., Strahler, A.H., Woodcock, C.E., Schaaf, C., Yao, T., Ranson, K.J., Sun, G., Blair, J.B., 2010. Assessing general relationships between aboveground biomass and vegetation structure parameters for improved carbon estimate from lidar remote sensing. J. Geophys. Res. Biogeosciences 115, n/a-n/a. https://doi.org/10.1029/2009jg000936

Nomura, K., Mitchard, E.T.A., Bowers, S.J., Patenaude, G., 2019. Missed carbon emissions from forests: Comparing countries' estimates submitted to UNFCCC to biophysical estimates. Environ. Res. Lett. 14. https://doi.org/10.1088/1748-9326/aafc6b

Novotný, J., Navrátilová, B., Janoutová, R., Oulehle, F., Homolová, L., 2020. Influence of site-specific conditions on estimation of forest above ground biomass from airborne laser scanning. Forests 11, 1–18. https://doi.org/10.3390/f11030268

Ntchisi District Assembly, 2014. Ntchisi District Socio-Economic Profile 2013-2018. Ntchisi District Assembly, Ntchisi, Malawi.

Ntchisi District Assembly, 2007. Strategic Forest Area Plan-Ntchisi Forest Reserve-June, 2007. Ntchisi District Forestry Office, Ntchisi, Malawi.

Nunes, L., Pasalodos-Tato, M., Alberdi, I., Sequeira, A.C., Vega, J.A., Silva, V., Vieira, P., Rego, F.C., 2022. Bulk Density of Shrub Types and Tree Crowns to Use with Forest Inventories in the Iberian Peninsula. Forests 13. https://doi.org/10.3390/f13040555

Nyasulu, M., Haque, M.M., Boiyo, R., Kumar, K.R., Zhang, Y.L., 2020. Seasonal climatology and relationship between AOD and cloud properties inferred from the MODIS over Malawi, Southeast Africa. Atmospheric Pollut. Res. 11, 1933–1952. https://doi.org/10.1016/j.apr.2020.07.023

Odipo, V.O., Nickless, A., Berger, C., Baade, J., Urbazaev, M., Walther, C., Schmullius, C., 2016. Assessment of aboveground woody biomass dynamics using terrestrial laser scanner and L-band ALOS PALSAR data in South African Savanna. Forests 7. https://doi.org/10.3390/f7120294

Panjvani, K., Dinh, A.V., Wahid, K.A., 2019. LiDARPheno – A low-cost LiDAR-based 3D scanning system for leaf morphological trait extraction. Front. Plant Sci. 10. https://doi.org/10.3389/fpls.2019.00147

Patenaude, G., Milne, R., Dawson, T.P., 2005. Synthesis of remote sensing approaches for forest carbon estimation: reporting to the Kyoto Protocol. Environ. Sci. Policy 8, 161–178. https://doi.org/10.1016/j.envsci.2004.12.010

Pearson, T., Walker, S., Brown, S., 2005. Sourcebook for land use, land-use change and forestry projects. Winrock International, USA.

Peters, C.M., 2005. Sustainable Harvest of Non-Timber Plant Resources in Tropical Moist Forest: An Ecological Primer. https://www.researchgate.net/publication/238066719_Sustainable_Harvest_of_Non-timber_Plant_Resources_in_Tropical_Moist_Forest_An_Ecological_Primer

Petrokofsky, G., Kanamaru, H., Achard, F., Goetz, S.J., Joosten, H., Holmgren, P., Lehtonen, A., Menton, M.C.S., Pullin, A.S., Wattenbach, M., 2012. Comparison of methods for the measurement and assessment of carbon stocks and carbon stock changes in terrestrial carbon pools. Environ. Evid. 1–21.

Pettorelli, N., Vik, J.O., Mysterud, A., Gaillard, J.M., Tucker, C.J., Stenseth, N.C., 2005. Using the satellite-derived NDVI to assess ecological responses to environmental change. Trends Ecol. Evol. 20, 503–510. https://doi.org/10.1016/j.tree.2005.05.011

Phalla, T., Ota, T., Mizoue, N., Kajisa, T., Yoshida, S., Vuthy, M., Heng, S., 2018. The importance of tree height in estimating individual tree biomass while considering errors in measurements and allometric models. Agrivita 40, 131–140. https://doi.org/10.17503/agrivita.v40i1.1730

Phillips, N., Blauvelt, C., Ziba, M., Sherman, J., Saka, E., Bancroft, E., Wilcox, A., 2016. Costs associated with the use of unmanned aerial vehicles for transportation of laboratory samples in Malawi. VillageReach.

https://www.updwg.org/resource/costs-associated-with-the-use-of-unmanned-aerial-vehicles-for-transportation-of-laboratory-samples-in-malawi/

Phiri, M., Nyirenda, H., 2022. Assessment of land use change in the Thuma forest reserve region of Malawi, Africa. Environ. Res. Commun. 4, 015002–015002. https://doi.org/10.1088/2515-7620/ac473c

Piponiot, C., Anderson-Teixeira, K.J., Davies, S.J., Allen, D., Bourg, N.A., Burslem, D.F.R.P., Cárdenas, D., Chang-Yang, C.H., Chuyong, G., Cordell, S., Dattaraja, H.S., Duque, Á., Ediriweera, S., Ewango, C., Ezedin, Z., Filip, J., Giardina, C.P., Howe, R., Hsieh, C.F., Hubbell, S.P., Inman-Narahari, F.M., Itoh, A., Janík, D., Kenfack, D., Král, K., Lutz, J.A., Makana, J.R., McMahon, S.M., McShea, W., Mi, X., Bt. Mohamad, M., Novotný, V., O'Brien, M.J., Ostertag, R., Parker, G., Pérez, R., Ren, H., Reynolds, G., Md Sabri, M.D., Sack, L., Shringi, A., Su, S.H., Sukumar, R., Sun, I.F., Suresh, H.S., Thomas, D.W., Thompson, J., Uriarte, M., Vandermeer, J., Wang, Y., Ware, I.M., Weiblen, G.D., Whitfeld, T.J.S., Wolf, A., Yao, T.L., Yu, M., Yuan, Z., Zimmerman, J.K., Zuleta, D., Muller-Landau, H.C., 2022. Distribution of biomass dynamics in relation to tree size in forests across the world. New Phytol. 234, 1664–1677. https://doi.org/10.1111/nph.17995

Plotnick, R.E., Gardner, R.H., O'Neill, R.V., 1993. Lacunarity indices as measures of landscape texture. Landsc. Ecol. 8, 201–211. https://doi.org/10.1007/BF00125351

Power, M.J., Marlon, J., Ortiz, N., Bartlein, P.J., Harrison, S.P., Mayle, F.E., Ballouche, A., Bradshaw, R.H.W., Carcaillet, C., Cordova, C., Mooney, S., Moreno, P.I., Prentice, I.C., Thonicke, K., Tinner, W., Whitlock, C., Zhang, Y., Zhao, Y., Ali, A.A., Anderson, R.S., Beer, R., Behling, H., Briles, C., Brown, K.J., Brunelle, A., Bush, M., Camill, P., Chu, G.Q., Clark, J., Colombaroli, D., Connor, S., Daniau, A.L., Daniels, M., Dodson, J., Doughty, E., Edwards, M.E., Finsinger, W., Foster, D., Frechette, J., Gaillard, M.J., Gavin, D.G., Gobet, E., Haberle, S., Hallett, D.J., Higuera, P., Hope, G., Horn, S., Inoue, J., Kaltenrieder, P., Kennedy, L., Kong, Z.C., Larsen, C., Long, C.J., Lynch, J., Lynch, E.A., McGlone, M., Meeks, S., Mensing, S., Meyer, G., Minckley, T., Mohr, J., Nelson, D.M., New, J., Newnham, R., Noti, R., Oswald, W., Pierce, J., Richard, P.J.H., Rowe, C., Sanchez Goñi, M.F., Shuman, B.N., Takahara, H., Toney, J., Turney, C., Urrego-Sanchez, D.H., Umbanhowar, C., Vandergoes, M., Vanniere, B., Vescovi, E., Walsh, M., Wang, X., Williams, N., Wilmshurst, J., Zhang, J.H., 2008. Changes in fire regimes since the last glacial maximum: An assessment based on a global synthesis and analysis of charcoal data. Clim. Dyn. 30, 887–907. https://doi.org/10.1007/s00382-007-0334-x

Prosperi, P., Bloise, M., Tubiello, F.N., Conchedda, G., Rossi, S., Boschetti, L., Salvatore, M., Bernoux, M., 2020. New estimates of greenhouse gas emissions from biomass burning and peat fires using MODIS Collection 6 burned areas. Clim. Change 161, 415–432. https://doi.org/10.1007/s10584-020-02654-0

Provost, E.J., Butcher, P.A., Coleman, M.A., Kelaher, B.P., 2020. Assessing the viability of small aerial drones to quantify recreational fishers. Fish. Manag. Ecol. 27, 615–621. https://doi.org/10.1111/fme.12452

Puliti, S., Breidenbach, J., Schumacher, J., Hauglin, M., Klingenberg, T.F., Astrup, R., 2021. Above-ground biomass change estimation using national forest

inventory data with Sentinel-2 and Landsat. Remote Sens. Environ. 265, 112644–112644. https://doi.org/10.1016/j.rse.2021.112644

Puliti, S., Saarela, S., Gobakken, T., Ståhl, G., Næsset, E., 2018. Combining UAV and Sentinel-2 auxiliary data for forest growing stock volume estimation through hierarchical model-based inference. Remote Sens. Environ. 204, 485–497. https://doi.org/10.1016/j.rse.2017.10.007

Pulliainen, J.T., Kurvonen, L., Hallikainen, M.T., 1999. Multitemporal behavior of L- and C-band SAR observations of boreal forests. IEEE Trans. Geosci. Remote Sens. 37, 927–937. https://doi.org/10.1109/36.752211

Qin, Z., Li, W., Li, M., Chen, Z., Zhou, G., 2003. A Methodology for True Orthorectification of Large-Scale Urban Aerial Images and Automatic Detection of Building Occlusions Using Digital Surface Model. Int. Geosci. Remote Sens. Symp. IGARSS 2, 729–731. https://doi.org/10.1109/igarss.2003.1293898

Racine, E.B., Coops, N.C., Bégin, J., Myllymäki, M., 2021. Tree species, crown cover, and age as determinants of the vertical distribution of airborne LiDAR returns. Trees - Struct. Funct. 35, 1845–1861. https://doi.org/10.1007/s00468-021-02155-2

Reitz, O., Graf, A., Schmidt, M., Ketzler, G., Leuchner, M., 2022. Effects of Measurement Height and Low-Pass-Filtering Corrections on Eddy-Covariance Flux Measurements Over a Forest Clearing with Complex Vegetation. Springer Link 184, 277–299. https://doi.org/10.1007/s10546-022-00700-1

Réjou-Méchain, M., Muller-Landau, H.C., Detto, M., Thomas, S.C., Le Toan, T., Saatchi, S.S., Barreto-Silva, J.S., Bourg, N.A., Bunyavejchewin, S., Butt, N., Brockelman, W.Y., Cao, M., Cárdenas, D., Chiang, J.M., Chuyong, G.B., Clay, K., Condit, R., Dattaraja, H.S., Davies, S.J., Duque, A., Esufali, S., Ewango, C., Fernando, R.H.S., Fletcher, C.D., N. Gunatilleke, I.A.U., Hao, Z., Harms, K.E., Hart, T.B., Hérault, B., Howe, R.W., Hubbell, S.P., Johnson, D.J., Kenfack, D., Larson, A.J., Lin, L., Lin, Y., Lutz, J.A., Makana, J.R., Malhi, Y., Marthews, T.R., Mcewan, R.W., Mcmahon, S.M., Mcshea, W.J., Muscarella, R., Nathalang, A., Noor, N.S.M., Nytch, C.J., Oliveira, A.A., Phillips, R.P., Pongpattananurak, N., Punchi-Manage, R., Salim, R., Schurman, J., Sukumar, R., Suresh, H.S., Suwanvecho, U., Thomas, D.W., Thompson, J., Uríarte, M., Valencia, R., Vicentini, A., Wolf, A.T., Yap, S., Yuan, Z., Zartman, C.E., Zimmerman, J.K., Chave, J., 2014. Local spatial structure of forest biomass and its consequences for remote sensing of carbon stocks. Biogeosciences 11, 6827–6840. https://doi.org/10.5194/bg-11-6827-2014

Ribeiro, N., Cumbana, M., Mamugy, F., Chaúque, A., 2012. Remote Sensing of Biomass in the Miombo Woodlands of Southern Africa: Opportunities and Limitations for Research. Remote Sens. Biomass Princ. Appl. 77–98. https://doi.org/10.5772/696

Ribeiro, N.-S., Syampungani, S., Matakala, N.-M., Nangoma, D., Ribeiro-Barros, A.I., 2015. Miombo Woodlands Research Towards the Sustainable Use of Ecosystem Services in Southern Africa. Intech 32, 137–144. https://doi.org/10.5772/59288

Ritchie, H., Roser, M., 2017. CO_2 and Greenhouse Gas Emissions - Our World in Data. OurWorldInData.org 1, 1–12. https://ourworldindata.org/co2-and-greenhouse-gas-emissions

Rodríguez-Veiga, P., Quegan, S., Carreiras, J., Persson, H.J., Fransson, J.E.S., Hoscilo, A., Ziółkowski, D., Stereńczak, K., Lohberger, S., Stängel, M., Berninger, A., Siegert, F., Avitabile, V., Herold, M., Mermoz, S., Bouvet, A., Le Toan, T., Carvalhais, N., Santoro, M., Cartus, O., Rauste, Y., Mathieu, R., Asner, G.P., Thiel, C., Pathe, C., Schmullius, C., Seifert, F.M., Tansey, K., Balzter, H., 2019. Forest biomass retrieval approaches from earth observation in different biomes. Int. J. Appl. Earth Obs. Geoinformation 77, 53–68. https://doi.org/10.1016/j.jag.2018.12.008

Romijn, E., Herold, M., Kooistra, L., Murdiyarso, D., Verchot, L., 2012. Assessing capacities of non-Annex I countries for national forest monitoring in the context of REDD+. Environ. Sci. Policy 19–20, 33–48. https://doi.org/10.1016/j.envsci.2012.01.005

Rosenqvist, A., Perez, A.,. Olfindo.N., 2018. A Layman's Interpretation Guide to L-Band and C-band Synthetic Aperture Radar data. Nihon Naika Gakkai Zasshi 107, Contents8–Contents8. https://doi.org/10.2169/naika.107.contents8

Routa, J., Kellomäki, S., Kilpeläinen, A., Peltola, H., Strandman, H., 2011. Effects of forest management on the carbon dioxide emissions of wood energy in integrated production of timber and energy biomass. GCB Bioenergy 3, 483–497. https://doi.org/10.1111/j.1757-1707.2011.01106.x

Roy, D.P., Kovalskyy, V., Zhang, H.K., Vermote, E.F., Yan, L., Kumar, S.S., Egorov, A., 2016. Characterization of Landsat-7 to Landsat-8 reflective wavelength and normalized difference vegetation index continuity. Remote Sens. Environ. 185, 57–70. https://doi.org/10.1016/J.RSE.2015.12.024

Roy, P.S., 1989. Spectral reflectance characteristics of vegetation and their use in estimating productive potential. Proc. Plant Sci. 99, 59–81. https://doi.org/10.1007/BF03053419

Ryan, C.M., Hill, T., Woollen, E., Ghee, C., Mitchard, E., Cassells, G., Grace, J., Woodhouse, I.H., Williams, M., 2012. Quantifying small-scale deforestation and forest degradation in African woodlands using radar imagery. Glob. Change Biol. 18, 243–257. https://doi.org/10.1111/j.1365-2486.2011.02551.x

Ryan, C.M., Williams, M., 2011. How does fire intensity and frequency affect miombo woodland tree populations and biomass? Ecol. Appl. 21, 48–60. https://doi.org/10.1890/09-1489.1

Ryan, C.M., Williams, M., Grace, J., 2011. Above- and Belowground Carbon Stocks in a Miombo Woodland Landscape of Mozambique. Biotropica 43, 423–432. https://doi.org/10.1111/j.1744-7429.2010.00713.x

Saarela, S., Holm, S., Grafström, A., Schnell, S., Næsset, E., Gregoire, T.G., Nelson, R.F., Ståhl, G., 2016. Hierarchical model-based inference for forest inventory utilizing three sources of information. Ann. For. Sci. 73, 895–910. https://doi.org/10.1007/s13595-016-0590-1

Saatchi, S.S., 1997. Coherent effects in microwave backscattering models for forest canopies. IEEE Trans. Geosci. Remote Sens. 35, 1032–1044. https://doi.org/10.1109/36.602545

Saatchi, S.S., Harris, N.L., Brown, S., Lefsky, M., Mitchard, E.T.A., Salas, W., Zutta, B.R., Buermann, W., Lewis, S.L., Hagen, S., Petrova, S., White, L., Silman, M., Morel, A., 2011. Benchmark map of forest carbon stocks in tropical regions across three continents. PNAS 108, 9899–9904. https://doi.org/10.1073/pnas.1019576108

Sakai, T., Birhane, E., Abebe, B., Gebremeskel, D., 2021. Applicability of Structure-from-Motion Photogrammetry on Forest Measurement in the Northern

Ethiopian Highlands. Sustain. Switz. 13, 1–14. https://doi.org/10.3390/su13095282

Sameen, M.I., Nahhas, F.H., Buraihi, F.H., Pradhan, B., Shariff, A.R.B.M., 2016. A refined classification approach by integrating Landsat Operational Land Imager (OLI) and RADARSAT-2 imagery for land-use and land-cover mapping in a tropical area. Int. J. Remote Sens. 37, 2358–2375. https://doi.org/10.1080/01431161.2016.1176273

Santoro, M., Cartus, O., Fransson, J.E.S., Shvidenko, A., McCallum, I., Hall, R.J., Beaudoin, A., Beer, C., Schmullius, C., 2013. Estimates of Forest Growing Stock Volume for Sweden, Central Siberia, and Québec Using Envisat Advanced Synthetic Aperture Radar Backscatter Data. Remote Sens. 5, 4503–4532. https://doi.org/10.3390/rs5094503

Santoro, M., Kay, H., Lucas, R., Quegan, S., 2021. CCI Biomass product user guide (year 3, version 3.0) (No. Version 3.0). Aberystwyth University and Gamma Remote Sensing AG, England, UK.

Saunders, J., 2014. Draft Data Standards Report (No. v1.0). Ministry of Water Development and Irrigation, Lilongwe, Malawi.

Sedgwick, P., 2014. Standardising outcome measures using z scores. BMJ Online 349, 31–33. https://doi.org/10.1136/bmj.g5878

Shen, X., Cao, L., 2017. Tree-species classification in subtropical forests using airborne hyperspectral and LiDAR data. Remote Sens. 9. https://doi.org/10.3390/rs9111180

Shimada, M., Isoguchi, O., Tadono, T., Isono, K., 2009. PALSAR radiometric and geometric calibration. IEEE Trans. Geosci. Remote Sens. 47, 3915–3932. https://doi.org/10.1109/TGRS.2009.2023909

Shimano, K., 1997. Analysis of the Relationship between DBH and Crown Projection Area Using a New Model. J. For. Res. 2, 237–242. https://doi.org/10.1007/BF02348322

Shoch, D., Eaton, J., Settelmyer, S., 2013. Project developer's guidebook to VCS REDD methodologies (No. Version 2.0, February 2013). Peoria, IL Metropolitan Area, USA.

Silva, C.A., Duncanson, L., Hancock, S., Neuenschwander, A., Thomas, N., Hofton, M., Fatoyinbo, L., Simard, M., Marshak, C.Z., Armston, J., Lutchke, S., Dubayah, R., 2021. Fusing simulated GEDI, ICESat-2 and NISAR data for regional aboveground biomass mapping. Remote Sens. Environ. 253, 1–24. https://doi.org/10.1016/j.rse.2020.112234

Sinha, S., Jeganathan, C., Sharma, L.K., Nathawat, M.S., 2015. A review of radar remote sensing for biomass estimation. Int. J. Environ. Sci. Technol. 12, 1779–1792. https://doi.org/10.1007/s13762-015-0750-0

Skole, D., Samek, J., 2016. Standard Operating Procedures Forest Carbon Inventory, Data Collection and Reporting Volume 1: Establishing the Inventory and Sample Plots. Global Observatory for Ecosystem Services, Department of Forestry, Michigan State University, Michigan State University.

Skole, D.L., Samek, J.H., Mbow, C., Chirwa, M., Ndalowa, D., Tumeo, T., Kachamba, D., Kamoto, J., Chioza, A., Kamangadazi, F., 2021. Direct Measurement of Forest Degradation Rates in Malawi : Toward a National Forest Monitoring System to Support REDD +. Forests 1–30. https://doi.org/10.3390/f12040426

Slik, J.W.F., Paoli, G., Mcguire, K., Amaral, I., Barroso, J., Bastian, M., Blanc, L., Bongers, F., Boundja, P., Clark, C., Collins, M., Dauby, G., Ding, Y., Doucet,

J.L., Eler, E., Ferreira, L., Forshed, O., Fredriksson, G., Gillet, J.F., Harris, D., Leal, M., Laumonier, Y., Malhi, Y., Mansor, A., Martin, E., Miyamoto, K., Araujo-Murakami, A., Nagamasu, H., Nilus, R., Nurtjahya, E., Oliveira, Á., Onrizal, O., Parada-Gutierrez, A., Permana, A., Poorter, L., Poulsen, J., Ramirez-Angulo, H., Reitsma, J., Rovero, F., Rozak, A., Sheil, D., Silva-Espejo, J., Silveira, M., Spironelo, W., ter Steege, H., Stevart, T., Navarro-Aguilar, G.E., Sunderland, T., Suzuki, E., Tang, J., Theilade, I., van der Heijden, G., van Valkenburg, J., Van Do, T., Vilanova, E., Vos, V., Wich, S., Wöll, H., Yoneda, T., Zang, R., Zhang, M.G., Zweifel, N., 2013. Large trees drive forest aboveground biomass variation in moist lowland forests across the tropics. Glob. Ecol. Biogeogr. 22, 1261–1271. https://doi.org/10.1111/geb.12092

Solberg, S., Gizachew, B., Næsset, E., Gobakken, T., Bollandsås, M.O., Mauya, W.E., Olsson, H., Malimbwi, R., Zahabu, E., 2015. Monitoring forest carbon in a Tanzanian woodland using interferometric SAR: A novel methodology for REDD+. Carbon Balance Manag. 10. https://doi.org/10.1186/s13021-015-0023-8

Specht, M., 2021. Determination of navigation system positioning accuracy using the reliability method based on real measurements. Remote Sens. 13. https://doi.org/10.3390/rs13214424

Streefkerk, I.N., van den Homberg, M.J.C., Whitfield, S., Mittal, N., Pope, E., Werner, M., Winsemius, H.C., Comes, T., Ertsen, M.W., 2022. Contextualising seasonal climate forecasts by integrating local knowledge on drought in Malawi. Clim. Serv. 25, 100268–100268. https://doi.org/10.1016/j.cliser.2021.100268

Sumida, A., Miyaura, T., Torii, H., 2013. Relationships of tree height and diameter at breast height revisited: Analyses of stem growth using 20-year data of an even-aged Chamaecyparis obtusa stand. Tree Physiol. 33, 106–118. https://doi.org/10.1093/treephys/tps127

Sun, G., Ranson, K.J., 1998. Radar modelling of forest spatial patterns. Int. J. Remote Sens. 19, 1769–1791. https://doi.org/10.1080/014311698215243

Syampungani, S., Geldenhuys, C.J., Chirwa, P.W., 2016. Regeneration dynamics of miombo woodland in response to different anthropogenic disturbances: forest characterisation for sustainable management. Agrofor. Syst. 90, 563–576. https://doi.org/10.1007/s10457-015-9841-7

Tang, L., Shao, G., 2015. Drone remote sensing for forestry research and practices. J. For. Res. 26, 791–797. https://doi.org/10.1007/s11676-015-0088-y

Tetra Tec and Winrock International, 2022. Modern Cooking for Healthy Forests in Malawi 2021 National Forest Inventory Analysis (No. January 2022). Winrock International, USA.

Tetra Tec and Winrock International, 2021. Modern Cooking for Healthy Forest in Malawi (MCHF) Site-Based Forest Inventory Analysis (February, 2021). Winrock International, USA.

The World Bank, 2022. Forest Carbon Partnership Facility Annual Report 2022, www.forestcarbonpartnership.org. The World Bank, Washington DC, USA.

The World Bank, 2018. Forest Carbon Partnership Facility Annual Report 2018. The World Bank, Washington DC, USA.

Theron, K., Bredenkamp, B.V., 2004. PLANTATION SILVICULTURE | Stand Density and Stocking in Plantations. Encycl. For. Sci. 829–836. https://doi.org/10.1016/b0-12-145160-7/00214-3

Torres, R., Snoeij, P., Geudtner, D., Bibby, D., Davidson, M., Attema, E., Potin, P., Rommen, B.Ö., Floury, N., Brown, M., Traver, I.N., Deghaye, P., Duesmann, B., Rosich, B., Miranda, N., Bruno, C., L'Abbate, M., Croci, R., Pietropaolo, A., Huchler, M., Rostan, F., 2012. GMES Sentinel-1 mission. Remote Sens. Environ. 120, 9–24. https://doi.org/10.1016/j.rse.2011.05.028

Townsend, A., Jiya, I.N., Martinson, C., Bessarabov, D., Gouws, R., 2020. A comprehensive review of energy sources for unmanned aerial vehicles, their shortfalls and opportunities for improvements. Heliyon 6, e05285–e05285. https://doi.org/10.1016/j.heliyon.2020.e05285

UNFCCC, 2021. Report on the technical assessment of the proposed forest reference level of Malawi submitted in 2019 (No. 9780761929277). UNFCCC, Bonn, Germany.

UNFCCC, 2014. Handbook on Measurement, Reporting And Verification For Developing Country Parties. United Nations Climate Change Secretariat, Bonn, Germany.

Urban, M., Berger, C., Mudau, T.E., Heckel, K., Truckenbrodt, J., Odipo, V.O., Smit, I.P.J., Schmullius, C., 2018. Surface moisture and vegetation cover analysis for drought monitoring in the southern Kruger National Park using Sentinel-1, Sentinel-2, and Landsat-8. Remote Sens. 10, 1–16. https://doi.org/10.3390/rs10091482

Urbazaev, M., Thiel, C., Cremer, F., Dubayah, R., Migliavacca, M., Reichstein, M., Schmullius, C., 2018. Estimation of forest aboveground biomass and uncertainties by integration of field measurements, airborne LiDAR, and SAR and optical satellite data in Mexico. Carbon Balance Manag. 13. https://doi.org/10.1186/s13021-018-0093-5

USAID PERFORM, 2017. Perform Site-Based Forest Inventory Report a Technical Report on Liwonde, Ntchisi and Perekezi Forest Reserves (No. February). Department of Forestry-Malawi, Lilongwe, Malawi.

Uyttendaele, M., Eden, A., Szeliski, R., 2001. Eliminating ghosting and exposure artifacts in image mosaics. Proc. IEEE Comput. Soc. Conf. Comput. Vis. Pattern Recognit. 2, II509–II516. https://doi.org/10.1109/CVPR.2001.991005

Vafaei, S., Soosani, J., Adeli, K., Fadaei, H., Naghavi, H., Pham, T.D., Bui, D.T., 2018. Improving accuracy estimation of Forest Aboveground Biomass based on incorporation of ALOS-2 PALSAR-2 and Sentinel-2A imagery and machine learning: A case study of the Hyrcanian forest area (Iran). Remote Sens. 10. https://doi.org/10.3390/rs10020172

Vanclay, J.K., Skovsgaard, J.P., Pilegaard Hansen, C., 1995. Assessing the quality of permanent sample plot databases for growth modelling in forest plantations. For. Ecol. Manag. 71, 177–186. https://doi.org/10.1016/0378-1127(94)06097-3

Vannière, B., Blarquez, O., Rius, D., Doyen, E., Brücher, T., Colombaroli, D., Connor, S., Feurdean, A., Hickler, T., Kaltenrieder, P., Lemmen, C., Leys, B., Massa, C., Olofsson, J., 2016. 7000-year human legacy of elevation-dependent European fire regimes. Quat. Sci. Rev. 132, 206–212. https://doi.org/10.1016/j.quascirev.2015.11.012

Vrieling, A., Meroni, M., Darvishzadeh, R., Skidmore, A.K., Wang, T., Zurita-Milla, R., Oosterbeek, K., O'Connor, B., Paganini, M., 2018. Vegetation phenology from Sentinel-2 and field cameras for a Dutch barrier island. Remote Sens. Environ. 215, 517–529. https://doi.org/10.1016/j.rse.2018.03.014

Wale, H.A., Bekele, T., Dalle, G., 2012. Floristic diversity, regeneration status, and vegetation structure of woodlands in Metema Area, Amhara National Regional State, Northwestern Ethiopia. J. For. Res. 23, 391–398. https://doi.org/10.1007/s11676-012-0275-z

Walker, S.M., Desanker, P.V., 2004. The impact of land use on soil carbon in Miombo Woodlands of Malawi. For. Ecol. Manag. 203, 345–360. https://doi.org/10.1016/j.foreco.2004.08.004

Wang, B., Jia, K., Liang, S., Xie, X., Wei, X., Zhao, X., Yao, Y., Zhang, X., 2018. Assessment of Sentinel-2 MSI spectral band reflectances for estimating fractional vegetation cover. Remote Sens. 10, 1–21. https://doi.org/10.3390/rs10121927

Wang, G., Oyana, T., Zhang, M., Adu-Prah, S., Zeng, S., Lin, H., Se, J., 2009. Mapping and spatial uncertainty analysis of forest vegetation carbon by combining national forest inventory data and satellite images. For. Ecol. Manag. 258, 1275–1283. https://doi.org/10.1016/j.foreco.2009.06.056

Wang, Y., Zhang, X., Guo, Z., 2021. Estimation of tree height and aboveground biomass of coniferous forests in North China using stereo ZY-3, multispectral Sentinel-2, and DEM data. Ecol. Indic. 126, 107645–107645. https://doi.org/10.1016/j.ecolind.2021.107645

Westoby, M.J., Brasington, J., Glasser, N.F., Hambrey, M.J., Reynolds, J.M., 2012. "Structure-from-Motion" photogrammetry: A low-cost, effective tool for geoscience applications. Geomorphology 179, 300–314. https://doi.org/10.1016/j.geomorph.2012.08.021

Wildlife Action Group, 2018. Dedza Salima Forest Reserve and Thuma Forest Reserve Hotspot Tree and Orchid Inventory Final Report -March 2018. Department of Forestry, PERFORM and Wildlife Acton Group, Salima, Malawi.

Wingate, V.R., Phinn, S.R., Kuhn, N., Scarth, P., 2018. Estimating aboveground woody biomass change in Kalahari woodland: Combining field, radar, and optical data sets. Int. J. Remote Sens. 39, 577–606. https://doi.org/10.1080/01431161.2017.1390271

Woodhouse, I.H., 2006. Introduction to Microwave Remote Sensing, II. ed. CRC Press Taylor & Francis Group, New York, US.

Woodhouse, I.H., Hoekman, D.H., 2000. A model-based determination of soil moisture trends in Spain with the ERS-scatterometer. IEEE Trans. Geosci. Remote Sens. 38, 1783–1793. https://doi.org/10.1109/36.851762

Xu, L., Saatchi, S.S., Yang, Y., Yu, Y., Pongratz, J., Anthony Bloom, A., Bowman, K., Worden, J., Liu, J., Yin, Y., Domke, G., McRoberts, R.E., Woodall, C., Nabuurs, G.J., De-Miguel, S., Keller, M., Harris, N., Maxwell, S., Schimel, D., 2021. Changes in global terrestrial live biomass over the 21st century. Sci. Adv. 7. https://doi.org/10.1126/sciadv.abe9829

Zerihun and Tesfaye, A., 2013. Training Manual on: Forest Inventory and Management in the Context of SFM and REDD+. Hawassa University, Ethiopia. https://www.forestcarbonpartnership.org/sites/fcp/files/fcp-docs/2015/October/Forest%20Inventory%20%26%20Management_Manual.pdf

Zhang, H., Hagan, D.F.T., Dalagnol, R., Liu, Y., 2021. Forest canopy changes in the southern amazon during the 2019 fire season based on passive microwave and optical satellite observations. Remote Sens. 13. https://doi.org/10.3390/rs13122238

Zhang, L., Xu, M., Qiu, S., Li, R., Zhao, H., Shang, H., Lai, C., Zhang, W., 2017. Improving the estimate of forest biomass carbon storage by combining two forest inventory systems. Scand. J. For. Res. 32, 297–305. https://doi.org/10.1080/02827581.2016.1226946

Zhang, S., Chen, H., Fu, Y., Niu, H., Yang, Y., Zhang, B., 2019. Fractional vegetation cover estimation of different vegetation types in the Qaidam Basin. Sustain. Switz. 11. https://doi.org/10.3390/su11030864

Zhang, X., Ni-meister, W., 2014. Remote Sensing of Forest Biomass. In: Hanes, J. (eds) Biophysical Applications of Satellite Remote Sensing. Springer Remote Sensing/Photogrammetry. Springer 63–98. https://doi.org/10.1007/978-3-642-25047-7_3

Zheng, H., Du, P., Chen, J., Xia, J., Li, E., Xu, Z., Li, X., Yokoya, N., 2017. Performance evaluation of downscaling sentinel-2 imagery for Land Use and Land Cover classification by spectral-spatial features. Remote Sens. 9. https://doi.org/10.3390/rs9121274

Zheng, X., Gong, P., Strome, M., 1995. Characterizing spatial structure of tree canopy using colour photographs and mathematical morphology. Can. J. Remote Sens. 21, 421–429. https://doi.org/10.1080/07038992.1995.10855165

Zhou, J., Proisy, C., Descombes, X., le Maire, G., Nouvellon, Y., Stape, J.L., Viennois, G., Zerubia, J., Couteron, P., 2013. Mapping local density of young Eucalyptus plantations by individual tree detection in high spatial resolution satellite images. For. Ecol. Manag. 301, 129–141. https://doi.org/10.1016/j.foreco.2012.10.007

Zhu, X., Helmer, E.H., Gwenzi, D., Collin, M., Fleming, S., Tian, J., Marcano-Vega, H., Meléndez-Ackerman, E.J., Zimmerman, J.K., 2021. Characterization of dry-season phenology in tropical forests by reconstructing cloud-free landsat time series. Remote Sens. 13. https://doi.org/10.3390/rs13234736

Zianis, D., Gitas, I., Radoglou, K., Karathanassi, V., Tsakiri-Strati, M., Woodhouse, I., Mallinis, G., 2016. Vegetation biomass estimation with remote sensing: focus on forest and other wooded land over the Mediterranean ecosystem. Int. J. Remote Sens. 38, 1940–1966. https://doi.org/10.1080/01431161.2016.1266113

Zimba, H., Coenders-Gerrits, M., Kawawa, B., Nyambe, I., Savenije, H., Winsemius, H., Zimba, H., Coenders-Gerrits, M., Kawawa, B., Nyambe, I., Savenije, H., Winsemius, H., 2022. Land Surface Temperature and Miombo forest canopy phenophases: what induces leaf fall and leaf flush?, in: EGU General Assembly 2020. p. 10389.

7.0 APPENDICES

APPENDIX I: KEY TREE PARAMETERS MEASURED DURING TERRESTRIAL INVENTORIES

Parameter	Description
Tree species	All species in 2m (clip plot), 6m, 12m, and 20m radius plots
Diameter at Breast Height	Arithmetic mean diameter of plant bole at the height of 1.3 meters above ground, measured in 6m, 12m, and 20m radius plots
Basal Area	Arithmetic sum of all individual trees basal area within a stand measured in 6m, 12m, and 20m radius plots
Mean Height	Arithmetic mean tree height of sample trees within the stand measured in 6m, 12m, and 20m radius plots
Crown/Canopy Cover	Percentage of ground covered by vertical projection of the outermost edges of the foliage of the plants measured in 6m, 12m, and 20m radius plots.
Stocking	Number of trees in an area as opposed to the desired number of trees for best growth measured in all plots
Stand Density	Quantitative measure of stocking on a per unit area basis [e.g. Volume/Area, Tree Numbers/Area, Canopy Cover/Area]

APPENDIX II: BASIC FIELD INVENTORY EQUIPMENT/TOOLS

Tool/Equipment	Primary Use
Aluminium tag/tree marker, tapes/staple-gun tucker	Identifying sampled trees
Botanical–press board	Collection of plant specimen for further identification
Calliper	Measuring tree diameter/dead wood diameter
Chalk/flag tape	Marking sampled trees and sub-plot boundary
Clipboard	Writing surface
Data Sheets	Recording measurements
Diameter measuring tape	*dbh*
GPS-(handheld receivers)	Navigation and plot layout (centre identification, marking waypoints, boundary demarcation)
Hammer	Driving metal rod into the soil on plot centre
Hypsometer	Height
Machete	Cut vegetation to create access, determine wood decay level
Metal rod	Monumenting plot centre
Pocket compass	Navigation, tree bearing
Ranging rod	Aligning and marking positions
Reel measuring tapes	Plot layout, crown diameter and horizontal distance
Scale	Weigh litter and herbaceous material
Slope Correction Table	Slope degree/angle adjustment
Spherical Densiometer	Density/crown/canopy cover

APPENDIX III: INDEX CODE FOR TREE SPECIES SAMPLED IN NTCHISI FOREST

Species	Index Code	Species	Index Code	Species	Index Code
Acacia_polyacantha	1	Combretum_apiculatum	15	Monotes_africanus	29
Acacia_goetzei	2	Combretum_collinum	16	Parinari_curatellifolia	30
Acacia_nigrescens	3	Combretum_zeyheri	17	Pseudolachnostylis_maprouneifolia	31
Anonna_senegalensis	4	Cussonia_arborea	18	Rhus_natalensis	32
Bauhinia_petersiana	5	Dalbergia_nitidula	19	Rothmania_engleriana	33
Brachystegia_longifolia	6	Diplorhynchus_condlylocarpon	20	Senna_spectabilis	34
Brachystegia_boehmii	7	Euclea_crapes	21	Stereospermum_kunthianum	35
Brachystegia_bussei	8	Faurea_rochetiana	22	Strychnos_potatorum	36
Brachystegia_floribunda	9	Friesoldielsia_obovata	23	Uapaca_kirkiana	37
Brachystegia_longifolia	10	Julbernadia_globiflora	24	Uapaca_sansibarica	38
Brachystegia_manga	11	Julbernadia_paniculata	25	Vernonia_amygdalina	39
Brachystegia_utilis	12	Lannea_discolor	26	Ximenia_caffra	40
Bridelia_micrantha	13	Margaritaria_discoidea	27		
Catunaregam_spinosa	14	Markhamia_obtusifolia	28		

APPENDIX IV: EFFECT OF LEAF PHENOLOGY, TOPOGRAPHY AND WIND SPEED ON FOREST CANOPY HEIGHT AND ABOVE GROUND BIOMASS ESTIMATION USING OPTICAL UAV DATA IN MALAWI'S MIOMBO WOODLANDS

Journal of Global Ecology and Environment

16(3): 28-42, 2022
ISSN 2454-2644

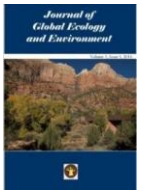

EFFECT OF LEAF PHENOLOGY, TOPOGRAPHY AND WIND SPEED ON FOREST CANOPY HEIGHT AND ABOVE GROUND BIOMASS ESTIMATION USING OPTICAL UAV DATA IN MALAWI'S MIOMBO WOODLANDS

HENRY KADZUWA [a,b*] AND EDWARD MISSANJO [c]

[a] University of Edinburgh, School of Geosciences, Drummond St, Edinburgh, EH8 9XP, UK.
[b] Department of Forestry Headquarters, P.O. Box 30048, Capital City, Lilongwe 3, Malawi.
[c] Department of Research, Malawi Assemblies of God University, P.O. Box 184, Lilongwe, Malawi.

AUTHORS' CONTRIBUTIONS

This work was carried out in collaboration between both authors. Both authors read and approved the final manuscript.

Received: 02 April 2022
Accepted: 09 June 2022
Published: 13 June 2022

Original Research Article

ABSTRACT

The study investigated the effect of tree leaf phenology, topography and wind speed on estimating forest canopy height (FCH) and above ground biomass (AGB) using optical drone data in Miombo Woodlands of Malawi. Data were acquired in 2019 from thirteen plots of Ntchisi Forest Reserve, in two-fold; tree measurements from 0.1ha *in-situ* plots and airborne RGB ortho-images overlaid on the terrestrial plots from 50 ha boxes. The imagery were acquired by DJI Phantom-4 Unmanned Aerial Vehicle (UAV) at ~7cm pixel resolution. These were processed using Structure-*from*-Motion photogrammetry algorithm in Agisoft Metashape Professional software. Malawi's local allometry was used to estimate AGB while the Analysis of Variance was employed to test accuracy. Results reveal that leaf phenology, topography and wind speed significantly (P<0.05) affected estimation of FCH and AGB using the airborne observations. Wind speed contributed highly (53.95% and 55.52%) to the total variation of FCH and AGB, respectively. Furthermore, wind speed upsurge >5m.s^{-1} (-666.90±27.62%; -64.78±8.47%), topography >15% slope (- 114.53±2.92%; -17.07±2.31%) and leaf-off condition (-188.45±25.62%; -27.80±7.98 %) bore higher errors for FCH and AGB, respectively. A significant variation of relationship (R^2=0.71; P<0.05) was observed between ground-based height and UAV canopy height. Nevertheless, the variation of the relationship strongly increased by 10% to R^2=0.81 when two plots highly affected by the wind speed were excluded from the analysis. Similarly, a significant variation of relationship (R^2=0.81; P<0.05) was registered between the ground-based and UAV-based AGB. Correspondingly, a very strong variation of relationship (R^2= 0.95; an increase by 14%) was yielded when the two plots highly affected by wind speed were excluded from the analysis. These findings imply that seasonal leaf-fall, slope and wind speed significantly influence the accuracy of FCH and AGB estimations in Miombo Woodlands. Hence, for accurate results, it is a pre-requisite to consider leaf-phenology, topography and wind speed prior to undertaking ground and airborne inventory

in the Woodlands.

Keywords: Phenology; UAV; Miombo; AGB; point-cloud; REDD+; Structure-*from*-Motion (S*f*M); Canopy Height Model (CHM); 3rd Dimension (3D).

**Corresponding author Email H.H.N.Kadzuwa@sms.ed.ac.uk;*

1. INTRODUCTION

Above ground-biomass (AGB) and forest canopy height (FCH) remain indispensable woody parameters to forest status and change assessments due to their relationship with the carbon cycle and ecosystems services [1-3]. However, accurate estimation of the two is mutually inclusive to the understanding of carbon (C) fluxes within the realms Climate Change mitigation, particularly under the 'Reducing Emissions from Deforestation and forest Degradation' (REDD+) global mechanism. Despite a plethora of REDD+ inventory studies focusing on AGB and FCH estimations for the past decades in Malawi's Miombo Woodlands and other tropical forests, literature, unfortunately reveals miniature efforts have been made to investigate how estimation of these two variables' accuracy is affected by leaf phenology and seasonality, topography and wind speed [2,4,5].

Research on monitoring the Southern Africa Savannas which are dominated by the Miombo Woodlands remains a challenge, partly due to a variety of uncertainties pertaining to; their fragmented vegetation cover, topographic variations, deciduous nature, seasonality and the associated anthropogenic activities such as fire and harvesting, affecting their spatial distribution patterns [6-12]. These attributes render categorical maps of limited value in the Savannas, in contrast to the Boreal forests which are characterised by well-defined patterns of overstory trees and understory vegetation strata expanding over given stands [10,13]. Besides, the Boreal's ever-green status positively corresponds to their wetter conditions [13].

While the seasonal leaf-behaviour dynamics of Miombo is characterised by the distinct exhibition of being deciduous i.e., leaf-fall (foliage shed) during dry season and leaf-on morphological changes during rainy seasons (Fig. 1), the former starkly poses a challenge to their monitoring using remote sensing [8], [11].

A key remote sensing study on Miombo cover observed that the woodland is influenced by seasonal changes (i.e., leaf-on leaf-off) that consequently affect spectral reflectance patterns which vary according to water availability during the short rainy season (November to March) and long dry season (April to October) [8], [11]. These consequently render difficulties interpreting woody cover such as biomass [11]. On the other hand, fire occurrence in these African Savannas has been estimated to account for 22% of biomass burned globally, with a higher frequency registered in Malawi during the hot-dry season [14,15]. In these woodlands, fire is induced by the presence of leaf litter in dry season. This has been singled out as an anthropogenic factor that poses a challenge to mapping of the ecosystem due to its significant contribution to the spatial heterogeneity (e.g., tree density and size) which results to uncertainties in canopy cover and structure estimation [11]. This predicament forms part of the motivation for this study, thus to attempt to establish in detail the effect of the interplay of the leaf-phenology and seasonality with regards to AGB and FCH estimation accuracy in the Miombo Woodlands of Malawi.

Fig. 1. Miombo phenology and seasonality affecting AGB in Ntchisi Forest Reserve 2019: *Left*- transition from leaf-on to leaf-fall towards the end of post rainy season, *Right*- leaf-fall induced by the peak of dry season in October

Due to various topographic forms that Malawi's Miombo Woodlands portray, slope adjustment, especially in the steep terrain (slope > 10°) distances to the subplots are required during ground-based forest inventories [16-18]. In this regard, tables of pre-calculated radii and slope degrees/percent for random plot allocation are provided to ensure accurate representation while saving inventory time [17], [18]. In spite of these efforts, there has not been any deliberate attempt in Malawi's forest studies to statistically correlate the degree of slope aspect with the accuracy it reflects in estimating AGB and FCH, at least to the authors' knowledge, yet the two are the common outputs of an inventory.

Domingo et al. [5], attempted to model the effect of slope on biomass and their findings revealed that steeper slopes, especially of >35% affect biomass predictions, though with a small magnitude. However, the simulation was based on 468ha only of Miombo Woodlands (Muyobe Forest), which statistically might not have been robust enough from which to draw generalised conclusions, compared to 9,720ha, an area for this incumbent Ntchisi Forest study.

Besides, the degree of slope variation in Muyobe Forest is relatively homogenous (contained within 1169–1413m above sea level) in contrast to Ntchisi whose terrain ranges from 600-1702m with 5-74% slope range (Table 1) [5], [17]. Ntchisi Forest is renowned for its cliffs, escarpments, rolling hills and undulating slopes. More striking is the fact that the Muyobe's study model did not attempt to systematically correlate slope percentage with AGB variation, let alone FCH, i.e., how much slope % leads to an underestimate or overestimate of a given amount of AGB and/or canopy height in Miombo Woodlands. Yet, most of the Malawi's Miombo REDD+ sites stretch over hilly and mountainous areas where escarpments, steep slopes are common [19]. Furthermore, the Muyobe study used a fixed- wing UAV which is renowned for relatively better flight endurance and wind resistance. Nonetheless, in order to acquire an in-depth understanding of the wind effect, it was inclining for this study to employ a multi-rotor craft which is associated with relatively different flight endurance, stability and more importantly, wind resistance.

Currently, Malawi relies on terrestrial forest inventories for monitoring AGB and C fluxes though records on forest airborne data acquisition trace back to the colonial era [18], [20]. Arguably, uncollated airborne observations covering forest surveys conducted in Malawi could be stored elsewhere, but, the available literature shows (as of 2012) that the only consistent and retrievable datasets comprising of 1955 analogue aerial photo-films are archived at the Surveys Department [21]. Acquired in greyscale (black and white) by manned drones, the photos (1742 in number) contain 35 rolls of analogue images covering forest reserves across the country. They were processed using stereoscopic geometry to derive height, a third dimension (3D) to the *xy*-Cartesian plane. Height (*ht.*) parameter was factored-in to provide key forest information such as stock density and volume. Even to date, biomass assessments are regarded more accurate if height is included in their estimations or allometric equations [22]. Nevertheless, the stereoscopic technology has currently revolved to the Structure-*from*-Motion (S*f*M) photogrammetry technique whereby sensors aboard a craft i.e. Unmanned Aerial vehicles (UAVs) acquire ortho-photos that are processed to render 3D information through digital modelling.

The S*f*M technique entails algorithmic generation and resolution of a 3D structure from a series of overlapping offset-images (with corresponding feature points) captured from a camera sensor that is formed to a scene (Fig. 2) [23]. The processed outputs include; the Digital Surface Model (DSM), and the Digital Terrain/Elevation Model (DT/EM) out of which a Canopy Height Model (CHM) is retrieved to estimate *ht.* in forests. The S*f*M has been explained in details under image processing sub-section of this paper. Integration of ground-based tree metrics and imagery acquired by S*f*M from UAVs has been recommended for the enhancement of biomass and C estimates accuracy, besides being comparatively cost- effective while covering large expanses simultaneously, thus, under the REDD+ global mechanism [24-27]. Hence, the technique further provides an edge to the Least Developed Countries (LDCs) or non-Annex 1 countries plying REDD+, i.e. Malawi, where finances pose a great constraint, yet they must provide robust estimates to meet the Measuring Reporting and Verification standard [28], [29]

During data acquisition, flight safety, stability and efficiency for UAVs, particularly in hilly and mountainous terrain beyond visual line of sights (BVLOS) are of paramount importance [30,31]. These may be compromised by wind and turbulence, consequently affecting the quality of data acquired by the sensor aboard the imaging craft (*ibid*). Since employment of UAV in conducting forest surveys is relatively novel, though it is increasing sharply in Malawi [5], [26], it was therefore of particular interest for this study to examine the effect of wind speed/turbulence in the mountainous terrain of Miombo Woodland of Ntchisi Forest. This is a

knowledge gap in as far as the Miombo Woodlands of Malawi are concerned, at least to the knowledge of the authors.

Although a number of studies have published on Miombo AGB and ecology of Malawi ([5], [18], [26], [32–35], they do not usually report in detail at forest level, i.e. the values (extent) that leaf-phenology and seasonality, slope and wind speed contribute to the estimation of AGB and FCH accuracy. Worse-still, they have not been succinctly modelled the aforesaid bio-physical factors on the woody cover, even though such data are pivotal to in-depth understanding of the C balances under climate change mitigation in Malawi. It is against this background that this study objectively examined the extent with which the estimation of AGB and FCH accuracy gets affected by: (i) tree leaf phenology (leaf-off and leaf-on conditions) in relation to season of the year; (ii) topography (terrain slope); and (iii) wind speed/turbulence experienced during the UAV flight missions.

2. MATERIALS AND METHODS

2.1 Study Site

The study site was Ntchisi Forest, a Malawi's Miombo Woodland declared as protected area in 1924. It is located in the central district named Ntchisi (Lat.,-13.3205 E and Long., 34.0419 S). Positioned at ~96km to the north-west of Lilongwe, Malawi's capital (Fig. 3) the reserve covers 9,720ha. The forest stretches on undulating mountainous terrain with a peak of 1702m and altitudinal range of 600-1675m above sea level (*asl*) registered from ground plots. Ntchisi Forest has a mix of gentle and extreme slopes that range from 5-74% (Table 1). It is a tourism attraction feature, especially to internationals who love picnic, cycling, hiking and scene viewing.

The site experiences a humid subtropical climate typified by alternating dry-winter and hot-summer seasons, and annual temperature and rainfall ranges of 19-25^{0}C and 1200-400mm, respectively [36]. Soils within the forest are classified by a mixture of poor sand and blackish-loam localised inside the *Brachystegia* and *Montane* dominated portions of the reserve, respectively. The reserve, whose eastern (windward) side is ~25km away from Lake Malawi, is not spared from the effects of the South-easterly winds, locally known as 'Mwera' that blow across the lake. The winds are known for their strong blowing effect that potentially damage vegetation and property, especially, fishing boats on the lake [37], [38]. The forest serves as a pilot study area for the Malawi REDD+ Programme [17], [18]. Nonetheless, forest fires and illegal wood harvesting (in form firewood, poles, charcoal and timber) have since 2007 been reported as some of the threats that may contribute to reduction of the woody component [36], [39], [40].

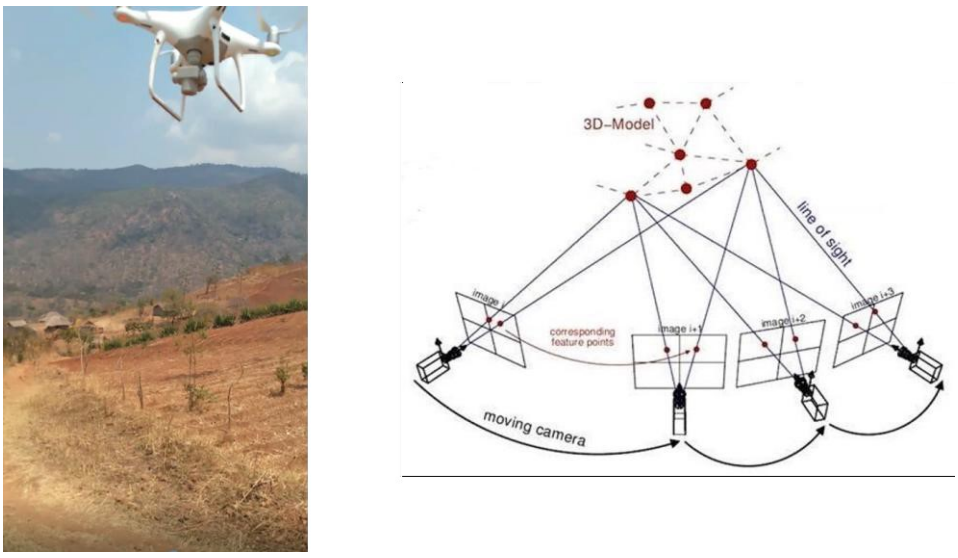

Fig. 2. Left-UAV (DJI-Phantom-4 Pro+ quadcopter) with camera sensor mounted on a gimbal, set at nadir angle of acquisition, vertically taking-off to Msankhire plot (P3) flight mission in Ntchisi Mountain Forest; Right-Structure *from* Motion (S*f*M) Photogrammetry technique

Source: (i) UAV picture- *taken by principal author during the 2019- Ntchisi Forest Inventory*
(ii) S*f*M picture- *Lecture-Introduction to Structure-from-Motion by Edwin Nissen -2021*

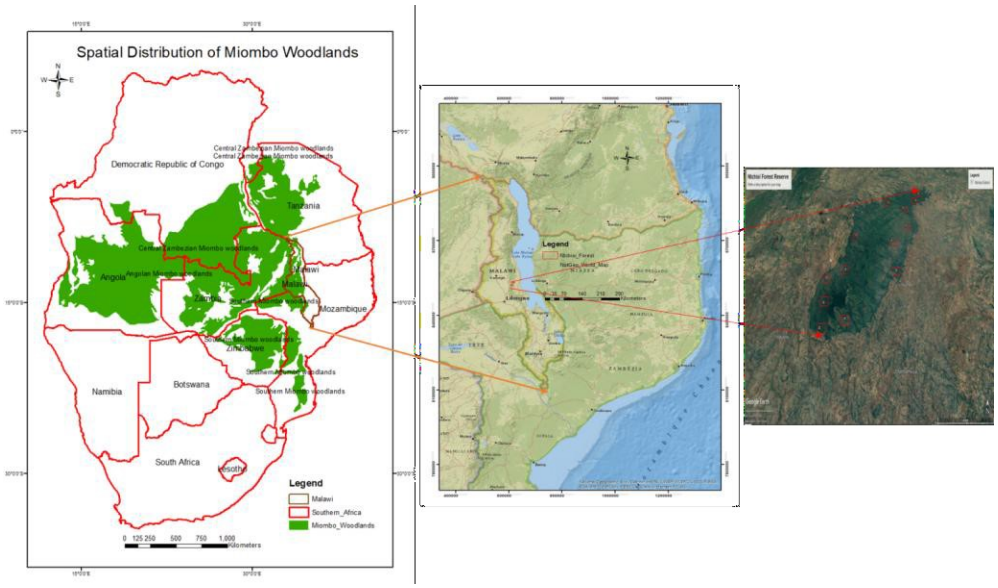

Fig. 3. Miombo Woodland spatial distribution-(Left), Map of Malawi (Middle), and Ntchisi Forest Reserve showing 50ha UAV plot boxes (red squares) and 20m radius plots (white circles)-(Right)

Table 1. Ntchisi Forest Plot location and elevation attributes

UAV plot	Ground Plot	UTM Easting	UTM Northing	Elevation (m)	Slope %	Slope Condition
1	Mndinda	0618875	8533606	681	12	Steep
2	Kajaliza	0618355	8532624	669	10	Steep
3	Msankhire	0614781	8532317	832	19	Very Steep
4	Mkomba	0616651	8531612	713	11	Steep
5	Chenche	0615166	8529363	716	10	Steep
6	Mandwe	0610894	8528310	1079	18	Steep
7	Chanika	0614888	8527699	847	36	Extremely steep
8	Chifwelekete	0609963	8524839	1206	74	Dangerously steep
9	Kasakula	0616733	8524713	764	5	Relatively flat
10	Mnguluwe	0608108	8524124	1212	37	Extremely steep
11	Sambakunsi	0608106	8522106	1498	32	Extremely steep
12	Mpamila	0610161	8520969	1344	48	Extremely steep
13	Nyanga	0607984	8520324	1332	12	Steep

2.2 Data Collection

Data for the study were two-fold, namely: (i) ground-based measurements of individual tree parameters, and (ii) digital airborne imagery data acquired by UAV in the visible (optical) window of the Red, Green and Blue (RGB) spectral bands of the Electromagnetic Spectrum (EMS).

2.2.1 Ground reference data

2.2.1.1 Sampling design and collection of ground-based measurements

Ground-based measurements were conducted from 17-21September 2019. Key variables and parameters measured include;

(i) individual tree diameter at breast height (*dbh*),
(ii) total tree height (*ht*)
(iii) crown diameter (*max.* and *min.*)
(iv) tree botanical names,
(v) trees *xy* coordinates,
(vi) plot centre *xy* coordinates (centroids),
(vii) bearing (in degrees) of each tree from the centre and,
(viii) horizontal distance of each tree from the centre.

Sampling design inherited permanent sample plots (PSPs) that were established following a multi-stage sampling approach which integrated stratified and random sampling techniques during the 2016 Malawi REDD+ site-based inventory. The stratified sampling

phase incorporated forest management units that were demarcated to cover forest management blocks that each of the 13 surrounding villages holds as management stake, thus, under co-management arrangement with the Department of Forestry [17], [40]. This was followed by a systematic random sampling phase whereby sampling unit plots were computed at a minimum spacing of 90meter square grids (network) encompassing the reserve. The network generated a minimum of 13 randomly sampled points that became plot centroids of 20metre radius circles (0.1ha) (Fig.4), sufficient to attain a Confidence Interval (CI) of 95%, with a precision error of 10% [17], [41].

At each sample plot, a four fixed concentric circular plot design bearing 2m, 6m, 12m and 20m radius each, respectively, was inventoried (Fig.4). For each tree measured, its code was documented using a species list catalogue provided by the Forestry Research Institute of Malawi (FRIM). The species were later deciphered to their full botanic names prior to transferring the records into Microsoft Excel data sheets for statistical computing and graphics. These were later uploaded into GenStat 18.1(Windows) for further modelling and analysis.

2.3 UAV Imagery Acquisition

Digital airborne RGB imagery were acquired using UAV in 4 days, thus from 23rd to 25th September and on 6th October, 2019. The survey flight missions were operated on DJI Phantom 4 Pro+ RTK (Real-time Kinematic) quadcopter platform carrying a 1" CMOS SENSOR (2.52µm-1) with a 20 Megapixel resolution (Fig.1).The UAV, a 2016 release, was manufactured by the Shenzhen DJI Sciences and Technologies Ltd, in Shenzhen City of Guangdong Province in China. The flights were programmed on a tablet using Map Inner (v3) software.

The sensor has 5472x3078 pixels fitted to a 3-axis stabilized gimbal to maintain nadir angled imagery (Fig. 1). It has an autofocus feature that enabled it to capture still JPEG scenes at 3-7cm pixel sensor resolution (Ground Sampling Distance). The sensor is embedded with a mechanical shutter which control light intensity besides removing the detrimental 'jello' effect, an attribute that ensures generation of professional images with absolutely low noise. In contrast to the fixed wing, the multirotor craft was preferred for easy vertical take-off/landing (VTOL) in the rough mountainous terrain of Ntchisi Forest (Fig. 1).

Imagery acquisition involved 13 flight missions of ~50ha square boxes (0.71km x0.71km) following the 13 randomly distributed terrestrial plots. The sampling inherited the multi-stage sampling approach (stratified and random techniques) employed during the ground reference collection data as explained in 2.2.1. This ensured that the UAV square boxes overlaid the terrestrial plot centroids in order to enhance geo-spatial referencing (Fig.3-Right), thus following [42]. Hence, at each ground plot centroid, ground control points (GCPs) were placed and their respective waypoints marked using handheld GPS sets (Garmin GPSMap 64x). The imagery were acquired in WGS84 (EPSG:4326) projection, at a flying altitudinal range of 120-150m above-ground- level (AGL). Detailed key flight settings have been depicted in (Table 3).

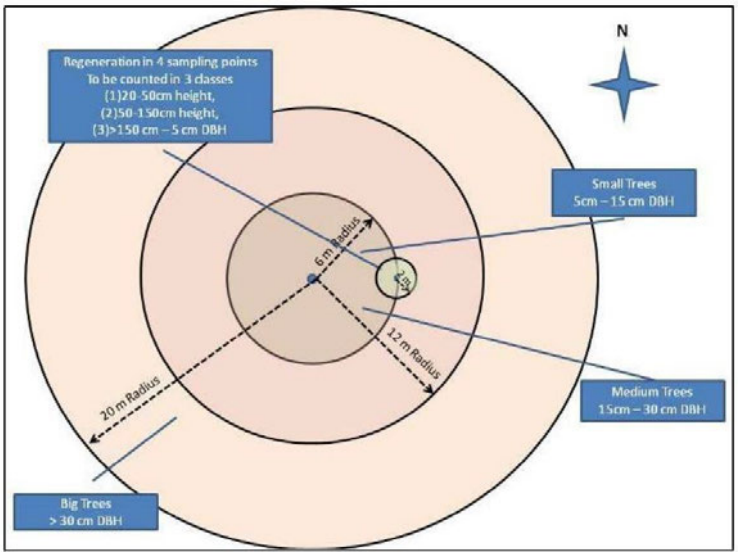

Fig. 4. Concentric ground plot design

Table 2. Plot dimensions and threshold for ground-based measurements

	DIMENSION		
Subplot	**Radius (m)**	**Area (ha)**	***dbh* Threshold (cm)**
Regeneration	2	0.001	<5
Small	6	0.011	5-14.9
Medium	12	0.045	15-29.9
Large	20	0.126	≥30

However, due to high costs that shot beyond the budget ceiling for this study, hiring of a Differential GPS/GNSS that would have been used to set a base station for enhancing global/absolute accuracy, was not possible. While this typifies the funding constraints of the non-Annex-I REDD+ countries under which the study site falls, the positional error (incurred by not setting of the reference point) was offset by the consistent setting of the GCPs as reference points. As aforementioned, this was achieved by deliberately overlaying the GCPs on the ground plot centroids *xy* coordinates (validated during both the 2016 and this incumbent study's) which were used as marks during the S*f*M as well as in delineating the 20m buffer for the circular plots (Fig. 6).

2.4 Plot-based AGB Computations

Using a threshold of *dbh* ≥5cm, 216 individual trees (observations) were measured from the entire 13 PSPs, i.e. *n=216* and used for AGB calculations. Prior to the calculations, a scaling factor (*SF*) was applied to scale up dimension (area) values for each subplot and convey estimates of C stock on a hectare basis. The step involved conversion of the subplot area unit measurements in squared meters (m^2) to a per hectare basis (1ha) as follows;

SF= 10,000/NA,

Where;

SF = Scaling Factor to convert per hectare basis (dimensionless)

10,000 = number of squared meters (m^2) in one hectare

NA= horizontal projected area of nested plot (in m^2)

Computation of AGB employed an allometry that was specifically developed for Malawi's Miombo trees, published by (Kachamba et al., 2016) as indicated in equation (1);

Where;

AGB = above-ground biomass in kilograms of dry matter (kg.d m.)

dbh = diameter at breast height in centimetres (cm) (vertical height of 1.3m)

ht = total tree height in metres (m)

A carbon fraction of 0.47 for all the individual Miombo tree species was used to calculate C from kilograms of dry matter (kg.d.m.), otherwise referred to as biomass (USAID PERFORM, 2017).

2.5 Airborne Data-Image processing

UAV imagery were processed using the generic S*f*M photogrammetry technique in Agisoft Metashape Professional 1.4 (Table 4) as follows. The first step involves alignment of photos whereby the software algorithmically searches for common points on photographs and matches them. This is followed by finding positions of the camera for each picture (Fig.1) and refining camera calibration parameters. Building of point-cloud comes second and it entails generation of data points that have matched. For this particular study, the point-clouds were classified into ground and vegetation feature classes. This was due to the fact that the prime interest was to separate the height of the tree vegetation (canopy height) from the ground level layer. The subsequent phase ensured exportation of the point-clouds to yield bare earth ground level input referred to as Digital Terrain Model (DTM) which is a product of Digital Elevation Model (DEM). Using the exported material, a surface mesh called Digital Surface Model (DSM), is generated in a process otherwise termed as mesh building. The fourth stage involves generation of orthomosaics which basically cascades the merging of geometrically rectified (aligned) photos into a large composition structure representing a 3D scene. The orthomosaics for each plot box were projected to WGS84 (EPSG::4326) global reference system. Relative absolute height values of the resulting dense point-clouds were normalised using the DTM obtained from the ortho-photos. Optical RGB spectral band information was used to generate 3D outputs in JPEG format. As a final step, the 3D outputs (orthomosaics, DSM, DTM and CHM) were converted into Tiff format for further analysis and interpretation (Fig. 5). The key steps and parameters set during the S*f*M photogrammetry image processing technique are depicted in Table 4.

Table 3. Key flight mission settings

UAV Make	Sensor Type	GSD	Flights Day^{-1}	Images plot^{-1} (mean)	Flight Endurance (min)	Flight Altitude AGL (m)	Wind Speed Resistance (m.s^{-1})	On-board GPS Accuracy (m)	Front and End Overlaps
DJI-Phantom-4 Pro+ Quadcopter	1" 20-Megapixel CMOS	3-7cm	2-3	338	20	120-150	20 Knots	5-6	83% (front) 84% (end)
	With mechanical Shutter	Terrain dependent	Access & weather dependent		Weather dependent	Terrain dependent	Max.	RTK	Terrain dependent

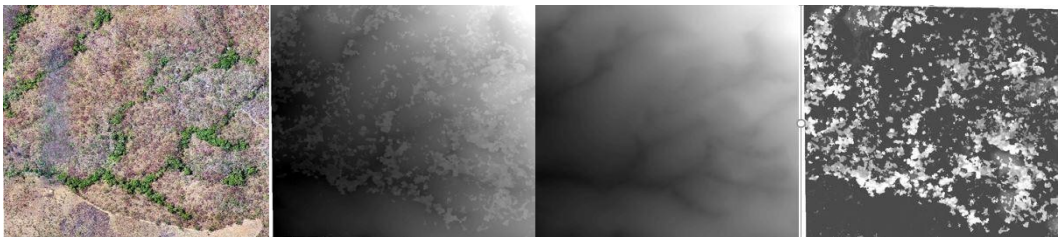

Fig. 5. Outputs of S*f*M Photommetry-P13 (L-R); RGB Orthomosaics, DSM, DTM and CHM (in greyscale) from 50ha UAV plots acquired with 3-7cm pixel resolution

Table 4. SfM Photogrammetry main steps and parameter settings

Task	Parameter
Align Photos	Accuracy: High Projection Type: Geographic WGS84 (EPSG::4326) Pair selection: Generic Preselection Reference preselection: Source Key Points Limit: 40,000 Tie points:4,000
Build Dense	Quality: High Depth Filtering: Moderate
Build Mesh	Source Detail: Dense cloud Surface Type: Arbitrary (3D) Quality face count: High Interpolation: Enabled Select Point Classes:
Build DEM	Source data: Dense cloud Interpolation: Enabled Surface Type: Arbitrary (3D) Quality face count: High Select Point classes: Ground
Build Orthomosaic	Surface: DEM Blending Mode: Mosaic Hole filling: Enabled

2.6 Canopy Height Model (CHM) Generation and Value Extraction

Application of an algorithm for each plot's 3D point-cloud data was set to conduct a geographic analysis in order to filter DTM from corresponding DSM mesh in ArcMap (10.8.1) software. Using the Map-Algebra function under Spatial Analysis Tool, each DTM was mathematically subtracted from a DSM using an Algebraic Boolean expression in the Raster Calculator. This yielded a preliminary CHM with values of vegetation mix growing on the ground i.e. grass, shrubs, herbs and trees, referred to as 'difference map' in this study. Since the minimum height of all the trees measured during ground- measurement was 2m, this was set as a threshold condition (i.e. >=2) in the Raster Calculator for filtering the preliminary CHM from lower vegetation.

Extraction of values from the CHM of 50ha UAV plot boxes to 20m radius plot size involved several steps as follows. The initial task was visual inspection of correct *xy* geo-locations (coinciding) of the point clouds in CHM and tree locations in the ground-based plots and in the RGB orthomosaics. This was done by overlaying all the three layers while using the GCPs as reference points for geo-rectification. A relative accuracy of ±3m was observed throughout. A buffer of 20m radius was created using the GCP/ground plot centroid waypoints and each plot's layer values were extracted using the 'Extract by Mask' function under the Spatial Analyst Tools in ArcMap. The values extracted from the CHM were later used for predicting forest biomass and C stocks for the reserve (Fig.6).

2.7 Statistical Data Analysis

Data on deviation percentage between ground-based field height and UAV canopy height as well as deviation percentage between ground-based field AGB and UAV estimated AGB were tested for

normality and homogeneity using Kolmogorov-Smirnov D and normal probability plot tests. In a few marginal cases, graphic residual analysis was also performed; however, no data transformation was deemed necessary. The data sets were then subjected to analysis of variance (ANOVA). Variance components for the sources of variation were also estimated. Statistical analysis was performed using GenStat 18.1 for Windows. Differences between treatment means were separated using Fischer's least significant difference (LSD) at the 0.05 level. Graphs were plotted using Microsoft Excel 16. Spearman's rank coefficient of determination (R^2) was computed to determine the variation explained by the relationship between ground-based height and UAV canopy height as well as between ground-based AGB and UAV estimated AGB.

The data sets were analysed using equation (2):

where: is the response variable (deviation percentage) of $ijkl^{th}$ observation; is the overall mean; is the fixed effect of slope %; is the fixed effect of wind speed; is the fixed effect of leaf phenology; is the effect of the interaction between slope and wind speed; is the effect of the interaction between slope and leaf phenology;

is the effect of the interaction between wind speed and leaf phenology; is the effect of the interaction among slope, wind speed and leaf phenology; and is the random error term.

All the interactions between parameters, except the interaction between slope and leaf phenology, were removed from the analysis because their contribution to the total variance was negligible. Furthermore, the variance component for these terms could not be estimated and/or was otherwise insignificant. Equation (2) was therefore reduced to equation (3):

Slope % was categorised into three classes: ≤10%; 11-15%; and finally, >15%. On the other hand, wind speed was categorised into two classes: <5 $m.s^{-1}$, and ≥5 $m.s^{-1}$ while, leaf phenology was categorised into two: leaf-on, and leaf-off conditions.

3. RESULTS AND DISCUSSION

3.1 Effect of Leaf Phenology, Topography and Wind speed on FCH Estimation Using UAV Data

Summary of the results on the effect of leaf phenology, topography and wind speed on forest canopy height estimation using Optical UAV data are presented in Tables 5 and 6 as well as in Fig. 7. The results indicate that leaf phenology, topography and wind speed significantly (P<0.05) affected forest canopy height (CHM) estimation using Optical UAV data. However, wind speed contributed the highest (53.95%) to the total variation.

Wind speed of ≥5 $m.s^{-1}$ had the highest (- 666.90±27.62) deviation percentage, while the leaf- off condition had a deviation percentage of - 188.45±25.62%. On the other hand, an increase in slope % resulted into a corresponding increase in deviation %. Hence slope of >15% had the highest (- 114.53±2.92%) deviation percentage compared to the slope of 11-15% (- 5.13±0.38%) and ≤10% (- 2.83±0.36%).

Fig. 6: Greyscale CHM Point Clouds for P9 (left) and P11 (right) 20m radius plots at ≥2m threshold. White colour denotes canopy cover while black denotes low or no canopy cover

Results on individual plots indicate that P11 (Sambakunsi) and P3 (Msankhire) had higher deviation of -1680.00% and -243.18%, respectively. The uncertainty on P3 canopy height estimation was attributed to the sharp rise of wind speed (south- easterly wind) that was registered during the flight mission covering the plot. Precisely, the back and head wind speed of the UAV sharply peaked from an average maximum of 10.4 $m.s^{-1}$ to 13.1 $m.s^{-1}$, rendering some degree of mobility to the tree crowns forming the canopy of the height. This resulted to a shift in the *xy* positions and maximum and lower limits of the crown as detected by RGB camera sensor aboard the UAV. The repercussions were that the shift affected the combinations of pixel values of features in the overlap images which would have become tie-points during S*f*M photogrammetric process as noted by [23], [43], [44]. As a result, the error was transferred to the CHM point-clouds and reflected in the CHM extracted values and contributed to higher deviations.

Furthermore, the higher deviation on P11 was attributed to the effect of the terrain which is extremely steep (32% slope, Table 1) and affected the determination of the ground level (DEM) during the S*f*M photogrammetric process. Fayad et al. [45], observed that the accuracy of a DEM in a forest is dependent on the topographic slope. In their study, they observed that for dominant height, an RMSE increase of 14% was observed from data acquired over slopes higher than 20%, in comparison to slopes between 10 and 20%. Hence, this is equally true for P11 which sits an extremely steep slope, a topographic condition that led to the higher deviation on the measured forest canopy height variable. The same applies to P3 which is characterised by a steep slope of 19%.

Further analysis portrayed a significant variation of relationship (R^2=0.71; P<0.05) between UAV canopy height and ground-based field height when all the 13 plots were included in the analysis (Fig. 7a). Exclusion of P11 and P3 which had higher deviation percentage, resulted in an increase in the relationship, thus, by 10% translating to R^2 =0.81 (Fig. 7b).

3.2 Effect of Leaf Phenology, Topography and Wind speed on AGB Estimation Using UAV Data

The AGB for ground-based and UVA data on average were 93.91±12.60 t/ha and 81.08±14.28 t/ha, respectively and the mean deviation was - 18.87±8.33% (Table 7). Slope, leaf phenology, and wind speed significantly (P<0.05) affected the estimation of AGB using Optical UAV data. Wind speed contributed the highest variation (55.52%) to the total variation, followed by slope % (29.72%) (Table 8).

Wind speed of ≥5 $m.s^{-1}$ had the highest deviation percentage (-64.78±8.47%), while leaf-off had a deviation percentage of -27.80±7.98 %. On the other hand, an increase in slope % resulted to an increased deviation %. Therefore, the slope of >15% yielded the highest deviation percentage (-17.07±2.31%) compared to the slope of 11-15% (-3.13±1.86%) and ≤10% (-0.83±0.42%).

The present findings support previous research highlights documented on Miombo Woodlands. Domingo et al. [5], observed that effect of wind speed and slope on biomass, especially for wind speed (≥5 $m.s^{-1}$) and steeper slopes (>35%) affects biomass predictions. These results imply that wind speed of ≥5 $m.s^{-1}$is not reliable for UAV estimation of AGB.

Table 5. Influence of leaf phenology, topography and wind speed on FCH Estimation using UAV data

Category	Ground-Based Height (m)	UVA Canopy Height (m)	Deviation (%)
Slope (%)			
≤10	18.46±3.11	17.62±2.79	-2.83±0.36^{b}
11 – 15	16.77±3.10	16.67±2.78	-5.13±0.38^{b}
>15	16.06±2.31	13.43±2.07	-114.53±2.92^{a}
Wind speed (m/s)			
<5	17.29±1.70	16.34±1.53	-6.90±0.56^{b}
≥5	11.97±3.09	3.87±2.78	-666.90±27.62^{a}
Leaf Phenology			
Leaf-on	17.02±1.90	16.71±1.71	-2.83±0.67^{b}
Leaf-off	16.58±2.92	12.15±2.62	-188.45±25.62^{a}
Mean	**16.05±1.33**	**13.57±1.89**	**-158.46±28.18**

Mean values are followed by standard errors; Deviation (%) means with different superscript within a column in the same category significantly differ (P<0.05)

Table 6. Variance components for deviation (%) between ground-field height and UAV canopy height

Source of Variation	*df*	Deviation	
		P-value	Var %
Slope (S)	2	0.011	22.93
Wind speed (W)	1	0.002	53.95
Leaf phenology (L)	1	0.023	14.41
S x L	1	0.898	0.03
R/S/W/L	7		8.68

Note: df is degrees of freedom, Var % is variance percentage.

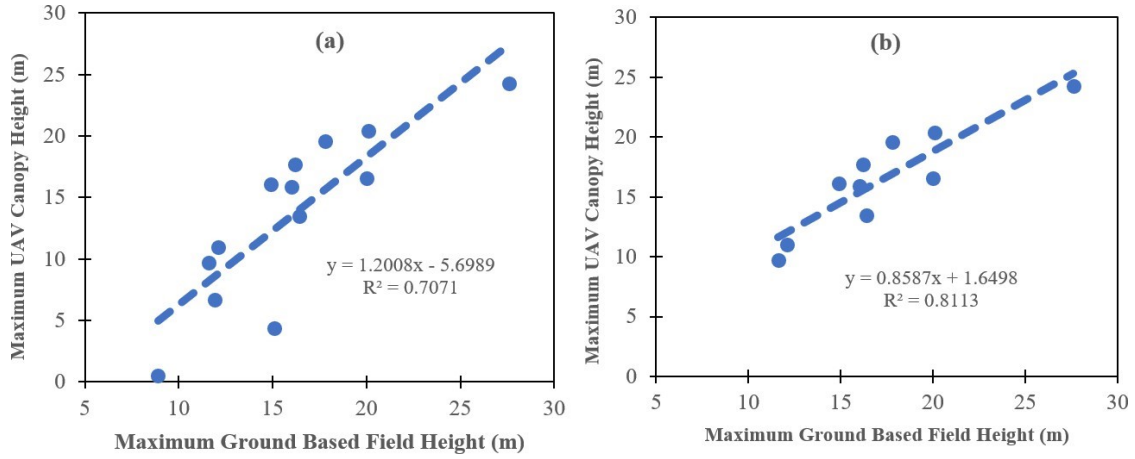

Fig. 7. Scatter plots of UAV canopy height vs ground-based canopy height for (a) inclusion of all 13 plots, and (b) exclusion of P11 and P3 which had higher deviation percentage

Table 7. Influence of leaf Phenology, topography and wind speed on AGB estimation using UAV data

Category	Ground-Based Field AGB (t/ha)	UVA AGB (t/ha)	Deviation (%)
Slope (%)			
≤10	89.20±3.15	88.44±6.79	-0.83±0.42^{b}
11 – 15	118.70±3.19	116.08±6.80	-3.13±1.86^{b}
>15	94.30±2.36	80.46±9.87	-17.07±2.31^{a}
Wind speed (m/s)			
<5	102.12±6.48	97.72±4.65	-4.55±2.65^{b}
≥5	65.66±9.97	22.11±6.63	-64.78±8.47^{a}
Leaf Phenology			
Leaf-on	102.69±1.90	101.34±6.36	-1.57±0.89^{b}
Leaf-off	91.23±8.28	68.63±5.13	-27.80±7.98^{a}
Mean	**93.91±12.60**	**81.08±14.28**	**-18.87±8.33**

Mean values are followed by standard errors; Deviation (%) means with different superscript within a column in the same category significantly differ (P<0.05)

Table 8. Variance components for deviation (%) between ground-field AGB and UAV AGB

Source of Variation	*df*	Deviation	
		P-value	Var %
Slope (S)	2	0.018	29.72
Wind speed (W)	1	0.001	55.52
Leaf phenology (L)	1	0.043	5.40
S x L	1	0.858	0.07
R/S/W/L	7		9.29

Note: df is degree of freedom, var % is variance percentage

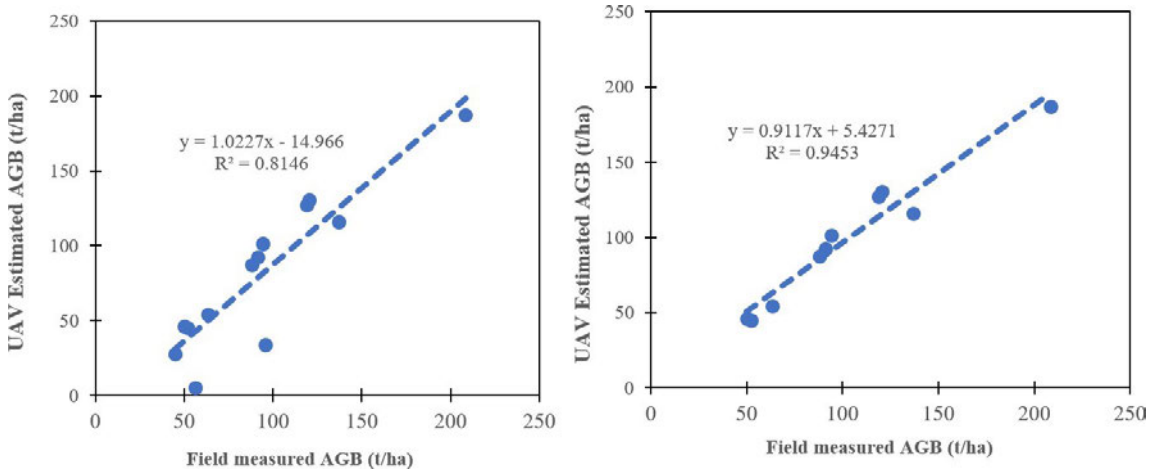

Fig. 8. Scatter plots of UAV AGB vs ground-based AGB for (a) inclusion of all 13 plots, and (b) exclusion of P11 and P3 which had higher deviation percentage

Further analysis conducted by this study indicates a significant variation of relationship (R^2=0.81; P<0.05) between UAV based AGB and ground-based AGB when all the 13 plots were included in the analysis (Fig. 8a). Omission of P11 and P3s which had higher deviations percentage, and resulted in the increase of the variation of the relationship, thus by 14% to R^2=0.95 (Fig. 8b). This suggests that careful analysis of the topographic attributes, wind speed, and tree leaf phenology has to be considered prior to undertaking terrestrial and airborne surveys in Miombo Woodlands thus for accurate results.

4. CONCLUSION

The study examined the effect of tree leaf phenology, topography and wind speed on estimating forest canopy height (FCH) and above-ground biomass (AGB) using optical drone data in Miombo Woodlands of Malawi. The results revealed that leaf phenology, topography, as well as wind speed significantly affected estimation of two variables. Wind speed contributed the highest to the total variation followed by topography. Precisely, wind speed of ≥5 $m.s^{-1}$, topography of greater than 15% slope, and leaf-off condition yielded higher errors. A significant variation of relationship (R^2=0.71) was observed between the ground-based height and UAV canopy height model. However, the variation of the relationship increased by 10% when two plots affected by wind speed were excluded from the analysis. Similarly, there was a significant variation of relationship (R^2=0.81) between ground-based and airborne based AGB. Likewise, the variation of the relationship increased by 14% when two plots affected by wind speed were excluded from the analysis. Therefore, for accurate results, this study recommends a careful analysis of the biophysical factors, particularly, tree leaf phenology, topography and wind speed, *inter alia,* prior to undertaking terrestrial and airborne surveys in Miombo Woodlands. It further encourages research on how other environmental factors such as fire and cloud cover affect accuracy of the woody components estimation in the Miombo Woodlands.

ACKNOWLEDGEMENTS

The authors are grateful Prof., Ian Woodhouse and Dr. Steven Hancock for their priceless guidance and encouragement. Thanks be to Mike Chirwa for his key role during ground data collection. A special mention goes to Owen Cardew, Managing Director for Precision (Malawi) where we hired the UAV. Last but not least, the authors salute Joseph Trindade, a Dedza-origin pilot for his unparalleled flying skills, particularly beyond visual line of sight (BVLOS) in the mountainous terrain of Ntchisi Forest.

COMPETING INTERESTS

Authors have declared that no competing interests exist.

REFERENCES

1. Burt A, et al. Assessment of Bias in Pan-Tropical Biomass Predictions. 2020;3. DOI: 103389/ffgc.2020.00012.
2. Naidoo L, Mathieu R, Main R, Wessels K, Asner GP. L-band Synthetic Aperture Radar imagery performs better than optical datasets at retrieving woody fractional cover in deciduous, dry savannahs," International Journal of

Applied Earth Observation and Geoinformation. 2016;52:54–64.
DOI: 101016/j.jag.2016.05.006.
3. Foody GM, Lucas RM, Curran PJ, Honzak M. Mapping Tropical Forest Fractional Cover from Coarse Spatial Resolution Remote Sensing Imagery Author (s): Giles M. Foody, Richard M. Lucas, Paul J. Curran and Miroslav Honzak Published by: Springer tropical sensing imagery fractional from resolute. 2014;131(2):143–154.
4. Cassells GF, Woodhouse IH, Mitchard ETA, Tembo MD. The use of alos palsar for supporting sustainable forest use in southern africa: A case study in Malawi, International Geoscience and Remote Sensing Symposium (IGARSS). 2009;2:206–209.
DOI: 101109/IGARSS.2009.5418042.
5. Domingo D, Ørka HO, Næsset E, Kachamba D, Gobakken T. Effects of UAV image resolution, camera type, and image overlap on accuracy of biomass predictions in a tropicalwoodland, Remote Sensing. 2019;11:8. DOI: 103390/rs11080935.
6. Campbell B. The Ecology of Miombo Woodlands; 1996. [Online]. Available:http://books.google.com/books?hl=nl&lr=&id=rpildJJVdU4C&pgis=1
7. Chidumayo E. Dry season watering alters the significance of climate factors influencing phenology and growth of saplings of savanna woody species in central Zambia, southern Africa, Austral Ecology. 2015;40(7):794–805. DOI: 101111/aec.12254.
8. Chidumayo EM. Miombo Ecology and Management : An Introduction. 1997;166(3): 276–277.
9. Chidumayo EN. Climate and Phenology of Savanna Vegetation in Southern Africa, Journal of Vegetation Science. 2001;12(3):347. DOI: 102307/3236848.
10. Higginbottom TP, Symeonakis E, Meyer H. van der Linden S. Mapping fractional woody cover in semi-arid savannahs using multi-seasonal composites from Landsat data, ISPRS Journal of Photogrammetry and Remote Sensing. 2018;139:88–102.
DOI: 101016/j.isprsjprs.2018.02.010.
11. Kamusoko C, Gamba J, Murakami H. Mapping woodland cover in the Miombo ecosystem: A comparison of machine learning classifiers, Land (Basel). 2014;3(2): 524–540. DOI: 103390/land3020524.
12. Frost P. The Ecology of Miombo Woodlands, The Miombo in Transition: Woodlands and Welfare in Africa. 1996;266, [Online]. Available:http://books.google.com/books?hl=nl&lr=&id=rpildJJVdU4C&pgis=1
13. Majasalmi T, Rautiainen M. The impact of tree canopy structure on understory variation in a boreal forest, Forest Ecology and Management. 2020;466:118100.
DOI: 101016/j foreco.2020.118100.
14. Nieman WA, van Wilgen BW, Leslie AJ. Correction to: A reconstruction of the recent fire regimes of Majete Wildlife Reserve, Malawi, using remote sensing (Fire Ecology. 2021;17,1,(4), DOI: 10.1186/s42408-020-00090-0)," Fire Ecology,
DOI: 101186/s42408-021-00122-3.
15. Ribeiro N, Cumbana M, Mamugy F, Chaúque A. Remote Sensing of Biomass in the Miombo Woodlands of Southern Africa: Opportunities and Limitations for Research, Remote Sensing of Biomass Principles and Applications. 2012;77–98.
DOI: 105772/696.
16. Biocarbon B, Development R, Biodev A. Field measurement guidelines for aboveground biomass and fuel wood stocks. 2014;0:4–5.
17. USAID PERFORM, "Forest Inventory Report; 2017.
18. Government of Malawi, Malawi National Forest Inventory 2018 Analysis Report; 2019.
19. Malawi Government, Malawi State of Environment and Outlook Report Environment for Sustainable Economic Growth; 2010.
20. United Nations, Summary of AG-004 Department of Economic and Social Affairs (DESA) (1955-present); 2015.
21. Department of Forestry, Forest Resource Mapping Final Report for Implementation Phase; 2012.
22. Iman Gerard FB, et al. Height-diameter allometry and above ground biomass in tropical montane forests : Insights from the Albertine Rift in Africa, Plos One. 2017;1–20.
23. Westoby MJ, Brasington J, Glasser NF, Hambrey MJ, Reynolds JM. Structure-from-Motion' photogrammetry: A low-cost, effective tool for geoscience applications, Geomorphology. 2012;179:300–314.
DOI: 101016/j.geomorph.2012.08.021.
24. Birdal AC, Avdan U, Türk T. Estimating tree heights with images from an unmanned aerial vehicle, Geomatics, Natural Hazards and Risk. 2017;8(2):1144–1156.
DOI: 101080/19475705.2017.1300608.
25. Mlambo R, Woodhouse IH, Gerard F, Anderson K. Structure from motion (SfM) photogrammetry with drone data: A low cost method for monitoring greenhouse gas

emissions from forests in developing countries, Forests. 2017;8:3.
DOI: 103390/f8030068.
26. Kachamba DJ, Ørka HO, Gobakken T, Eid T, Mwase W. Biomass estimation using 3D data from unmanned aerial vehicle imagery in a tropical woodland, Remote Sensing. 2016; 8(11):1–18.
DOI: 103390/rs8110968.
27. Fankhauser K, Strigul N, Gatziolis D. Augmentation of Traditional Forest Inventory and Airborne Laser Scanning with Unmanned Aerial Systems and Photogrammetry for Forest Monitoring, Remote Sensing. 2018;10:10. DOI: 103390/rs10101562.
28. Neeff T. A Roadmap for Developing Malawi's National Forest Monitoring System, no; 2015.
29. Malawi Redd+ Programme, Malawi REDD+ Readiness Program: Final Report on Carbon Inventory in Malawi's Forests Capacity to Support REDD+ and National forest Inventory Activities; 2015.
30. Zmarz A, Rodzewicz M, Dąbski M, Karsznia I, Korczak-Abshire M, Chwedorzewska KJ. Application of UAV BVLOS remote sensing data for multi-faceted analysis of Antarctic ecosystem," Remote Sensing of Environment. 2018;217:375–388.
DOI: 10.1016/j rse.2018.08.031.
31. Wood K, et al. BVLOS UAS Operations in Highly-Turbulent Volcanic Plumes, Frontiers in Robotics and AI. 2020;7:1–15.
DOI: 103389/frobt.2020.549716.
32. Mueller A. Development of Integrated Monitoring Systems for REDD + in the Southern African Development Community (SADC) Design of REDD MRV : SADC Field Inventory Manual – Draft; 2012.
33. Berry N, Utila H, Clunas C, Viergever K, Tipper R. Avoiding Unplanned Mosaic Deforestation and Degradation in Malawi. 2009;45.
34. Beedy TL, Chanyenga TF, Akinnifesi FK, Sileshi GW, Nyoka BI, Gebrekirstos A. Allometric equations for estimating above-ground biomass and carbon stock in Faidherbia albida under contrasting management in Malawi, Agroforestry Systems. 2016;90(6): 1061–1076.
DOI: 10.1007/s10457-015-9883-x.
35. Chanyenga T, Fehrmann L, Bertram A, Kleinn C, Meke G. Performance Of Different Sampling Plot-Designs In The Estimation Of Stocking Densities , Basal Area And Diameter Distribution Of Some Miombo Species In Phirilongwe Forest Reserve In Malawi; 2005.
36. Assembly ND. Ntchisi District Socio-Economic Profile; 2013-2018," 2014.
37. Magrath J, Sukali E. The winds of change: Climate change, poverty and the environment in Malawi; 2009. [Online].
Available: www.oxfam.org
38. Streefkerk IN, et al. Contextualising seasonal climate forecasts by integrating local knowledge on drought in Malawi, Climate Services, vol. 25, no. October 2021, p. 100268, 2022,
DOI: 101016/j.cliser.2021.100268.
39. Chinangwa L, Pullin AS, Hockley N. Livelihoods and Welfare Impacts of Forest Comanagement, International Journal of Forestry Research; 2016.
DOI: 10.1155/2016/5847068.
40. Ntchisi District Assembly, "Strategic Forest Area Plan-Ntchisi Forest Reserve-June,2007.
41. Pearson T, Walker S, Brown S. Sourcebook for land use, land-use change and forestry projects, Winrock International, Little Rock, Arkansas, 2005.
42. Puliti S, Saarela S, Gobakken T, Ståhl G, Næsset E, Combining UAV and Sentinel-2 auxiliary data for forest growing stock volume estimation through hierarchical model-based inference," Remote Sensing of Environment. 2017;204:485–497.
DOI: 10.1016/j.rse.2017.10.007.
43. Uyttendaele M, Eden A, Szeliski R. Eliminating ghosting and exposure artifacts in image mosaics, Proceedings of the IEEE Computer Society Conference on Computer Vision and Pattern Recognition. 2001;2:II509–II516.
DOI:10.1109/CVPR.2001.991005.
44. Chen J, Li Z, Peng C, Wang Y, Gong W. UAV Image Stitching Based on Optimal Seam and Half-Projective Warp, Remote Sensing. 2022; 14(5):1068.
DOI: 103390/rs14051068.
45. Fayad I, et al. Terrain slope effect on forest height and wood volume estimation from gedi data, Remote Sensing. 221;13:11. DOI:103390/rs13112136.

Journal of Global Ecology and Environment

16(2): 7-27, 2022
ISSN 2454-2644

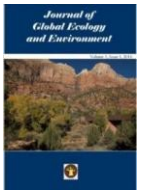

COMPARISON OF VARIED FOREST INVENTORY METHODS AND OPERATING PROCEDURES FOR ESTIMATING ABOVE-GROUND BIOMASS IN MALAWI'S MIOMBO WOODLANDS

HENRY KADZUWA [a,b*] AND EDWARD MISSANJO [c]

[a] Department of Forestry Headquarters, P.O. Box 30048, Capital City, Lilongwe 3, Malawi.
[b] University of Edinburgh, C/O 3/1, 21 Meadowbank Terrace, Edinburgh, EH8 7AS, UK.
[c] Department of Research, Malawi Assemblies of God University, P.O. Box 184, Lilongwe, Malawi.

AUTHORS' CONTRIBUTIONS

This work was carried out in collaboration between both authors. Both authors read and approved the final manuscript.

Received: 02 March 2022
Accepted: 06 May 2022
Published: 11 May 2022

Original Research Article

ABSTRACT

This study assessed forest inventory methods and standard operating procedures (SOPs) for estimating above-ground biomass (AGB) and carbon, as employed in the key REDD+ Miombo Forest Reserves of Malawi. Analysis of Variance statistical technique was applied to investigate the following methods and SOPs: (i) allometry, (ii) sample plot configuration, and (iii) dendrometric measurements. Results indicate that the allometric equations parameter significantly (P<0.001) affected the AGB estimations and was the highest contributor (97.95%) of the total variation. Malawi's specific allometry provided the highest AGB estimate (113.08±1.56 t/ha). In contrast, the Pan-Tropical/generalized allometric models substantially underestimated AGB within the range of 16.7-67.9%. Furthermore, the findings demonstrate that the use of varied sampling plot sizes significantly (P<0.001) affected the estimates of AGB. However, the plot size parameter contributed only 1.65% to the total variation. The 20m radius plot size registered the highest AGB (75.31±0.77 t/ha) compared to the 17.84m radius plot (66.12±1.61 t/ha). This signifies that the plot size of 17.84m radius underestimated the AGB by 12.2%. However, results on dendrometric measurements showed no significant (P>0.05) differences in the AGB estimates between the use of diameter tape (D-tape) and calliper in measuring *dbh* of individual trees despite the former yielding higher estimates of AGB (74.65±0.93 t/ha) than the latter (72.53±0.98 t/ha). This demonstrates that the use of calliper in measuring *dbh* underestimated AGB t/ha by only 2.8% compared to the use of D-tape. Therefore, the study recommends; employment of local allometry, adoption of a circular sampling design of 20m radius, and consistent use of D-tape in measuring *dbh* for AGB in Malawi's Miombo Woodlands. In conclusion, incorporation of these changes is envisaged to facilitate quick realisation of Malawi's REDD+ carbon payments, smooth running of the National Forest Inventory system, robust implementation and global recognition of the REDD+ efforts.

Keywords: Miombo; REDD+; above ground biomass; standard operating procedures; sampling design; allometry; D-tape; calliper.

*Corresponding author Email h.h.n.kadzuwa@sms.ed.ac.uk;

1. INTRODUCTION

Acquisition of consistent and accurate forest biomass and carbon estimates that are accorded through the measurement, reporting and verification (MRV) etiquette remains a significant challenge for successful implementation of the global mechanism on reducing emissions from deforestation and forest degradation (REDD+). Malawi, a non-Annex 1 Party, submits primarily, but, not exclusively, her Greenhouse gas (GHG) estimates to the United Nations Framework Convention on Climate Change (UNFCCC) as part of efforts on climate change mitigation [1–3]. The country relies on ground-based forest inventory as its MRV system for monitoring and collecting data pertaining to above-ground biomass (AGB) and carbon (C) [4,5].

Nevertheless, significant inaccuracies and inconsistencies pertaining to methods and Standard Operating Procedures (SOPs) have been observed in forest inventories conducted over the past three decades in Malawi [4,6,7]. These include sampling strategies/design, sampling plot-unit configuration, stem diameter measurements and allometry. Critical about these flaws is that they have contributed to the generation of forest AGB and C datasets that are incomparable, thereby leading to the accreditation of Malawi's REDD+ efforts at a lower tier [4-7]. More importantly, this has affected the C financial payments standards. A technical report on assessment of Malawi's proposed forest reference level (emissions) which was submitted in 2019 as the last requirement prior to assessing procedures considered for C payments was not passed by the UNFCCC due to issues bordering the aforementioned inconsistencies and flaws [8]. These genuinely pose a stumbling block to the development of Malawi's National Forestry Inventory (NFI) system which is underway. Hence, in the absence of recognising and estimating their extent and impact, it is not certain how the country can achieve its carbon financial awards and better-still sufficiently improve in attaining its goals for climate change mitigation in Malawi under the global REDD+ initiative.

Discrepancies and flaws detected in the approaches and operating procedures for estimating forest biomass and C remain a significant gap to the understanding and robust management of REDD+ and NFI particularly in the tropical woodlands [9,10]. As REDD+ global standards have been laid for comparability and repeatability sake, thus to curtail flaws, their implementation critically depends on reliable ground-based MRV protocol of biomass and C storage which inversely is reliant on the accuracy involved [11]. The standards govern recognition of definitions, measuring parameters and C domains that embrace terms such as forest, deforestation and forest degradation [12,13]. Within such realms, the most overarching role of forests with regards to Climate Change has been identified as the C sink domain entailing majority of above and below- ground terrestrial regenerative C stored as biomass [14,15].

Arguably, this prompted categorisation of forest biomass into five main pools constituting; (i) AGB, (ii) Below-Ground Biomass (BGB), (iii) Dead Wood (DW), (iv) Litter, and (v) Soil Organic Carbon [16,17]. The AGB category consists of woody and herbaceous biomass of living vegetation above the soil surface that includes; stems, stumps, branches, bark, seeds and foliage of trees, shrubs, palms, bamboo, vines and other living plants (ibid.). Comparatively, AGB constitutes the major pool of biomass in tropical forests [18]. Besides, AGB is moderately easier to measure often used as the basis for estimating other terrestrial C pools including BGB. This is why research efforts on biomass estimations favour it. In Malawi's Miombo Woodlands, forest biomass assessments for the past years deliberately focused only on AGB in contrast to litter and/or BGB. This is because the former's quantity has been quite minimal and negligible while the latter is practically estimated through destructive sampling which is deemed expensive worldwide [4,14,19–21]. However, the UNFCCC has highlighted a number of serious inconsistencies and flaws pertaining to data, methodology and procedures that Malawi follows to estimate AGB in its Miombo Woodlands under the REDD+ programme [8].

Notwithstanding ground-based and remote sensing methods for estimating forest AGB and C stocks; accurate assessment methods and data remain indispensable to sound management strategies and decision making [9]. The salient challenge in most African woodlands, Malawi inclusive, remains lack of evaluation of these data collection systems (i.e., inadequate capacity to compare the different methods) due to the paucity of data besides the various methods and procedures [9,22]. This has potentially led to the quandary of uncoordinated efforts and sometimes acquisition of redundant and contradictory datasets, a phenomenon that is no exception to Malawi [22,23]. It is against such a background that this study aimed at obtaining a deeper insight into the methods and SOPs that estimation of AGB in Miombo Woodlands, in the light of Malawi's REDD+ and NFI that are under development.

Studies on the REDD+ MRV protocol in relation to the IPCC guidelines observed that uncertainties in the

estimation of biomass and C stocks in tropical forests may emanate from poor stratification or representativeness of the sampling network, improper sampling design, sampling unit size, wrong allometric models and inaccurate measurement of variables, i.e., instrument and calibration errors as a result of deviating from the standards [24, 25].

Paradoxically, this is against the backdrop that Malawi started piloting REDD+ schemes as early as 2008, besides officially embracing the UN REDD+ partnership in 2014 [2,5,19]. Ryan et al. [26] observed that data on land use change emissions from the African Woodlands are generated from unreliable and inconsistent sources which have consequently provided difficulties in making comparisons or used under global REDD+ purposes [27].

Under the Forest Carbon Partnership Facility (FCPF) of the World Bank, payments for verified emission reductions from REDD+ programs are provided to countries that register considerable progress [24,28]. By August 2019, 18 countries including Mozambique, DRC and Ghana, some of which border with Malawi and have Miombo woodlands as well, presented emission reduction programs to the FCPF [24,28]. However, Malawi unfortunately, still lags behind these advancements. Worse-still, despite piloting REDD+ activities for more than a decade the country operates within lower Tiers of 1 and 2, indicative of lesser methodological accuracy with regards to the IPCC standards [1,3]. If left unchecked, these may jeopardise the effectiveness of REDD+ and ultimately the climate change mitigation path-way that Malawi has taken.

In an attempt to illuminate the pertinent challenges associated with methods and SOPs in estimating AGB in Miombo Woodlands of Malawi, a comprehensive review of the forest inventories has been conducted by this study covering the past 3 decades by; (i) first identifying the challenges, and (ii) analysing their effect of their impact with regards to AGB estimation in statistical terms. This is a novel initiative applied on Malawi's Miombo woodlands, at least to the knowledge of the authors. Some of the forest inventories and sampling designs employed for the past 3 decades in Malawi are presented in Table 1.

Therefore, the study's objective was to assess forest inventory methods and SOPs engaged in estimating AGB in Malawi's Miombo Woodlands for the past three decades (1991-2021). The parameters assessed include: (i) allometry for AGB estimation, (ii) sampling plot configuration, and (iii) stem diameter measurements. The hypothesis of the study was that Malawi's AGB estimated in Miombo landscape for the past three decades (1991-2021) has registered flaws and inconsistencies heterogeneous to their methods and SOPs.

2. MATERIALS AND METHODS

2.1 Study Area, Meta-Analysis Approach and Database

This study covered the forest inventories conducted in the Miombo Woodlands of Malawi. Malawi is a Southern tropical country that lies between latitudes 9°22' and 17°03', south of the Equator and longitudes 33°40' and 35°55' east of the Greenwich meridian. The country is bordered by Tanzania in the north and north-east, Mozambique in the south-west, south and the east; and Zambia in the west (Fig. 1). It lies in the general tropical continental Savanna climate characterised by a single rainy season lasting from October to April. This alternates with a dry season running from May to September. The mean annual rainfall ranges between 500 mm in low-lying marginal rainfall areas to over 3,000 mm on high altitude plateaus while 12° to 32°C is the mean annual temperature range [3]. The climate is greatly influenced by varied altitudinal range (35-3000m *asl.*) plus its proximity to Lake Malawi, a water body covering ~two thirds of the country's length.

Malawi's forests cover 23,677 km^2 representing 25% of the country's total surface land area, out of which 22,857 km^2 expanses over Miombo landscape. Almost 90% of Malawi's forest area is indigenous vegetation which is dominated by the Miombo Woodland [7]. The Miombo Forest Ecosystem spreads across the entire 3 regions of the country covering a number of protected areas (PAs) some of which lie along the country border. The PAs include; forest reserves, national parks and wildlife reserves which cover almost one million hectares (Fig. 2). The Malawi's Miombo comprise open forests of low carbon stocks, ranging from 35 to 45 Mg ha^{-1} and in some cases as low as 8 Mg ha^{-1} [7]. More than 96% of Malawi's population rely on fuelwood in form of charcoal and firewood while forest products and services contribute 6.9% of the country's GDP through domestic and export product sales, employment, and tourism [29].

This study conducted a meta-analysis with a focus on forest assessment methods and procedures for estimating AGB in Miombo Woodlands under the REDD+ mechanism and NFI schemes. The following key sites and links provided relevant literature for the study;

Table 1. Traceable Forest Inventories in Malawi's Miombo Woodlands: 1991-2021

Forest Inventory	Location	Sampling & Sample Plot Design	Sample Size	Parameter Measured	Carbon Pool
National Forest Inventory (1991-93)	Nation-wide	*NA*	*NA*	*dbh*, *ht*, clear length, species.	*AGB*
Dzalanyama Reserve (1994-95)	Dzalanyama Reserve,	*NA*	*NA*	*dbh*, *ht*, clear length, species.	*NA*
Miombo Inventories (1995-96)	Chimaliro & Liwonde	*NA*	*NA*	*dbh*, *ht*, clear length, species.	*AGB*
Bark Harvesting Project (2005)	Phirilongwe Forest Reserve	Randomized (branch), using K- tree methods	*NA*	*dbh*, *ht*, species.	*ABG*
Tree Planting and Management for Carbon Sequestration and Other Ecosystem Services (2006-2011)	Countrywide	Stratified random sampling, samples collected in 0-10, 10-20 & 20-30 cm soil depths.	300	*dbh*, *ht*, root collar, diameter, Soil organic Carbon (SOC), litter, species.	*AGB, BGB, SOC, Litter*
Tree Survey for Right of Way: Malawi Mozambique Interconnector Power-line (2009)	Balaka & Mwanza	Systematic sampling, (covering a stretch of 75km), concentric nested circular plots of 2m, 5m, 25m, laid at 250m apart	294	*dbh*, *ht*, disc (growth rings of stem disc for age determination), species.	*AGB*
Avoiding Unplanned Mosaic Deforestation and Degradation in Malawi (2008-2009)	Mkuwazi & Nyika,	Random sampling, Square plots of 30m x30m & circular plots of 17.84 m radius	203	*dbh, ht*, *cd*, clear length, species.	*AGB, DW, BGB*
Biomass of *Faidherbia albida* under Different Management Regimes (2010)	Karonga, Bolero, Makanjila, Salima, Bwanje & Mwanza	Complete randomised block design, 30m interval	83	*dbh, ht & crown area*	*AGB*
Lake Chilwa Change Adaptation Programme (2010-17)	Lake Chilwa Basin (Machinga, Phalombe & Zomba)	Random Sampling	*NA*	*dbh, ht*, species.	*AGB*
Forest Resource Mapping under Forest Preservation Programme (2011-12)	17 forest reserves across the country,	Systematic sampling. Nested-Circular nested plots of 5.64m & 17.84m radius each respectively. **(0.1ha)**	278	*dbh, ht*, *cd*, clear length, species.	*AGB, DW, BGB*
Development of Integrated Monitoring Systems for REDD+ in the SADC Project (2013)	Trans-boundary between Malawi & Zambia	Stratified random sampling. Nested T-Shaped Cluster (**0.3ha**)	150	*dbh, ht*, *cd*, clear length, species, saplings.	*AGB, DW, BGB*
Distribution and Population Structures of *Adansonia digitata* (2013)	Countrywide,	Systematic random sampling. followed 500m grid interval	26 sites	*dbh, ht*, bole height, *cd*, shape of trunk, species.	*AGB*
Liwonde, Ntchisi and Perekezi Forest Reserves (2016)	Liwonde, Ntchisi and Perekezi Forest Reserves,	Stratified random sampling. Nested T-Shaped Cluster (**0.3ha**)	86	*dbh, ht*, *cd*, clear length, species, saplings	*AGB, DW, BGB*
Dzalanyama Forest Reserve	Dzalanyama Forest	Systematic sampling 2-Circular nested	*68*	*dbh, ht*, *cd*, clear length, species.	*AGB, DW,*

Forest Inventory	Location	Sampling & Sample Plot Design	Sample Size	Parameter Measured	Carbon Pool
Conservation Project (2017)	Reserve	plots of 5.64m and 17.84m radius each respectively **(0.1ha)**			*BGB*
Thuma and Dedza-Salima Escarpment Forest Reserves (2017)	Thuma and Dedza-Salima Escarpment Forest Reserve,	Stratified random sampling Nested T-Shaped Cluster (3 totalling to **0.3ha**)	33	*dbh, ht*, crown diameter, clear length, species.	*AGB, DW, BGB*
National Forest Inventory (2018)	North and South (except Central Region Forests)	Random sampling T- cluster design 6m, 12m, 20m radius plots (**0.3ha**)	94	*dbh, ht*, *cd*, clear length, species.	*AGB, DW, BGB*

***Source**: Malawi National Forest Inventory Analysis-2018*

***Key**: DW=Dead Wood; N/A=Not Applicable (information or data not Available or Applicable), ht=height, dbh=diameter at breast height, cd=crown diameter, AGB=Above ground biomass, BGB=Below ground biomass.*

(i) https://www.unredd.net/regions-and-countries/africa/malawi html
(ii) https://www.dof.gov.mw/
(iii) http://www.ead.gov.mw/green-house-gas-inventory
(iv) https://www.tetratech.com/en/projects/protecting-ecosystems-and-restoring-forests-in-malawi
(v) https://unfccc.int/
(vi) https://www.giz.de/en/worldwide/15908 html
(vii) https://discovered.ed.ac.uk/discovery/search?
(viii) https://www.ipcc-nggip.iges.or.jp/public/2006gl/vol4.html
(ix) https://scholar.google.co.uk/scholar?

These sites were accessed between March 2021 and January 2022. The search involved the following keywords 'forest biomass and carbon assessment in Malawi', 'national forest inventory of Malawi' and 'national forest monitoring system of Malawi'. The major focus for the meta-analysis was on 6 recent studies that pursue the REDD+ initiative and have traceable inventory data which include:

a) Avoiding Unplanned Mosaic Deforestation and Degradation in Malawi (2008-2009),
b) Forest Resource Mapping under Forest Preservation Programme (2011-12),
c) Development of Integrated Monitoring Systems for REDD + in the Southern African Development Community (SADC) Design of REDD MRV (2013),
d) Dzalanyama Forest Reserve Conservation Project (2017),
e) Liwonde, Ntchisi and Perekezi Forest Reserves Inventory (2016) and,
f) Malawi National Forest Inventory (2018).

For conciseness, these studies have been named after their site and/or funder followed by year of study interchangeably hereinafter as follows; (a) Nyika-Mkuwazi-2008, (b) FPP/JICA-2012, (c) SADC-GIZ-2013, (d) DFRP-2017, (e) LIW-NTZ-PER-2016 and, (f) NFI-2018, respectively.

2.2 Sample Plot and Data Collection

Data for testing (analysis) was specifically acquired from forest inventories that were conducted in Liwonde Forest Reserve (Fig. 2) in 2012 and 2016. The reserve is located between the latitude $15^0$21'S and longitude $35^0$21'E. The altitude of the area ranges from 800 m to 2080 m above sea level. The mean annual rainfall range is 840–960 mm while the mean annual temperature range is 18ºC – 25ºC. The area experiences a 5–6-month dry season thus from May to October. The reserve is dominated by ferrallitic latosols soils with an average pH of 5.2 [30].

2.2.1 Measurement procedure

Navigation to the sample plot centre was the initial stage that was preceded by *a priori* entry of plot centroid (*xy* coordinates) in handheld GPS receiver. Attainment minimum positional accuracy of +or -3m by the receiver was ensured prior to marking the *xy* positions of any other target feature. This was followed by monumenting the plot centre using metal bars. Plot alignment and plot boundary demarcation steps followed. These were done using pocket-prismatic compass, adjustable ranging rods, tape-measure and coloured flagging tape and/or chalk.

2.2.2 Key variables

Enumeration began with saplings from the regeneration subplot and was sequentially followed by small, medium and large subplots. While saplings' height was used as a threshold in the regeneration subplot, a given dbh threshold determines the trees to measure in the rest of the subplots (Table 3). Tree parameter measurements were carried out following Azimuth direction, thus beginning from the plot- centre stretching outward in clockwise direction. Each measured tree was tagged using an identification number (ID). GPS camera (in built) and/or a steel camera (embedded with GPS function) were also used to capture tree IDs to ascertain georeferenced locations. Other features depicting the plot status i.e., regenerants, standing trees, lying/leaning trees, deadwood or vegetation and terrain status that were deemed important were captured as well.

Key variables and parameters recorded include; (i) *dbh* taken at 1.3m above-ground-using diameter tape (*D*-tape) or calliper, (ii) height–using hypsometer, (iii) crown diameter using *D*-tape, (iv) tree and regenerants botanical names, (v) trees *xy* geocoordinates using handheld-GPS set, (vi) plot- centre geo-coordinates (*xy*) using handheld GPS set. Normally, deadwood was recorded though its quantity has usually been deemed too insignificant to account in Malawi's forests [4].

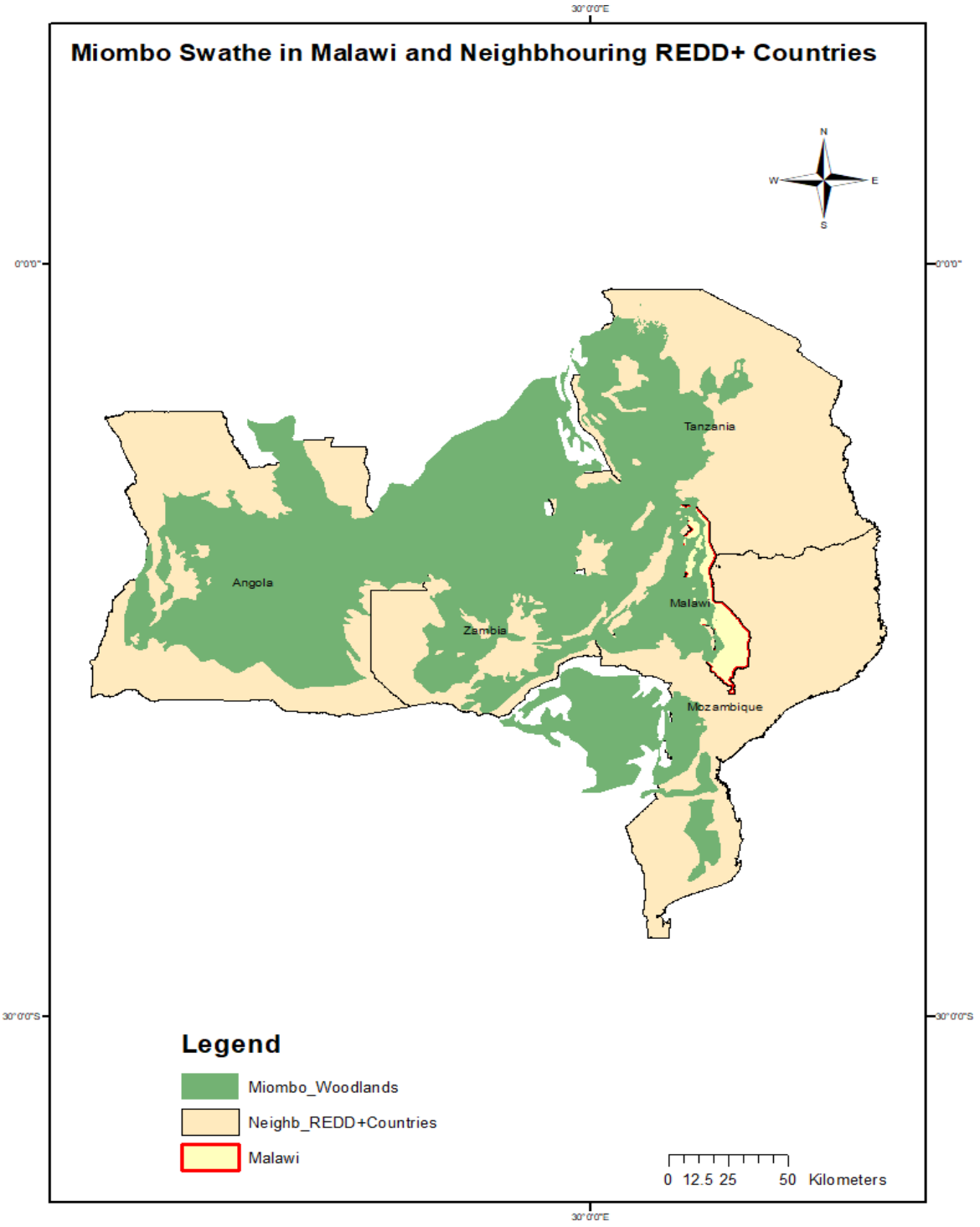

Fig. 1. Miombo Swathe in Malawi and Neighbouring Countries

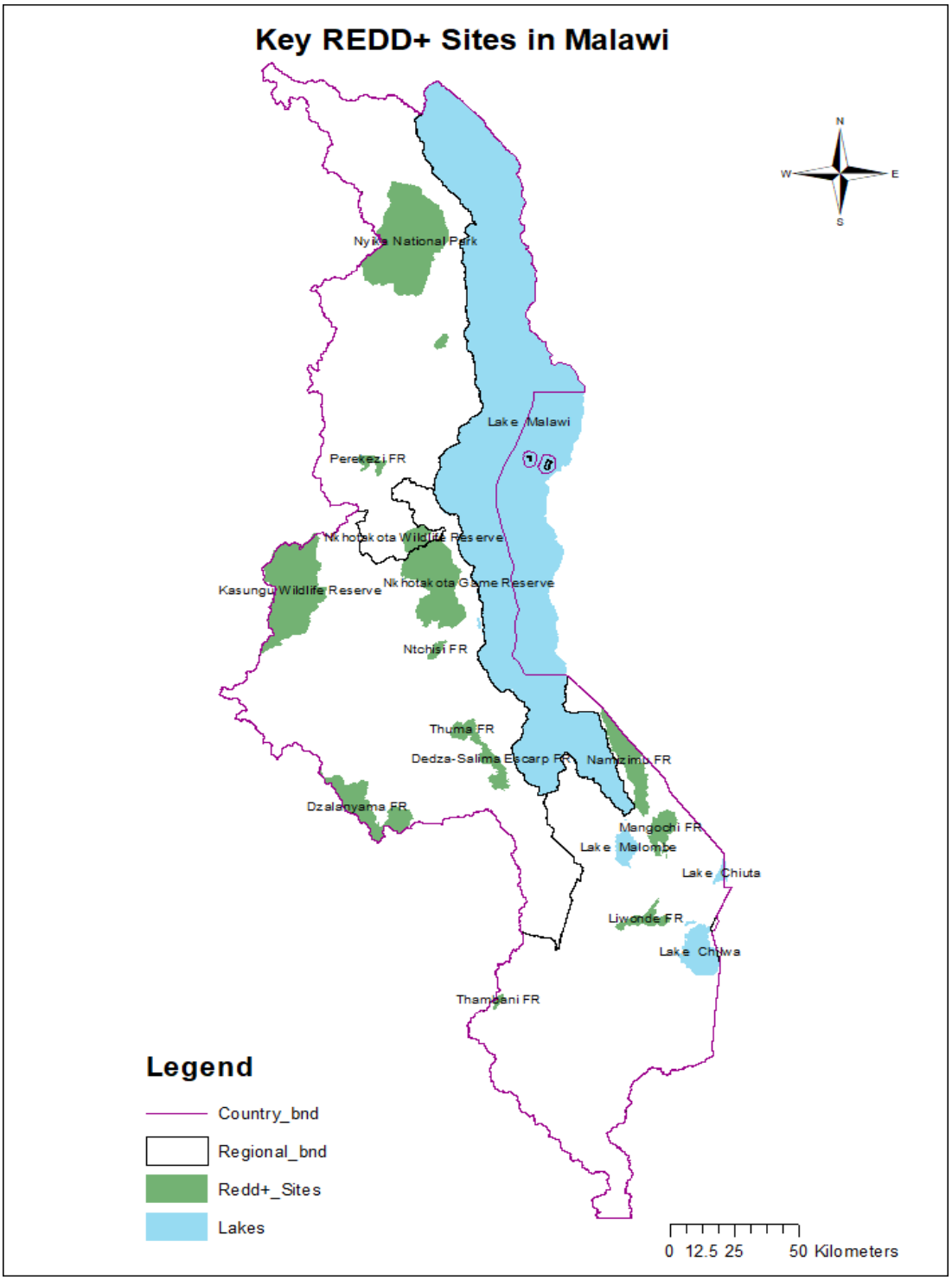

Fig. 2. Key REDD+ Sites in Malawi

Source: Country and Protected areas shapefile- Surveys Department of Malawi.

The number of sample plots and other parameters used in the study are presented in Table 2. The following measurements were taken for each tree in the plot and were recorded: *dbh* using caliper or *D*- tape; height using vertex; distance and bearing from the centre using vertex and hand-held compass, respectively. However, trees were measured using the following threshold small plot (5cm ≤ dbh ≥ 14.9 cm); medium plot (15cm ≤ dbh ≥ 29.9 cm); and large plots (dbh ≥ 30cm). The botanical name of each tree

measured was also identified and recorded. Furthermore, the present study simulated the calliper measurements for the *dbh* of trees for the 2016-forest inventory and the diameter tape measurements for the 2012-forest inventory as shown in Table 2.

2.3 Calculation of AGB

Calculation of AGB encompasses all live trees measured in the sampling plots. It covers a number of stages that have been exemplified using a T-cluster circular nested sample design (Fig. 4) in this study and categorised as follows; (i) sampled plot area, (ii) scaling factor, and (ii) employment of allometry. The allometry used is the one that was developed by Kachamba et al. [20].

2.3.1 Sampled plot area

Prior to AGB estimation, the initial stage involves establishing the extent of area that the biomass covers which is calculated based on the sample plot size and shape. While calculation of square or rectangular shaped plot is regarded as straight forward, most of the studies under focus employed circular sample plot.

Area calculation of the nested circular plots is based on the following formula; $A= \pi R^2$,

where:

A= the area of the nest (circle) π
=pi (3.14)
R= the radius of the nest

2.3.2 Scaling factor

Prior to AGB calculations, a scaling factor (SF) is used to scale up dimension (area) values for each subplot in order to convey estimates of C stock on a hectare basis. This involved conversion of the subplot area unit measurements (in m^2) to a per hectare basis (1ha) as follows:

SF= 10,000/NA,

where;
SF = Scaling Factor to convert per hectare basis (dimensionless)
10,000 = number of squared meters (m^2) in one hectare
NA = horizontal projected area of nested plot (in m^2)

Table 2. Parameters employed during plot-based inventories in Liwonde Forest

No.	Parameter	Inventory Year	
		2012	2016
1	**Number of sample plots**	16	70
2	**Plot-size**	0.1 ha (Circular plots of 17.84 m radius) (Figure 3)	0.13 ha (Circular plots of 20 m radius) (Figure 4)
3	**DBH Measurement tool**	Calliper (Figures 5 and 6)	*D*-tape (Figures 5 and 6)

Fig. 3. Concentric nested sampling plot design
Source: Makungwa [31] and DoF [32]

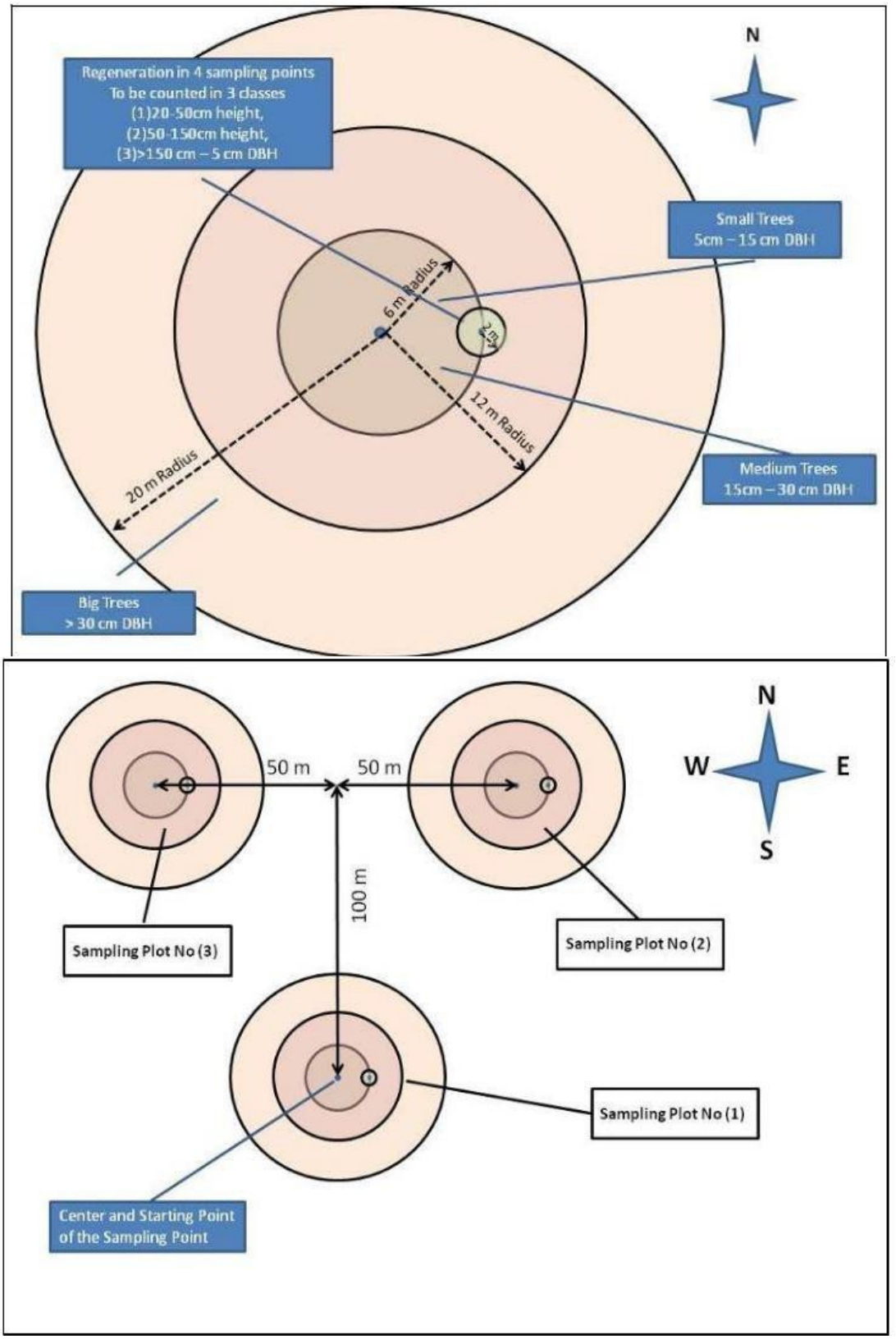

Fig. 4. T-Shaped cluster sampling plot design
Source: Mueller [33]

Fig. 5. *dbh* Measuring tools used in Malawi Inventories (Vertex and Transponder-*far-left*, Calliper-*middle* and Diameter tape (rolled) (*far-right*)
Source: Mueller [33]

Fig. 6. Site-specific Ground-based inventory in Malawi's Miombo Woodlands-inconsistencies in measuring *dbh* by using both D-tape and calliper regardless of stem diameter geometry resulting to error in AGB estimation: (top-left) and (top-right) measuring *dbh* using *D*-tape on fine hardwood species of big, but leaning tree and small, but upright tree respectively. Bottom-left-measuring *dbh* using calliper on smooth rounded evergreen species, and (bottom-right) measuring mid-diameter of deadwood using a calliper on fine hardwood species with rough outer bark

Table 3. Different allometry used for AGB calculations

No.	AGB Allometric Equation	Source
1	$AGB=0.0267dbh^{2.5996}$	Ryan et al. [35] (Mozambique)
2	$AGB=0.5(0.2035dbh^{2.3196})$	Brown et al. [36] (Mozambique)
3	$AGB=\exp(-1.996+2.32^{*\ln(dbh)})$	Brown [37] (Mozambique)
4	$AGB=BD \times \exp\{-0.667+1.784 \times \ln(dbh) + 0.207[\ln(dbh)]^2 - 0.0281 \times [\ln(dbh)]^3\}$	Chaves et al. [38]
5	$AGB= 0.21691 * dbh^{2.318391}$	Kachamba et al. [20] (Malawi)

Key: AGB=Above-ground Biomass in kg C, dbh=diameter at breast height in cm, BD=Basic Wood density (oven-dry. tonne/moist m^3)

2.3.5 Employment of allometry

This stage involves factoring of AGB allometric equation. As aforementioned, this study employed a local allometry specifically developed for Malawi's Miombo trees that was published by Kachamba et al. [20] as a standard one thus, indicated below:

$AGB_t = 0.21691*dbh^{2.318391}$

where;

AGB_t = above-ground biomass of tree *t*; kilograms of dry matter (kg.d m.)
dbh = diameter at breast height in centimeters (cm)
ht = total tree height (m) taken at breast height

The results obtained are in kilograms of dry matter (kg.d m.) otherwise referred to as AGB. As a final step, a carbon fraction of 0.47 for all the Miombo tree species measured is multiplied to the AGB to calculate Carbon [4, 21].

AGB allometric equation presented in Table 3 were used for the meta-analysis.

2.4 Statistical Analysis

Datasets on AGB were tested for normality and homogeneity with Kolmogorov-Smirnov D and normal probability plot tests. After the two criteria were met, the datasets were subjected to the analysis of variance (ANOVA) technique. Variance components for the sources of variation were also estimated. Statistical analysis was performed using GenStat 18.1 for Windows. Differences between treatment means were separated using Fischer's least significant difference (LSD) at the 0.05 level. The data were analysed using equation 1.

(1)

where:

- is the response variable (Above ground biomass) of the *j*th observation in the *i*th treatment;
- is the overall mean;
- is the fixed effect of the allometric equation (*i* = 1, 2, 3, …, 5);
- is the fixed effect of plot size (j =1, 2);
- is the fixed effect of DBH tool measurement (k=1, 2);
- is the effect of the interaction between the allometric equation and plot size;
- is the effect of the interaction between the allometric equation and DBH tool measurement;
- is the effect of the interaction between plot size and DBH tool measurement;
- is the effect of the interaction among allometric equation, plot size, and DBH tool measurement;
- is the random residual effect, ~ N ( ).

3. RESULTS AND DISCUSSION

3.1 Influence of Allometric equations on AGB

Summary of the results on the influence of allometric equations in the estimation of AGB in Malawi's Miombo woodland are presented in Tables 4 and 5. Allometric equations significantly ($P<0.001$) affected the estimation of AGB and contributed the highest (97.95%) of the total variation. The site-specific allometric equation developed by Kachamba et al. [20] estimated the highest (113.08±1.56 t/ha) AGB. The other allometric equations underestimated the AGB within the range of 16.7% to 67.9%.

The present findings are in line with those in the literature [39, 40]. For example, the generalized model developed by Chave et al. [38] overestimated and underestimated tree volume in the Miombo Woodlands of Dindili and Rondo forests in Tanzania, respectively, compared to the site-specific models developed by Mugasha et al. [39]. Similarly, the generalized model [34] underestimated and overestimated the mean tree volume by 41.7% and 12.4% in *Pinus patula* and *Pinus oocarpa* in Malawi,

respectively, compared to the site-specific models developed by Malata et al. [40]. Though to some extent the degree of disparity may be due to differences in site characteristics and the type of data used in the development of allometry [41], the studies clearly indicate that the default values used in the generalized allometry (rather than the local values) greatly affected the results.

is the allometric equations; is plot size; is DBH tool measurement; is the interaction between allometric equation and plot size; is the interaction between allometric equation and DBH- tool measurement; is the interaction between plot-size and DBH-tool measurement; and is the interaction among allometric equation, plot-size and DBH-tool-measurement.

3.2 Effect of Plot Size on the Estimation of AGB

Results on the effect of plot size on the estimation of AGB in Malawi's Miombo woodland are presented in Tables 5 and 6. The plot size of 20m radius (0.13ha) had the highest (75.31±0.77 t/ha) AGB compared to 66.12±1.61 t/ha for the plot size of 17.84 m radius (0.1ha). This indicates that the plot size of radius 17.84 m underestimated the AGB t/ha by 12.2% compared to the plot size of 20m radius plot. The results portray that plot size significantly (P<0.001) affected the AGB estimates.

Nevertheless, the overall effect of plot size was 1.65% to the total variation (Table 4). Though the magnitude of the plot size contribution appears to be minimal, it has the potential to become substantial if assessed on large-scale forest areas where fine hardwood Miombo tree species intermix with ever green *afro-montane* species, such as the Mkuwazi Forest Reserve and Nyika National Park [42]. A study conducted by Mauya et al. [43] in Miombo Woodlands of Tanzania on the effect of plot size on prediction of the accuracy of AGB indicated that the plot size increases correspondingly with an increase in plot size where the adjusted R^2 increased from 0.35 to 0.74 while RMSE 63.6 to 29.2%.

Table 4. Variance components for AGB

Source of variations	df	AGB (t/ha)	
		P-value	Var %
	4	<0.001	97.95
	1	<0.001	1.65
	1	0.125	0.15
	4	0.452	0.23
	4	0.990	0.02
	1	0.935	0.00
	4	0.999	0.00

Table 5. Influence of Allometry, plot size and *dbh* measurement tool on AGB Estimation

Category	AGB (t/ha)
Allometric equation	
Brown et al. [36]	53.26±1.16^{d}
Brown [37]	71.23±1.51^{c}
Chaves et al. [38]	94.17±1.06^{b}
Ryan et al. [35]	36.28±1.65^{e}
Kachamba et al. [20]	113.08±1.56^{a}
Plot size	
Circular plot of 20m radius (0.13ha)	75.31±0.77^{a}
Circular plot of 17.84 m radius (0.1 ha)	66.12±1.61^{b}
DBH tool measurement	
Diameter tape	74.65±0.93^{a}
Calliper	72.53±0.98^{a}

Note: means with different superscripts within the same category significantly differ (P<0.05)

The plot size contribution can as well display remarkable differences in either underestimations or over estimations AGB in areas where topography is rugged i.e., steep slopes, undulating terrain cliffs etc. Topographic variables such as slope and elevation have been known to explain ~21% variations in AGB within human impacted tropical dry forest landscapes [44]. In this regard, this study encourages further research on the effect of the plot size and configuration bearing in mind the diverse topographical that the Miombo Woodlands of not only Malawi, but the entire Eco-biome expanse in Southern Africa.

The findings of the present study have also demonstrated the importance of choosing appropriate the field plot sizes (dimensions and configuration) during forest inventory of Miombo Woodlands. They have demonstrated the positive effects of increasing plot size on the improved predictive power of the AGB model. Increasing sample plot size minimizes the plot boundary affects that arise due to smaller circumference to area ratio [43]. Similar trends have been reported and discussed by other authors in tropical forests [45, 46].

3.3 Influence of dbh (Dendrometric) Measurements Tool

Summary of the results on the influence of *dbh* tool measurement on the estimation of AGB in Malawi's Miombo Woodland are presented in Tables 4 and 5. The results indicate that there were no significant (P>0.05) differences on the AGB between the use of diameter tape and calliper in measuring *dbh* of trees. However, AGB estimated using D-tape was higher (74.65±0.93 t/ha) compared to the one estimated using calliper (72.53±0.98 t/ha). This indicates that the use of calliper in measuring *dbh* underestimated the AGB t/ha by 2.8% compared to the use of *D*-tape in measuring *dbh*.

Nonetheless, much as the measuring of *dbh* looks straight-forward, Wilson et al. [47] noted that it can be difficult if no consideration is made to the discrepancies that may arise as a function of the geometric relationships upon which they are designed. While conventional callipers and *D*-tapes are generally regarded more accurate and faster than any of the optical dendrometers such as vertex clinometers; the sliding arm of a calliper can be damaged and may not always be perpendicular to the scale when read thereby introducing a bias. In spite of this, the majority of studies have recommended *D*-tapes on the grounds that they are more consistent and precise than callipers as their measurements represent an average of all diameters over all directions [47, 48]. Hence, as way forward, this study recommends further research on the accuracy assessment of AGB results propagated when using *D*-tape*s* and callipers in Miombo Woodlands of other countries for enhancing the understanding in the light of the REDD+ mechanism.

3.4 Inconsistences and Inaccuracies in Methods and SOPs for estimating AGB in Malawi

3.4.1 Varied sampling designs

The Nyika-Mkuwazi-2008 study engaged a more complex, sampling design which determined sampling plot locations considering the variant vegetation strata of the study sites. First, it employed a regular 250m grid for areas where understory vegetation did not inhibit movement [49]. Second, it involved selecting a random distance along existing paths and a random distance from the path (between 20m and 200m) in more densely vegetated areas. In total the design yielded 203 sampling plots (Fig. 7 and Table 1).

A quite different grid dimensional approach was engaged by both the FPP/JICA-2012 and DFRP-2017 studies which though employed the systematic random sampling, each target forest reserve was instead overlaid at a systematic grid interval of 1km, 2km and 4km (Fig. 7) [31,32]. In contrast to the Nyika-Mkuwazi-2008 study, the intersection points during the FPP/JICA and DFRP inventories became centroids for the sample plots for both of these studies. The FPP/JICA-2012 drew 278 plots for the entire 17 forest reserves surveyed while the DFRP- 2017 drew 68 for its study site (Table 1).

The SADC-GIZ-2013 inventory used a unique system altogether. It administered a multi-stage stratified (restricted) random sampling design whereby distribution of sample points was first based on stratification of the area into forest land and non- forest land and further into intact and non-intact forest strata [33]. The approach yielded an overlay of forest mask comprising 325 squares of 9km by 9km each randomly selected within an inventory unit. These were located inside the squares and became plot centroids (Figs. 4 and 7). This in contrast to the design followed by FPP/JICA-2012 and DFRP-2017 studies whereby the plot centroids fell at the grid intersections.

Much as the LIW-NTZ-PER-2016 study imitated the stratified and random sampling techniques laid by the SADC-GIZ-2013 study, it differently engaged a multi-stage sampling design whereby the forest reserves were further stratified by using the existing

management blocks [4, 21, 50]. The study yielded a total of 81 cluster sampling units.

In contrast, the NFI-2018 used random stratified sampling design which distributed plot points within the sampling frame with several stratification approaches. Applied a landscape-based approach that grouped lands into larger contiguous zones generally no smaller than 25km by 25km [4]. However, its full sampling approach largely followed the LIW-NTZ-PER-2016 study, even though the stratification part was based on visual (arbitrary) interpretation [4].

Fig. 7. Varied Forest Inventory Sampling Designs: (i) SADC-GIZ-2013-top, (ii) FPP/JICA-2012 and the DFRP-2017-bottom

Source: Makungwa [31] & DoF [32]

Table 6. Inconsistencies in sampling design and Dendrometers for AGB

	DIMENSION						
Name of Inventory	**Subplot**	**Dimensions/ Radius**	**Shape**	**Area**	**Threshold *for dbh***	**Instrument for *dbh***	**Source**
Nyika-Mkuwazi-2008	Small	10m x 10m	Square	0.01ha	5-20cm		(USAID Malawi [42])
	Medium	20m x 20m	Square	0.04ha	20-50cm	*D*-tape	
	Large	30m x 30m	Square	0.09ha	>50cm		
	Small	5.64m	Circular	0.01ha	5-20cm		
	Large	17.84m	Circular	0.1ha	>20cm		
FPP/JICA-2012	Small	5.64m	Circular	0.01ha	5-20cm	*D*-tape	(Department of Forestry, [32])
	Large	17.84m	Circular	0.13ha	>20cm		
SADC-GIZ-2013	Regeneration	2m	Circular	-	<5cm	calliper &	(Mueller, [33])
	Small	6m		-	5-14.9cm	*D*-tape	
	Medium	12m		-	15-29.9cm		
	Large	20m		0.3ha	≥30cm		
LIW-NTZ-PER-2016	Regeneration	2m	Circular	-	<5cm	calliper &	(USAID PERFORM, [21])
	Small	6m		-	5-14.9cm	*D*-tape	
	Medium	12m		-	15-29.9cm		
	Large	20m		0.3ha	≥30cm		
DFRP-2017	Regeneration	2m	Circular	-	<5cm		(Makungwa, [13])
	Small	5.68m		-	5-14.9cm	vertex	
	Medium	11.28m		-	15-29.9cm		
	Large	17.87m		0.13ha	≥30cm		
NFI-2018	Regeneration	2m	Circular	-	<5cm	calliper &	(Government of Malawi, [46])
	Small	5.68m		-	5-14.9cm	*D*-tape	
	Medium	11.28m		-	15-29.9cm		
	Large	17.87m		0.3ha	≥30cm		

Note: dbh=diameter at breast height, ha=hectare,

3.4.2 Varied sample plot unit design and configuration

The Nyika-Mkuwazi-2008 study employed a nested sample plot design whereby square plots were laid in dense understorey vegetation while circular ones were laid in areas with more open vegetation structure (Table 6) [49]. The square subplots' dimensions were; 10m x 10m, 20m x 20m, and 30m x 30m. An entire sampling unit was 0.09 ha. The circular subplots were of 5.64m and 17.84m radius each and the total for each cluster was 0.1ha. Nevertheless, the minimum *dbh* threshold was 5cm for both plot shapes while the maximum for the circular and square plots were >20cm and >50cm respectively.

The SADC-GIZ-2012, LIW-NTZ-PER-2016 and NFI-2018 studies laid clusters of 3-T shaped circular sampling plot units that effected a min. and max. *dbh* threshold of 5cm and >30cm respectively (Table 6 and Fig. 4) [33]. The circular subplots were of 2m, 6m, 12m, and 20m radius. Each individual concentric subplot gave a total of 0.1ha while the entire 3-T sampling unit amounted to 0.3ha.

A different sampling plot design was also employed by both the FPP/JICA-2012 and the DFRP-2017 studies which favoured nested circular plots of 2m, 5.64m, 11.28m and 17.84m radius (Fig. 3). Although the min. and max. *dbh* threshold was similar to the one used by the Nyika-Mkuwazi-2008 study, the FPP/JICA-2012 and the DFRP-2017 studies employed one nested concentric plot as their sampling unit (Fig. 3), thus in contrast to the 3-T cluster design (Fig. 4) used by the former. Hence, this implies that the entire sampling unit amounted to 0.1ha, as opposed to 0.3ha.

3.4.3 Varied Allometry employed for AGB estimation

Over the past 3 decades, a number of allometric equations (Pan-Tropical and others) have been used to estimate AGB in Miombo Woodlands of Malawi (Table 7).

Table 7. Different AGB Allometry used in Miombo Woodlands of Malawi

No.	Inventory Name	AGB Allometry	Source
1	Nyika-Mkuwazi-2008	(i)$AGB=0.0267dbh^{2\,5996}$ (ii)$AGB=0.5(0.2035dbh^{2\,3196}$	Mozambique (Ryan et al. [35]) (Brown et al. [36])
2	SADC-GIZ- 2013	AGB=exp. (-1.996+2.32* ln (dbh))	(Brown [37])
3	FPP/JICA-2012	(i) $AGB=BD$ x exp. {-0.667+1.784 x ln (dbh) + 0.207 [ln(dbh)]^2 -0.0281 x[ln(dbh)]^3} (ii) $AGB=BD$ x exp. {-1.499+2.148 x ln (dbh) + 0.207 [ln(dbh)]^2 -0.0281 x[ln(dbh)]^3}	(Chaves et al. [38]) (Chaves et al. [38])
4	LIW-NTZ-PER-2016	AGB= 0.21691$*dbh^{2\,318391}$	Malawi, (Kachamba et al. [20])
5	NFI-2018	AGB= 0.21691$*dbh^{2\,318391}$	Malawi (Kachamba et al. [20])

Key: AGB=Above-ground Biomass in kg C, dbh=diameter at breast height in cm, b= basal area in cm^2, BD=Basic Wood density (oven-dry. tonne/moist m^3)

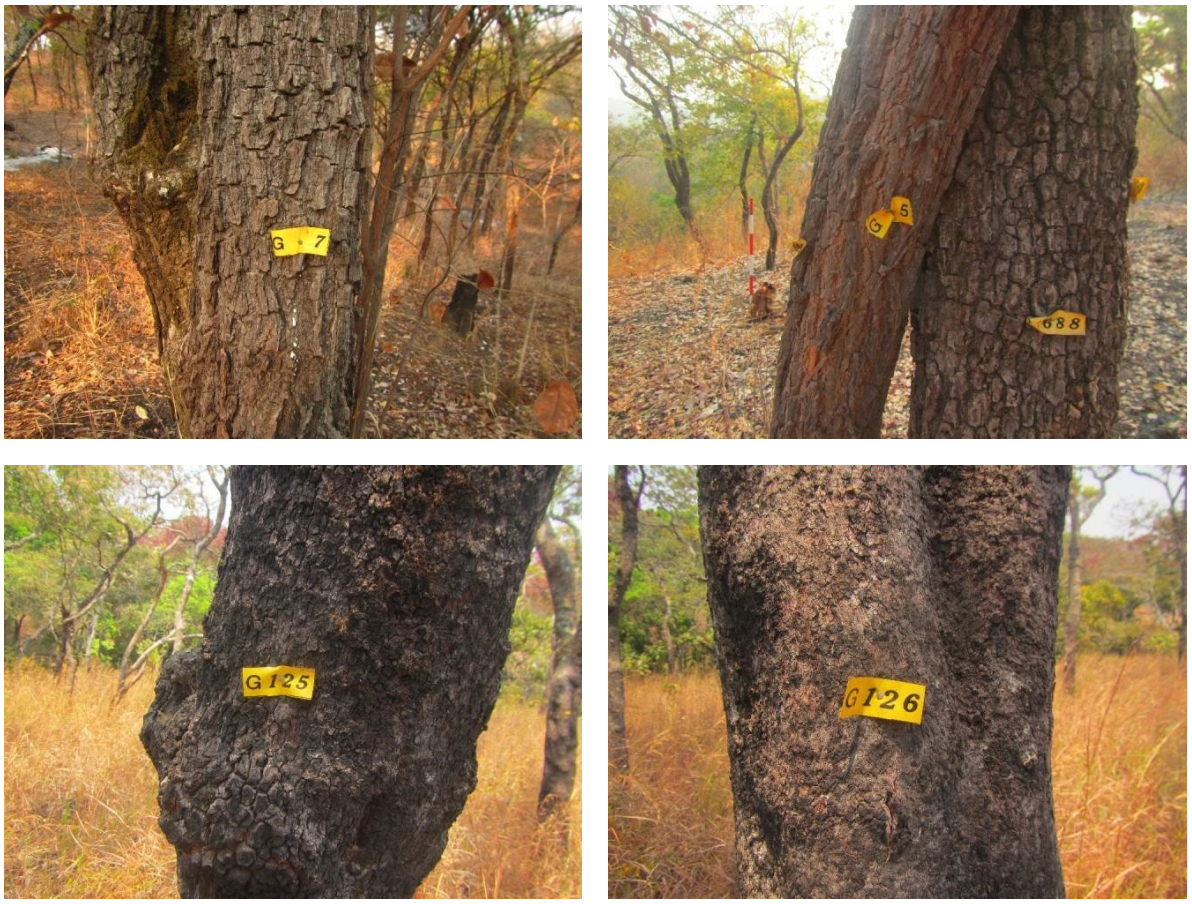

Fig. 8. Irregular outer-bark stem diameter shapes of Miombo warranting *D*-tape more than calliper for better *dbh* accuracy-Ntchisi Forest Reserve-Malawi

3.4.4 Stem diameter measurement (Dendrometric) errors

For the purpose of this write-up, dendrometers imply the many types of diameters measuring instruments such as callipers, diameter tapes (*D*-tapes), range finders, forks and others possessing widely differing properties (e.g., accuracy, precision, cost, operation, simplicity etc.) [48]. Diameter at breast height (*dbh*) is the measurement of a standing trees' out-side-bark stem diameter at 1.3m above level ground and the two common dendrometers referred in this study include callipers and *D*-tapes [51,52]. Basically, a *D*-tape consists of a tape measure that wraps around the circumference (girth) of a tree with a calibrated scale in pi (π) cm units of a diameter (i.e.,1cm=3.14cm on the scale). *D*-tapes directly measure diameter on one side and often have standard length (equals the

circumference) on the other side of the tape while callipers measure the distance between parallel tangents of a closed convex region [48,51,52].

With *dbh* alone or in combination with other parameters such as *ht*, basal area, one is able to estimate volume, tree growing stock and more importantly biomass and carbon [33,51,52]. The parameter is also important for determination of size- frequency distributions in irregular structure stands
[51]; hence, *dbh* remains an indispensable parameter to the estimation AGB in Miombo woodlands of Malawi [34]. Under REDD+, callipers are recommended for measuring deadwood especially the one lying on the ground (Fig. 6, right bottom). However, due to other factors, they have been used interchangeably with *D-t*apes to measure *dbh* of standing trees of Miombo during field inventories in Malawi, thus regardless of the stem geometry (Fig. 8).

Some fine hardwood Miombo tree species stems of Malawi possess rugged outer-barks (Fig. 8). Besides, they may overhang or overlay on each other and even grow bigger than the size of calliper leading to errors when their dbh is measured using calliper in comparison to *D*-tape.

4. CONCLUSION

This study assessed, methods and operating procedures for estimating AGB estimation in Miombo Woodlands of Malawi for the past three decades. It has revealed significant gaps associated with (i) sampling design, (ii) sample plot configuration, (iii) allometry, and (iv) dendrometric measurements which were analysed using the ANOVA statistical package. Results indicate that employment of varied allometric equations significantly affected the AGB estimations ($P<0.001$) among the rest of the parameters followed by sampling plot unit configuration. However, the influence of the dendrometric measurements tool was minimal as no significant differences were observed on the use of either a *D*-tape or calliper in measuring *dbh* ($P>0.05$). The study recommends adoption of a circular sampling design of 20m radius, consistent use of *D*-tape in measuring *dbh*, and employment of local of allometry for AGB in Malawi's Miombo Woodlands. Incorporation of these changes is envisaged to facilitate not only smooth running of the Malawi's NFI system but also robust implementation and global recognition of the REDD+ efforts carried out. Besides working to the quick realisation of REDD+ carbon payments, the study advises that embracing the changes will ensure a swift means of advancing methodological framework for assessing and reporting C stock fluxes and GHG emissions, thus, from lower levels to Tier 3, thus indicative of high-level accuracy. The study also advocates integration of the current ground-based system with cost-effective remotely sensed EO such as free and open source, but high-resolution imagery from ALOS-PALSAR and SENTINEL 1 and 2 missions would go a long way in enhancing the accuracy of AGB estimations in Miombo Woodlands of Malawi. Finally, the study encourages further research on the effects of plot size/configuration as well as on the use of *D*-tape and calliper for measuring *dbh* in the Miombo Woodlands.

DATA AVAILABILITY

The data that support the findings of this study can be obtained from the corresponding author upon request.

ACKNOWLEDGEMENTS

The authors are thankful to the staff of Forestry Department Headquarters and Forestry Research Institute of Malawi (FRIM) for the provision of the data that was used in this study. A special mention goes to the officers who provided some of the field photos.

COMPETING INTERESTS

Authors have declared that no competing interests exist.

REFERENCES

1. Government of Malawi, The Second National Communication of the Republic of Malawi to the Conference of the Parties (COP) of the United Nations Framework Convention on Climate Change October, 2011; 2011.
2. Malawi Redd+ Programme, "Malawi REDD+ Readiness Program: Final Report on Carbon Inventory in Malawi's Forests Capacity to Support REDD+ and National Forest Inventory Activities,"; 2015.
3. Ministry of Forestry and Natural and Resources, "The Third National Communication of the Republic of Malawi to the Conference of the Parties (COP) of the United Nations Framework Convention on Climate Change (UNFCCC),"; 2020.
4. Government of Malawi, "Malawi National Forest Inventory 2018 Analysis Report,"; 2019.
5. Neeff T. A Roadmap for Developing Malawi's National Forest Monitoring System; 2015.
6. McGann M. Malawi REDD + Readiness Program: Land Use / Land Cover Technical Detail Final Report; 2015.

7. Skole DL et al. Direct measurement of forest degradation rates in Malawi: Toward a National Forest Monitoring System to Support REDD; 2021.
8. UNFCCC. Report on the technical assessment of the proposed forest reference level of Malawi submitted in 2019; 2021. [Online].
Available:http://unfccc.int/resource/docs/2014/tar/bra01.pdf
9. Petrokofsky G, et al. Comparison of methods for measuring and assessing carbon stocks and carbon stock changes in terrestrial carbon pools. How do the accuracy and precision of current methods compare? A systematic review protocol. Environmental Evidence. 2012;1(1): 1–21.
DOI: 10.1186/2047-2382-1-6
10. Shi L, Liu S. Methods of estimating forest biomass: A review. Biomass Volume Estimation and Valorization for Energy; 2017.
DOI: 10.5772/65733.
11. Chave J, et al. Improved allometric models to estimate the aboveground biomass of tropical trees. Global Change Biology. 2014;20(10): 3177–3190.
DOI: 10.1111/gcb.12629
12. [FAO] Food and Agriculture Organization of the United Nations, "Food and Agriculture Organization of the United Nations: Global Forest Resources Assessment 2020: Terms and Definition FRA," Global Forest Resources Assessment -Terms and Definitions. 2020;32.
Available:http://www.fao.org/forestry/58864/e n/
13. Gaucher C, Domingues-Hamdi É, Prin-Mathieu C, Menu P, Baudin-Creuza V. Good practice guidance for land use, land-use change and forestry. 2015;338(2).
DOI: 10.1016/j.crvi.2014.11.004
14. Novotný J, Navrátilová B, Janoutová R, Oulehle F, Homolová L. Influence of site-specific conditions on estimation of forest above ground biomass from airborne laser scanning. Forests. 2020;11(3):1–18.
DOI: 10.3390/f11030268.
15. Dixon RK, Brown S, Houghton RA, Solomon AM, Trexler MC, Wisniewski J. Carbon pools and flux of global forest ecosystems. Science. 1979;263(5144):185–190.
DOI: 10.1126/science.263.5144.185.
16. Goetz S, Dubayah R. Advances in remote sensing technology and implications for measuring and monitoring forest carbon stocks and change. Carbon Management. 2011;2(3): 231–244.
DOI: 10.4155/cmt.11.18
17. Bhattarai T, Skutsch M, Midmore D, Shrestha HL. Carbon measurement: An overview of forest carbon estimation methods and the role of geographical information system and remote sensing techniques for REDD+ implementation. Journal of Forest and Livelihood. 2016;13(1): 69–86.
DOI: 10.3126/jfl.v13i1.15367.
18. Iman Gerard FB, et al. Height-diameter allometry and above ground biomass in tropical montane forests: Insights from the Albertine Rift in Africa. Plos One. 2017;1–20.
19. Kachamba DJ. Biomass estimation models and methods for miombo woodlands of Malawi using field and remotely sensed data; 2016.
20. Kachamba DJ, Eid T, Gobakken T. Above- and belowground biomass models for trees in the miombo woodlands of Malawi. Forests. 2016; 7(2).
DOI: 10.3390/f7020038.
21. USAID PERFORM. Forest Inventory Report; 2017.
22. Haack B, Mahabir R, Kerkering J. Remote sensing-derived national land cover land use maps: A comparison for Malawi. Geocarto International. 2015;30(3):270–292.
DOI: 10.1080/10106049.2014.952355
23. Malawi Government, Malawi State of Environment and Outlook Report Environment for Sustainable Economic Growth; 2010.
24. Köhl M, Neupane PR, Mundhenk P. REDD+ measurement, reporting and verification – A cost trap? Implications for financing REDD+MRV costs by result-based payments. Ecological Economics. 2019;168:106513.
DOI: 10.1016/j.ecolecon.2019.106513
25. Petrokofsky G, et al. Comparison of methods for the measurement and assessment of carbon stocks and carbon stock changes in terrestrial carbon pools. Environmental Evidence. 2012; 1–21.
Available:https://environmentalevidencejournal.biomedcentral.com/articles/10.1186/2047- 2382-1-6
26. Sinha S, Jeganathan C, Sharma LK, Nathawat MS. A review of radar remote sensing for biomass estimation. International Journal of Environmental Science and Technology. 2015; 12(5):1779–1792.
DOI: 10.1007/s13762-015-0750-0.

27. Ryan CM, et al. Quantifying small-scale deforestation and forest degradation in African woodlands using radar imagery. Global Change Biology. 2012;18(1):243–257.

DOI: 10.1111/j.1365-2486.2011.02551.x.

28. The World Bank. Forest Carbon Partnership Facility Annual Report 2018; 2018.

29. Drigo R. Woodfuel Integrated Supply/Demand Overview Mapping (WISDOM) Malawi: Analysis of Woodfuel Demand, Supply, and Harvesting Sustainability. 2019;144. [Online].

Available:http://www.mbaula.org/wp-content/uploads/2019/09/PERFORM-WISDOM-Malawi-Draft-Final.pdf

30. Review Reviewed Work (s): A Preliminary silvicultural classification of Malawi. Forest Research Record No. 57 by Review by: C. E. Duff Source: The Commonwealth Forestry Review. 1979;58(3):177.

Published by: Com. 2022;58(57):3–5.

31. Makungwa S. Field results of the 2017 forest inventory of Dzalanyama Forest Reserve; 2017.

DOI: 10.1016/j knee.2017.11.005

32. Department of Forestry. Forest Resource Mapping Final Report for Implementation Phase; 2012.

33. Mueller A. Development of integrated monitoring systems for REDD + in the Southern African Development Community (SADC) Design of REDD MRV: SADC Field Inventory Manual – Draft; 2012.

34. Kachamba DJ, Ørka HO, Gobakken T, Eid T, Mwase W. Biomass estimation using 3D data from unmanned aerial vehicle imagery in a tropical woodland. Remote Sensing. 2016; 8(11):1–18.

DOI: 10.3390/rs8110968.

35. Ryan C, Williams M, Grace J. Above- and belowground carbon stocks in a Miombo woodland landscape of Mozambique. Biotropica. 43(4):423–432.

DOI: 10.1111/j.1744-7429.2010.00713.x.

36. Brown S, Gillespie AJR, Lugo AE. Biomass estimation methods for tropical forests with applications to forest inventory data. Forest Science. 1989;35(4):881–902.

37. Brown S. Estimating biomass and biomass change of tropical forests: A primer. (FAO Forestry Paper - 134).

Available:http://www.fao.org/docrep/w4095e/w4095e00 htm," FAO Forestry Paper 134, no. January 1997, pp. 1–4, 1997.

38. Chave J, et al. Tree allometry and improved estimation of carbon stocks and balance in tropical forests," Oecologia. 2005;145(1):87–99.

DOI: 10.1007/s00442-005-0100-x

39. Mugasha WA, et al. Allometric models for estimating tree volume and aboveground biomass in Lowland Forests of Tanzania. International Journal of Forestry Research; 2016.

DOI: 10.1155/2016/8076271.

40. Malata H, Ngulube ES, Missanjo E. Site specific stem volume models for *Pinus patula* and *Pinus oocarpa.* International Journal of Forestry Research; 2017.

DOI: 10.1155/2017/3981647

41. Makungwa SD, Chittock A, Skole DL, Kanyama-Phiri GY, Woodhouse IH. Allometry for biomass estimation in Jatropha trees planted as boundary hedge in farmers' fields. Forests. 2013;4(2):218–233.

DOI: 10.3390/f4020218

42. USAID Malawi, Estimating Carbon Stocks: Toward Forest Conservation in Mkuwazi Forest Reserve and Thazima of Nyika Park in Malawi; 2008.

43. Government of Malawi, The Second National Communication of the Republic of Malawi to the Conference of the Parties (COP) of the United Nations Framework Convention on Climate Change October; 2011.

44. Malawi Redd+ Programme. Malawi REDD+ Readiness Program: Final Report on Carbon Inventory in Malawi's Forests Capacity to Support REDD+ and National Forest Inventory Activities; 2015.

45. Ministry of Forestry and Natural and Resources. The Third National Communication of the Republic of Malawi to the Conference of the Parties (COP) of the United Nations Framework Convention on Climate Change (UNFCCC); 2020.

46. Government of Malawi. Malawi National Forest Inventory 2018 Analysis Report; 2019.

47. Neeff T. A roadmap for developing Malawi's national forest monitoring system; 2015.

48. McGann M. Malawi REDD + Readiness Program: Land Use / Land Cover Technical Detail Final Report; 2015.

49. Skole DL, et al. Direct measurement of forest degradation rates in Malawi: Toward a national forest monitoring system to support REDD; 2021.

50. UNFCCC. Report on the technical assessment of the proposed forest reference level of Malawi submitted in 2019; 2021. [Online]. Available:http://unfccc.int/resource/docs/2014/tar/bra01.pdf

51. Petrokofsky G, et al. Comparison of methods for measuring and assessing carbon stocks and carbon stock changes in terrestrial carbon pools. How do the accuracy and precision of current methods compare? A systematic review protocol. Environmental Evidence. 2012;1(1): 1–21.
DOI: 10.1186/2047-2382-1-6

52. Shi L, Liu S. Methods of Estimating forest biomass: A review. Biomass Volume Estimation and Valorization for Energy; 2017. DOI: 10.5772/65733.

APPENDIX VI: MODELLING ABOVE-GROUND BIOMASS USING MACHINE LEARNING ALGORITHM: CASE STUDY MIOMBO WOODLANDS OF MALAWI

Journal of Global Ecology and Environment

Volume 17, Issue 3, Page 1-15, 2023; Article no.JOGEE.11407
ISSN: 2454-2644

Modelling Above-ground Biomass Using Machine Learning Algorithm: Case Study Miombo Woodlands of Malawi

Henry Kadzuwa [a,b*] and Edward Missanjo [c]

[a] School of GeoSciences, The University of Edinburgh, C/O LG/1, Holyrood Court, Dumbiedykes Road, Edinburgh, EH8 8AN, UK.
[b] Department of Forestry Headquarters-Malawi, Nkhalango House, P.O. Box-30048, Lilongwe 3, Malawi.
[c] Department of Research, Malawi Assemblies of God University (MAGU), P.O. Box-184, Lilongwe, Malawi.

Authors' contributions

This work was carried out in collaboration between both authors. Author HK acquired both the ground and satellite imagery datasets, observed the variable selection bias in randomForest, set up and performed experiments, studied the sources of the selection bias, ran the functions, analysed the datasets and drafted the manuscript. Author EM contributed to the acquisition of the ground-datasets, design of the paper, theoretical investigations of the problem, validated the analysis and shaped the manuscript. Both authors read and approved the final manuscript.

Article Information

DOI: 10.56557/JOGEE/2023/v17i38178

Received: 21/01/2023 Accepted: 25/03/2023 Published: 30/03/2023

Original Research Article

ABSTRACT

Malawi's Miombo Woodlands provide critical wood products and ecosystem services, including carbon storage through above ground-biomass (AGB). However, accurate and efficient estimation of AGB and C remains a huge challenge due to the complexity of heterogeneous natural and anthropogenic environmental factors exacerbated by choice of data collection and analysis techniques. A study was conducted to explore the potential of Machine Learning (ML) algorithmic on modelling AGB in Malawi's Miombo Woodlands using remotely sensed data. A combination of

**Corresponding author: E-mail: h.h.n.Kadzuwa@sms.ed.ac.uk, henharkadzuwa@gmail.com;*

AGB field measurements and Sentinel 2 Multi-Spectral Instrument (S2 MSI) imagery, and environmental data were employed to train and evaluate the performance of Random Forest (RF) regression ML model, thus against the backdrop of traditional simple linear and multiple linear regression models used in the past. The *randomForest* package in Rstudio R-3.6.1 software was used to model the S2 median seasonal composite band imagery datasets acquired in 2019 over Ntchisi Forest. Results demonstrate an outstanding performance of the RF with Mean Decrease in Accuracy (MDA) importance of >80 acquired from the Green, Blue and Near-Infra-Red (NIR) bands of the post-rainy season imagery while the dry season scene registered a MDA importance of >52 obtained from the Red, Blue and NIR bands. These findings underscore the superiority of the RF, revealing its ability to model AGB using different spectral bands, and more importantly, in different seasons. The outcomes have also revealed the better accuracy that the RF render in generating AGB maps (providing a minimum range of 25-33 $tCha^{-1}$, which is in line with the ground reference estimates). Overall, the study has shown that RF Regression is a better technique to estimate AGB in Miombo Woodlands using the S2 MSI imagery under the given conditions. In conclusion, the research has further shown that the optical band combination of NIR and the Red regions of the Electro-Magnetic Spectrum are indispensable variables for successful modelling of AGB as well as delineating forest cover from non-forest attributes in the Miombo Woodlands. However, the study recommends exploring modelling the AGB using averaged vegetation indices i.e., NDVI, SAVI, and MSAVI, for robust results.

Keywords: Above-ground biomass (AGB); Miombo woodlands; algorithm; Sentinel-2 MSI; random forest; out-of-bag (OOB); Rstudio; Google Earth Engine (GEE); JavaScript; mean decrease in accuracy (MDA).

1. INTRODUCTION

Accurate and low-cost methods for estimating and modelling forest above-ground biomass (AGB) are critical for better understanding and monitoring of the tropical Miombo Woodlands which are under huge threat from anthropogenic activities, especially within the non-Annex-I REDD+ parties [1] of Southern Africa, Malawi inclusive. Malawi primarily relies on the traditional method of ground-based measurements for her AGB and carbon (C) estimates [1]. While measurement of tree biomass under this system may not require sophisticated technology; the datasets sampled might not be economically practical for broad- scale assessments, and worse-still, not comprehensively representative of the study site spatially, due to the system's limitation of access to fragile areas such as cliffs, peaks and ridges that pose danger to human life [2,3]. This inarguably, renders key advantage to remote sensing technology (*ibid*), which is often regarded as the icing on the biomass estimations' cake.

Availability of free and open/unrestricted imagery from LandSat, and currently Sentinel-1 and 2, and ALOS–PALSAR-2 satellite missions provides the leverage for advancing the global mechanism on Reducing Emissions from Deforestation and forest Degradation (REDD+), not only as a low-cost means, but with enhanced accuracy as well. Malawi has been conducting a series of site-based AGB estimations in its Miombo Woodlands, largely under the global REDD+ umbrella [1,4]. Nevertheless, the choice of accurate, but, cost-effective remote sensing methods has never been adequately addressed, an area that poses a key problem to the Least Developed Countries (LDCs) where financial backstopping remains the major constraint [5,6].

Worse-still, Miombo Woodlands are characterised by a plethora of intertwined challenges associated with their morphology, seasonality, and the interplay of anthropogenic disturbances that include forest fire and wood harvesting which cumulatively render difficulties to correctly estimate and map AGB [2,7,8]. Despite these *rarae-avis,* the unrestricted medium-resolution Sentinel-2 Multi-Spectral Instrument (MSI) imagery datasets and the ground measurements have not yet been modelled for AGB in these woodlands of Malawi, at least to the best of the authors' knowledge. Paradoxically, mapping of land cover and AGB estimations of Malawi's Miombo Woodlands has been associated with significant inconsistences

[1] *Non-Annex I partners are developing countries that do not have legally binding greenhouse gas emissions reductions targets under the Kyoto Protocol.*

and inaccuracies that compromise biomass results and C quantifications [1,9,10].

In spite of the cost implications, the accuracy challenges and the method inconsistencies associated with the reliance on the ground-based system for measuring biomass; no study has attempted to explore and/or enhance the accuracy associated with AGB estimates through either modelling and/or evaluating the performance aligned with the Random Forest Machine Learning algorithm using low-cost remotely sensed Earth Observations in Malawi's Miombo Woodlands.

While a study on biomass estimation using 3D data from unmanned aerial vehicle imagery in a Tropical Woodland of Malawi was key in introducing the need for exploring statistical regression methods for modelling AGB [2]; unfortunately, no further research has endeavoured to examine the performance of Machine Learning (ML) algorithms i.e., Decision Tree and Random Forest in modelling AGB of Malawi's rugged Miombo woodlands, despite the well-known record of rendering improved accuracy [5,11,12]. Hence, against such a backdrop, it was of interest for this study to; (i) model tree AGB (computed from ground measurements) using unrestricted Sentinel-2 imagery acquired over Miombo Woodlands, and (ii) explore the accuracy of the Random Forest (RF) Regression Machine Learning technique in the Miombo Woodlands of Malawi.

2. MATERIALS AND METHODS

2.1 Study Site

The study was conducted in Ntchisi Forest, a reserve declared as one of Malawi's protected areas in 1924. The forest is located in a central district named Ntchisi (Latitude, -13.3205 E and Longitude, 34.0419 S), ~96km to the north-west of Lilongwe, the capital city of Malawi. The reserve is predominantly a Miombo Woodland covering 9,720ha. It stretches on undulating mountainous terrain with an altitudinal range of 600-1675m above sea level. Due to the rugged nature of its terrain, it is difficult to physical access every part of the forest. This arguably contributes to its improved conservation as depicted by its relatively high mean AGB (45tCha^{-1}) compared to those of Liwonde (35tCha^{-1}) and Perekezi (42tCha^{-1}) Forest managed for the REDD+ purposes as well [13].

The site experiences a humid subtropical climate that is characterised by alternating dry-winter and hot-summer seasons with annual temperature range of 19-25^{0}C and rainfall range of 1200- 400mm per annum. Soils within the forest are typically a mixture of poor sand and blackish- loam, localised within the *Brachystegia* and *Montane* dominated areas of the reserve, respectively. Administratively, the management regime of the forest falls under co-management arrangement whereby; the roles and responsibilities of governing the forest are shared between the Central Government of Malawi through the Department of Forestry (DoF) and the villages surrounding the forest. These villages include those within the jurisdiction of Traditional Authorities; Vuso Jere, Kasakula and Nthondo. Currently, the forest serves as a pilot study area for the REDD+ mechanism [13].

2.2 Data Collection

Data for the study was two-fold, *vis-a-vis;* ground-based individual tree level parametric measurements, out of which AGB was computed, and the median seasonal Sentinel-2 MSI imagery acquired from Google Earth Engine (GEE) online platform. The GEE uses *JavaScript* Application Programming Interface (API) which enables two programming languages (software) components to communicate with each other using a set of definitions and protocols [14]. In this study, the API enabled the *JavaScript* to communicate with *RStudio* used in analysing the datasets.

2.2.1 Sampling Design and Collection of Ground-based Measurements

Ground-based measurements were conducted from 17-21 September 2019. The key variables and parameters measured include;

i. Individual tree diameter at breast height (*dbh*),
ii. Total tree height (*ht*),
iii. Crown diameter (*max.* and *min.*),
iv. Tree botanical names (species),
v. Tree *xy* coordinates,
vi. Plot centre *xy* coordinates (centroids),
vii. Bearing (in degrees) of each tree from the centre, and,
viii. Horizontal distance of each tree from the centre.

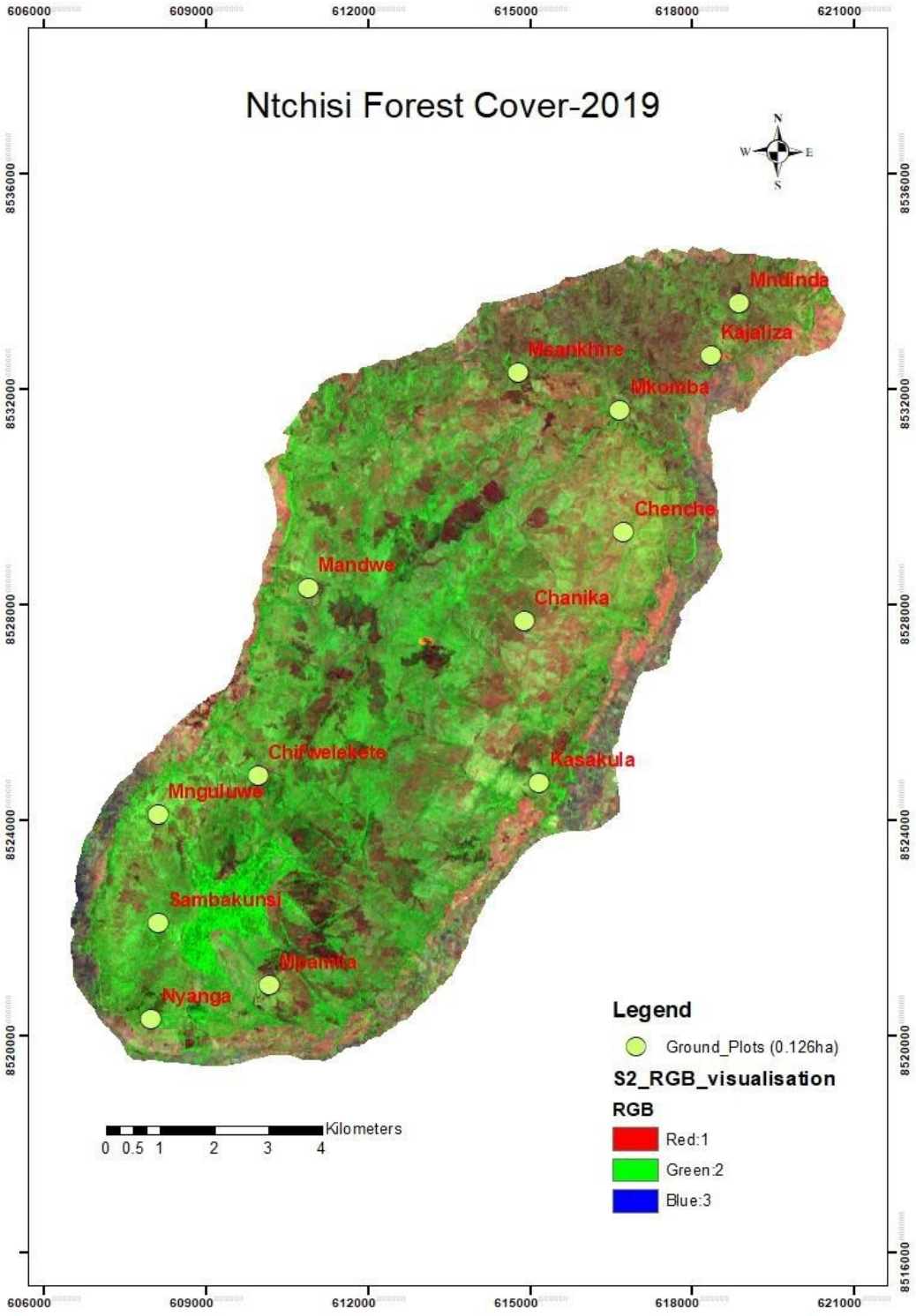

Fig. 1. Map of Ntchisi reserve (study site) showing (i) 2019 forest cover displayed in Sentinel-2 imagery red, green, blue (RGB) visualisation, and (ii) ground-sampling plot units (0.126ha or 20m radius) distribution denoted by circles

Ground data collection inherited permanent sample plots (PSPs) established following a multi-stage sampling design which integrated stratified and random sampling techniques during the 2016 Malawi REDD+ site-based inventory [1,13]. The stratified sampling phase incorporated forest management units demarcated to cover forest management blocks that each of the 13 villages surrounding Ntchisi Forest holds as management stake, thus, under co-management arrangement with the DoF [15,16]. The sampling plot units were named after each of the villages (Fig. 1). This was followed by a systematic random sampling phase: whereby sampling unit plots were computed at a minimum spacing of 90-meter square grids (network) covering the entire reserve. The network generated a minimum of 13 randomly sampled points that became plot centroids of 20metre radius circles (0.126ha) (Fig. 1), sufficient to attain a Confidence Level (CL) of 95% with a precision of 10% error [13,16]. At each sample plot, a four fixed concentric circular plot design bearing 2m, 6m, 12m and 20 m radius each, respectively, was inventoried (Table 1 and Fig. 2).

For each tree measured, its code was documented using a species list catalogue provided by the Forestry Research Institute of Malawi. The species were decoded to their full botanic names prior to transferring all records into Microsoft-excel data sheets. The data were converted to *CSV* format and exported to Rstudio R-3.6.1, for statistical computing and graphics.

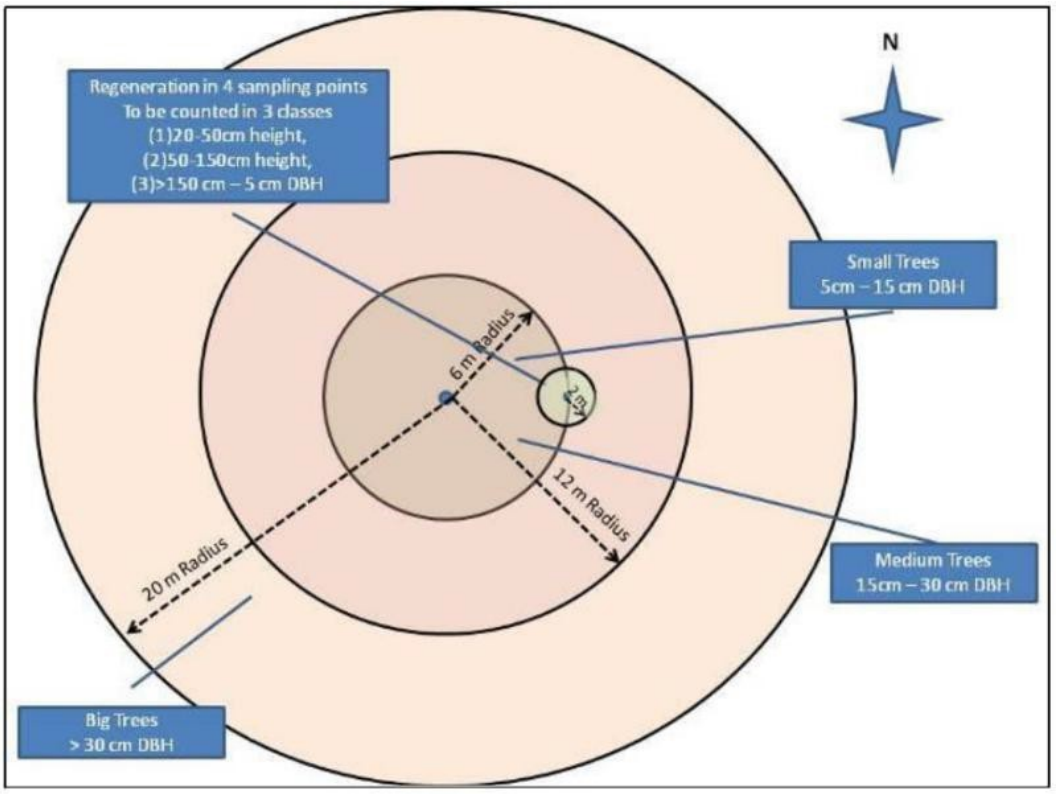

Fig. 2. Concentric ground-based sampling plot unit design used in Ntchisi Forest during 2019 inventory that sampled 13 plots at 95% Confidence Interval and 10% precision error

Table 1. Dimensions and threshold for ground plot measurements

	Dimensional Threshold		
Subplot	**Radius (m)**	**Area (m^2)**	***dbh* (cm)**
Regeneration	2m	0.001ha	<5cm
Small	6m	0.011ha	5-14.9cm
Medium	12m	0.045ha	15-29.9cm
Large	20m	0.126ha	≥30cm

2.2.2 AGB computations

Using a threshold of *dbh* ≥5cm, a total number of 216 individual trees (observations) were measured from the entire 13 PSPs, i.e., *n=216* were used for AGB calculations. Prior to the calculations, a scaling factor (*SF*) was applied to scale up dimension (area) values for each subplot and convey estimates of C stock on a hectare basis. The step involved conversion of the subplot area unit measurements in squared meters (m^2) to a per hectare (1ha) basis as follows;

SF= 10,000/NA

where;

SF = *Scaling Factor* to convert per hectare basis (dimensionless),
10,000 = number of squared meters (m^2) in one hectare, and
NA= horizontal projected area of nested plot (in m^2).

Computation of AGB involved the two sets of the local AGB allometry specifically tested and developed for Malawi's Miombo trees and published by [2]. Between the two, one employs both height and diameter at breast height (dbh) while the other factors-in dbh only [13,17]. This study preferred the later, due to its capability of yielding higher accuracy [13,17], indicated below;

$AGB = 0.21691 \times dbh^{2.318391}$ [17 ,18]
where;

AGB = above-ground biomass in kilograms of dry matter (kg.d.m.)
dbh = diameter at breast height in centimetres (cm)
h = total tree height in metres (m) taken at breast height (vertical height of 1.3m)

A carbon fraction of 0.47 for the entire individual Miombo tree species was used to calculate C from kilograms of dry matter (kg.d.m.) otherwise referred to as biomass [13].

2.3 Sentinel-2 Imagery Acquisition and Preprocessing

Optical median seasonal composite Sentinel-2 MSI 2019 imagery from GEE platform were acquired over Ntchisi Forest Reserve in July 2021. Preference of the datasets, notwithstanding being free and open (unrestricted), was due to its imaging sensors' red-edge (RE) of the Near-InfraRed (NIR) window that is used to detect vegetation at moderate spectral resolution of 10-20 m (Table 2).

The NIR red-edge spectral region is located in the sharp change of canopy reflectance range between 680nm and 750nm where a slope occurs, providing an advantage to mapping vegetation [19], forest AGB inclusive. The RE band has low reflectance over vegetation canopy due to its strong absorption of chlorophyll rendering a high correlation with various physiological vegetation parameters, such as nitrogen and eventually biomass [19]. It offers the RE the significant verge for describing the status of plant pigments and health.

Using GEE online platform, the Ntchisi Forest Reserve perimeter boundary layer was imported and overlaid on Sentinel-2 (S2) imagery to define the domain of interest. This was followed by cloud masking the imagery using '*maskS2clouds*' function contained in the '*ggplot2*' library, a process which subtracts the contribution of the atmosphere from the signal at the satellite to obtain desirable radiance that is used for further analysis [8,20].

The next step involved image filtering using cloud-pixel percentage and seasonal dates as threshold i.e.; post-rainy season covering the period 1 April to 30 June 2019 and the dry season from 1 July to 30 October 2019, respectively. Dual seasonal datasets were preferred to mono seasonal imagery because the former provide the leverage to discriminate and account for the seasonality and phenology changes, attributes which characterise the deciduous formations of Miombo trees' spectral reflectance behaviour [8].

The subsequent phase involved selection of the 10 desirable spectral bands (B2, B3, B4, B5, B6, B7, B8, B8A, B11 and B12) covering both the post-rainy and dry seasons. The study excluded the spectral band 1 (B1) because this coastal aerosol channel (Table 2) is better at estimating suspended sediment in water, an attribute which was not of interest for this research. The 10 bands selected largely comprise the RE, NIR and the Short-Wave Infrared (SWIR). The preference for the RE region is due to its capability of being more sensitive to vegetation [19,21] which is vital for this study's AGB estimations in the Miombo Woodlands. As afore-mentioned, the NIR red

edge renders high correlation with various physiological vegetation parameters, such as nitrogen, and eventually biomass [19] which forms the gist of this study.

Conversely, the SWIR preference was due to its capabilities of; being negatively correlated to water content, but indispensably better at detecting newly burnt land, features that reflect highly in these channels [22]. These contrasting artefacts remain ideal for mapping and modelling the Miombo Woodlands (trees) during the both the wet and dry seasons [5,23]. This in order to efficiently detect the effect fire and loss of trees in relation to AGB during the dry period, in contrast to the effect the abundant moisture and the leaf-on conditions that typify the wet season and affect AGB modelling as well [5,23].

The final product of this stage was generation of the S2 median composite imagery which was clipped using the boundary layer of Ntchisi Forest Reserve. The composite images were exported into a GEE repository (Google-drive) in the spatial reference WGS84 UTM Zone 36S coordinate system. The S2 imagery were separately uploaded as layer stacks in QGIS
3.10. They were further inspected for proper overlay with the ground-based data layer prior to exploratory data analysis and statistical modelling.

2.4 Modelling AGB Using Random Forest Algorithm

Recent studies have shown that biomass estimation and modelling using remotely sensed data is usually done using either parametric approaches (i.e., regression-based models, such as multiple linear regression) or non-parametric techniques, such as K-nearest neighbor (K-NN), Artificial Neural Network (ANN), Regression Tree, RF, Support Vector Machine (SVM) and Maximum Entropy (MaxEnt), among others [24– 27]. While most of these are well-known for their;
(i) nature of being independent to the effects of normal distribution assumptions, (ii) sensitivity to outliers, and (iii) its ability to quantify input variables into measures of importance, the RF Regression analysis was preferred for this study primarily, but, not exclusively for its ability to automatically balance datasets when a class is more infrequent than others in the observations [25–27]. It was further advantageous to employ the RF model due to its capability of limiting the over-fitting attribute that is managed by aggregating many decision trees, thereby enhancing accuracy (minimising error bias) [*ibid*].

2.4.1 Development and evaluation of random forest regression model

Exploratory data analysis: The Random Forest Regression model was run using *randomForest* package (loaded from the *randomForest* library in Rstudio R-3.6.1 software [28]. The data set were partitioned into 60% and 40% as training (loaded from the *random Forest* library) and validation subsets, respectively [20,28]. The process was trailed by an exploratory data analysis (EDA) as depicted in the whisker and box plots (Figs. 3 and 4).

2.5 Model Parameters Optimisation

2.5.1 Tuning parameters

A pre-defined value of 27 was set as the initial random number of seed to generate a sequence of repeatable results. According to [18], the pinnacle of model development rests in its parameters, elements that constitute the engine room of the model. The process critically involves discovering the best combination of parameters to optimally run the model while minimising errors. In this RF Regression analysis model, the *ntree/fitcontrol* and *mtry* tuning parameters were engaged [20,28]. The *ntree* controls number of trees to grow in a model. In this study it was achieved by subjecting the model to '*fitcontrol*' that applied the train control method using the *repeatedcv package* embedded in the caret libray [20,28]. The step involved 5 repeats of 5- fold cross-validation, implying that training dataset were randomly divided into 5 parts and used each of the 5 parts as testing dataset. The *mtry* controls number of predictor variables randomly sampled as candidates at each split [*ibid*].

The RF regression model generated a data frame comprising of 216 individual trees that were randomly distributed across Ntchisi Forest Reserve (following the ground PSP design) from which AGB computations were based. In total there were 11variables comprising of ten S2 imagery band predictor variables and AGB as the eleventh and response one. The RF algorithm employed regression and RMSE techniques to select the optimal model using the smallest value out of which 2 (*mtry*) was the final one available for splitting at each tree node. The number of trees tried randomly was 500 (*n=500*) [20,28]. This yielded a MSE of 50320.31 and a percentage Var explained of 3.03 for the post– rainy season dataset and 50705.61 and percentage Var explained of 2.29 for the dry season.

Table 2. Sentinel-2 MSI spectral and spatial resolution

SENTINEL-2A MSI			
Band	**Spectral Region**	**Wavelength Range (nm)**	**Spatial Resolution (m)**
B1	Coastal aerosols	443	60
B2	Blue	458-523	10
B3	Green peak	543-578	10
B4	Red	650-680	10
B5	Vegetation Red Edge	698-713	20
B6	Vegetation Red Edge	733-748	20
B7	Vegetation Red Edge	773-793	20
B8	NIR	785-899	10
B8A	NIR (Vegetation Red Edge)/narrow	855-875	20
B11	SWIR	1565-1655	20
B12	SWIR	2100-2280	20

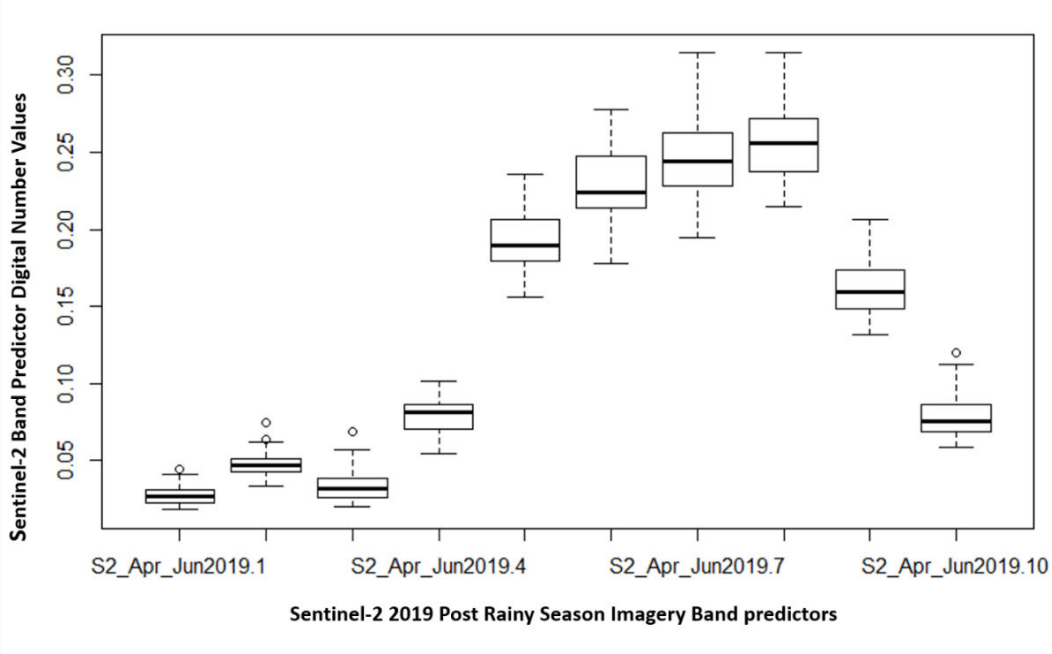

Fig. 3. Sentinel-2 MSI imagery for post-rainy season acquired over Ntchisi Forest. The X variables are Sentinel-2 imagery band (predictors) for post-rainy season (for the period 01April to 30June 2019), denoted as (S2-Apr_Jun2019.1 to S2_Apr_Jun2019.10). They represent the following bands; B2, B3, B4, B5, B6, B7, B8, B8A, B11 and B12, respectively. The Y (response) variable is the Digital Number (DN) band value(s) correlating to AGB stock

2.6 Variable Importance

Variable Importance technique was employed after training the RF algorithm to enhance the understanding of the contribution of each variable in the model. The process intuitively invokes variables that have the most predictive power. It is based on experiments on out-of-bag (OOB) samples, via destroying the predictive power of a feature without changing its marginal distribution [28,29]. The OOB error is the average error for each feature calculated using predictions from the trees that do not contain in their respective bootstrap sample [29]. This allows the *RandomForestClassifier* to be fit and validated whilst being trained. Hence, the OOB sample data are used to evaluate performance, while the importance measures are computed based on the proportion between misclassifications and the OOB sample [28].

The Variable Importance technique is derived from two measures; the first bases on accuracy level of model predictions that decreases when one variable value is permuted (excluded) between instances, otherwise, known as the

mean decrease in accuracy (MDA) [30]. The process is further categorised into outcome classes i.e., the larger the MDA, the more the variable contributes to the accuracy of the model [31]. The second bases its measure on the decrease of *Gini* impurity when a variable is chosen to split a node. The implication, therefore, is that variables with high importance drive the outcome and consequently, their values bear significant impact on the outcome values. Conversely, the variables with low importance might be omitted, thereby, rendering it simpler and faster to fit and predict a model.

3. RESULTS AND DISCUSSION

3.1 Forest Masks/Band Contribution

Generally, forests are distinguished by both low Near-Infrared Radiation (NIR) and Red-edge values [32]. The contribution of different S2-band parameters to the AGB model is shown in Figs. 5 and 6 for this study. For both the post- rainy and dry seasons, the NIR infrared (B8) and NIR-vegetation red edge (B8A) have emerged the most important input variables for delineating the forest cover distribution and determining the AGB with Digital Number (DN) maximum value of
50. This can be attributed to the spectral reflectance behaviour of the Miombo forest cover (trees) in both seasons which has high values in the NIR and, RED and relatively high in the Red- edge channels of S2 imagery, as these parameters contribute the most in forest biomass recognition.

This is further explained by the fact that vegetation spectral reflectance in the visible window of the Electromagnetic Spectrum (EMS) is based on chlorophyll and water absorption in the leaves [19,21,33]. Hence; under normal circumstances, healthy tree leaves absorb Red and Blue bands and thereby leaving the Green band to scatter and reflect highly [21]. However, for the post-rainy season the magnitude of the Vegetation Red-Edge (B5, B6 and B7) is also significantly apparent in delineating forest cover and determining AGB of Ntchisi Forest. This can be attributed to the fact that during the post-rainy season (which technically comes immediately after the rains stopped and coincides with winter in Malawi) the Miombo tree species still have leaves on (had green leaves) whereas other lower vegetation such as grasses have theirs withered, thereby giving a clear spectral distinction between the trees and other non-tree features and consequently providing a relatively normal reflectance.

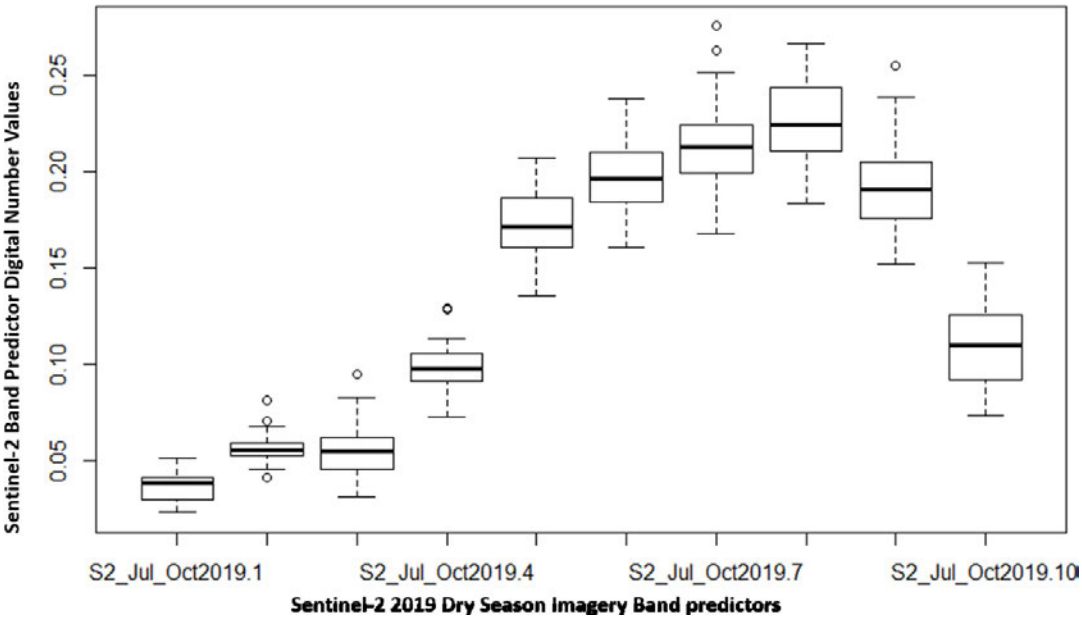

Fig. 4. Sentinel-2 MSI imagery for dry season acquired over Ntchisi Forest. The X variables are Sentinel-2 imagery band (predictors) for dry season (for the period 1 July - 30 October 2019), denoted as (S2-Jul_Oct2019.1 to S2_Jul_Oct2019.10). They represent the following bands; B2, B3, B4, B5, B6, B7, B8, B8A, B11 and B12 respectively. Similarly, the Y (response) variable is the Digital Number (DN) band value(s) correlating to AGB stock

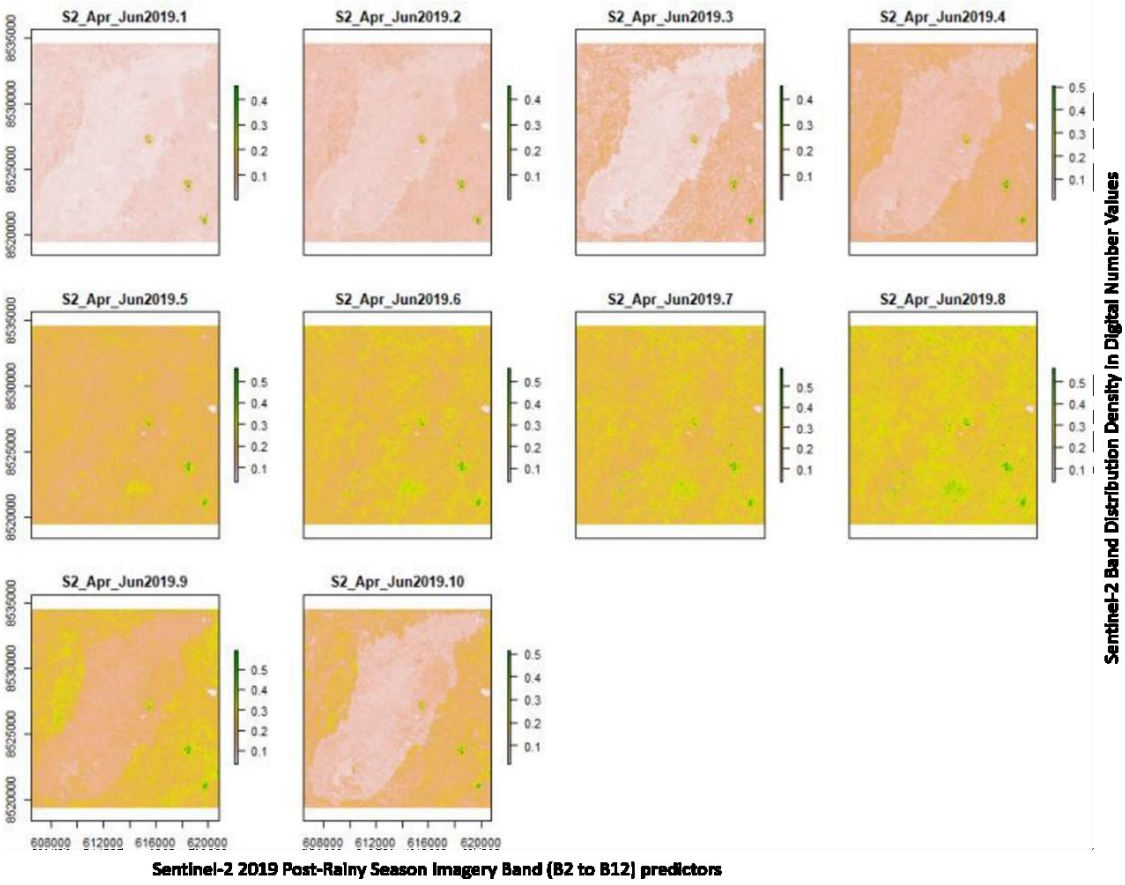

Fig. 5. Ntchisi Forest Band Distribution Density (in Digital Number values) for Post-Rainy Season (S2 imagery covering 2ndApril to 30th June 2019). (S2-Apr_Jun2019.1 to S2_Apr_Jun2019.10 =B2, B3, B4, B5, B6, B7, B8, B8A, B11 and B12)

Differently, the effect of dry season on spectral reflectance is conspicuously depicted in the magnitude range of 0.05-0.04 DN values for B2-B8A (Fig. 6) which ranged between 0.1-0.5 for the same bands during the post rainy season. The relatively lower spectral reflectance in the dry season of Miombo Woodlands is characterised by the hot season and fires [34,35], attributes which correspondingly resulted to less chlorophyll and water absorption. These phenomena simultaneously increased water loss, thus signifying unhealthy conditions that contributed to slightly enhanced scattering in the Blue band (B2) which registered the lowest range (0.05-0.2) during the dry season. This could be ascribable also to the fact that the 2019 dry season (1st July-30th October) registered one of the extreme weather conditions (hottest and driest) in Malawi, attained its peak in October when the mean daily temperatures ranged from
29.2°C to 42.1°C [24]. In Southern Africa Tropics, Miombo Woodlands inclusive, dry periods lead to an additional decrease in surface moisture that affects all land cover classes [36].

A study on Miombo Woodlands of Malawi observed that any changes in moisture pattern i.e., early rains or late rains, reduced or prolonged dry season are likely to affect reflectance pattern in [37]. The extreme heat and dry condition must have affected the surface moisture of the tree biomass reflectance below the required threshold in the dry season. It is, therefore, not a surprise that several studies have recommended the use of averaged Vegetation Indices (VI) for detailed investigations of the seasonal trends of forests that involve retrieval of vegetation cover and reflectivity [27,38,39]. These include, but are not limited to Normalised Difference Vegetation Index (NDVI), Enhanced Vegetation Index (EVI), SAVI (Soil-Adjusted Vegetation Index) and MSAVI (Modified Soil-Adjusted Vegetation Index).

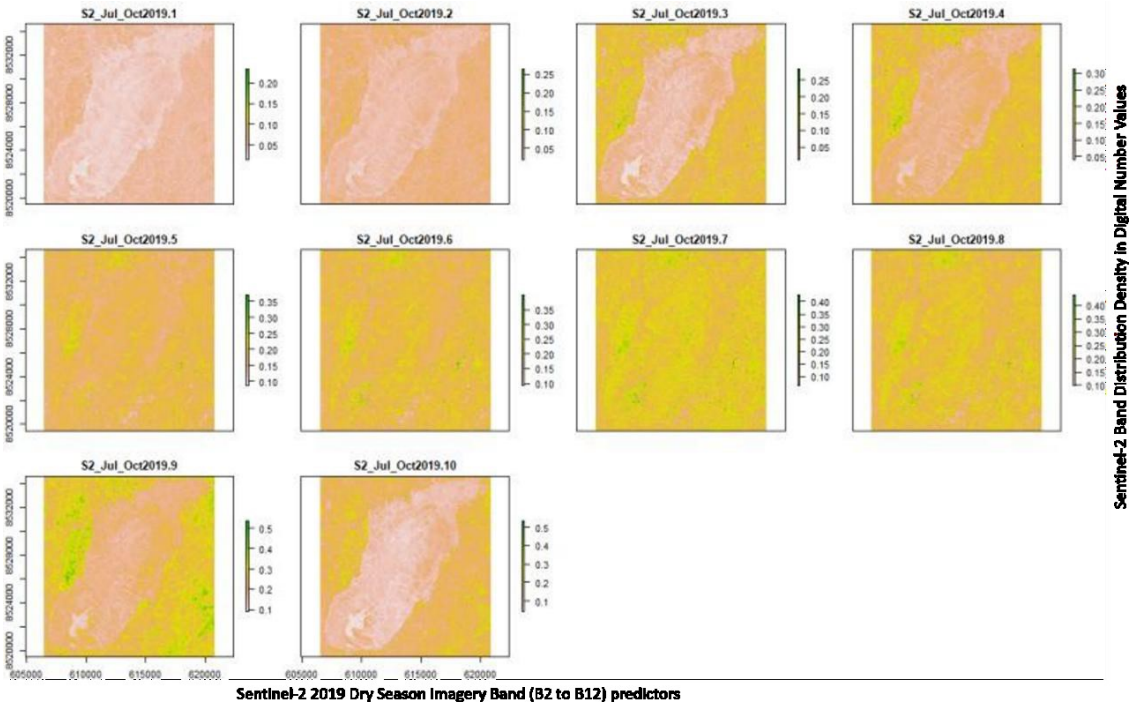

Fig. 6. Ntchisi Forest Band Distribution Density (in Digital Number values) for Dry Season (S2 imagery covering 1st July to 30th October 2019). (S2-July_Oct2019.1 to S2_July_Oct2019.10 =B2, B3, B4, B5, B6, B7, B8, B8A, B11 and B12)

Fig. 7. Dry Season attributes affecting AGB modelling in Ntchisi Forest: (Top-left) Tree leaf-off condition and (Top-right) rock outcrop during ground survey. (Bottom-left) Forest fire (burnt area) and (Bottom-right) rock outcrop depicted from aerial orthomosaics

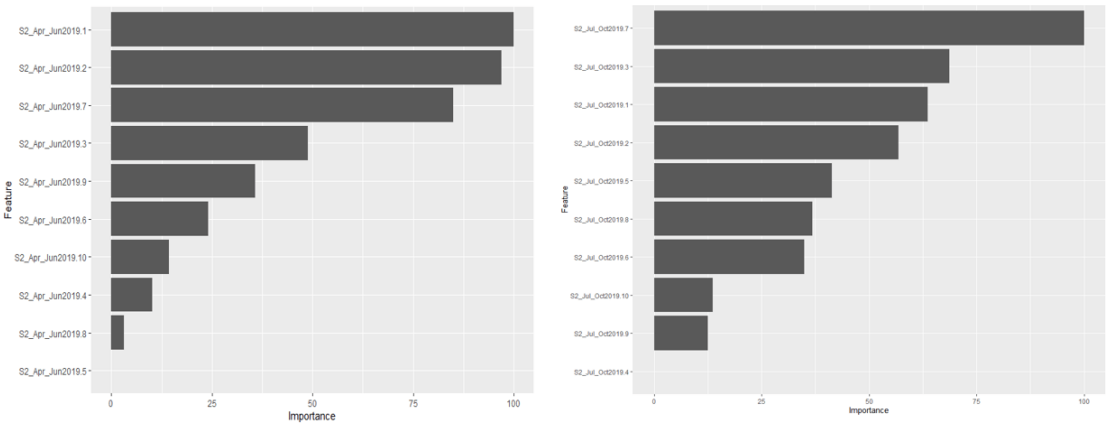

Fig. 8. Random forest variable importance for post-rainy season (left) and dry season (right)

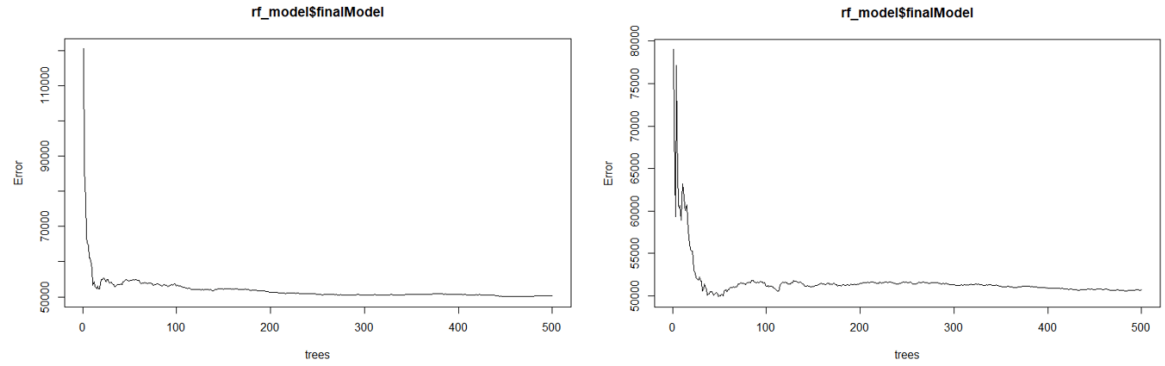

Fig. 9. Random forest final model performance for post-rainy season (left) and dry season (right)

3.2 Performance of RF Classifier for Ntchisi Forest Cover Classification

Summary of the performance of RF Classifier is depicted in Fig. 9. For both seasons, the RF regression algorithm optimal final RMSE value selected for the model (*mtry*) for splitting at each tree node was 2 while the number of trees tried randomly was 500 [20,28]. Through Variable Importance techniques the study analysed the relative importance of the contribution of the most important band variables for estimating AGB in two seasons. The greatest contributions (MDA >80) for the post-rainy season (between 01April and 30June 2019) were derived from the following 3 bands; Blue (S2-Apr_Jun2019.1), Green (S2-Apr_Jun2019.2), and NIR (S2- Apr_Jun2019.7). For the dry season (between 01 July and 30 October 2019), the highest contributions (MDA >52) originated from the following 3 bands; (i) NIR (S2-July_Oct2019.7), Red (S2-July_Oct2019.3), and Blue (S2-July_Oct 2019.1), respectively. As afore-mentioned, the trend observed confirms the importance of the NIR bands in AGB mapping. It further underscores the importance of dual or multi- seasonal datasets as opposed to mono-seasonal ones in understanding AGB estimations, given the rugged terrain, complex seasonal and morphological aspects of Miombo forest vegetation in the study area.

The >80 and >52 MDA difference values observed in the post-rainy and dry seasons can be attributed to the leaf-on and leaf-off conditions experienced in the two different seasons, respectively. Overall, these results show the effectiveness of the RF regression, i.e., its ability to model AGB using different spectral and seasonal spatial variables during the classification.

The results further indicate that during the post-rainy season, the AGB ranged from 25-78t*C*ha^{-1}. On the other hand, the range for the dry season was 33-82t*C*ha^{-1}. The results for 2016 REDD+ terrestrial inventory conducted in the same forest

estimated a mean AGB of 45tCha^{-1} with a standard deviation of 19.4tCha^{-1} [13]. Therefore, the AGB estimates/results obtained from the *Randomforest* model for this current study agree with the expected stocks assessed and projected during the 2016 ground-based inventory [13]. However, the interplay of forest fire and wood harvesting (poles, firewood, timber, medicine and charcoal making) characterise the study area as well [9,40,41]. These anthropogenic activities can be attributed to the differences observed in the mean AGB stock estimated in this study and the one estimated during 2016 inventory.

4. CONCLUSIONS

The study has revealed that RF Regression model Machine Learning technique is an effective method for estimating and modelling AGB in the rugged terrain Miombo Woodlands of Malawi. It has underlined the importance of Near- Infra-Red and the Red regions of the EMS for successful modelling of AGB as well as delineating forest cover from non-forest attributes in the Woodlands, under the given conditions**.** Furthermore, the RF model has produced AGB maps whose minimum estimates agree with the previous terrestrial findings, thereby underscoring its accuracy. However, the study recommends modelling and mapping of AGB using averaged VIs that includes, but are not limited to NDVI, SAVI, and MSAVI, for robust results.

DATA AVAILABILITY STATEMENT

The datasets supporting the findings of this study can be obtained from the corresponding author upon request.

ACKNOWLEDGEMENTS

The first author was funded under the Commonwealth Scholarship Scheme for a PhD programme at the University of Edinburgh, School of GeoSciences in the United Kingdom.

COMPETING INTERESTS

Authors have declared that no competing interests exist.

REFERENCES

1. Government of Malawi. Malawi national forest inventory 2018 analysis report; 2019.
2. Kachamba DJ, Ørka HO, Gobakken T, Eid T, Mwase W. Biomass estimation using 3D data from unmanned aerial vehicle imagery in a tropical woodland. Remote Sens. 2016;8(11):1-18.
DOI: 10.3390/rs8110968.
3. Kumar L, Mutanga O. Remote sensing of above-ground biomass. Remote Sens. 2017;9(9):1-8. DOI: 10.3390/rs9090935.
4. Malawi redd+ programme. Malawi REDD+ Readiness Program: final Report on Carbon Inventory in Malawi's Forests Capacity to Support REDD+ and National forest Inventory Activities; 2015.
5. Kamusoko C, Gamba J, Murakami H. Mapping woodland cover in the Miombo ecosystem: A comparison of machine learning classifiers. Land. 2014;3(2):524-40. doi: 10.3390/land3020524.
6. Neeff T. A road map for developing malawi's national forest monitoring system; 2015.
7. Halperin J, LeMay V, Chidumayo E, Verchot L, Marshall P. Model-based estimation of above-ground biomass in the miombo ecoregion of Zambia. Forest Ecosyst. 2016;3(1):1-17.
DOI: 10.1186/s40663-016-0077-4
8. Kamusoko C, Gamba J, Murakami H. Mapping woodland cover in the Miombo ecosystem: A comparison of machine learning classifiers. Land. 2014;3(2):524-40.
DOI: 10.3390/land3020524
9. Chinangwa L, Pullin AS, Hockley N. Livelihoods and welfare impacts of forest comanagement. Int J For Res. 2016;2016:1-12.
DOI: 10.1155/2016/5847068
10. Haack B, Mahabir R, Kerkering J. Remote sensing-derived national land cover land use maps: a comparison for Malawi. Geocarto Int. 2015;30(3):270-92.
DOI: 10.1080/10106049.2014.952355
11. Kamusoko C. Remote sensing: image analysis image classification. 2019;52.
12. Pandit S, Tsuyuki S, Dube T. Estimating above-ground biomass in sub-tropical buffer zone community forests, Nepal, using Sentinel 2 data. Remote Sens. 2018;10(4).
DOI: 10.3390/rs10040601
13. USAID, PERFORM. Forest Inventory Report; 2017.
14. Benzell SG, Van Alstyne MW. The role of APIs in firm performance. SSRN Electron J. 2016(November).
DOI: 10.2139/ssrn.2843326
15. Chidumayo EN. Changes in miombo woodland structure under different land

tenure and use systems in central Zambia. J Biogeography. 2002;29(12):1619-26.
DOI: 10.1046/j.1365-2699.2002.00794.x

16. Davis MJ. Contrast coding in multiple regression analysis: strengths, weaknesses, and utility of popular coding structures. J Data Sci. 2021;8(1):61-73. DOI: 10.6339/JDS.2010.08(1).563
17. Kachamba DJ, Eid T, Gobakken T. Above- and belowground biomass models for trees in the miombo woodlands of Malawi. Forests. 2016;7(2).

DOI: 10.3390/f7020038

18. Kachamba DJ. Biomass estimation models and methods for miombo woodlands of Malawi using field and remotely sensed data; 2016.
19. Wang B, Jia K, Liang S, Xie X, Wei X, Zhao X et al. Assessment of Sentinel-2 MSI spectral band reflectances for estimating fractional vegetation cover. Remote Sens. 2018;10(12):1-21. DOI: 10.3390/rs10121927
20. Kamusoko C. Explainable machine learning for land cover classification: An introductory guide. 2019;1:105-12.
21. Wang Y, Zhang X, Guo Z. Estimation of tree height and aboveground biomass of coniferous forests in North China using stereo ZY-3, multispectral Sentinel-2, and DEM data. Ecol Indic. 2021;126:107645-. DOI: 10.1016/j.ecolind.2021.107645
22. Benseghir L, Bachari NEI. Shortwave infrared vegetation index-based modelling for aboveground vegetation biomass assessment in the arid steppes of Algeria. Afr J Range Forage Sci. 2021;38(4):281-90.

DOI: 10.2989/10220119.2021.1882575.

23. Chidumayo EN. Climate and phenology of savanna vegetation in Southern Africa. J Veg Sci. 2001;12(3):347.

DOI: 10.2307/3236848

24. Kachamba DJ, Ørka HO, Gobakken T, Eid T, Mwase W. Biomass estimation using 3D data from unmanned aerial vehicle imagery in a tropical woodland. Remote Sens. 2016;8(11):1-18.

DOI: 10.3390/rs8110968.

25. Li Y, Li M, Li C, Liu Z. Forest aboveground biomass estimation using Landsat 8 and Sentinel-1A data with machine learning algorithms. Sci Rep. 2020;10(1):9952. DOI: 10.1038/s41598-020-67024-3, PMID 32561836
26. Liu K, Wang J, Zeng W, Song J. Comparison and evaluation of three methods for estimating forest above ground biomass using TM and GLAS data. Remote Sens. 2017;9(4).

DOI: 10.3390/rs9040341

27. Pandit S, Tsuyuki S, Dube T. Estimating above-ground biomass in sub-tropical buffer zone community forests, Nepal, using Sentinel 2 data. Remote Sens. 2018;10(4).

DOI: 10.3390/rs10040601

28. Kamusoko C, Kamusoko OW, Chikati E, Gamba J. Mapping urban and peri-urban land cover in Zimbabwe: challenges and opportunities. Geomatics. 2021;1(1):114-47.

DOI: 10.3390/geomatics1010009

29. Strobl C, Boulesteix AL, Zeileis A, Hothorn T. Bias in random forest variable importance measures: illustrations, sources and a solution. BMC Bioinformatics. 2007;8:25.

DOI: 10.1186/1471-2105-8-25

30. Palczewska A, Palczewski J, Robinson Daniel RMN. Interpreting random forest classification models using a feature contribution method. In : Interpreting Random Forest Classification Models Using a Feature Contribu; 2014.
31. Murray K, Conner MM. Methods to quantify variable importance: Implications for the analysis of noisy ecological data (Ecology (2009) 90 (348-355)). Ecology. 2009;90(5):1425-.

DOI: 10.1890/0012-9658-90.5.1425

32. Bilous A, Myroniuk V, Holiaka D, Bilous S, See L, Schepaschenko D. Mapping growing stock volume and forest live biomass: A case study of the Polissya region of Ukraine. Environ Res Lett. 2017; 12(10).

DOI: 10.1088/1748-9326/aa8352

33. Li C, Zhou L, Xu W. Estimating aboveground biomass using sentinel-2 msi data and ensemble algorithms for grassland in the shengjin lake wetland, China. Remote Sens. 2021; 13(8).

DOI: 10.3390/rs13081595

34. Chidumayo EN. Management implications of tree growth patterns in miombo woodlands of Zambia. Forest Ecol Manag. 2019;436(January):105-16.

DOI: 10.1016/j.foreco.2019.01.018

35. Chidumayo EN, Gumbo DJ. The dry forests and woodlands of Africa: Managing

for products and services. 2010; 288.
DOI: 10.4324/9781849776547.
36. Government of Malawi, 'Malawi 10-day Weather and Agrometeorological Bulletin. 2019;265:1-2.
37. Cassells GF, Woodhouse IH, Mitchard ETA, Tembo MD. The use of Alos palsar for supporting sustainable forest use in southern Africa: A case study in Malawi. Int Geosci Remote Sens Symp (IGARSS). 2009;2:II-206.
DOI: 10.1109/IGARSS.2009.5418042
38. Patenaude G, Milne R, Dawson TP. Synthesis of remote sensing approaches for forest carbon estimation: Reporting to the Kyoto Protocol. Environ Sci Policy. 2005;8(2):161-78.
DOI: 10.1016/j.envsci.2004.12.010
39. Puliti S, Ørka HO, Gobakken T, Næsset E. Inventory of small forest areas using an unmanned aerial system. Remote Sens. 2015;7(8):9632-54.
DOI: 10.3390/rs70809632
40. N. D. Assembly. Ntchisi District socio-economic profile 2013-2018; 2014.
41. Ntchisi District assembly. Strategic forest area plan-Ntchisi forest reserve-June 2007; 2007.